INSIGHTS AND REGULATION OF PLANT CARBON METABOLISM

EDITED BY: Maria Grazia Annunziata, Diana Santelia and Rubén Vicente

PUBLISHED IN: Frontiers in Plant Science

frontiers Research Topics

frontiers

ISSN 1664-8714
ISBN 978-2-88976-879-0
DOI 10.3389/978-2-88976-879-0

About Frontiers

Frontiers is more than just an open-access publisher of scholarly articles: it is a pioneering approach to the world of academia, radically improving the way scholarly research is managed. The grand vision of Frontiers is a world where all people have an equal opportunity to seek, share and generate knowledge. Frontiers provides immediate and permanent online open access to all its publications, but this alone is not enough to realize our grand goals.

Frontiers Journal Series

The Frontiers Journal Series is a multi-tier and interdisciplinary set of open-access, online journals, promising a paradigm shift from the current review, selection and dissemination processes in academic publishing. All Frontiers journals are driven by researchers for researchers; therefore, they constitute a service to the scholarly community. At the same time, the Frontiers Journal Series operates on a revolutionary invention, the tiered publishing system, initially addressing specific communities of scholars, and gradually climbing up to broader public understanding, thus serving the interests of the lay society, too.

Dedication to Quality

Each Frontiers article is a landmark of the highest quality, thanks to genuinely collaborative interactions between authors and review editors, who include some of the world's best academicians. Research must be certified by peers before entering a stream of knowledge that may eventually reach the public - and shape society; therefore, Frontiers only applies the most rigorous and unbiased reviews.
Frontiers revolutionizes research publishing by freely delivering the most outstanding research, evaluated with no bias from both the academic and social point of view. By applying the most advanced information technologies, Frontiers is catapulting scholarly publishing into a new generation.

What are Frontiers Research Topics?

Frontiers Research Topics are very popular trademarks of the Frontiers Journals Series: they are collections of at least ten articles, all centered on a particular subject. With their unique mix of varied contributions from Original Research to Review Articles, Frontiers Research Topics unify the most influential researchers, the latest key findings and historical advances in a hot research area! Find out more on how to host your own Frontiers Research Topic or contribute to one as an author by contacting the Frontiers Editorial Office: frontiersin.org/about/contact

INSIGHTS AND REGULATION OF PLANT CARBON METABOLISM

Topic Editors:
Maria Grazia Annunziata, University of Potsdam, Germany
Diana Santelia, ETH Zürich, Switzerland
Rubén Vicente, Universidade NOVA de Lisboa, Portugal

Citation: Annunziata, M. G., Santelia, D., Vicente, R., eds. (2022). Insights and Regulation of Plant Carbon Metabolism. Lausanne: Frontiers Media SA. doi: 10.3389/978-2-88976-879-0

Table of Contents

frontiers | Frontiers in Plant Science

TYPE Editorial
PUBLISHED 31 August 2022
DOI 10.3389/fpls.2022.1011224

OPEN ACCESS

EDITED AND REVIEWED BY
Massuo Jorge Kato,
University of São Paulo, Brazil

*CORRESPONDENCE
Rubén Vicente
ruben.vicente@itqb.unl.pt

SPECIALTY SECTION
This article was submitted to Plant Metabolism and Chemodiversity, a section of the journal Frontiers in Plant Science

RECEIVED 04 August 2022
ACCEPTED 15 August 2022
PUBLISHED 31 August 2022

CITATION
Vicente R, Annunziata MG and Santelia D (2022) Editorial: Insights and regulation of plant carbon metabolism. *Front. Plant Sci.* 13:1011224. doi: 10.3389/fpls.2022.1011224

Editorial: Insights and regulation of plant carbon metabolism

Rubén Vicente[1]*, Maria Grazia Annunziata[2] and Diana Santelia[3]

[1]Plant Ecophysiology and Metabolism Group, Instituto de Tecnologia Química e Biológica António Xavier (ITQB NOVA), Universidade Nova de Lisboa, Oeiras, Portugal, [2]Department of Molecular Biology, Institute of Biochemistry and Biology, University of Potsdam, Potsdam, Germany, [3]Institute of Integrative Biology, ETH Zurich, Zurich, Switzerland

KEYWORDS

carbohydrates, crop production, fluctuating environment, metabolic regulation, phenotyping, photosynthesis, plant carbon metabolism, source-to-sink dynamics

Editorial on the Research Topic
Insights and regulation of plant carbon metabolism

In their natural environments, plants use sunlight to obtain the energy needed to carry out the fixation of atmospheric CO_2 (photosynthesis) and other anabolic processes that are necessary for their growth and development. This energy is also used for the daily challenge of survival during the night, when the absence of light forces the plant to use the carbon reserves accumulated during the day. In addition to these daily fluctuations, plants efficiently regulate their carbon metabolism at the whole plant level to adapt to changes in environmental conditions. During the day, the autotrophic organs ("sources") supply carbon and energy, mainly in the form of sucrose, to maintain plant metabolism and ensure the development of heterotrophic organs ("sinks"), such as roots and reproductive structures. When carbon fixation exceeds its demand, carbon is accumulated in transient carbon pools (mainly starch and soluble sugars) to be used during the night or at later growth stages. Carbon metabolism is highly susceptible to environmental changes, being involved in stress sensing and signaling that allow plants to adapt to the new growth conditions. Moreover, efficient source-to-sink transport of sugars is essential for plant growth processes and enables fine-tuned carbon partitioning across plant organs through the phloem. Despite huge progress over the last decades in understanding plant carbon metabolism, knowledge about its regulation and coordination at the whole-plant level is still fragmentary.

This Research Topic aims at providing novel insights into the regulation of plant carbon metabolism. Matiolli et al. studied one of the key mechanisms regulating carbon metabolism: the post-translational modifications (PTMs) of proteins involved in primary metabolism. The authors provided a holistic overview of PTMs in plant carbon metabolism, showing how they can regulate carbon sensing, fixation, storage, remobilization, transport, and cytosolic glycolysis. PTMs lead to fast, often reversible, adjustments of processes such as protein-protein interactions, enzymatic activities, stability and subcellular localization, which allow to optimize plant fitness in the ever-changing environment. Among the most relevant examples, the role of three

conserved kinases (SnRK1, TOR, and HXK1) and the ferredoxin/thioredoxin system controlling carbon-energy-nutrient homeostasis were highlighted. Furthermore, Paul reviewed one of the most controversial points about carbon metabolism over the past years: is photosynthesis one of the main targets to focus on to improve crop yields? While some studies suggest that photosynthesis is not the main limiting process for crop improvement, other studies have shown that its manipulation led to significant improvements. However, the improvement of the plant carbon status has to be accompanied by other crucial factors, such as optimized nitrogen and water supplies and source-sink interactions. Martínez-Peña et al. studied source-sink dynamics in field-grown durum wheat (*Triticum turgidum* L. ssp. *durum*) by integrating canopy phenotyping with metabolic analyses of different plant photosynthetic organs. This novel approach allowed them to investigate the coordination between carbon and nitrogen metabolism at the whole plant level. Interestingly, the authors observed that non-foliar organs (e.g. ear organs such as awns, glumes, and lemmas) play a crucial role in late grain filling and grain quality, although their metabolic activity is quantitatively not comparable to flag leaves. These findings lead to the suggestion that non-foliar organs may represent novel targets for crop breeding.

Photoassimilates are the main source of carbon and energy in sink organs that are transported from sources by various mechanisms. The transport of sugars through the phloem requires the subsequent unloading via sugars transporters, as highlighted in the study of Li et al. The authors revealed the role of the hexose transporter CsSWEET7a, localized in the phloem region of the receptacle and nectary in both male and female flowers of cucumber (*Cucumis sativus* L.), in supplying sugars for flower anthesis and nectar secretion to reward pollinators. Continuing with the reproductive phase of flowering plants, Wang et al. further showed the involvement of carbon metabolism in pollen germination in *Arabidopsis thaliana*. This study reveals that starch and sucrose metabolism were induced during the transition from mature to hydrated pollen, while the metabolites palmitic acid, oleic acid, linolenic acid, quercetin, luteolin/kaempferol, and γ-aminobutyric acid (GABA) may contribute to activate pollen tube emergence. Hence, sugars play an essential role in plant fertilization, seed formation, and yield. Photoassimilates also play a primary role in root growth, as Kang et al. demonstrated in radish (*Raphanus sativus* L.) with the levels of fructose determining root length and color. Glucose was the main sugar in radish roots, while sucrose was majorly transported to roots by the apoplasmic pathway, where it was metabolized. Sucrose and cellulose synthases were correlated at transcript levels, suggesting tightly coordinated cell wall synthesis, while the excess fructose generated by sucrose synthases was predominantly phosphorylated by fructokinases.

New findings on the reserve polysaccharide starch are reported by Ribeiro et al. which highlights its central role in plant responses to biotic and abiotic stresses. Starch synthesis is generally decreased under abiotic stresses (e.g., salt, drought, heat, and cold stresses) due to lower photosynthetic rates, while its content also decreases to reallocate carbon or to synthesize osmo/cryoprotectants to minimize the impact of stress. In response to pathogen infection, starch usually accumulates, which may restrict CO_2 diffusion. However, the dynamics of starch metabolism in response to stress is dependent on several factors, and further research studies should consider carefully the strength and duration of the stress, and short- (daily fluctuations regulated by circadian clock) and long-term responses. In line with this, Calderan-Rodrigues et al. reports novel findings on the role of proteogenic dipeptides in the control of metabolic fluxes during the day-night cycle of *Arabidopsis thaliana*. Intriguingly, they found rhythmic dipeptides under short- and long-day diel cycles that could be regulated by the Target of Rapamycin (TOR) signaling pathway. The authors hypothesized that altered levels of proline and proline-containing didpeptides (e.g., Pro-Gln) under limited carbon availability may act as alternative respiratory substrates to allow plant survival and modulate protein activity. External application of metabolic compounds is also a direct way to improve plant growth and stress response. Abd Elbar et al. applied GABA to leaves of tomato (*Solanum lycopersicum* L.) plants under chilling stress at the reproductive and fruit set stages. This non-proteinogenic amino acid, known to be associated with stress tolerance, led to fruit yield improvement under such stress. This response was mainly associated with an upregulation of sugar metabolism (acting as osmolytes), modulation of pigment composition and secondary metabolism, alleviation of oxidative damage by promoting antioxidant system and maintenance of the integrity of plastids' ultrastructure.

Concluding remarks

The regulation of carbon metabolism is key to the understanding of how plants use their internal reserves to respond to the environment and develop a specific phenotype, which ultimately has an essential impact on plant growth, development and yield. Over the past decades, much research has been carried out to understand the mechanisms regulating carbon fixation and its utilization in model plants, mainly *Arabidopsis thaliana*. However, the knowledge gained studying model species is more and more applied to crops of economic or environmental interest and, in addition, researchers have understood the importance of conducting experiments under conditions as close as possible to the real growing environments. In this Research Topic and throughout the aforementioned studies, we highlight the need to advance the study of mechanisms regulating carbon metabolism as the backbone for crop improvement. Holistic studies should be promoted that

(i) integrate approaches at different levels, from molecular and biochemical methods to high-precision phenotyping techniques, (ii) encompass the whole plant (source-sink dynamics) at different stages of its development, and (iii) include the different crops of interest under present and future growth conditions.

Author contributions

RV wrote the manuscript, while MA and DS revised and edited it. All authors approved the submitted version for publication.

Funding

RV acknowledges the support by FCT - Fundação para a Ciência e a Tecnologia, I.P., through GREEN-IT - Bioresources for Sustainability R&D Unit (UIDB/04551/2020, UIDP/04551/2020) and LS4FUTURE Associated Laboratory (LA/P/0087/2020). MA acknowledges funding by the Deutsche Forschungsgemeinschaft (DFG) of the Collaborative Research Center 973 Priming and Memory of Organismic Responses to Stress (www.sfb973.de) and by the European Union's Horizon 2020 Research and Innovation Programme, project PlantaSYST (SGA-CSA No. 739582 under FPA No. 664620). DS acknowledges the support by Swiss National Science Foundation (Grant no. 310030_185241) and by ETH Zurich.

Acknowledgments

The Guest Editors would like to thank all the people involved in this Research Topic; the authors for their valuable contributions and the reviewers for their time, dedication and rigor during the review process.

Conflict of interest

The authors declare that the research was conducted in the absence of any commercial or financial relationships that could be construed as a potential conflict of interest.

Publisher's note

frontiers in Plant Science

OPINION
published: 21 September 2021
doi: 10.3389/fpls.2021.743862

Improving Photosynthetic Metabolism for Crop Yields: What Is Going to Work?

*Matthew J. Paul**

Plant Science, Rothamsted Research, Harpenden, United Kingdom

Keywords: photosynthesis, crop yield improvement, source-sink, Rubisco, cereals

INTRODUCTION

Photosynthesis is an indispensable process that provides the oxygen we breathe, regulates climate, and drives biological processes including crop yields. An important and obvious challenge for crop improvement is: Is photosynthesis and its regulation in crops amenable to improvement to stimulate yields? If so, how could this be done? Photosynthesis is a well-studied process with models of the limitations in the photosynthetic pathway (Zhu et al., 2010). The past 10 years have seen a major effort into improving photosynthesis with a justification that improvements in crop yields need to be quick and large because of the yield plateauing of major crops. The harvest index has been optimized, and therefore, the next bottleneck is proposed as photosynthesis. However, crop yields are yet to benefit from this research despite some tantalizing examples of genetic interventions in models (Arabidopsis and tobacco) including field studies (Glowacka et al., 2018; South et al., 2019). The focus on photosynthesis has been controversial given long-standing evidence with well-reasoned arguments going back to the 1970s that carbon input is not limiting for crop growth and yield (Sinclair et al., 2019). Failure to produce tangible benefits in crops so far from the photosynthetic research effort is attracting gathering criticism (Araus et al., 2021) with arguments for a more balanced approach (Reynolds et al., 2021). However, a recent study overexpresses Rubisco in paddy rice which increases yield in the field under good nitrogen supply by 17–28% (Yoon et al., 2020). This appears to be the first successful direct targeting of photosynthesis in the field in a major food security cereal crop. This article gathers information from recent literature on the photosynthetic improvement of both heavily reductionist approaches and broader-based strategies to provide a balanced opinion of the way forward for the photosynthesis field for crop yield improvement.

PHOTOSYNTHESIS AS PART OF A REGULATED SYSTEM

Biological systems consist of parts that make up a whole system. These parts such as photosynthesis need to be considered in themselves to understand the reductionist fundamental molecular science of their makeup and function. This has given rise to photosynthetic models of limiting steps in the process where improvements could be made (Zhu et al., 2010). However, of all biological processes within the plant, photosynthesis is perhaps the most intimately integrated into the system. Therefore, it could be argued that photosynthesis in terms of increasing crop yields cannot be seen like the engine of a motor car where improvements in one or several components could make the engine drive faster or consume less petrol. This is because "the car" in biological terms is not just driven by the engine, photosynthesis, but the car (rest of the plant) strongly interacts and regulates the engine itself. Crop yield is a product of the whole system, not just photosynthesis. So, photosynthesis provides the carbon and energy on which the entire system depends, but this

OPEN ACCESS

Edited by:
Rubén Vicente, Universidade NOVA de Lisboa, Portugal

Reviewed by:
Rosa María Morcuende, Institute of Natural Resources and Agrobiology of Salamanca (IRNASA), Spain

***Correspondence:**
Matthew J. Paul
matthew.paul@rothamsted.ac.uk

Specialty section:
This article was submitted to Plant Metabolism and Chemodiversity, a section of the journal Frontiers in Plant Science

Received: *19 July 2021*
Accepted: *24 August 2021*
Published: *21 September 2021*

Citation:
Paul MJ (2021) Improving Photosynthetic Metabolism for Crop Yields: What Is Going to Work? Front. Plant Sci. 12:743862. doi: 10.3389/fpls.2021.743862

interaction is not linear and depends on numerous factors such as development, leaf and canopy structure and architecture, source-sink feedback, and how photosynthesis is affected within a crop stand in the field. Further, photosynthesis and growth are strongly regulated by the field environment that is significantly different from the laboratory or greenhouse. Photosynthesis is strongly affected by such interactions and feedbacks, such that knowledge of individual components as limiting factors for yield becomes almost lost and meaningless among the noise of the system. Sinclair et al. (2019) made a particularly strong case that long-standing evidence shows that past crop yield increases are not associated with increased photosynthesis. For numerous crops, there has been no rise in carbon exchange rate per unit leaf area. The conclusion was that yield was a multifaceted outcome of many resources and processes; photosynthetic input was almost never the critical variable limiting yield (Evans, 1994; Boote and Sinclair, 2006).

TRANSGENIC PADDY RICE OVEREXPRESSING RUBISCO INCREASES YIELD IN THE FIELD

A recent article (Yoon et al., 2020) goes against this prevailing view that increasing the photosynthetic rate will do nothing for crop yield. Rubisco was overexpressed in rice with its own promoter. Convincing increases in filled spikelets gave grain yields up to 28% higher in paddy fields. The total biomass was also higher (11–23%). Effects were greatest at nitrogen application rates 100–170 kg per hectare peaking at 28% higher yield at 141 kg nitrogen per hectare. This resulted in more yield gain for nitrogen added, indicating that nitrogen use efficiency was increased. The variety Notohikari has been used since 1985; so potentially, an older variety like this could be more amenable to improvement. However, 6 tonnes per hectare in wild type is a good rice crop yield.

THE CRUCIAL CONSIDERATION OF NITROGEN AND WATER FOR PHOTOSYNTHETIC IMPROVEMENT

There may be two factors in this study to explain the success of this genetic intervention, specifically the role of nitrogen and water. The main conclusion from Sinclair et al. (2019) was that yield increases are closely dependent on nitrogen accumulation as an essential and quantitative component of seeds. Carbon accumulation in the absence of additional nitrogen does not increase yield. Overexpression of Rubisco in Yoon et al. (2020) increased nitrogen uptake and content particularly just before full heading and through the ripening stages. This could fulfill the requirement laid down by Sinclair et al. (2019) of nitrogen to accompany carbon. As Rubisco is such a large component of leaf nitrogen, increasing photosynthesis by targeting other photosynthetic proteins might not increase nitrogen uptake. Second, increases in photosynthetic gas exchange are normally attenuated by water availability, as much of agricultural production is rainfed rather than irrigated. Intermittent drought can limit yields to at least to some extent each year. The challenge faced is that enhanced photosynthesis leads to more rapid depletion of water. Cross-scale system modeling through the crop life cycle by Wu et al. (2019) shows that enhanced photosynthesis improves biomass gain early in the season when soil water is more abundant, but depletes soil water, leaving less for later crop development. This impinges yields in all but the most hydrated agricultural environments. Yoon et al. (2020) performed their work in a rice paddy where water is not limiting, and hence, photosynthesis is not likely to have been compromised. The filling of existing spikelets was improved, which depends on high photosynthesis later during the life cycle. Therefore, at a system level, both the major limiting factors to crop yield, nitrogen and water, were able to match the enhanced carbon uptake.

BESPOKE PHOTOSYNTHETIC IMPROVEMENT?

It is possible that overexpressing Rubisco may only work where water and nitrogen availability and uptake will not hold back the benefits of extra carbon, such as in paddy rice. Overexpressing Rubisco where water supply limits yield even to a small extent may provide little or no worthwhile benefit to yield according to Wu et al. (2019). Hence, paddy rice or heavily irrigated crops only may benefit. Intervention in photosynthesis may need to be tailored to environmental conditions. Protection measures such as against reactive oxygen species may be beneficial in situations where water limits yield, as shown in maize in the field (Simmons et al., 2021). Recovery from photoprotection may also be amenable to transgenic intervention, as shown in tobacco (Kromdijk et al., 2016). This approach will not increase the yield potential but enables the existing photosynthetic potential to cope better with insufficient water. Photoprotection may be particularly beneficial in very sunny environments. In a recent study involving the wheat high biomass association panel (HiBAP) conducted in Mexico, Joynson et al. (2021) showed marker-trait associations relating to leaf pigment content that could prevent the propagation of free radicals to improve radiation use efficiency and yield. Selection or genetic intervention in photoprotection may not involve large interactions with the whole system and, therefore, may be relatively straightforward compared with other strategies. However, other approaches that do alter the whole system like optimizing source-sink interactions could potentially benefit crops for both yield potential and abiotic stress resilience.

THE CRUCIAL CONSIDERATION OF SOURCE-SINK INTERACTION TO IMPROVE PHOTOSYNTHESIS

There are examples where the promotion of sink strength increases photosynthesis and carbon gain for yield. Maize expressing a rice trehalose phosphate phosphatase gene in phloem tissue in developing cobs had higher yield at a range of water availabilities in extensive field trials, at 9–49% higher than wild type with no or mild drought and

31–123% higher with more severe drought (Nuccio et al., 2015). Lower trehalose 6-phosphate (T6P) in phloem tissue enhanced SWEET expression resulting in stronger movement of sucrose into kernels improving kernel set (Oszvald et al., 2018). This genetic intervention prevented the normal decline of photosynthesis in associated leaves over time giving almost 50% greater photosynthetic rates at specific time points showing that stimulation of sink can exert a strong pull on the source. Beechey-Gradwell et al. (2020) overexpressed diacylglycerol acyltransferase to drive triacylglycerol biosynthesis in *Lolium perenne*. High lipid *L. perenne* plants not only accumulated lipid but also had up to 28% higher photosynthetic rate. Diversion of carbohydrates into a lipid carbon sink may sequester carbon away from carbon-sensing mechanisms. This could mitigate the signals that would normally downregulate photosynthesis as part of carbon and energy metabolic homeostasis, meaning that photosynthesis is "blind" to carbon accumulation and can carry on unimpeded while carbon accumulates. This is another example of the strong effect sink can have on source as a consideration in improving photosynthesis. Source-sink modifications for cereals could work where photosynthesis is maximized around grain set before anthesis to establish a large sink through floret initiation and retention. This large sink may then sustain photosynthesis during grain filling (Reynolds et al., 2021). Optimizing canopy structures such as upright leaves to allow more light interception is an approach shown to work to increase wheat photosynthesis to maximize grain set (Richards et al., 2019). Lines with erectophile leaves had a 13% higher yield. Griffiths et al. (2020) showed that effects of drought pre- or post-anthesis affect grain yield parameters differently. Yield is strongly related to grain number when drought is pre-anthesis but has a stronger element of grain size as a yield determinant when drought is applied at anthesis. Environments with intermittent drought need to ideally include germplasm with elements of tolerance to both pre- and post-anthesis drought that also have good yield potential. There were only three such lines out of 150 that fulfilled this requirement (Griffiths et al., 2020). It is proposed that genes that enable high yields in all three conditions may be genes that coordinate source and sink. Source-sink coordination at crucial times in development may be important. Wang et al. (2019) and Wang et al. (2020) showed that genetic regions could be identified containing genes for high source and high sink that could be combined in breeding. For different crops where water is often limiting unpredictably, combining beneficial source and sink genes is likely to be a way forward.

CONCLUSION: WAYS AHEAD FOR PHOTOSYNTHESIS

Transgenic crops with modified photosynthesis that successfully increase yield in the field in major food security cereals may be rare. The example of Yoon et al. (2020) may have worked because of the special paddy conditions in that experiment. In more water-restricted environments, overexpressing Rubisco may be less successful, and consideration of photoprotection could offer some benefits. Strategies to optimize source-sink would represent a promising way forward given the significant effects that a strong sink can exert on photosynthesis and the strong determination of grain number and also grain size on the source and yield. A stronger sink strength can increase yield with and without drought (Oszvald et al., 2018). Creating a stronger sink strength has the advantage over photoprotection that yield potential is increased too. It may be possible to identify genetic regions for the strong source and sink through GWAS (Wang et al., 2019, 2020). More than anything, improving crop photosynthesis in the field will require larger-scale collaborations involving expertise from experts in institutes and universities, CGIAR centers, and the private sector. This will require adopting strategies critically assessed as likely to work in field conditions by all stakeholders.

AUTHOR CONTRIBUTIONS

The author confirms being the sole contributor of this work and has approved it for publication.

FUNDING

Rothamsted Research receives strategic funding from the Biotechnological and Biological Sciences Research Council of the United Kingdom.

ACKNOWLEDGMENTS

Support is acknowledged from the Designing Future Wheat Institute Strategic Programme (BB/P016855/1).

REFERENCES

Araus, J. L., Sanchez-Bragado, R., and Vicente, R. (2021). Improving crop yield and resilience through optimisation of photosynthesis: panacea or pipe dream? *J. Exp. Bot.* 72, 3936–3955. doi: 10.1093/jxb/erab097

Beechey-Gradwell, Z., Cooney, L., Winichayakul, S., Andrews, M., Hea, S. Y., Crowther, T., et al. (2020). Storing carbon in leaf lipid sinks enhanced perennial ryegrass carbon capture especially under high N and elevated CO_2. *J. Exp. Bot.* 71, 2351–2361. doi: 10.1093/jxb/erz494

Boote, K. J., and Sinclair, T. R. (2006). Crop physiology: significant discoveries and our changing perspectuive on research. *Crop Sci.* 46, 2270–2277. doi: 10.2135/cropsci2006.01.0039gas

Evans, L. T. (1994). "Crop physiology: prospects for the retrospective science," in *Physiology and Determniantion of Crop Yield*, eds Boote K. J. et al. (ASA-CSSA-SSSA), 19–35. doi: 10.2134/1994.physiologyanddetermination.c2

Glowacka, K., Kromdijk, J., Kucera, K., Xie, J., Cavanagh, A. P., Leonelli, L., et al. (2018). Photosystem II subunit S overexpression increases the efficiency of water use in a field-grown crop. *Nat. Comm.* 9:868. doi: 10.1038/s41467-018-03231-x

Griffiths, C. A., Reynolds, M. P., and Paul, M. J. (2020). Combining yield potential and drought resilience in a spring wheat diversity panel. *Food Energy Secur.* 9:e241. doi: 10.1002/fes3.241

Joynson, R., Molero, G., Coombes, B., Gardiner, Rivera-Amado, C., Piñera-Chávez, F. J., Evans, J. R., et al. (2021). Uncovering candidate genes involved in

photosynthetic capacity using unexplored genetic variation in Spring Wheat. *Plant Biotechnol. J.* 19, 1537–1552. doi: 10.1111/pbi.13568

Kromdijk, J., Glowacka, K., Leonelli, L., Gabilly, S. T., Iwai, M., Niyogi, K. K., et al. (2016). Imporving photosynthesis and crop productivity by accelerating recovery from photoprotection. *Science* 354, 857–861. doi: 10.1126/science.aai8878

Nuccio, M. L., Wu, J., Mowers, R., Zhou, H.-P., Meghji, M., Primavesi, L. F., et al. (2015). Expression of trehalose 6-phosphate phosphatase in maize ears improves yield in well-watered and drought conditions. *Nat. Biotech.* 33, 862–869. doi: 10.1038/nbt.3277

Oszvald, M., Primavesi, L. F., Griffiths, C. A., Cohn, C., Basu, S. S., Nuccio, M. L., et al. (2018). Trehlaose 6-phosphate in maize reproductive tissue regulates assimilate partitioning and photosynthesis. *Plant Physiol.* 176, 2623–2638. doi: 10.1104/pp.17.01673

Reynolds, M., Atkin, O. K., Bennett, M., Cooper, M., Dodd, I. C., Foulkes, M. J., et al. (2021). Addressing research bottlenecks to crop productivity. *Trends Plant Sci.* 16, 607–630. doi: 10.1016/j.tplants.2021.03.011

Richards, R. A., Cavanagh, C. R., and Riffkin, P. (2019). Selection for erect canopy architecture can increase yield and biomass of spring wheat. *Field Crops Res.* 244:107649. doi: 10.1016/j.fcr.2019.107649

Simmons, C. R., Lafitte, H. R., Reimann, K. S., Brugiere, N., Roesler, K., Albertsen, M. C., et al. (2021). Successes and insights of an industry biotech program to enhance maize agronomic traits. *Plant Sci.* 307:110899. doi: 10.1016/j.plantsci.2021.110899

Sinclair, T. R., Rufty, T. W., and Lewis, R. S. (2019). Increasing photosynthesis: unlikely solution for world food problem. *Trends Plant Sci.* 24, 1032–1039. doi: 10.1016/j.tplants.2019.07.008

South, P. F., Cavanagh, A. P., Liu, H. W., and Ort, D. R. (2019). Synthetic glycolate metabolism pathways stimulate crop growth and productivity in the field. *Science* 363:eaat9077. doi: 10.1126/science.aat9077

Wang, Y., Pang, Y., Chen, K., Zhai, L., Shen, C., Wang, S., et al. (2019). Genetic bases of source-, sink-, and yield-related traits revealed by genome-wide association study in rice. *Crop J.* 8, 119–131. doi: 10.1016/j.cj.2019.05.001

Wang, Y., Wang, J., Zhai, L., Liang, C., Chen, K., and Xu, J. (2020). Identify QTLs and candidate genes underlying source-, sink-, and grain yield-related traits in rice by integrated analysis of bi-parental and natural populations. *PLoS ONE* 15:e0237774. doi: 10.1371/journal.pone.0237774

Wu, A., Hammer, G. L., Doherty, A., von Caemmerer, S., and Farquhar, G. D. (2019). Quantifying impacts of enhancing photosynthesis on crop yield. *Nat. Plants* 5, 380–388. doi: 10.1038/s41477-019-0398-8

Yoon, D.-K., Ishiyama, K., Suganami, M., Tazoe, Y., Watanabe, M., Imaruoka, S., et al. (2020). Transgenic rice overproducing Rubisco exhibits increased yields with improved nitrogen-use efficiency in an experimental paddy field. *Nat. Food* 1, 134–139. doi: 10.1038/s43016-020-0033-x

Zhu, X. G., Long, S. P., and Ort, D. R. (2010). Improving photosynthetic efficiency for greater yield. *Annu. Rev. Plant Biol.* 61, 235–261. doi: 10.1146/annurev-arplant-042809-112206

Conflict of Interest: The author declares that the research was conducted in the absence of any commercial or financial relationships that could be construed as a potential conflict of interest.

Publisher's Note: All claims expressed in this article are solely those of the authors and do not necessarily represent those of their affiliated organizations, or those of the publisher, the editors and the reviewers. Any product that may be evaluated in this article, or claim that may be made by its manufacturer, is not guaranteed or endorsed by the publisher.

frontiers in Plant Science

ORIGINAL RESEARCH
published: 18 October 2021
doi: 10.3389/fpls.2021.663750

Protective Effect of γ-Aminobutyric Acid Against Chilling Stress During Reproductive Stage in Tomato Plants Through Modulation of Sugar Metabolism, Chloroplast Integrity, and Antioxidative Defense Systems

*Ola H. Abd Elbar[1], Amr Elkelish[2], Gniewko Niedbała[3], Reham Farag[1], Tomasz Wojciechowski[3], Soumya Mukherjee[4], Ayman F. Abou-Hadid[5], Hussien M. El-Hennawy[5], Ahmed Abou El-Yazied[5], Hany G. Abd El-Gawad[5], Ehab Azab[6], Adil A. Gobouri[7], Nihal El Nahhas[8], Ahmed M. El-Sawy[9], Ahmed Bondok[10] and Mohamed F. M. Ibrahim[1]**

[1] Department of Agricultural Botany, Faculty of Agriculture, Ain Shams University, Cairo, Egypt, [2] Department of Botany, Faculty of Science, Suez Canal University, Ismailia, Egypt, [3] Department of Biosystems Engineering, Faculty of Environmental and Mechanical Engineering, Poznań University of Life Sciences, Poznań, Poland, [4] Department of Botany, Jangipur College, University of Kalyani, West Bengal, India, [5] Department of Horticulture, Faculty of Agriculture, Ain Shams University, Cairo, Egypt, [6] Department of Food Science and Nutrition, College of Science, Taif University, Taif, Saudi Arabia, [7] Department of Chemistry, College of Science, Taif University, Taif, Saudi Arabia, [8] Department of Botany and Microbiology, Faculty of Science, Alexandria University, Alexandria, Egypt, [9] Department of Climate Modification, Central Laboratory for Agriculture Climate, Agriculture Research Center, Giza, Egypt, [10] Department of Plant Pathology, Faculty of Agriculture, Ain Shams University, Cairo, Egypt

OPEN ACCESS

Edited by:
Diana Santelia,
ETH Zürich, Switzerland

Reviewed by:
Tianhu Sun,
Cornell University, United States
Parvaiz Ahmad,
Sri Pratap College Srinagar, India

***Correspondence:**
Mohamed F. M. Ibrahim
ibrahim_mfm@agr.asu.edu.eg

Specialty section:
This article was submitted to Plant Metabolism and Chemodiversity, a section of the journal Frontiers in Plant Science

Received: *22 February 2021*
Accepted: *13 August 2021*
Published: *18 October 2021*

Citation:
Abd Elbar OH, Elkelish A, Niedbała G, Farag R, Wojciechowski T, Mukherjee S, Abou-Hadid AF, El-Hennawy HM, Abou El-Yazied A, Abd El-Gawad HG, Azab E, Gobouri AA, El Nahhas N, El-Sawy AM, Bondok A and Ibrahim MFM (2021) Protective Effect of γ-Aminobutyric Acid Against Chilling Stress During Reproductive Stage in Tomato Plants Through Modulation of Sugar Metabolism, Chloroplast Integrity, and Antioxidative Defense Systems. Front. Plant Sci. 12:663750. doi: 10.3389/fpls.2021.663750

Despite the role of γ-aminobutyric acid (GABA) in plant tolerance to chilling stress having been widely discussed in the seedling stage, very little information is clear regarding its implication in chilling tolerance during the reproductive stage of the plant. Here, we investigated the influence of GABA (1 and 2 mM) as a foliar application on tomato plants (*Solanum lycopersicum* L. cv. Super Marmande) subjected to chilling stress (5°C for 6 h/day) for 5 successive days during the flowering stage. The results indicated that applied GABA differentially influenced leaf pigment composition by decreasing the chlorophyll a/b ratio and increasing the anthocyanin relative to total chlorophyll. However, carotenoids were not affected in both GABA-treated and non-treated stressed plants. Root tissues significantly exhibited an increase in thermo-tolerance in GABA-treated plants. Furthermore, applied GABA substantially alleviated the chilling-induced oxidative damage by protecting cell membrane integrity and reducing malondialdehyde (MDA) and H_2O_2. This positive effect of GABA was associated with enhancing the activity of phenylalanine ammonia-lyase (PAL), catalase (CAT), superoxide dismutase (SOD), and ascorbate peroxidase (APX). Conversely, a downregulation of peroxidase (POX) and polyphenol oxidase (PPO) was observed under chilling stress which indicates its relevance in phenol metabolism. Interesting correlations were obtained between GABA-induced upregulation of sugar metabolism coinciding with altering secondary metabolism, activities

of antioxidant enzymes, and maintaining the integrity of plastids' ultrastructure Eventually, applied GABA especially at 2 mM improved the fruit yield and could be recommended to mitigate the damage of chilling stress in tomato plants.

Keywords: tomato (*Solanum lycopersicum* L.), gamma-aminobutyric acid, chilling stress, chloroplast ultrastructure, oxidative stress, antioxidants, fruit yield

INTRODUCTION

Tomato (*Solanum lycopersicum* L.) is a cosmopolitan economical vegetable crop cultivated worldwide, distributed in diverse climate zones. This leads to cultivation exposing the plant to various environmental stresses (Chaudhary et al., 2019). Most cultivated genotypes are sensitive to low temperatures in all growth stages (Foolad and Lin, 2000). As tomato is a warm-season crop which grows well in the range of 25–28°C, growth will be limited when the plants are exposed to low temperature (5–13°C; Aghdam et al., 2012).

In recent decades, global climate change has caused sudden, variable, and extreme weather changes repeatedly leading to high losses of crop productivity and yield (Alam et al., 2019; Ahanger et al., 2020; Ahmad et al., 2020; Jan et al., 2020; Kaya et al., 2020). Particularly, chilling stress is deleterious to the growth and development of crops that have originated in temperate zones (Zhang et al., 2004; Ma et al., 2018). Chilling stress causes a rapid and synchronized change in the thermodynamic microclimate of every plant cell, including in the molecular makeup of all organelles. Enzymatic reactions are slowed due to a reduction in the diffusion rates of substrates (Kratsch and Wise, 2000). This in turn will affect photosynthesis performance including carbon fixation, stomatal conductance, electron transport, and the functional roles of PSI and PSII (Allen and Ort, 2001; Sun et al., 2008; Liu et al., 2012; Zhang et al., 2014). Consequently, this has resulted in the generation of reactive oxygen species (ROS; Ahmad et al., 2010, 2019; Kohli et al., 2019) and instantly caused damage for membranes, resulting in an interruption in transport processes across membranes and membrane-bound enzyme activity (Ahmad et al., 2010, 2019; Zhang et al., 2014, 2015; Kohli et al., 2019). Moreover, chilling causes ultrastructural injures particularly for the chloroplasts, which we are considering the most severely impacted organelles. The symptoms observed are swelling and disorganization of the chloroplast and dilation of thylakoids thus leading to a subsequent increase in plastoglobule numbers (Musser et al., 1984; Zbierzak et al., 2013; Karim et al., 2014). Various symptoms of chilling stress include grana disorganization, changes in thylakoid and chloroplast membrane followed by accumulation of lipid droplets, and darkening of the stroma (Musser et al., 1984; Kratsch and Wise, 2000; Zbierzak et al., 2013; Karim et al., 2014). However, plants resistant to chilling stress exhibit a reduction in the size and number of starch grains (Kratsch and Wise, 2000; Zhuang et al., 2019), and more condensed grana disks are present (Garstka et al., 2007). Structural and physiological changes are closely related to the accumulation of ROS in the chloroplast, which is considered the main site for generating ROS under unfavorable stress conditions thereby damaging the photosynthetic apparatus (Partelli et al., 2011; Kim, 2020). These injuries are proportional to the length of time spent at the damaging temperature and the physiological age of the plant.

Various priming molecules have been suggested to induce chilling stress tolerance in plants (Malekzadeh et al., 2014; Han et al., 2016; Zhao et al., 2016). γ-aminobutyric acid (GABA), is an important non-proteinogenic amino acid present in very low levels in plant tissue and involved in some physio-biochemical functions related to plant growth and development (Sita and Kumar, 2020). It can be rapidly accumulated in plant tissue as a response to several biotic and abiotic stresses (Roberts, 2007). Exogenous application of GABA plays a substantial role in the alleviation of a wide array of abiotic stresses such as drought (Abd El-Gawad et al., 2020), salinity (Wu et al., 2020), chilling (Malekzadeh et al., 2014; Wang et al., 2014), heavy metals (Seifikalhor et al., 2020), low light, and nitrogen starvation (Kinnersley and Lin, 2000). These effects can be explained *via* regulating osmotic pressure, pH scale, H^+ in cytosol, C and N metabolism, and scavenging free radicals (Gilliham and Tyerman, 2016). Consequently, exogenous applied-GABA can enable plants to enhance their photosynthetic capacity by affecting the level of ROS by altering the activities of antioxidant enzymes and maintaining the membrane integrity (Aghdam et al., 2015).

Although several studies have confirmed that GABA can alleviate chilling injuries in tomato plants, all have focused on the seedling stage (Aghdam et al., 2012; Malekzadeh et al., 2014). To date, insufficient information exists on the role of GABA in alleviating chilling injuries during the reproductive and fruit set stages. In this study, we provided evidence of the implication of GABA in mitigation of the chilling-induced damages in tomato plants through the protection of the chloroplast ultrastructure, altering several primary and secondary metabolism pathways and reducing the oxidative damage during reproductive and fruit set stage. These findings could be further elucidating the mechanism of GABA in plant tolerance to chilling stress.

MATERIALS AND METHODS

Experimental Design and Growth Conditions

Tomato seeds (*Solanum lycopersicum* L. cv. Super Marmande) were sterilized for 4 min with 0.7% (w/v) NaOCl and washed with distilled water several times. Seeds were germinated in trays with 50 individual cells (4 × 4 × 6 cm) containing peat and vermiculite (3/1 v/v) at temperature (25/18°C) and a 16/8 h light/dark cycle. About 4-week-old tomato seedlings at the four-leaf stage homogenized in shape and size were grown into 15-L plastic pots filled with sterilized sandy-loamy soil (2:1 w/w) during the period from 10th November 2019 to 4th March 2020 in a

greenhouse at the Department of Plant Pathology, Faculty of Agriculture, Ain Shams University, Cairo, Egypt. Average air temperature and relative humidity (**Table 1**) of the greenhouse were recorded by digital Thermo/hygrometer Art placed in the middle of the greenhouse (No.30.5000/30.5002, TFA, Germany). All pots were irrigated with half-strength Hoagland's solution 2–3 times a week according to the growth stage of the plants. When the first floral bud started emerging, the plants were divided into three groups; each plant in the first group was sprayed three times with 15 ml distilled water plus 0.05% Tween-20, (V/V) as a non-ionic surfactant (one time every 3 days). Whereas, each plant in the second and third group was sprayed every time with 15 ml of 1 and 2 mM γ-aminobutyric acid, GABA (Sigma-Aldrich, Munich, Germany) plus 0.05% Tween-20 (V/V) respectively. The first group was divided into the Control subgroup (normal conditions), and the chilling subgroup (exposed to 5°C for 6 h/day for 5 successive days). The second and third groups were divided into GABA subgroup under normal conditions, and GABA subgroup with chilling stress. Subsequently, all subgroups of chilling stressed plants were transferred to the normal conditions for 2 days of recovery. Then, the leaves were collected and stored at −80°C for further physiological and biochemical examination. The experimental layout was a complete randomized Design (CRD) with three replicates. Each replicate contained 30 individual plants (five plants × six treatments). Six plants from each treatment (two plants/replicate) were left to the end of the season to evaluate the eventual fruit yield. The timeline infographic for the treatments and samples' collection was shown in **Figure 1**.

Determination of Leaf Pigments

Chlorophyll a, b, and total chlorophyll were determined as described by Costache et al. (2012) with some modification, small pieces of fresh leaves (0.5 g) were submerged into 10 ml pure acetone for 24 h/4°C. The absorbance was measured at 645 and 663 nm, respectively. The concentration was calculated using the following equations:

$$\text{Chlorophyll a}\left(\text{mg / g FW}\right) = 11.75\,A662 - 2.350\,A645 \times \left(V / 1000 \times W\right).$$

$$\text{Chlorophyll b}\left(\text{mg / g FW}\right) = 18.61\,A645 - 3.960\,A662 \times \left(V / 1000 \times W\right).$$

Where A is the absorbance at 645 and 663 nm, V is the Final volume of chlorophyll extract in pure acetone and W is the fresh weight of tissue extract. Total chlorophyll was calculated as the sum of chlorophyll a + b.

TABLE 1 | Summary of the monthly mean climate condition, maximum (T_{max}) and minimum (T_{min}), mean (T_{ave}) daily temperatures and relative humidity (RH), inside the greenhouse.

Month	T_{max}	T_{min}	T_{ave}	RH (%)
November	32.15	19.32	25.74	72.25
December	27.55	15.30	21.43	76.31
January	24.95	14.50	19.74	79.84
February	29.73	15.63	22.68	74.14
March	30.11	18.54	24.33	75.77

Carotenoids were quantified using the acetone and petroleum ether method as described by De Carvalho et al. (2012) using the following formula:

$$\text{Carotenoids}\left(\text{mg / g FW}\right) = A_{450}\ \text{x}\ V\left(\text{ml}\right)\text{x}\,10 / \left[A^{1\%}{}_{1\text{cm}}\ \text{x}\ W\left(\text{g}\right)\right].$$

Where A_{450} = Absorbance at 450 nm, V = Total extract volume; W = sample weight; $A^{1\%}{}_{1\text{cm}} = 2{,}592$ (β-carotene coefficient in petroleum ether). Anthocyanin was determined according to Harvaux and Kloppstech (2001). A fresh weight (0.4 g) was ground into 10 ml acidified methanol (99 MeOH: 1 HCl; v/v). The samples were centrifuged (4,000 rpm/10 min), then the absorption was recorded on a spectrophotometer at 530 nm, the concentration of anthocyanin was expressed as Δ O.D/100 mg FW.

The specific wavelengths for all estimated leaf pigments were determined using UV–visible spectrophotometer (UV-1601PC; Shimadzu, Tokyo, Japan).

Determination of Reducing/Non-reducing and Total Soluble Sugars

Total soluble sugars were estimated using the colorimetric method of anthrone and sulfuric acid (Yemm and Willis, 1954), whereas, the reducing sugars were determined using the method of 3, 5-Dinitrosalicylic acid (DNS) as described by Miller (1959). Non-reducing sugar content was estimated using the difference between the total soluble sugar content and the reducing sugars.

Determination of Leaf Oxidative Damage

Hydrogen peroxide was quantified by the colorimetric method of potassium iodide as described by Velikova et al. (2000). A fresh weight (0.5 g) of leaf tissues was homogenized in 3 ml of 1% (w/v) tri-chloroacetic acid (TCA). The homogenate was centrifuged at 10,000 rpm at 4°C for 15 min. Subsequently, 0.75 ml of the supernatant was added to 0.75 ml of 10 mM K-phosphate buffer (pH 7.0) and 1.5 ml of 1 M KI. The mixture was measured at 390 nm using a spectrophotometer (UV-1601PC; Shimadzu, Tokyo, Japan) and the concentration was calculated according to a previously prepared standard curve.

Lipid peroxidation as malondialdehyde (MDA) was determined using thiobarbituric acid (TBA) as described by Heath and Packer (1968) with some minor modifications. A fresh weight of leaves (0.2 g) was homogenized with 0.1% trichloroacetic acid homogenates (TCA; m/v) and 5% PVP (m/v). The homogenate was centrifuged at 5000 rpm for 15 min. Around 3 ml of the supernatant were added to the reaction medium consisting of 0.5% (m/v) thiobarbituric acid (TBA) and 10% (w/v) TCA. The mixture was heated in boiling water for 30 min then cooled rapidly in ice. The absorbance of reddish color was measured at 535 and 600 nm using a spectrophotometer (UV-1601PC; Shimadzu, Tokyo, Japan). The concentration of the MDA/TBA complex was calculated using the following equation:

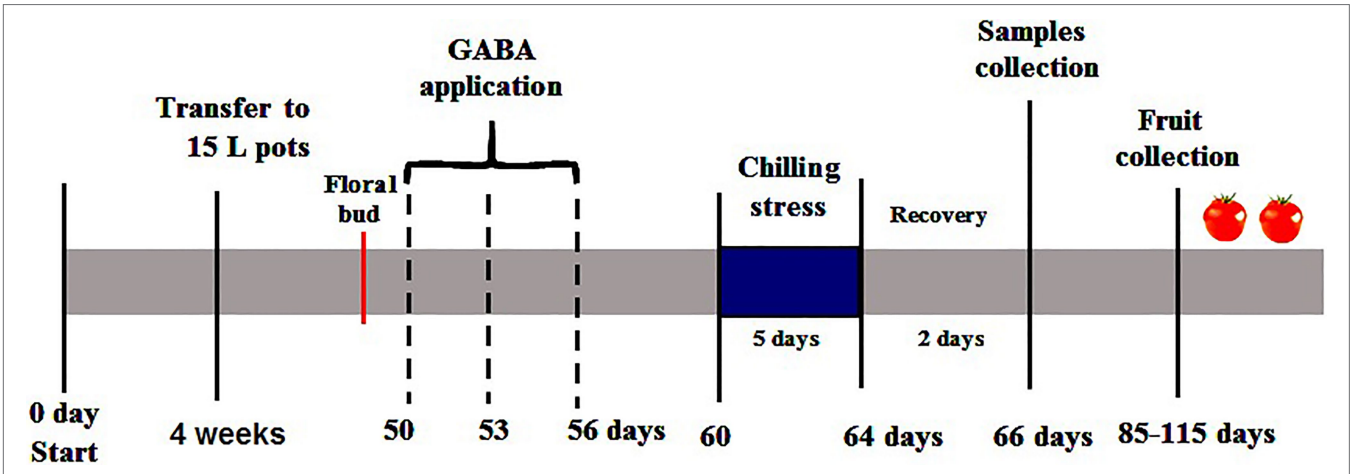

FIGURE 1 | The timeline infographic for the treatments of GABA as a foliar application and the samples' collection of tomato plants subjected chilling stress in the reproductive stage.

$$\mathrm{MDA}\left(\mathrm{nmol}\cdot\mathrm{g}^{-1}\,\mathrm{FW}\right)=\left(\mathrm{A535}-\mathrm{A600}\right)/\varepsilon.$$

Where ε is the extinction coefficient = 155 mM^{-1} cm^{-1}.

Electrolyte leakage was measured as a percentage between readings of EC meter (DOH-SD1, TC-OMEGA, United States/Canada) before and after killing leaf tissues by autoclave at 120°C for 20 min as described by Singh et al. (2008) with some minor modifications. Eight leaf discs (2 cm diameter) were taken by a cork borer, cleaned well and incubated in 10 ml deionized water for 24 h on a shaker. The EC of the solution was measured twice, the first one immediately after the incubation period and the second after killing the leaf tissue by autoclave.

Determination of Root Thermotolerance

After sampling, roots were collected and washed with tap water several times. The root tissues were cut into small pieces and incubated in darkness for 24 h/37°C with a solution containing 0.6% 2,3,5 triphenyltetrazolium chloride (TTC). The red color of formazan was extracted in 95% ethanol and the absorbance was observed on a spectrophotometer (UV-1601PC; Shimadzu, Tokyo, Japan) at 490 nm (Xu and Huang, 2008).

Total Soluble Protein and Enzyme Assays

To prepare the extraction of enzyme and soluble proteins, fresh leaves (0.5 g) were homogenized in 4 ml 0.1 M sodium phosphate buffer (pH 7.0) containing 1% (w:v) polyvinylpyrrolidone (PVP) and 0.1 mM EDTA, centrifuged at 10,000 × g for 20 min at 4°C and then the supernatant was used for assays. Soluble proteins were evaluated by the method of Bradford (1976). All studied enzyme activities and protein concentration in the crude enzyme extract were measured using a spectrophotometer (UV-1601PC; Shimadzu, Tokyo, Japan) as follows:

Superoxide dismutase (SOD) assay was based on the method described by Beyer and Fridovich (1987). The reaction mixture with a total volume of 3 ml contained 100 µl crude enzyme, 50 mM phosphate buffer (pH 7.8), 75 µM NBT, 13 mM L-methionine, 0.1 mM EDTA, and 0.5 mM riboflavin. The reaction was initiated by the addition of riboflavin then the reaction mixture was illuminated for 20 min with a 20 W fluorescent lamp. One unit of enzyme activity was defined as the amount of enzyme required to result in a 50% inhibition in the rate of nitro blue tetrazolium (NBT) reduction at 560 nm.

Catalase (CAT) activity was measured by monitoring the decrease in absorbance at 240 nm as described by Cakmak et al. (1993). The reaction mixture with a total volume of 3 ml contained 15 mM H_2O_2 in 50 mM phosphate buffer (pH = 7). The reaction was initiated by adding 50 µl crude enzyme. The activity was calculated from the extinction coefficient (ε = 40 mM^{-1} cm^{-1}) for H_2O_2. One unit of enzyme activity was defined as the decomposition of 1 µmol of H_2O_2 per minute.

The activity of ascorbate peroxidase (APX) was determined according to Nakano and Asada (1981). The decrease of absorbance at 290 nm was monitored for 3 min. The reaction mixture with a total volume of 3 ml included 100 µl crude enzyme, 50 mM phosphate buffer (pH 7), 0.1 mM EDTA, 0.5 mM ascorbic acid, and 0.1 mM H_2O_2. The reaction was initiated by the addition of H_2O_2. One unit of enzyme activity was defined as the amount of enzyme required for oxidation of 1 µmol of ascorbate per minute. The rate of ascorbate oxidation was calculated using the extinction coefficient (ε = 2.8 mm^{-1} cm^{-1}).

Polyphenol oxidase (PPO) activity was determined according to Oktay et al. (1995). The reaction mixture consisted of 100 µl crude enzyme, 600 µl catechol, and 2.3 ml phosphate buffer (0.1 M, pH 6.5). The absorbance at 420 nm was recorded at zero time and after 1 min using a spectrophotometer.

Peroxidase (POX) activity was quantified by the method of Dias and Costa (1983) with some minor modifications. The assay mixture (100 ml) contained 10 ml of 1% (v/v) guaiacol, 10 ml of 0.3% H_2O_2 and 80 ml of 50 mM phosphate buffer (pH = 6.6). The volume of 100 µl of the crude enzyme was added to 2.9 ml of the assay mixture to start the reaction. The absorbance was recorded every 30 s for 3 min at 470 nm.

The activity of phenylalanine ammonia-lyase (PAL) was determined as Trans-cinnamic acid as described by Lister et al. (1996). The PAL assay reaction consisted of 100 µl crude extract and 900 µl of 6 µmol phenylalanine in 500 mM tris-HCl buffer (pH 8.5). The mixture was incubated at 37°C for 1 h and measured spectrophotometrically at 290 nm. Trans-cinnamic acid was used as standard.

Sample Preparation and Observation by Transmission Electron Microscopy

Small leaf pieces (~3 mm × 1.5 mm) were cut and fixed in 3% glutaraldehyde rinsed in 0.1 m phosphate buffer (pH = 7.6) for 6 h. at 4°C and post-fixed in 1% potassium permanganate solution for 5 min at room temperature. The samples were dehydrated in an ethanol series ranging from 10 to 90% for 15 min in each alcohol dilution and finally with absolute ethanol for 30 min. Samples were infiltrated with EPON 812 epoxy resin (Sigma-Aldrich) and acetone through a graded series till finally in pure resin. For light microscopy, semi-thin leaf-cross sections were stained with toluidine blue and observed using LEICA light microscope model DM-500. Ultrathin sections were collected on copper grids. Sections were then double-stained in uranyl acetate followed by lead citrate. Stained sections were observed with a JEOL – JEM 1010 transmission electron microscope at 70 kV at The Regional Center for Mycology and Biotechnology (RCMB), Al-Azhar University (Frankl et al., 2015).

Statistics

One way ANOVA procedure was followed using SAS (1988) software. Means ± SE were calculated from three replicates and the Duncan multiple range test ($p \leq 0.05$) was used to determine significant differences between means. Linear regression between some variables was also performed.

RESULTS

Changes in Leaf Pigment Composition

Chilling-stress in tomato plants resulted in a significant ($p \leq 0.05$) decrease in chl a (19%) content in comparison with control plants while chl b exhibited marginal decrease (10.3%) during chilling stress (**Figures 2A,B**). Interestingly, exogenous GABA (1

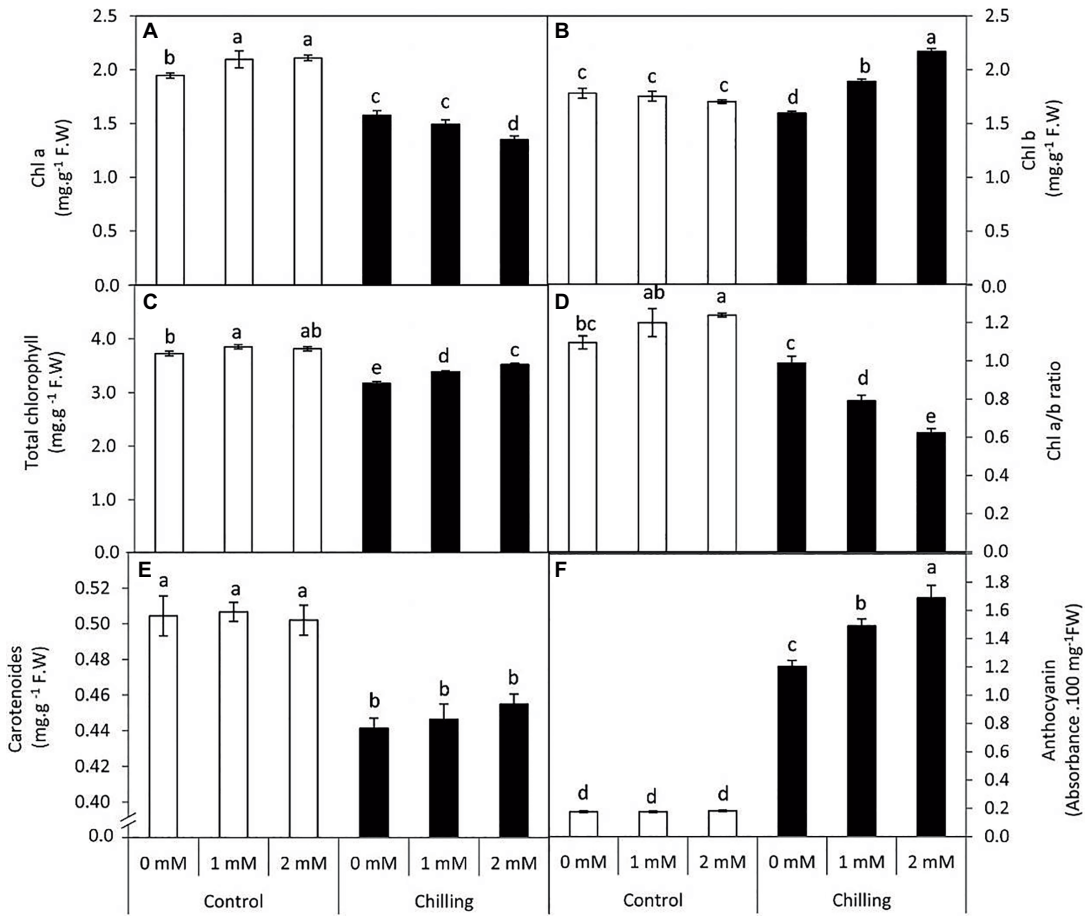

FIGURE 2 | Effect of γ-aminobutyric acid (GABA) as a foliar application at 1 and 2 mM on leaf pigments concentration of tomato plants cv "Super marmende" growing under normal (25°C/20°C day/night) and chilling conditions (5 days/4ºC for 6 h/day) followed by 2 days recovery. **(A)**, chlorophyll a; **(B)**, chlorophyll b; **(C)**, total chlorophyll; **(D)**, chlorophyll a/b ratio; **(E)**, carotenoids, and **(F)**, anthocyanin. Data followed by the same letters ± SE are not significant according to Duncan multiple rang test at $P \leq 0.05$. The white columns refer to the control conditions and the black columns refer to the chilling stress.

and 2 mM) application exerted contrasting effects on chla and chl b content during chilling stress. During Chilling stress chl a content underwent an obvious decrease in the presence of GABA treatments (23.3 and 30.7%) respectively. This decrease was accompanied by a steady increase in chl b (6.2 and 21.9%) content either in the presence of 1 or 2 mM GABA, respectively. However, GABA application to non-stressed plants exhibited a marginal increase in chl a content, while changes were insignificant ($p \leq 0.05$) in chl b content. Thus, GABA applications (1 and 2 mM) during chilling stress resulted in a distinct and significant ($p \leq 0.05$) decrease in chl a/b ratio (27.8 and 43.2% lower than the control) followed by a marginal increase in total chl content (**Figures 2C,D**). Contrastingly, chilling stress induced a significant ($p \leq 0.05$) decrease in the carotenoid content, which was observed to exhibit negligible effects upon GABA treatment (**Figure 2E**). Anthocyanin content exhibited a significant ($p \leq 0.05$) increase in the presence of chilling stress which all the more increases were observed in the presence of GABA (2 mM; **Figure 2F**). Generally, under chilling stress, anthocyanin was the most affected pigment by the treatment of 2 mM GABA (9.6-fold over the unstressed control plants) while this increase amounted to just 6.8 folds in the GABA untreated and chilling stressed plants.

Changes in Leaf Sugar Metabolism

In the present work, chilling stress resulted in a significant ($p \leq 0.05$) increase in reducing, non-reducing, and total soluble sugars (**Figures 3A–C**). Although exogenous GABA application marginally increased the levels of all three types of sugars, 2 mM GABA exerted significant ($p \leq 0.05$) positive effects on the non-reducing sugar content with an average increase of 71.7%. In general exogenous GABA (1 and 2 mM) had a positive effect on the accumulation of sugars in tomato leaves both in the absence and presence of chilling stress.

Changes in Chilling-Induced Oxidative Damage and Root Thermo-Tolerance

Chilling stress in tomato plants resulted in a significant ($p \leq 0.05$) increase in reactive oxygen species (H_2O_2 content), membrane lipid peroxidation (MDA content), and electrolytic leakage, while a significant decrease in root thermo-tolerance was observed (**Figures 4A–D**). The accumulation of H_2O_2, MDA reached 5.4, 3.8–fold, respectively over the unstressed control plants. However, GABA application (1 and 2 mM) during chilling stress resulted in a steady decrease in the extent of H_2O_2, lipid peroxidation (MDA) and electrolytic leakage, respectively. However, control plants subjected to GABA treatment did not exhibit any significant changes in these parameters. In contrast, root thermo-tolerance exhibited a marginal increase upon GABA application under chilling stress.

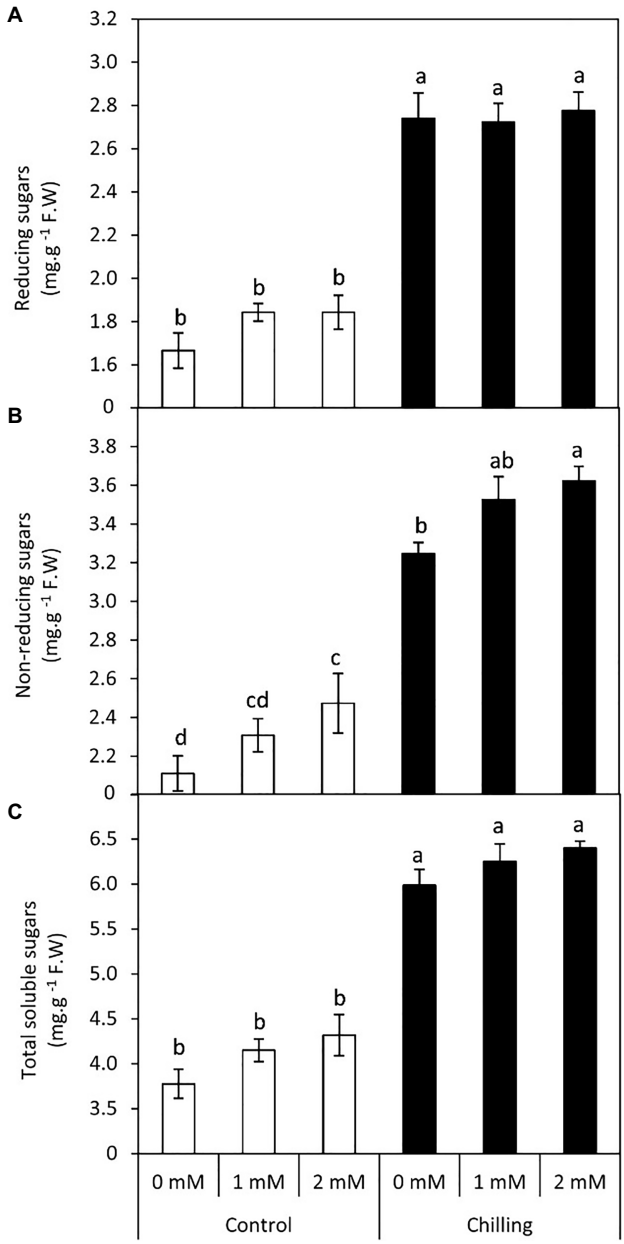

FIGURE 3 | Effect of γ-aminobutyric acid (GABA) as a foliar application at 1 and 2 mM on carbohydrate concentration of tomato plants cv "Super marmende" growing under normal (25°C/20°C day/night) and chilling conditions (5 days/4°C for 6 h/day) followed by 2 days recovery. **(A)**, reducing sugars; **(B)**, non-reducing sugars and **(C)**, total soluble sugars. Data followed by the same letters ± SE are not significant according to Duncan multiple rang test at $P \leq 0.05$. The white columns refer to the control conditions and the black columns refer to the chilling stress.

Changes in the Antioxidant and Phenolic Related Enzymes

Superoxide dismutase and CAT activity were increased in the presence of chilling stress wherein catalase activity was elevated to almost 1.5-fold in comparison with control (**Figures 5A,B**). Under chilling stress, the exogenous GABA treatments, particularly 2 mM, enhanced SOD and CAT activities, with increases of 97.7 and 140%, respectively. PPO activity was also analyzed during chilling stress and GABA application in tomato leaves (**Figure 5C**). Chilling stress significantly resulted in a decrease in PPO activity in comparison with control. PPO activity did not exhibit any significant changes in the presence of GABA application during chilling stress. Peroxidase activity

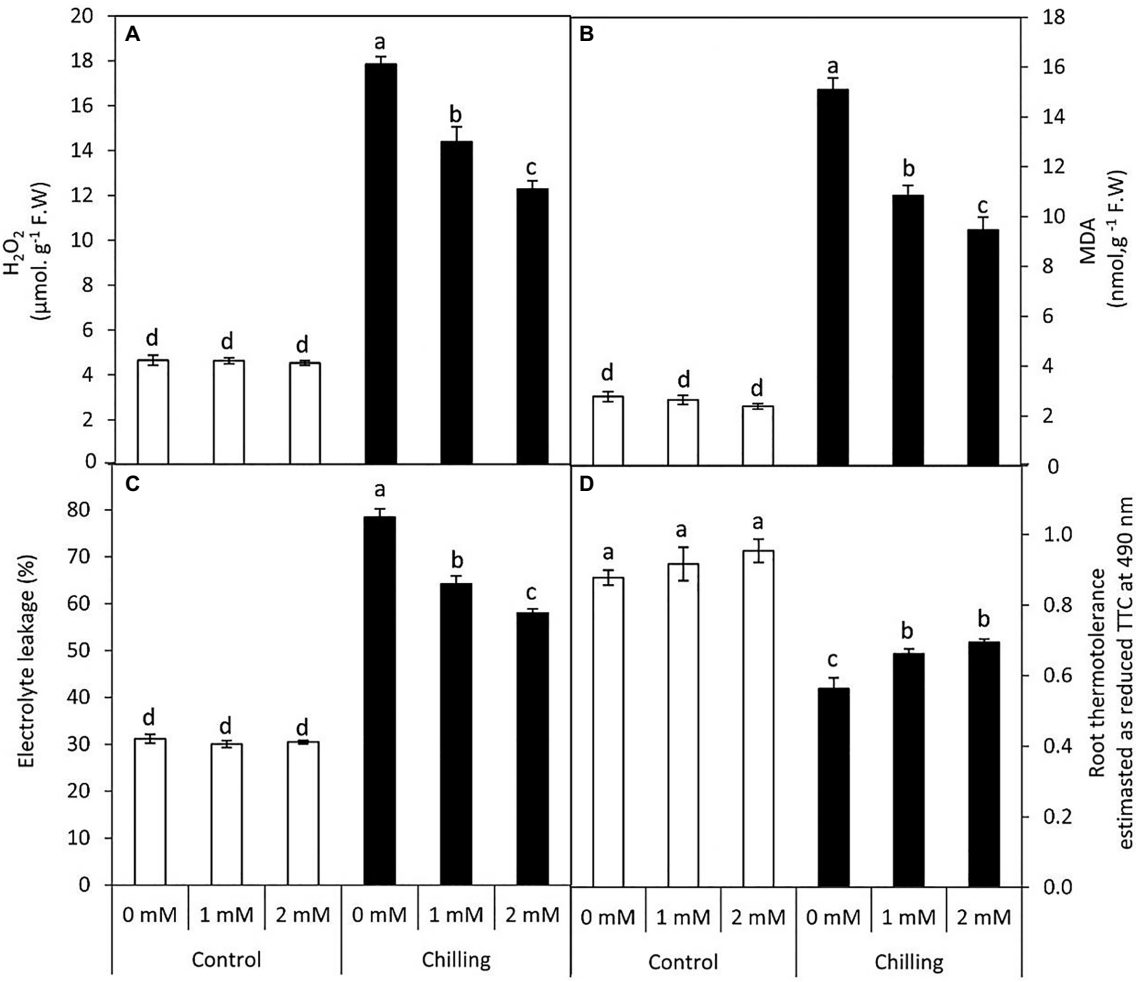

FIGURE 4 | Effect of γ-aminobutyric acid (GABA) as a foliar application at 1 and 2 mM on leaf oxidative damage and root tissues thermotolerance of tomato plants cv "Super marmende" growing under normal (25°C/20°C day/night) and chilling conditions (5 days/4°C for 6 h/day) followed by 2 days recovery. **(A)**, hydrogen peroxide (H_2O_2); **(B)**, malondialdehyde (MDA); **(C)**, electrolyte leakage, and **(D)**, root thermotolerance as reduced TTC. Data followed by the same letters ± SE are not significant according to Duncan multiple rang test $P \leq 0.05$. The white columns refer to the control conditions and the black columns refer to the chilling stress.

(POD) was negatively upregulated in the presence of chilling stress and GABA application, respectively (**Figure 5D**). However, APX activity showed a gradual increase by the average of 35.2, 43.2, and 51%, respectively in the presence of chilling stress and GABA treatments (**Figure 5E**). PAL activity showed a noticeable increase in the presence of chilling stress (**Figure 5F**). Exogenous GABA positively upregulated PAL activity both in the absence and presence of chilling stress.

Relationship Between the Form of Soluble Carbohydrates and Secondary Metabolism

To further illuminate the relationships between the accumulation of soluble sugars and the secondary metabolism of GABA-treated and untreated tomato plants under chilling stress, linear regression analysis was performed (**Figure 6**). It can be observed that PAL and anthocyanin were positively and significantly correlated with the accumulation of reducing sugars, non-reducing sugars, and total soluble sugars in leaves. Precisely, PAL was more correlated with the non-reducing sugars ($R^2 = 0.9767$, $p = 0.0002$) than reducing and total soluble sugars, while anthocyanin exhibited a highly significant correlation with non-reducing sugars ($R^2 = 0.969$, $p = 0.0004$) and total soluble sugars ($R^2 = 0.9686$, $p = 0.0004$) compared to the reducing sugars. These results specifically imply that in the flowering stage, GABA-pretreatment may induce its protective effect against chilling stress in tomato plants through a close linkage between the transformation of soluble carbohydrates to non-reducing form (the major transport form) and the simultaneous upregulation of flavonoid pathway (secondary metabolism).

Relationship Between the Form of Soluble Carbohydrates and Antioxidant Enzymes

Several previous studies have reported that soluble carbohydrates can play an important role in reducing cold-induced oxidative damage in plants. To gain further insights into the effect of

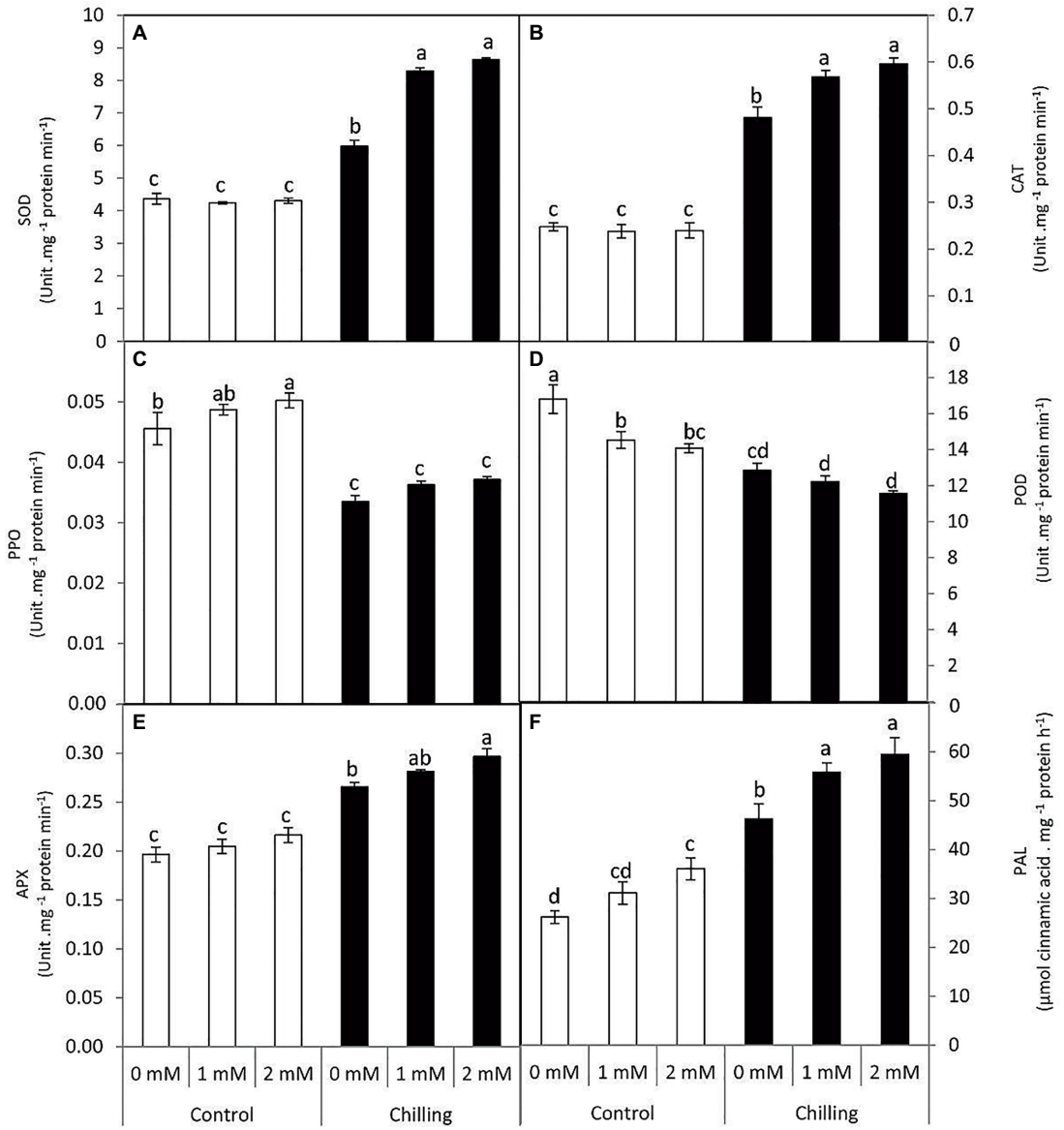

FIGURE 5 | Effect of γ-aminobutyric acid (GABA) as a foliar application at 1 and 2 mM on antioxidant and phenolic-related enzymes of tomato plants cv "Super marmende" growing under normal (25°C/20°C day/night) and chilling conditions (5 days/4ºC for 6 h/day) followed by 2 days recovery. **(A)**, superoxide dismutase (SOD); **(B)**, catalase (CAT); **(C)**, polyphenol oxidase (PPO); **(D)**, peroxidase (POD); **(E)**, ascorbate peroxidase (APX), and **(F)**, phenylalanine ammonia lyase (PAL). Data followed by the same letters ± SE are not significant according to Duncan multiple rang test at $P \leq 0.05$. The white columns refer to the control conditions and the black columns refer to the chilling stress.

applied-GABA on chilling-stressed tomato plants during the reproductive stage, we analyzed the relationships between the accumulation of different forms of soluble sugars (Reducing, non-reducing, and total soluble sugars) and the activities of antioxidant enzymes in leaves (**Figure 7**). The results indicated that PPO and POD negatively and significantly correlated with different forms of soluble sugars which mean PPO and POD did not contribute to control the level of ROS in the cold leaf stressed tissues of tomato plants, while positive and significant correlations were observed with APX, CAT, and SOD in this respect. More precisely, POD ($R^2 = 0.8772$, $p = 0.0059$), CAT ($R^2 = 0.9632$, $p = 0.0005$), and SOD ($R^2 = 0.8945$, $p = 0.0043$) were highly correlated with non-reducing sugars than the reducing ones; Whereas, APX was strongly correlated with both reducing and non-reducing sugars at the same level of significance ($p \leq 0.001$). On the other hand, PPO exhibited an obvious negative correlation with total sugars ($R^2 = 0.8611$, $p = 0.0060$) more than any individual type of sugars.

Changes in the Fruit Yield

Plants exposed to chilling stress demonstrated a significant decrease in fruit yield compared to the unstressed plants by an average of 64.3% (**Figure 8**). Plants treated by GABA especially at 2 mM achieved the highest significant increases

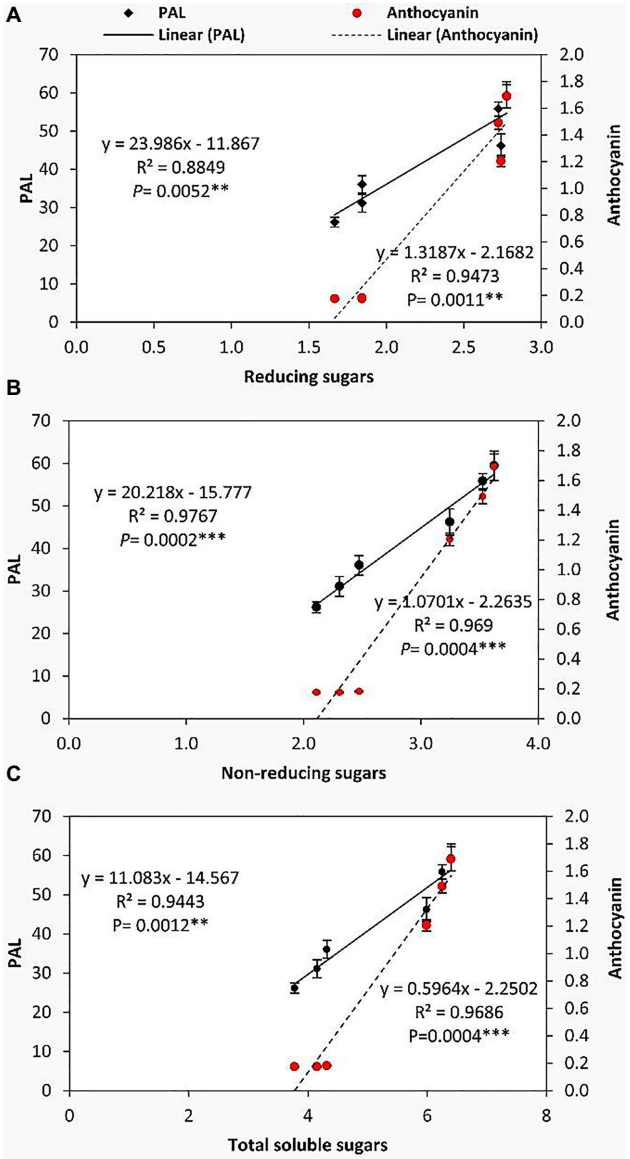

FIGURE 6 | Linear regression analysis elucidates the relationship between the soluble sugars, PAL enzyme activity, and anthocyanin contents in tomato plants cv "Super marmende" treated by γ-aminobutyric acid (GABA) as a foliar application at 1 and 2 mM and growing under normal (25°C/20°C day/night) and chilling conditions (5 days/4ºC for 6 h/day) followed by 2 days recovery. ns. non-significant; $^{*}P \leq 0.05$; $^{**}P \leq 0.01$; and $^{***}P \leq 0.001$.

in the fruit yield in both chilling stress and non-stressed plants. These results indicate the possible role of GABA in fruit set and mitigation of low temperatures in tomato plants.

Exogenous GABA Application Alleviates Chloroplast Damage and Maintains Starch Grain Integrity in Chilling-Stressed Tomato Leaves

Tomato leaves grown under standard conditions at 25°C have a normal green color. Whereas leaves exposed to chilling stress changed color from green to dark red or purple. The red color appeared firstly on the leaf margins and gradually spread throughout the leaf surface, the major and minor veins gaining the blue or purple colors.

Examination of leaf anatomy under control conditions revealed that the leaf consists of the common epidermal layers enclosed in between the mesophyll, which is intervened by some vascular bundles (**Figure 9A**). Mesophyll ultra-structures pointed out that the outer cell membrane was attached well with the cell wall, organelles could be observed clearly; chloroplasts, nucleus, mitochondria as well as the vacuole (**Figure 9B**). The chloroplasts distribute regularly and have an elongated or ellipsoidal shape with distinct normal envelopes. It was characterized by well-developed grana and stromal thylakoids. Sometimes, starch grains appeared with acceptable size (**Figures 9B,C**). During chilling, stress plastids are affected more than other organelles. It aggregated together in clusters and became swollen with a more rounded shape compared to ellipsoidal recorded in control plants (**Figures 10A,B**). The chloroplast envelope was disintegrated or completely disappeared. The starch grains became larger, with a spherical shape; the membranes of granal and stromal thylakoids were indistinct, with a noticeable accumulation of lipid droplets in the dark stroma (**Figure 10C**). Sometimes, the outer cellular membrane ruptured and partially disconnected from the cell wall (**Figures 10D,E**).

Exogenous GABA application reduced chloroplast damage caused by chilling stress by recovery of the plastid shape, starch grains were observed in smaller size and as having an elongated shape, granal lamellae were better integrated than those from chilling stress in untreated plants (**Figures 11A–D**).

DISCUSSION

The present work provides evidence on the beneficial role of GABA treatment (foliar spray) on tomato plants subjected to chilling stress. The tomato plants were subjected to GABA pre-treatment (50–56 days) at the initial stage of the reproductive phase, which was characterized by the emergence of floral bud. The reproductive stage of tomato plants is associated with rapid translocation of organic solute to the emerging floral buds and flowers in the pre and post-pollination phase. Followed by GABA application the tomato plants were subjected to chilling stress for 5 days at an age of 60–64 days. Interestingly, GABA application resulted in modulation of pigment composition, secondary metabolism, sugar accumulation, and antioxidative defense during chilling stress exposure at a later stage. Thus, GABA application appears to be a good priming option for developing tolerance to chilling stress in tomato plants prior to the fruiting stage.

Current findings reveal that exogenous GABA (2 mM) exerts differential effects on chl-a and chl-b content in the presence of chilling stress. Exposure of tomato plants to chilling stress resulted in a decrease in both chl a and chl b content in leaves, while plants pretreated with exogenous GABA exhibited a significant increase in chl b content. Exogenous GABA is an effective priming molecule that is known to protect the

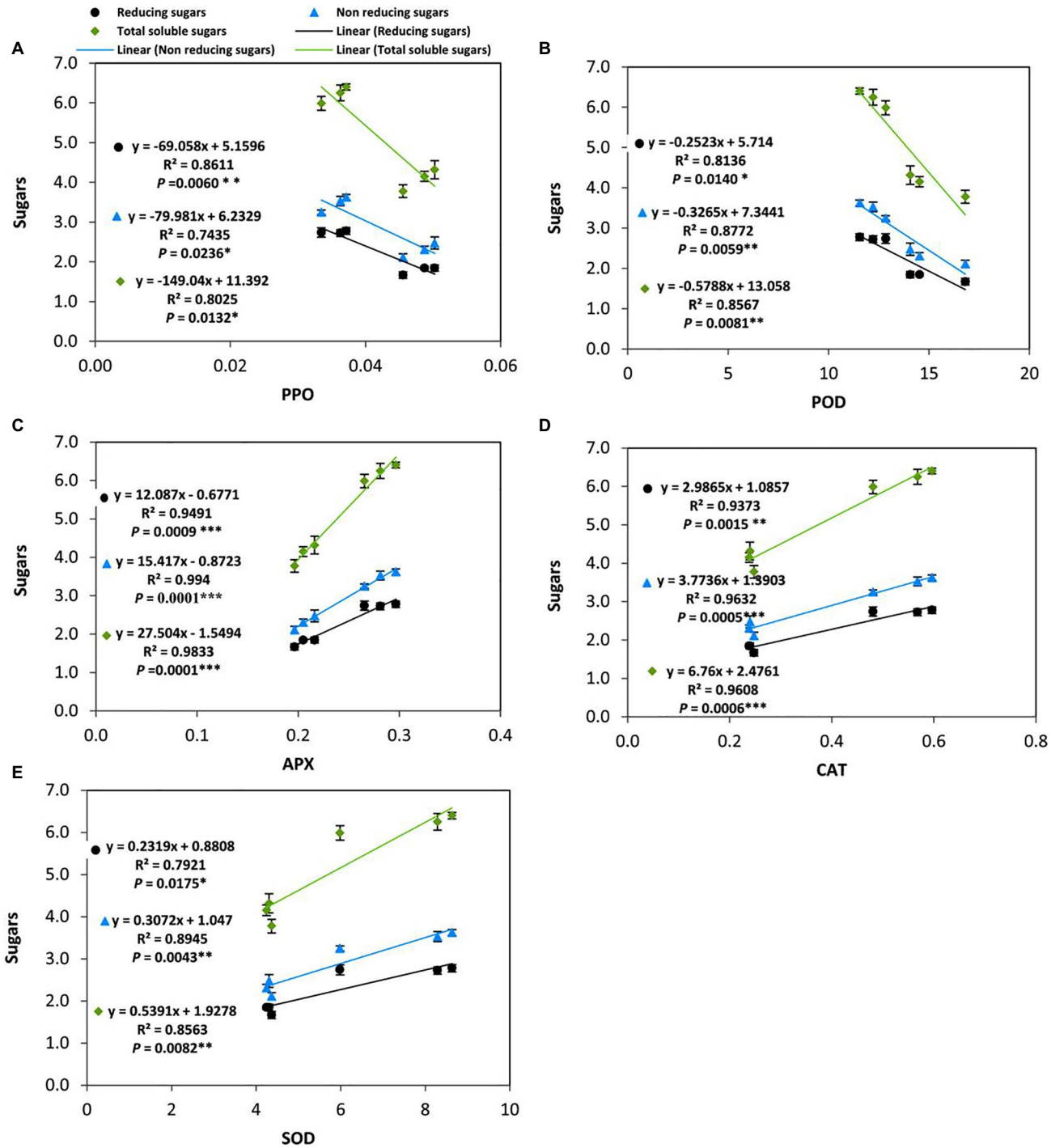

FIGURE 7 | Linear regression analysis elucidates the relationship between the soluble sugars, antioxidant enzyme activities, superoxide dismutase (SOD), catalase (CAT), polyphenol oxidase (PPO), and peroxidase (POD), ascorbate peroxidase (APX) in tomato plants cv "Super marmende" treated by γ-aminobutyric acid (GABA) as a foliar application at 1 and 2 mM and growing under normal (25°C/20°C day/night) and chilling conditions (5 days/4ºC for 6 h/day) followed by 2 days recovery. ns. non-significant; $^{*}P \leq 0.05$; $^{**}P \leq 0.01$; and $^{***}P \leq 0.001$.

structure and function of the PSII center in the chloroplast of musk melon plants subjected to alkalinity and salinity stress (Xiang et al., 2016). Although chl b content did not exhibit significant changes after chilling stress, GABA-induced increase in chl b content is attributed to modulation of photosynthetic capacity achieved by optimum light-harvesting efficiency. PSII functioning and net photosynthesis rate are known to be upregulated in response to GABA application during salinity

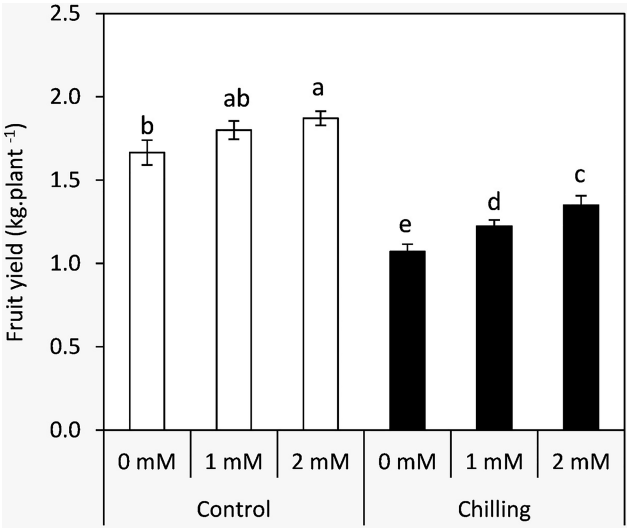

FIGURE 8 | Effect of γ-aminobutyric acid (GABA) as a foliar application at 1 and 2 mM on fruit yield of tomato plants cv "Super marmende" growing under normal (25°C/20°C day/night) and chilling conditions (5 days/4ºC for 6 h/day) followed by 2 days recovery. Data followed by the same letters ± SE are not significant according to Duncan multiple rang test at $P \leq 0.05$. The white columns refer to the control conditions and the black columns refer to the chilling stress.

stress in wheat plants (Li et al., 2016). Thus, GABA-treated tomato plants subjected to chilling stress (present work) are expected to exhibit improved photosynthetic efficiency. Chilling stress significantly increased anthocyanin content in the leaves of tomato plants which was all the more high in GABA-pretreated plants. However, GABA treatment did not exhibit any significant changes to chilling stress-induced reduction in carotenoid content. Anthocyanin accumulation in response to chilling stress and GABA-pretreatment indicate upregulation of flavonoid pathway (secondary metabolism) associated with tolerance to chilling stress. Although carotenoid content exhibits decreases due to chilling stress, a surge in chl b and anthocyanin is attributed to an increase in the light-harvesting efficiency of chilling stressed tomato leaves. A surge in anthocyanin biosynthesis and associated secondary metabolites has been known to be a tolerance mechanism to cold stress (Ahmed et al., 2015; Li et al., 2016; Sicilia et al., 2020). Apart from its role as a free radical scavenger, anthocyanin accumulation in the leaves of chilling stressed tomato plants (present work) is expected to be associated with reduced osmotic potential and delayed freezing of cells *via* surface nucleators (Chalker-Scott, 1999; Nagata et al., 2003).

Interestingly, GABA application appears to be a positive regulator of sugar accumulation (reducing and non-reducing) in the leaves of tomato plants both in the absence and presence of chilling stress. However, non-reducing sugars exhibited a significant increase in GABA-pretreated tomato leaves subjected to chilling stress. GABA-induced increments in non-reducing sugar coincided with changes in the shape of starch grains in the chloroplast of the leaves, as visualized by transmission electron microscopy. Chilling stress (in the absence of GABA) treatment exhibited clustered accumulation of chloroplast which was swollen and round in shape with indistinct thylakoid and filled with large-sized spherical starch grains. It is noteworthy that GABA pretreatment in chilling-stressed tomato leaves normalized the structure of the chloroplast and starch grains mostly appeared to be ellipsoidal in shape. An increase in both non-reducing and reducing sugars in the leaves after exposure to chilling stress depict upregulation of starch biosynthesis and sugar accumulation as osmolytes in cells, respectively. Optimum levels of carbon assimilation are preferably maintained by improved photosynthetic efficiency and increased transport of assimilates. Leaves are important source tissue that exhibit precise regulation of starch-sugar inter-conversion during abiotic stress signals (Thalmann and Santelia, 2017; Thitisaksakul et al., 2017). In the present work, GABA treatment induces a surge in starch accumulation which is likely to function as a reserve for inducing sucrose (osmolyte accumulation) formation in the later stages of flower and fruit development. Chilling stress brings about a significant increase in the reducing and soluble sugar content which, therefore, does not exhibit any significant increase in the presence of GABA treatment. GABA-induced increase in sugar content during abiotic stress depicts its role as an inducer of osmoprotectant (Wang et al., 2017). Osmotic stress results in alteration in the transport of organic assimilate (Yang et al., 2002; Rizhsky et al., 2004; Cramer et al., 2007) between the source and sink organs. In the present work, the leaves were obtained from plants with emerging floral buds. Thus, high levels of TSS after chilling stress indicate prior adaptive mechanisms for optimum transport and nutrient allocation in buds and floral parts. GABA-pretreatment resulted in a marginal increase in TSS. In addition to the function of starch as a storage molecule, it is known to exhibit transient changes during abiotic stress thus indicating its role in the metabolic fitness of plants (Pressel et al., 2006; Cuellar-Ortiz et al., 2008; Yin et al., 2010; Thalmann and Santelia, 2017). Starch degradation during abiotic stress is associated with improved osmotic tolerance attained by higher sugar accumulation. Thus, in the present work higher starch accumulation in GABA-treated chilling-stressed plants indicates signaling events preceding further osmolyte accumulation in leaves (Rezaei-Chiyaneh et al., 2018). Recent investigations from the author's laboratory have also revealed GABA-induced accumulation of soluble sugars in drought-stressed snap bean leaves (Abd El-Gawad et al., 2020). GABA-induced abatement of nitrogen stress in green microalga *Tetraselmis sub cordiformis* has been known to be associated with increased starch accumulation (Ran et al., 2020).

γ-aminobutyric acid-induced alleviation of chilling stress in tomato leaves is evident from reduced lipid peroxidation (MDA content), which is in congruence with decreased electrolytic leakage. The present findings are in line with various earlier investigations which reported GABA-induced osmotic tolerance and reduced lipid peroxidation (Nayyar et al., 2014; Wang et al., 2017; Cheng et al., 2018; Abd El-Gawad et al., 2020). Furthermore, GABA-pretreated tomato plants subjected to chilling stress exhibited a marginal increase in root thermotolerance. Foliar application of GABA, therefore, seems to exert a long-distance signaling effect from foliage to roots

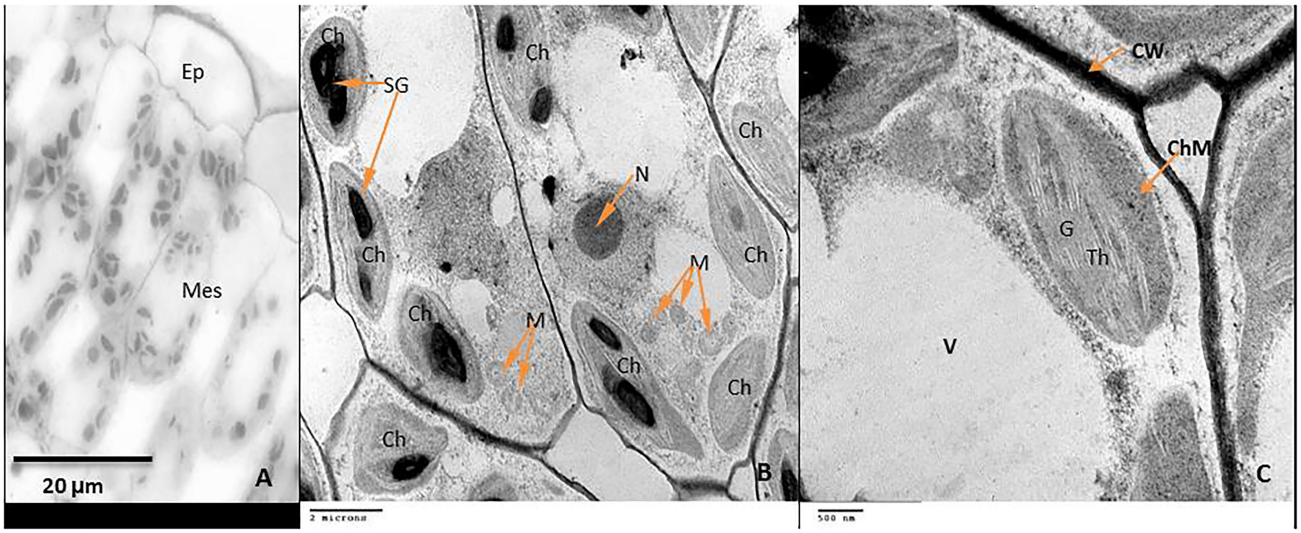

FIGURE 9 | Anatomical structure of Tomato leaf cv "Super marmende" growing under standard condition 25ºC. **(A)**. Part of leaf cross-section showed the upper epidermis (Ep) and the two mesophyll layers (Mes); note the regular arrangement of chloroplasts. **(B)**. TEM micrograph showed mesophyll ultra-structures: Mitochondria (M), nucleus (N), chloroplasts (Ch) with elongate shape, and starch grains (SG). **(C)**. Ultra-structure of one chloroplast showed it has normal envelope or membrane (ChM), well-developed granal lamella (G), and stromal thylakoids (Th), note that the outer cellular membrane was attached well with the cell wall (CW).

by imparting thermotolerance during chilling stress. Chilling stress in tomato plants resulted in a significant increase in hydrogen peroxide content accompanied by increased catalase activity. Although hydrogen peroxide priming has been known to be beneficial for abiotic stress tolerance in plants (Hossain et al., 2015; Arfan et al., 2019) higher levels appear toxic to plant cells. Higher catalase activity in leaves of tomato plants subjected to chilling stress and GABA-pretreatment is also accompanied by upregulation of SOD and APX activity. Redox balance in leaves is crucial to maintain the optimum efficiency of metabolic enzymes and the electron-transport cascade of the photosystem in the chloroplast. Thus, increased chlorophyll b and anthocyanin content (responsible for light harvest efficiency) is associated with elevated antioxidative defense in the leaves of tomato plants subjected to GABA-pretreatment before chilling stress. Present findings are in congruence with earlier reports of GABA-induced elevation of SOD, CAT, and APX activity in chilling stressed-tomato seedlings (Malekzadeh et al., 2014). GABA has been known to function as an important regulator of ROS scavengers in plant systems (Nayyar et al., 2014; Vijayakumari and Puthur, 2016; Carillo, 2018). According to Cheng et al. (2018) GABA-induced antioxidative defense in white clover is mediated by upregulation of Cu/ZnSOD, MnSOD, FeSOD, GPOX, CAT, APX, MDHAR, GST, and GPX genes. In the present work, GABA-induced elevation in CAT and APX activity is accompanied by reduced POD activity during chilling stress. POD is represented by several isoforms in plant organs with a different k_m value for its substrate (hydrogen peroxide). Our findings reveal a negative correlation between CAT and POD activity during GABA treatment and wherein, hydrogen peroxide detoxification mostly appears to be catalyzed by CAT and APX activity.

Analysis of enzymes associated with phenol metabolism revealed differential regulation of chilling stress on the modulation of PPO and PAL activity. It is noteworthy that although chilling stress decreased the activity of PPO, a significant surge in PAL activity was observed in the leaves. PAL activity was all the more elevated in presence of GABA treatment. PPO is a crucial enzyme localized in the thylakoid lumen and known to be associated with the restoration of photosynthetic functions. Although PPO catalyzes the activity of vacuolar localized monophenols, further investigations are required to decipher its direct role in oxidative stress or the regulation of photosynthetic efficiency. However, higher PPO activity in chloroplasts might be associated with the protection of the electron transport mechanism (Boeckx et al., 2015). In the present work, GABA-induced elevation in antioxidative defense is associated with a reduction in PPO activity. A similar report of GABA-induced downregulation of PPO activity has been reported in chilling stressed mango fruits (Rastegar et al., 2020). Our findings are incongruent with reports of Rastegar et al. (2020), where reduced PPO activity is associated with elevated CAT activity. GABA application and chilling stress positively upregulated PAL activity in tomato leaves thus suggesting the possible involvement of pheynyl-propanoid pathways in chilling tolerance. Thus, in support of earlier evidence of GABA-mediated upregulation of PAL activity in banana and barley (Wang et al., 2014; Ma et al., 2018), present findings indicate events of chilling tolerance to be associated with PAL activity in tomato leaves.

In the present study, linear regression analysis under cold stress and GABA as a foliar application demonstrated a number of close linkages between the soluble carbohydrates (specifically the non-reducing sugars) and secondary metabolisms in respect of the upregulation of PAL activity and biosynthesis of

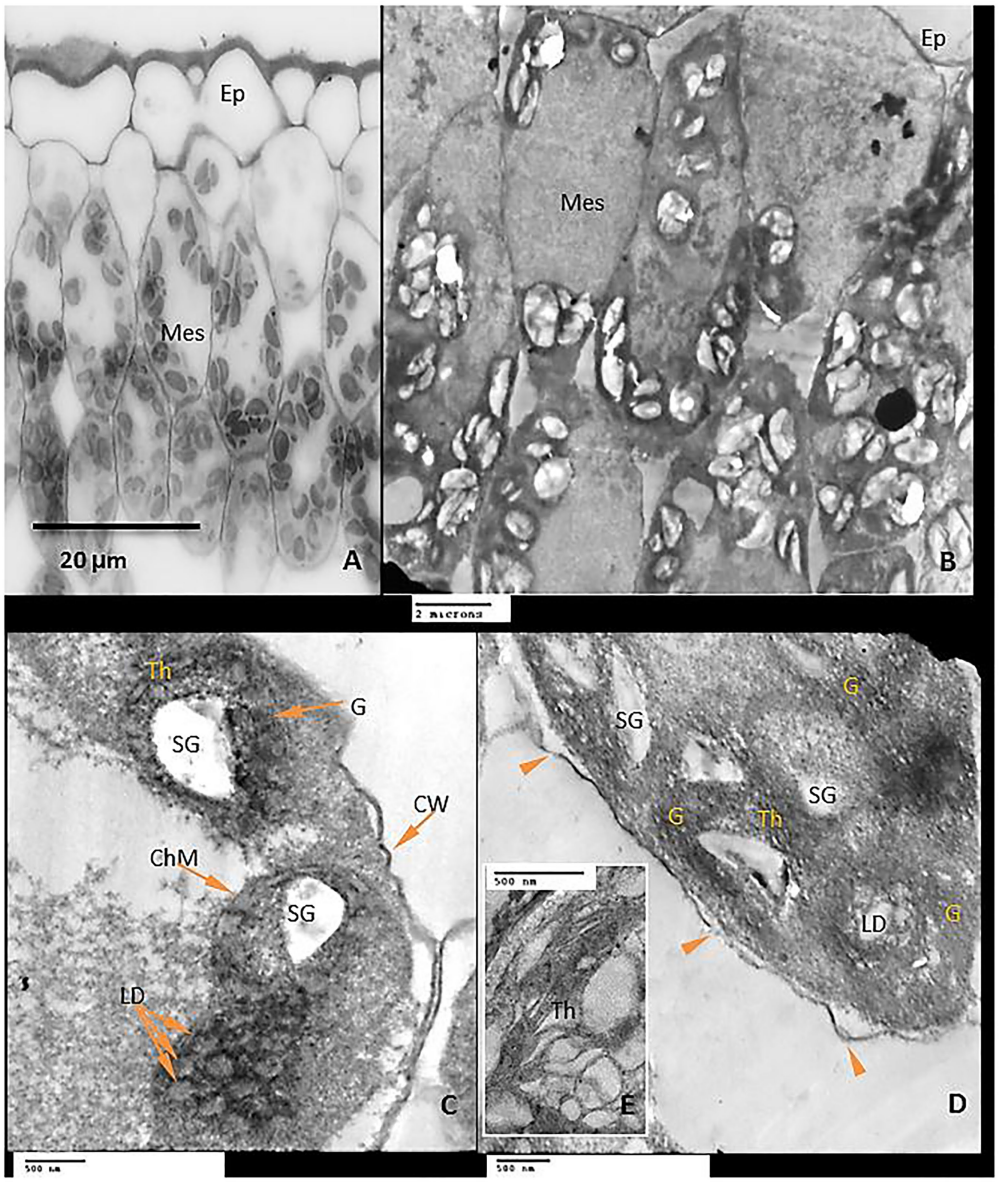

FIGURE 10 | Anatomical structure of Tomato leaf cv "Super marmende" growing under chilling conditions 5 days/4ºC for 6 h/day. **(A)** Leaf cross-section showed the upper epidermis (Ep) and the two mesophyll layers (Mes); note that chloroplasts were accumulated together in clusters. **(B)** TEM micrograph showed mesophyll ultra-structures: Chloroplasts became swollen with more rounded shape. **(C)** High magnification of two chloroplasts showed large starch spherical grains (SG) with accumulation of lipid droplets (LD) in stroma and the membranes of granal (G) and stromal thylakoids (Th) were indistinct. **(D,E)**, note the unstacking of grana and dilation of thylakoids. Arrowheads pointed to disintegration the outer cellular membrane which disconnected partly from the cell wall.

anthocyanin. The primary metabolites of photosynthesis can play a crucial role in the secondary metabolism specifically the biosynthesis of flavonoid-based compounds. This effect can occur through two distinct pathways, including the shikimic acid pathway generating the phenylpropanoids (C6-C3) skeleton, and the acetate pathway that serving as a building block for polymeric 2-carbon units (Croteau et al., 2000). Furthermore, soluble sugars can function as signaling molecules or primary messengers in signal transduction (Yuanyuan et al., 2009), which gives them the ability to regulate cold-induced gene expression (Tabaei-Aghdaei et al., 2003).

Moreover, multiple correlations were detected between the soluble sugars (reducing/non-reducing) and the activity of antioxidant enzymes. Soluble sugars can protect plant cells from chilling stress through interacting with the lipid bilayer of membranes and serving as osmoprotectants (Yuanyuan et al., 2009). Additionally, soluble sugars have been reported to be involved in the balance of ROS and consequently the responses to oxidative damage (Couée et al., 2006). Several metabolic reactions related to the production of ROS in plant cells have been found to be directly correlated with soluble sugars i.e., photosynthesis and mitochondrial respiration. However, soluble sugars have been found to be involved in the

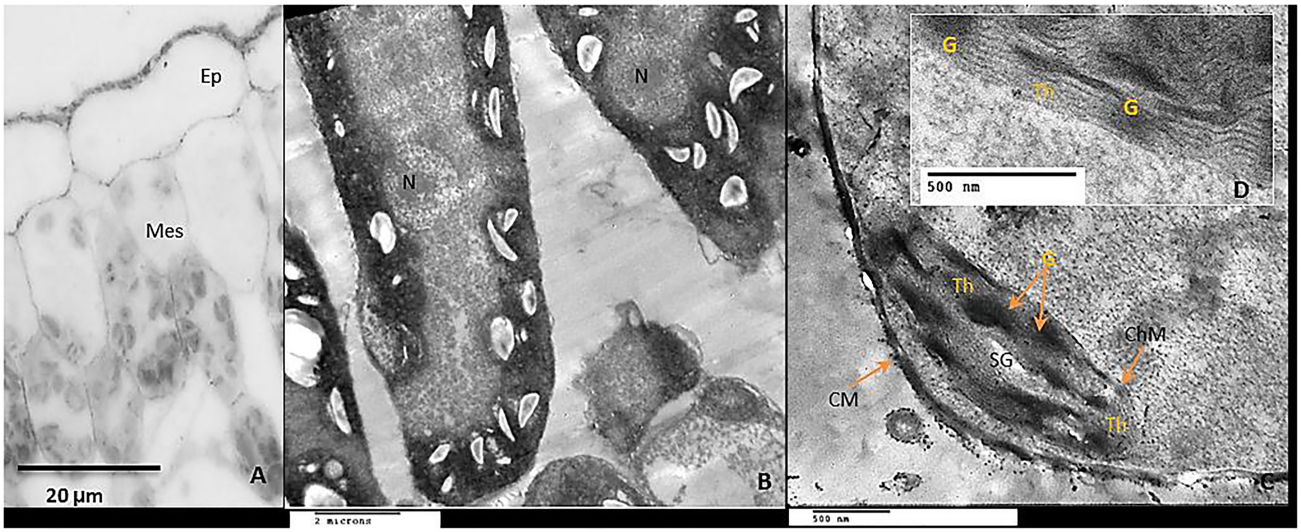

FIGURE 11 | Anatomical structure of Tomato leaf cv "Super marmende"growing under stress chilling conditions 5 days/4ºC for 6 h/day treated with GABA at 2 mM. **(A)** Leaf cross-section showed the upper epidermis (Ep) and the two mesophyll layers (Mes); note that chloroplasts were accumulated together in clusters. **(B)** TEM micrograph showed mesophyll ultra-structures: There are expansions in the size of the plastids due to the large starch grains in them, but with a tendency to elongate shape. **(C,D)** high magnification of one chloroplast showed normal chloroplast membrane (ChM), well-developed grana (G), and stromal thylakoids (Th), the cell wall (CW) was attached well with the outer cellular membrane.

anti-oxidative processes, such as the oxidative pentose-phosphate pathway and carotenoid biosynthesis (Couée et al., 2006). In this study, the author found that POD, CAT, and SOD were highly correlated with non-reducing sugars than the reducing ones. These results may be related to activate sucrose-specific signaling pathways by GABA application.

The structure of mesophyll cells, including the chloroplasts, is the main component for the photosynthesis process and play a crucial role in determining the photosynthetic assimilation capacity (Araki et al., 2012). Under stress conditions, the morphology and ultrastructure of chloroplasts are directly disturbed causing a significant decrease in photosynthetic efficiency, accumulation of dry matter, and loss of crop yield (Weston et al., 2000; Shao et al., 2014). Previous studies confirmed that the chloroplasts in plants subjected to abiotic stress are considered the primary sites for generating ROS (Sun et al., 2002; Gill and Tuteja, 2010). Our results showed that chilling stress affects chloroplast ultrastructure including swollen and abnormal shape, disintegration of the chloroplast envelope or complete disappearance, and dilation of thylakoids. Over time, small lipid droplets accumulated in chloroplast (**Figures 10A–E**). These results were coincided with a reduction in chlorophyll content (**Figures 2A–D**). At the same time, chloroplast ultrastructure might be damaged by chilling stress resulting from accumulation of ROS (**Figures 4A,B,D**). Changes in thylakoid membranes with the slowing in enzymatic reactions caused by chilling stress directly affect chlorophyll content and photosynthetic activities (Liu et al., 2018). However, GABA application measurably reduced chilling injury by protecting thylakoid membranes, chloroplast envelopes, and diminishing swelling (**Figures 11A–D**). This, in turn, improves the photosynthesis process *via* alleviating chlorophyll degradation (**Figures 2A–D**). In addition, chilling injury affects membranes by disintegrating the outer cellular membrane which is disconnected partly from the cell wall (**Figure 10D**). This was synchronized with increasing in H_2O_2, MDA, and electrolyte leakage contents, which are regarded as biochemical markers for the occurrence of ROS under chilling stress (**Figure 4A**). Whereas, exogenous application of GABA kept the stability of membranes *via* reducing the construction of lipid peroxidation products (**Figure 4B**). In addition significant enhancement of the activities of SOD, CAT, APX, and PAL antioxidant enzymes which create a defense system against chilling stress and protect membrane damage (**Figures 5A–F**) was noted.

To sum up, the present work provides a correlation between GABA-induced alleviation of chloroplast damage and the modulation of pigment composition in chilling stressed tomato leaves (**Figure 7**). Furthermore, increased chl b and anthocyanin content is accompanied by elevated starch levels and improved osmotic tolerance evident from reduced MDA content and electrolytic leakage. Further investigations are required to decipher the detailed role of GABA in the modulation of carbohydrate and phenol metabolism in tomato plants subjected to chilling stress.

DATA AVAILABILITY STATEMENT

The raw data supporting the conclusions of this article will be made available by the authors, without undue reservation.

AUTHOR CONTRIBUTIONS

OE, AE, and MI: conceptualization. OE, AE, GN, TW, RF, SM, AA-H, HE-H, AE-Y, HE-G, EA, AG, NN, AE-S, AB, and

MI: methodology, validation, resources, and writing – review and editing. OE, SM, GN, TW, AA-H, EA, AG, NN, AE-S, AB, and MI: software. OE, AE, RF, SM, AA-H, HE-H, NN, AE-S, AB and MI: formal analysis. RF, SM, AA-H, HE-H, AE-Y, HE-G, EA, AG, NN, AE-S, and AB: investigation. OE, AE, GN, TW, RF, SM, and MI: data curation. OE, SM, and MI: writing – original draft preparation. RF, SM, AA-H, HE-H, AE-Y, HE-G, EA, AG, NN, AE-S, AB, and MI: supervision. AE-Y, GN, TW, HE-G, MI, SM, AE-Y, EA, HE-G, AG, RF, and NN: project administration. OE, AE, GN, TW, EA, AG, RF, and MI: funding acquisition. All authors contributed to the article and approved the submitted version.

ACKNOWLEDGMENTS

We thank Taif University Researchers Supporting Project number (TURSP -2020/13), Taif University, Taif, Saudi Arabia.

REFERENCES

Abd El-Gawad, H. G., Mukherjee, S., Farag, R., Elbar, O. H. A., Hikal, M., El-Yazied, A. A., et al. (2020). Exogenous γ-aminobutyric acid (GABA)-induced signaling events and field performance associated with mitigation of drought stress in *Phaseolus vulgaris* L. *Plant Signal. Behav.* 16:1853384. doi: 10.1080/15592324.2020.1853384

Aghdam, M. S., Asghari, M., Farmani, B., Mohayeji, M., and Moradbeygi, H. (2012). Impact of postharvest brassinosteroids treatment on PAL activity in tomato fruit in response to chilling stress. *Sci. Hortic.* 144, 116–120. doi: 10.1016/j.scienta.2012.07.008

Aghdam, M. S., Naderi, R., Sarcheshmeh, M. A., and Babalar, M. (2015). Amelioration of postharvest chilling injury in anthurium cut flowers by γ-aminobutyric acid (GABA) treatments. *Postharvest Biol. Technol.* 110, 70–76. doi: 10.1016/j.postharvbio.2015.06.020

Ahanger, M. A., Aziz, U., Alsahli, A. A., Alyemeni, M. N., and Ahmad, P. (2020). Influence of exogenous salicylic acid and nitric oxide on growth, photosynthesis, and ascorbate-glutathione cycle in salt stressed Vigna angularis. *Biomolecules* 10:42. doi: 10.3390/biom10010042

Ahmad, P., Alyemeni, M. N., Al-Huqail, A. A., Alqahtani, M. A., Wijaya, L., Ashraf, M., et al. (2020). Zinc oxide nanoparticles application alleviates arsenic (As) toxicity in soybean plants by restricting the uptake of as and modulating key biochemical attributes, antioxidant enzymes, ascorbate-glutathione cycle and glyoxalase system. *Plants* 9:825. doi: 10.3390/plants9070825

Ahmad, P., Jaleel, C. A., Salem, M. A., Nabi, G., and Sharma, S. (2010). Roles of enzymatic and nonenzymatic antioxidants in plants during abiotic stress. *Crit. Rev. Biotechnol.* 30, 161–175. doi: 10.3109/07388550903524243

Ahmad, P., Tripathi, D. K., Deshmukh, R., Pratap Singh, V., and Corpas, F. J. (2019). Revisiting the role of ROS and RNS in plants under changing environment. *Environ. Exp. Bot.* 161, 1–3. doi: 10.1016/j.envexpbot.2019.02.017

Ahmed, N. U., Park, J.-I., Jung, H.-J., Hur, Y., and Nou, I.-S. (2015). Anthocyanin biosynthesis for cold and freezing stress tolerance and desirable color in *Brassica rapa*. *Funct. Integr. Genomics* 15, 383–394. doi: 10.1007/s10142-014-0427-7

Alam, P., Albalawi, T. H., Altalayan, F. H., Bakht, M. A., Ahanger, M. A., Raja, V., et al. (2019). 24-Epibrassinolide (EBR) confers tolerance against NaCl stress in soybean plants by up-regulating antioxidant system, ascorbate-glutathione cycle, and glyoxalase system. *Biomolecules* 9:640. doi: 10.3390/biom9110640

Allen, D. J., and Ort, D. R. (2001). Impacts of chilling temperatures on photosynthesis in warm-climate plants. *Trends Plant Sci.* 6, 36–42. doi: 10.1016/S1360-1385(00)01808-2

Araki, H., Hamada, A., Hossain, M. A., and Takahashi, T. (2012). Waterlogging at jointing and/or after anthesis in wheat induces early leaf senescence and impairs grain filling. *Field Crop Res.* 137, 27–36. doi: 10.1016/j.fcr.2012.09.006

Arfan, M., Zhang, D.-W., Zou, L.-J., Luo, S.-S., Tan, W.-R., Zhu, T., et al. (2019). Hydrogen peroxide and nitric oxide crosstalk mediates brassinosteroids induced cold stress tolerance in *Medicago truncatula*. *Int. J. Mol. Sci.* 20:144. doi: 10.3390/ijms20010144

Beyer, W. F., and Fridovich, I. (1987). Assaying for superoxide dismutase activity: some large consequences of minor changes in conditions. *Anal. Biochem.* 161, 559–566. doi: 10.1016/0003-2697(87)90489-1

Boeckx, T., Webster, R., Winters, A. L., Webb, K. J., Gay, A., and Kingston-Smith, A. H. (2015). Polyphenol oxidase-mediated protection against oxidative stress is not associated with enhanced photosynthetic efficiency. *Ann. Bot.* 116, 529–540. doi: 10.1093/aob/mcv081

Bradford, M. M. (1976). A rapid and sensitive method for the quantitation of microgram quantities of protein utilizing the principle of protein-dye binding. *Anal. Biochem.* 72, 248–254. doi: 10.1016/0003-2697(76)90527-3

Cakmak, I., Strbac, D., and Marschner, H. (1993). Activities of hydrogen peroxide-scavenging enzymes in germinating wheat seeds. *J. Exp. Bot.* 44, 127–132. doi: 10.1093/jxb/44.1.127

Carillo, P. (2018). GABA shunt in durum wheat. *Front. Plant Sci.* 9:100. doi: 10.3389/fpls.2018.00100

Chalker-Scott, L. (1999). Environmental significance of anthocyanins in plant stress responses. *Photochem. Photobiol.* 70, 1–9. doi: 10.1111/j.1751-1097.1999.tb01944.x

Chaudhary, J., Alisha, A., Bhatt, V., Chandanshive, S., Kumar, N., Mir, Z., et al. (2019). Mutation breeding in tomato: advances, applicability and challenges. *Plants* 8:128. doi: 10.3390/plants8050128

Cheng, B., Li, Z., Liang, L., Cao, Y., Zeng, W., Zhang, X., et al. (2018). The γ-aminobutyric acid (GABA) alleviates salt stress damage during seeds germination of white clover associated with Na+/K+ transportation, dehydrins accumulation, and stress-related genes expression in white clover. *Int. J. Mol. Sci.* 19:2520. doi: 10.3390/ijms19092520

Costache, M. A., Campeanu, G., and Neata, G. (2012). Studies concerning the extraction of chlorophyll and total carotenoids from vegetables. *Romanian Biotechnol. Lett.* 17, 7702–7708.

Couée, I., Sulmon, C., Gouesbet, G., and El Amrani, A. (2006). Involvement of soluble sugars in reactive oxygen species balance and responses to oxidative stress in plants. *J. Exp. Bot.* 57, 449–459. doi: 10.1093/jxb/erj027

Cramer, G. R., Ergül, A., Grimplet, J., Tillett, R. L., Tattersall, E. A., Bohlman, M. C., et al. (2007). Water and salinity stress in grapevines: early and late changes in transcript and metabolite profiles. *Funct. Integr. Genomics* 7, 111–134. doi: 10.1007/s10142-006-0039-y

Croteau, R., Kutchan, T. M., and Lewis, N. G. (2000). Natural products (secondary metabolites). *Biochem. Mol. Biol. Plants* 24, 1250–1319.

Cuellar-Ortiz, S. M., De La Paz Arrieta-Montiel, M., Acosta-Gallegos, J., and Covarrubias, A. A. (2008). Relationship between carbohydrate partitioning and drought resistance in common bean. *Plant Cell Environ.* 31, 1399–1409. doi: 10.1111/j.1365-3040.2008.01853.x

De Carvalho, L. M. J., Gomes, P. B., De Oliveira Godoy, R. L., Pacheco, S., Do Monte, P. H. F., De Carvalho, J. L. V., et al. (2012). Total carotenoid content, α-carotene and β-carotene, of landrace pumpkins (*Cucurbita moschata* Duch): a preliminary study. *Food Res. Int.* 47, 337–340. doi: 10.1016/j.foodres.2011.07.040

Dias, M. A., and Costa, M. M. (1983). Effect of low salt concentrations on nitrate reductase and peroxidase of sugar beet leaves. *J. Exp. Bot.* 34, 537–543. doi: 10.1093/jxb/34.5.537

Foolad, M. R., and Lin, G. (2000). Relationship between cold tolerance during seed germination and vegetative growth in tomato: germplasm evaluation. *J. Am. Soc. Hortic. Sci.* 125, 679–683. doi: 10.21273/JASHS.125.6.679

Frankl, A., Mari, M., and Reggiori, F. (2015). Electron microscopy for ultrastructural analysis and protein localization in *Saccharomyces cerevisiae*. *Microb. Cell* 2, 412–428. doi: 10.15698/mic2015.11.237

Garstka, M., Venema, J. H., Rumak, I., Gieczewska, K., Rosiak, M., Koziol-Lipinska, J., et al. (2007). Contrasting effect of dark-chilling on chloroplast structure and arrangement of chlorophyll–protein complexes in pea and tomato: plants with a different susceptibility to non-freezing temperature. *Planta* 226:1165. doi: 10.1007/s00425-007-0562-7

Gill, S. S., and Tuteja, N. (2010). Reactive oxygen species and antioxidant machinery in abiotic stress tolerance in crop plants. *Plant Physiol. Biochem.* 48, 909–930. doi: 10.1016/j.plaphy.2010.08.016

Gilliham, M., and Tyerman, S. D. (2016). Linking metabolism to membrane signaling: the GABA–malate connection. *Trends Plant Sci.* 21, 295–301. doi: 10.1016/j.tplants.2015.11.011

Han, Y., Wang, S., Zhao, N., Deng, S., Zhao, C., Li, N., et al. (2016). Exogenous abscisic acid alleviates cadmium toxicity by restricting Cd 2+ influx in *Populus euphratica* cells. *J. Plant Growth Regul.* 35, 827–837. doi: 10.1007/s00344-016-9585-2

Harvaux, M., and Kloppstech, K. (2001). The protective functions of carotenoid and flavonoid pigments against excess visible radiation at chilling temperature investigated in *Arabidopsis* npq and tt mutants. *Planta* 213, 953–966. doi: 10.1007/s004250100572

Heath, R. L., and Packer, L. (1968). Photoperoxidation in isolated chloroplasts: I. Kinetics and stoichiometry of fatty acid peroxidation. *Arch. Biochem. Biophys.* 125, 189–198. doi: 10.1016/0003-9861(68)90654-1

Hossain, M. A., Bhattacharjee, S., Armin, S.-M., Qian, P., Xin, W., Li, H.-Y., et al. (2015). Hydrogen peroxide priming modulates abiotic oxidative stress tolerance: insights from ROS detoxification and scavenging. *Front. Plant Sci.* 6:420. doi: 10.3389/fpls.2015.00420

Jan, S., Noman, A., Kaya, C., Ashraf, M., Alyemeni, M. N., and Ahmad, P. (2020). 24-Epibrassinolide alleviates the injurious effects of Cr (VI) toxicity in tomato plants: insights into growth, physio-biochemical attributes, antioxidant activity and regulation of ascorbate–glutathione and glyoxalase cycles. *J. Plant Growth Regul.* 39, 1587–1604. doi: 10.1007/s00344-020-10169-2

Karim, S., Alezzawi, M., Garcia-Petit, C., Solymosi, K., Khan, N. Z., Lindquist, E., et al. (2014). A novel chloroplast localized Rab GTPase protein CPRabA5e is involved in stress, development, thylakoid biogenesis and vesicle transport in *Arabidopsis*. *Plant Mol. Biol.* 84, 675–692. doi: 10.1007/s11103-013-0161-x

Kaya, C., Ashraf, M., Alyemeni, M. N., Corpas, F. J., and Ahmad, P. (2020). Salicylic acid-induced nitric oxide enhances arsenic toxicity tolerance in maize plants by upregulating the ascorbate-glutathione cycle and glyoxalase system. *J. Hazard. Mater.* 399:123020. doi: 10.1016/j.jhazmat.2020.123020

Kim, C. (2020). ROS-driven oxidative modification: its impact on chloroplasts-nucleus communication. *Front. Plant Sci.* 10:1729. doi: 10.3389/fpls.2019.01729

Kinnersley, A. M., and Lin, F. (2000). Receptor modifiers indicate that 4-aminobutyric acid (GABA) is a potential modulator of ion transport in plants. *Plant Growth Regul.* 32, 65–76. doi: 10.1023/A:1006305120202

Kohli, S. K., Khanna, K., Bhardwaj, R., Allah, E. F. A., Ahmad, P., and Corpas, F. J. (2019). Assessment of subcellular ROS and NO metabolism in higher plants: multifunctional signaling molecules. *Antioxidants* 8:641. doi: 10.3390/antiox8120641

Kratsch, H., and Wise, R. R. (2000). The ultrastructure of chilling stress. *Plant Cell Environ.* 23, 337–350. doi: 10.1046/J.1365-3040.2000.00560.X

Li, M., Guo, S., Yang, X., Meng, Q., and Wei, X. (2016). Exogenous gamma-aminobutyric acid increases salt tolerance of wheat by improving photosynthesis and enhancing activities of antioxidant enzymes. *Biol. Plant.* 60, 123–131. doi: 10.1007/s10535-015-0559-1

Lister, C. E., Lancaster, J. E., and Walker, J. R. (1996). Phenylalanine ammonia-lyase (PAL) activity and its relationship to anthocyanin and flavonoid levels in New Zealand-grown apple cultivars. *J. Am. Soc. Hortic. Sci.* 121, 281–285. doi: 10.21273/JASHS.121.2.281

Liu, Y., Qi, M., and Li, T. (2012). Photosynthesis, photoinhibition, and antioxidant system in tomato leaves stressed by low night temperature and their subsequent recovery. *Plant Sci.* 196, 8–17. doi: 10.1016/j.plantsci.2012.07.005

Liu, X., Zhou, Y., Xiao, J., and Bao, F. (2018). Effects of chilling on the structure, function and development of chloroplasts. *Front. Plant Sci.* 9:1715. doi: 10.3389/fpls.2018.01715

Ma, X., Chen, C., Yang, M., Dong, X., Lv, W., and Meng, Q. (2018). Cold-regulated protein (SlCOR413IM1) confers chilling stress tolerance in tomato plants. *Plant Physiol. Biochem.* 124, 29–39. doi: 10.1016/j.plaphy.2018.01.003

Malekzadeh, P., Khara, J., and Heydari, R. (2014). Alleviating effects of exogenous gamma-aminobutiric acid on tomato seedling under chilling stress. *Physiol. Mol. Biol. Plants* 20, 133–137. doi: 10.1007/s12298-013-0203-5

Miller, G. L. (1959). Use of dinitrosalicylic acid reagent for determination of reducing sugar. *Anal. Chem.* 31, 426–428. doi: 10.1021/ac60147a030

Musser, R. L., Thomas, S. A., Wise, R. R., Peeler, T. C., and Naylor, A. W. (1984). Chloroplast ultrastructure, chlorophyll fluorescence, and pigment composition in chilling-stressed soybeans. *Plant Physiol.* 74, 749–754. doi: 10.1104/pp.74.4.749

Nagata, T., Todoriki, S., Masumizu, T., Suda, I., Furuta, S., Du, Z., et al. (2003). Levels of active oxygen species are controlled by ascorbic acid and anthocyanin in *Arabidopsis*. *J. Agric. Food Chem.* 51, 2992–2999. doi: 10.1021/jf026179

Nakano, Y., and Asada, K. (1981). Hydrogen peroxide is scavenged by ascorbate-specific peroxidase in spinach chloroplasts. *Plant Cell Physiol.* 22, 867–880. doi: 10.1093/OXFORDJOURNALS.PCP.A076232

Nayyar, H., Kaur, R., Kaur, S., and Singh, R. (2014). γ-Aminobutyric acid (GABA) imparts partial protection from heat stress injury to rice seedlings by improving leaf turgor and upregulating osmoprotectants and antioxidants. *J. Plant Growth Regul.* 33, 408–419. doi: 10.1007/s00344-013-9389-6

Oktay, M., Küfreviolu, I., Kocaçalişkan, I., and Şaklrolu, H. (1995). Polyphenoloxidase from Amasya apple. *J. Food Sci.* 60, 494–496. doi: 10.1111/j.1365-2621.1995.tb09810.x

Partelli, F., Batista-Santos, P., Scotti-Campos, P., Pais, I., Quartin, V., Vieira, H., et al. (2011). Characterization of the main lipid components of chloroplast membranes and cold induced changes in Coffea spp. *Environ. Exp. Bot.* 74, 194–204. doi: 10.1016/j.envexpbot.2011.06.001

Pressel, S., Ligrone, R., and Duckett, J. G. (2006). Effects of de-and rehydration on food-conducting cells in the moss *Polytrichum formosum*: a cytological study. *Ann. Bot.* 98, 67–76. doi: 10.1093/AOB/MCL092

Ran, W., Xiang, Q., Pan, Y., Xie, T., Zhang, Y., and Yao, C. (2020). Enhancing photosynthetic starch production by γ-aminobutyric acid addition in a marine green microalga tetraselmis subcordiformis under nitrogen stress. *Ind. Eng. Chem. Res.* 59, 17103–17112. doi: 10.1021/acs.iecr.0c00398

Rastegar, S., Khankahdani, H. H., and Rahimzadeh, M. (2020). Effect of γ-aminobutyric acid on the antioxidant system and biochemical changes of mango fruit during storage. *J. Food Meas. Character.* 14, 778–789. doi: 10.1007/s11694-019-00326-x

Rezaei-Chiyaneh, E., Seyyedi, S. M., Ebrahimian, E., Moghaddam, S. S., and Damalas, C. A. (2018). Exogenous application of gamma-aminobutyric acid (GABA) alleviates the effect of water deficit stress in black cumin (*Nigella sativa* L.). *Ind. Crop. Prod.* 112, 741–748. doi: 10.1016/j.indcrop.2017.12.067

Rizhsky, L., Liang, H., Shuman, J., Shulaev, V., Davletova, S., and Mittler, R. (2004). When defense pathways collide. The response of *Arabidopsis* to a combination of drought and heat stress. *Plant Physiol.* 134, 1683–1696. doi: 10.1104/pp.103.033431

Roberts, M. R. (2007). Does GABA act as a signal in plants? Hints from molecular studies: hints from molecular studies. *Plant Signal. Behav.* 2, 408–409. doi: 10.4161/psb.2.5.4335

SAS (1988). SAS/STAT User's Guide: Release 6.03 edition. SAS Inst. Inc., Cary, NC.

Seifikalhor, M., Aliniaeifard, S., Bernard, F., Seif, M., Latifi, M., Hassani, B., et al. (2020). γ-Aminobutyric acid confers cadmium tolerance in maize plants by concerted regulation of polyamine metabolism and antioxidant defense systems. *Sci. Rep.* 10, 1–18. doi: 10.1038/s41598-020-59592-1

Shao, Q., Wang, H., Guo, H., Zhou, A., Huang, Y., Sun, Y., et al. (2014). Effects of shade treatments on photosynthetic characteristics, chloroplast ultrastructure, and physiology of *Anoectochilus roxburghii*. *PLoS One* 9:e85996. doi: 10.1371/journal.pone.0085996

Sicilia, A., Scialò, E., Puglisi, I., and Lo Piero, A. R. (2020). Anthocyanin biosynthesis and DNA methylation dynamics in sweet orange fruit [*Citrus sinensis* L.(Osbeck)] under cold stress. *J. Agric. Food Chem.* 68, 7024–7031. doi: 10.1021/acs.jafc.0c02360

Singh, A., Kumar, J., and Kumar, P. (2008). Effects of plant growth regulators and sucrose on post harvest physiology, membrane stability and vase life of cut spikes of gladiolus. *Plant Growth Regul.* 55:221. doi: 10.1007/s10725-008-9278-3

Sita, K., and Kumar, V. (2020). Role of gamma amino butyric acid (GABA) against abiotic stress tolerance in legumes: a review. *Plant Physiol. Rep.* 25, 1–10. doi: 10.1007/s40502-020-00553-1

Sun, W., Van Montagu, M., and Verbruggen, N. (2002). Small heat shock proteins and stress tolerance in plants. *Biochim. Biophys. Acta* 1577, 1–9. doi: 10.1016/S0167-4781(02)00417-7

Sun, S., Zhang, L., Wang, J.-X., Wang, S.-M., Gao, H.-J., and Gao, H.-Y. (2008). Effects of low temperature and weak light on the functions of photosystem in *Prunus armeniaca* L. leaves in solar greenhouse. *J. Appl. Ecol.* 19, 512–516

Tabaei-Aghdaei, S. R., Pearce, R. S., and Harrison, P. (2003). Sugars regulate cold-induced gene expression and freezing-tolerance in barley cell cultures. *J. Exp. Bot.* 54, 1565–1575. doi: 10.1093/jxb/erg173

Thalmann, M., and Santelia, D. (2017). Starch as a determinant of plant fitness under abiotic stress. *New Phytol.* 214, 943–951. doi: 10.1111/nph.14491

Thitisaksakul, M., Arias, M. C., Dong, S., and Beckles, D. M. (2017). Overexpression of GSK3-like kinase 5 (OsGSK5) in rice (*Oryza sativa*) enhances salinity tolerance in part via preferential carbon allocation to root starch. *Funct. Plant Biol.* 44, 705–719. doi: 10.1071/FP16424

Velikova, V., Yordanov, I., and Edreva, A. (2000). Oxidative stress and some antioxidant systems in acid rain-treated bean plants: protective role of exogenous polyamines. *Plant Sci.* 151, 59–66. doi: 10.1016/S0168-9452(99)00197-1

Vijayakumari, K., and Puthur, J. T. (2016). γ-Aminobutyric acid (GABA) priming enhances the osmotic stress tolerance in *Piper nigrum* Linn. Plants subjected to PEG-induced stress. *Plant Growth Regul.* 78, 57–67. doi: 10.1007/s10725-015-0074-6

Wang, Y., Gu, W., Meng, Y., Xie, T., Li, L., Li, J., et al. (2017). γ-Aminobutyric acid imparts partial protection from salt stress injury to maize seedlings by improving photosynthesis and upregulating osmoprotectants and antioxidants. *Sci. Rep.* 7:43609. doi: 10.1038/srep43609

Wang, Y., Luo, Z., Huang, X., Yang, K., Gao, S., and Du, R. (2014). Effect of exogenous γ-aminobutyric acid (GABA) treatment on chilling injury and antioxidant capacity in banana peel. *Sci. Hortic.* 168, 132–137. doi: 10.1016/j.scienta.2014.01.022

Weston, E., Thorogood, K., Vinti, G., and López-Juez, E. (2000). Light quantity controls leaf-cell and chloroplast development in *Arabidopsis thaliana* wild type and blue-light-perception mutants. *Planta* 211, 807–815. doi: 10.1007/s004250000392

Wu, X., Jia, Q., Ji, S., Gong, B., Li, J., Lü, G., et al. (2020). Gamma-aminobutyric acid (GABA) alleviates salt damage in tomato by modulating Na+ uptake, the GAD gene, amino acid synthesis and reactive oxygen species metabolism. *BMC Plant Biol.* 20:465. doi: 10.1186/s12870-020-02669-w

Xiang, L., Hu, L., Xu, W., Zhen, A., Zhang, L., and Hu, X. (2016). Exogenous γ-aminobutyric acid improves the structure and function of photosystem II in muskmelon seedlings exposed to salinity-alkalinity stress. *PLoS One* 11:e0164847. doi: 10.1371/journal.pone.0164847

Xu, C., and Huang, B. (2008). Root proteomic responses to heat stress in two *Agrostis* grass species contrasting in heat tolerance. *J. Exp. Bot.* 59, 4183–4194. doi: 10.1093/jxb/ern258

Yang, J., Zhang, J., Wang, Z., Zhu, Q., and Liu, L. (2002). Abscisic acid and cytokinins in the root exudates and leaves and their relationship to senescence and remobilization of carbon reserves in rice subjected to water stress during grain filling. *Planta* 215, 645–652. doi: 10.1007/s00425-002-0789-2

Yemm, E. W., and Willis, A. J. (1954). The estimation of carbohydrates in plant extracts by anthrone. *Biochem. J.* 57, 508–514. doi: 10.1042/bj0570508

Yin, Y.-G., Kobayashi, Y., Sanuki, A., Kondo, S., Fukuda, N., Ezura, H., et al. (2010). Salinity induces carbohydrate accumulation and sugar-regulated starch biosynthetic genes in tomato (*Solanum lycopersicum* L. cv.'micro-tom') fruits in an ABA-and osmotic stress-independent manner. *J. Exp. Bot.* 61, 563–574. doi: 10.1093/jxb/erp333

Yuanyuan, M., Yali, Z., Jiang, L., and Hongbo, S. (2009). Roles of plant soluble sugars and their responses to plant cold stress. *Afr. J. Biotechnol.* 8, 2004–2010.

Zbierzak, A. M., Porfirova, S., Griebel, T., Melzer, M., Parker, J. E., and Dörmann, P. (2013). A TIR–NBS protein encoded by *Arabidopsis* chilling sensitive 1 (CHS 1) limits chloroplast damage and cell death at low temperature. *Plant J.* 75, 539–552. doi: 10.1111/tpj.12219

Zhang, X., Fowler, S. G., Cheng, H., Lou, Y., Rhee, S. Y., Stockinger, E. J., et al. (2004). Freezing-sensitive tomato has a functional CBF cold response pathway, but a CBF regulon that differs from that of freezing-tolerant *Arabidopsis*. *Plant J.* 39, 905–919. doi: 10.1111/j.1365-313X.2004.02176.x

Zhang, G., Liu, Y., Ni, Y., Meng, Z., Lu, T., and Li, T. (2014). Exogenous calcium alleviates low night temperature stress on the photosynthetic apparatus of tomato leaves. *PLoS One* 9:e97322. doi: 10.1371/journal.pone.0097322

Zhang, D., Ren, L., Chen, G.-Q., Zhang, J., Reed, B. M., and Shen, X.-H. (2015). ROS-induced oxidative stress and apoptosis-like event directly affect the cell viability of cryopreserved embryogenic callus in *Agapanthus praecox*. *Plant Cell Rep.* 34, 1499–1513. doi: 10.1007/s00299-015-1802-0

Zhao, H., Ye, L., Wang, Y., Zhou, X., Yang, J., Wang, J., et al. (2016). Melatonin increases the chilling tolerance of chloroplast in cucumber seedlings by regulating photosynthetic electron flux and the ascorbate-glutathione cycle. *Front. Plant Sci.* 7:1814. doi: 10.3389/fpls.2016.01814

Zhuang, K., Kong, F., Zhang, S., Meng, C., Yang, M., Liu, Z., et al. (2019). Whirly1 enhances tolerance to chilling stress in tomato via protection of photosystem II and regulation of starch degradation. *New Phytol.* 221, 1998–2012. doi: 10.1111/nph.15532

Conflict of Interest: The authors declare that the research was conducted in the absence of any commercial or financial relationships that could be construed as a potential conflict of interest.

Publisher's Note: All claims expressed in this article are solely those of the authors and do not necessarily represent those of their affiliated organizations, or those of the publisher, the editors and the reviewers. Any product that may be evaluated in this article, or claim that may be made by its manufacturer, is not guaranteed or endorsed by the publisher.

frontiers in Plant Science

ERRATUM
published: 19 November 2021
doi: 10.3389/fpls.2021.812646

Erratum: Protective Effect of γ-Aminobutyric Acid Against Chilling Stress During Reproductive Stage in Tomato Plants Through Modulation of Sugar Metabolism, Chloroplast Integrity, and Antioxidative Defense Systems

*Frontiers Production Office**

Frontiers Media SA, Lausanne, Switzerland

Keywords: tomato (*Solanum lycopersicum* L.), gamma-aminobutyric acid, chilling stress, chloroplast ultrastructure, oxidative stress, antioxidants, fruit yield

An Erratum on

Protective Effect of γ-Aminobutyric Acid Against Chilling Stress During Reproductive Stage in Tomato Plants Through Modulation of Sugar Metabolism, Chloroplast Integrity, and Antioxidative Defense Systems

by Abd Elbar, O. H., Elkelish, A., Niedbała, G., Farag, R., Wojciechowski, T., Mukherjee, S., Abou-Hadid, A. F., El-Hennawy, H. M., Abou El-Yazied, A., Abd El-Gawad, H. G., Azab, E., Gobouri, A. A., El Nahhas, N., El-Sawy, A. M., Bondok, A., and Ibrahim, M. F. M. (2021). Front. Plant Sci. 12:663750. doi: 10.3389/fpls.2021.663750

Owing to a production error, the author Nihal El Nahhas was not included in the original article when published.

In addition, the contributions of the authors Gniewko Niedbała and Tomasz Wojciechowski were not included in the *Author Contributions* section of the original article when published. The correct *Author Contributions* section is presented here:

"OE, AE, and MI: conceptualization. OE, AE, GN, TW, RF, SM, AA-H, HE-H, AE-Y, HE-G, EA, AG, NN, AE-S, AB, and MI: methodology, validation, resources, and writing – review and editing. OE, SM, GN, TW, AA-H, EA, AG, NN, AE-S, AB, and MI: software. OE, AE, RF, SM, AA-H, HE-H, NN, AE-S, AB, and MI: formal analysis. RF, SM, AA-H, HE-H, AE-Y, HE-G, EA, AG, NN, AE-S, and AB: investigation. OE, AE, GN, TW, RF, SM, and MI: data curation. OE, SM, and MI: writing – original draft preparation. RF, SM, AA-H, HE-H, AE-Y, HE-G, EA, AG, NN, AE-S, AB, and MI: supervision. AE-Y, GN, TW, HE-G, MI, SM, AE-Y, EA, HE-G, AG, RF, and NN: project administration. OE, AE, GN, TW, EA, AG, RF, and MI: funding acquisition. All authors contributed to the article and approved the submitted version."

The publisher apologizes for these mistakes. The original article has been updated.

OPEN ACCESS

Approved by:
Frontiers Editorial Office, Frontiers Media SA, Switzerland

***Correspondence:**
Frontiers Production Office
production.office@frontiersin.org

Specialty section:
This article was submitted to Plant Metabolism and Chemodiversity, a section of the journal Frontiers in Plant Science

Received: *10 November 2021*
Accepted: *10 November 2021*
Published: *19 November 2021*

Citation:
Frontiers Production Office (2021) Erratum: Protective Effect of γ-Aminobutyric Acid Against Chilling Stress During Reproductive Stage in Tomato Plants Through Modulation of Sugar Metabolism, Chloroplast Integrity, and Antioxidative Defense Systems. Front. Plant Sci. 12:812646. doi: 10.3389/fpls.2021.812646

frontiers in Plant Science

ORIGINAL RESEARCH
published: 21 October 2021
doi: 10.3389/fpls.2021.716782

Analysis of Phenotypic Characteristics and Sucrose Metabolism in the Roots of *Raphanus sativus* L.

*Ji-Nam Kang, Jung Sun Kim, Si Myung Lee, So Youn Won, Mi-Suk Seo and Soo-Jin Kwon**

Genomics Division, National Institute of Agricultural Sciences, Rural Development Administration, Jeonju, South Korea

The taproot of radish (*Raphanus sativus* L.) is an important sink organ; it is morphologically diverse and contains large amounts of secondary metabolites. Sucrose metabolism is believed to be important in the development of sink organs. We measured the amounts of glucose, fructose, and sucrose in the roots of sixty three radish accessions and analyzed the association between the sugar content and the root phenotype. Fructose content correlated with the root color and length characteristics, glucose was the most abundant sugar in the roots, and the sucrose content was very low, compared to that of the hexoses in most of the accessions. Expression analysis of the genes involved in sucrose metabolism, transportation, starch synthesis, and cell wall synthesis was performed through RNA sequencing. The genes encoding sucrose synthases (SUSY) and the enzymes involved in the synthesis of cellulose were highly expressed, indicating that SUSY is involved in cell wall synthesis in radish roots. The positive correlation coefficient (*R*) between the sucrose content and the expression of cell wall invertase and sugar transporter proteins suggest that hexose accumulation could occur through the apoplastic pathway in radish roots. A positive *R* score was also obtained when comparing the expression of genes encoding SUSY and fructokinase (FK), suggesting that the fructose produced by SUSY is mostly phosphorylated by FK. In addition, we concluded that sucrose was the most metabolized sugar in radish roots.

Keywords: sucrose metabolism, sugar content, phenotypic analysis, sucrose synthases, radish roots

OPEN ACCESS

Edited by:
Diana Santelia,
ETH Zürich, Switzerland

Reviewed by:
Thomas J. Bach,
Université de Strasbourg, France
Shifeng Cao,
Zhejiang Wanli University, China

***Correspondence:**
Soo-Jin Kwon
sjkwon67@korea.kr

Specialty section:
This article was submitted to Plant Metabolism and Chemodiversity, a section of the journal Frontiers in Plant Science

Received: *29 May 2021*
Accepted: *04 October 2021*
Published: *21 October 2021*

Citation:
Kang J-N, Kim JS, Lee SM, Won SY, Seo M-S and Kwon S-J (2021) Analysis of Phenotypic Characteristics and Sucrose Metabolism in the Roots of Raphanus sativus L. Front. Plant Sci. 12:716782. doi: 10.3389/fpls.2021.716782

INTRODUCTION

Radish (*Raphanus sativus* L.) is a nutritionally important root crop belonging to the Brassicaceae family, which includes cabbage, kale, and broccoli. The roots of radish are mainly used for human consumption in the East Asian countries, including Korea and Japan (Kang et al., 2020). In particular, the taproot of radish contains large amounts of secondary metabolites, minerals, vitamins, and carbohydrates, which is its most remarkable trait (Mitsui et al., 2015). The phenotypes of radish roots are well characterized; radish roots are diverse in shape, longitudinal section, length, diameter, weight, skin surface texture, and skin color (International Board for Plant Genetic Resources, and Commission of the European Communities, 1990; Mitsui et al., 2015).

Sucrose, a disaccharide, is either broken down into monosaccharides for metabolism in the sink organ or stored in the form of starch and cellulose, in most of the higher plants. Sucrose is also stored specifically in the stems or roots, such as in sugar cane and sugar beets (McCormick et al., 2009; Stein and Granot, 2018). Sucrose is the final product of photosynthesis and is the main form of carbon generally transported from the "source" to the "sink" organ through the phloem, in higher plants (Yu et al., 2016; Stein and Granot, 2019). Sucrose metabolism is considered essential for root growth and development in radish, because it is active when the tuberous roots begin to develop. In addition, it is a signal molecule regulating the expression of transcription factors, microRNAs, plant hormones, and many other genes (Stokes et al., 2013; Xiong et al., 2013; Mitsui et al., 2015; Yu et al., 2016). The main pathways and enzymes involved in sucrose metabolism in plants are well described (**Figure 1**; Wang et al., 2016; Verbančič et al., 2018; Stein and Granot, 2019). When sucrose arrives at sink tissues, it is transported from the sieve element/companion cell complex (SE/CC) to the apoplast; it is then hydrolyzed by cell wall invertase (CWINV) to produce glucose and fructose. Sucrose can also pass directly from the phloem to the cytosol through plasmodesmata (Stein and Granot, 2019). In the cytosol, sucrose is cleaved by sucrose synthase (SUSY) to generate uridine diphosphate glucose (UDP-G) and fructose, while cytosolic invertase (CINV) can hydrolyze sucrose to glucose and fructose, which are then converted to glucose-6-phosphate (G6P) and fructose-6-phosphate (F6P) by hexokinase (HK) and fructokinase (FK), respectively (Stein and Granot, 2019). UDP-G is converted to glucose-1-phosphate (G1P) by UGPase. G1P and G6P are transferred into plastids and are used mainly for starch biosynthesis (Wang et al., 2016). Phosphoglucose isomerase (PGI) and phosphoglucomutase (PGM) are involved in the transformation of G6P to F6P, which can convert G1P to UDP-G. F6P is used to resynthesize sucrose by combining it with UDP-G in the cytosol. This complex is converted to sucrose-6-phosphate (S6P) by sucrose-6-phosphate synthase (SPS), S6P can be dephosphorylated by sucrose-phosphate phosphatase (SPP) to form sucrose (Stein and Granot, 2019). G6P and F6P can also be used for glycolytic respiration in the cytosol and plastids (Granot et al., 2013; Stein and Granot, 2018).

Sugar transport is a process that involves cell-to-cell transport and transport between multiple organelles such as the phloem, apoplast, cytosol, and vacuole. The accumulation, compartmentalization, and storage of sugar in plants is regulated by sugar transporters such as sucrose transporter protein (SUC), monosaccharide transporter (MST), and SWEET (Sugars Will Eventually be Exported Transporter) (Eom et al., 2015; Wang et al., 2016; Julius et al., 2017). SUCs are H^+-coupled symporters and are essential for the translocation of sucrose via phloem loading (Chen, 2014; Julius et al., 2017). The MST family includes the sugar transporter protein (STP) and tonoplast monosaccharide transporter (TMT) (Wang et al., 2016). STPs play a role in the transport of hexose from the apoplast to the cytosol (Büttner, 2007) and TMTs are responsible for sugar transport in the tonoplast (Eom et al., 2015; Jung et al., 2015). SWEETs are structurally different from other transporters such as MSTs and SUCs; they are responsible for the secretion of sucrose as a prerequisite for SUC1-mediated phloem loading (Chen, 2014; Eom et al., 2015).

Sucrose is not only the source of carbon skeletons, but is also important in the biosynthesis of essential metabolites, such as starch and cellulose (Yu et al., 2016). SUSY is a potential factor responsible for cell wall production, because it directly supplies UDP-G to cellulose and callose synthases (Amor et al., 1995; Persia et al., 2008; Verbančič et al., 2018). CINV also contributes to cellulose synthesis by supplying UDP-G (Rende et al., 2017; Barnes and Anderson, 2018). Starch synthesis is occurred through the catalysis of SUSY and UDPase in sink organs (Kleczkowski et al., 2004; Zhang et al., 2017; Stein and Granot, 2019). Cellulose and starch are the most abundant biosynthetic compounds in the world and are the primary carbon sinks in plants (Baroja-Fernández et al., 2012). Starch synthesis commonly occurs in amyloplasts, catalyzed by starch synthase (SS), whereas cellulose and callose are synthesized in the plasma membrane by cellulose synthase (CESA) and callose synthase (CALS), respectively, for cell wall formation in sink organs (Persia et al., 2008; Noronha et al., 2018; Stein and Granot, 2019).

Large amounts of transcriptomic information are generated for understanding the growth and development mechanisms of plants (Yu et al., 2016). Recently, the draft genome of *R. sativus* var. *hortensis* was sequenced and published (Mitsui et al., 2015). Global transcriptome analysis was performed in radish roots, using RNA sequencing (RNA-seq) (Mitsui et al., 2015; Yu et al., 2016). In this study, we focused on the association between the sugar content and the phenotypic characteristics of radish roots. In addition, we tried to understand the sugar accumulation by analyzing the expression of genes involved in sucrose metabolism. The amount of the individual sugars in the roots of sixty three radish accessions was investigated, and the expression of genes involved in sucrose metabolism, sugar transport, starch synthesis, and cell wall synthesis were comprehensively analyzed using RNA-seq.

MATERIALS AND METHODS

Radish Materials and Sample Preparation

The radish accessions used in this study were the same as that from our previous study (Kang et al., 2020). Seeds of sixty three radish accessions were collected from the National Agrodiversity Center (Korea, IT-), the Leibniz Institute of Plant Genetics and Crop Plant Research (Germany, RA-), and the National Agriculture and Food Research Organization (Japan, JP-). Seven young plants from each accession were grown in plastic pots and transferred to the field for plant growth. After 8 weeks, three independent plants from each accession were gently harvested from the ground, and the morphological characteristics of the taproot, including length, weight, and color, were recorded. The central part of the taproot was cut into two pieces. One piece was freeze-dried for sugar content analysis and the other piece was stored at −80°C for RNA sequencing.

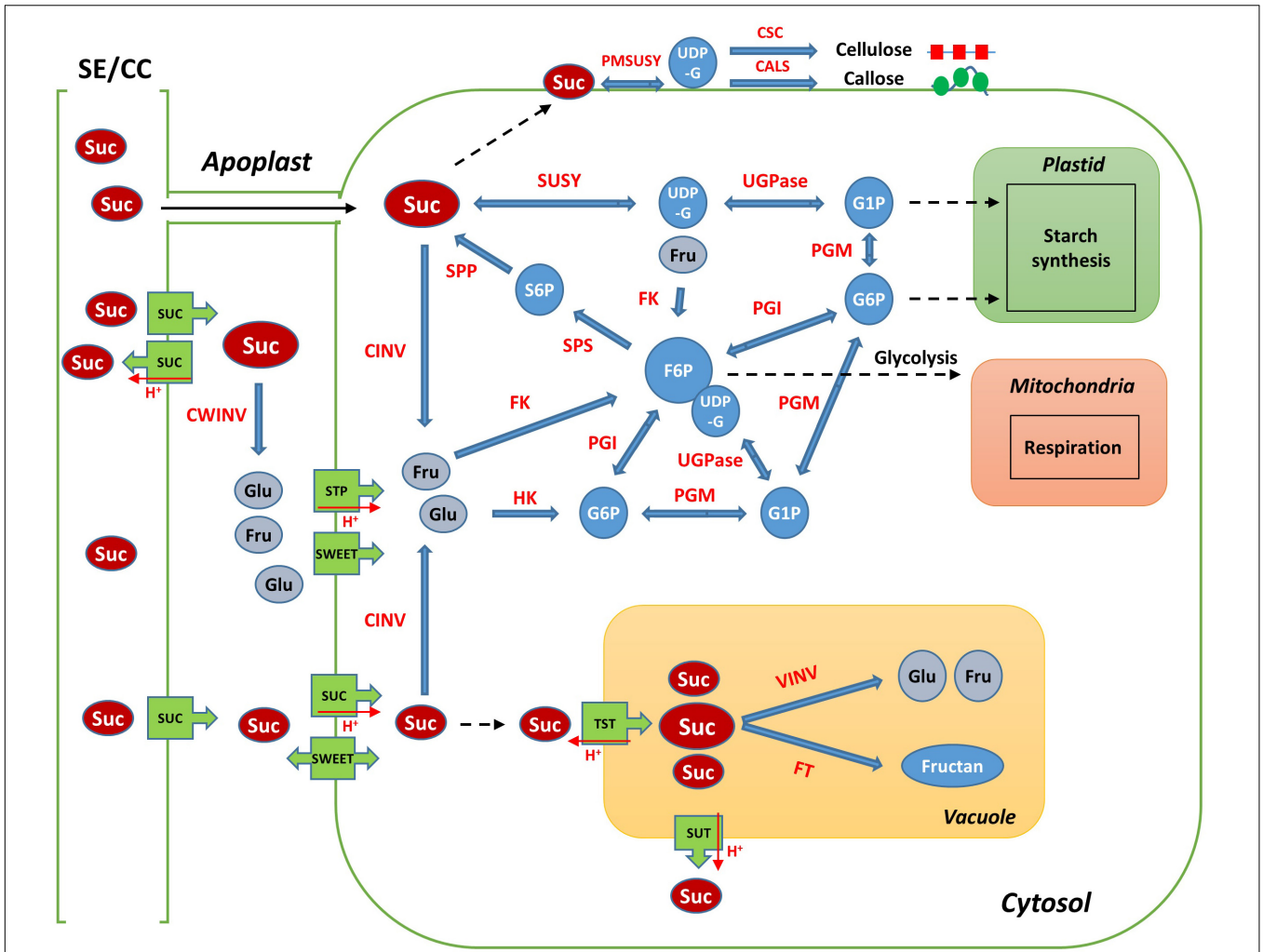

FIGURE 1 | Schematic map of sucrose metabolism in plant sink cell. SE/CC, sieve element/companion cell; Suc, sucrose; Glu, Glucose; Fru, Fructose; UDP-G, uridine diphosphate glucose; G1P, glucose-1-phosphate; G6P, glucose-6-phosphate; F6P, fructose-6-phosphate; S6P, sucrose-6-phosphate; SUSY, sucrose synthase; CWINV, cell-wall invertase; CINV, cytosol invertase; VINV, vacuole invertase; UGPase, UDP-glucose pyrophosphorylase; PGM, phosphoglucomutase; PGI, phosphoglucose isomerase; FK, fructokinase; HK, hexokinase; SPS, sucrose-6-phosphate synthase; SPP, sucrose-phosphate phosphatase; VINV, vacuolar invertase; FT, fructosyltransferase; SUC, sucrose transporter protein; SWEET, sugars will eventually be exported transporter; STP, sugar transporter protein; TST, tonoplast sucrose transporter; PMSUSY, plasma membrane-associated SUSY; CSC, cellulose synthase complex; CALS, callose synthase.

Determination of Individual Sugar Content

High-performance anion-exchange chromatography (HPAEC) was used for quantifying the reducing sugars. A mixture of 100 mg freeze-dried powder of radish roots and 1.5 mL of 5% trichloroacetic acid (TCA) solution was stirred thoroughly for 1 min. The mixture was centrifuged (5 min at 13,000 × g), the supernatant was filtered, and the eluent was used for the quantitative analysis of reducing sugars. The soluble sugar content was analyzed using a PHAEC system (Dionex, United States) with a CarboPac^{TM} PA1 column (4 mm × 250 mm). Mobile phases A and B contained 150 mM NaOH and 600 mM sodium acetate with 150 mM NaOH, respectively. The flow rate was 1 mL/min and separation was performed under the following gradients: 0–5 min, 0% B; 5–10 min, 10% B; 15–20 min, 100% B; 20–30 min, 0%. The concentration of individual soluble sugars was quantified against the standards for sucrose, glucose, and fructose.

RNA Sequencing and Gene Annotation

Total RNA was isolated from the roots of two radish accessions, JP-61 and JP-64, using a Hybrid-R kit (GeneAll, Korea), according to the manufacturer's instructions. The quality of the RNA was assessed; 2 μg of total RNA was used to construct RNA-seq libraries and libraries with an insert size of 300 bp were generated using an Illumina TruSeq RNA Sample Preparation Kit (Illumina, United States), according to the manufacturer's instructions. The Illumina HiSeq X platform was employed for RNA-seq at Macrogen Co. (Seoul, Korea), and paired-end reads of 101 bp were obtained from the pooled libraries. Mapping of

reads and gene annotation was performed according to Kang et al. (2020). The adapter sequences followed by the low quality and duplicated reads were removed using the Trimmomatic program (ver. 0.38). High-quality RNA-seq reads were mapped using HISAT2[1] in the coding region of the radish genome sequences of *R. sativus* var. *hortensis* cv. Aokubi is a double haploid line (Mitsui et al., 2015). The mapped reads were counted using HTSeq-count[2] and the fragments per kilobase of transcript per million (FPKM) values were calculated for the gene expression analysis. Gene annotation was performed using nrBLAST, InterProScan, and Araport11 for predicting the gene function. Sequencing data for the IT-15, RA-82, RA-92, RA-74, and IT-8 accessions, excluding JP-61 and JP-64, were obtained from our previous study (Kang et al., 2020). Information on genes involved in sucrose metabolism, transportation of sugar, synthesis of cellulose and callose, and starch synthesis was obtained from previous studies (Jung et al., 2015; Wang et al., 2016; Yu et al., 2016; Julius et al., 2017; Stein and Granot, 2019).

RESULTS

Analysis of Sugar Content and Phenotype Characteristics in Radish Roots

Sixty three radish accessions, including *R. sativus* var. *sativus*, *R. sativus* convar. *sativus* (radish group), *R. sativus* convar. *sativus* (small radish group), *R. sativus* var. *longipinnatus* (daikon group), *R. sativus* convar. *caudatus*, and *Raphanus* sp. were used for the analysis of sugar content and the phenotypic characteristics of radish roots (**Supplementary Figure 1**). Fructose, glucose, and sucrose were detected in the roots. The median value of fructose was 90.32 mg·g^{-1} dry weight (DW) within the range of 7.02–310.91 mg·g^{-1} DW, and that of glucose was 137.65 mg·g^{-1} DW within the range of 25.07–292.89 mg·g^{-1} DW. The median value of sucrose was 25.18 mg·g^{-1} DW in the range of 0–200.02 mg·g^{-1} DW. Glucose, fructose, and sucrose accounted for 47.15, 30.87, and 8.58% of the total content, respectively, based on the median values (**Supplementary Figure 2A**). The total DW and root length were distributed in the range of 1.11–61.39 g and 4.33–37.60 cm and their median values were 22.39 g and 18.93 cm, respectively. The diameter of central part of the taproot was in the range of 1.97–12.9 cm, and the median value was 6.3 cm (**Supplementary Figure 2B**). Skin color types, including white, pink, brown, and green, were identified among the sixty three radish accessions (**Supplementary Figure 1**). Detailed information on sugar content and phenotypic characteristics is indicated in **Supplementary Table 1**.

Correlation Analysis Between the Sugar Content and Root Phenotypes

Principal component analysis (PCA) was performed using 189 radish samples (three individual samples from each accession) to confirm the association between the sugar content and root phenotypes. PC1 and PC2 represented 55.19% of the seven variables (**Figure 2A**). When the five radish groups were reflected in seven variables, only the small radish (C) and daikon (D) groups were distinguishable. The root phenotypes of the small radish group were spheric or transverse elliptic with pink and brown skin color, except for one accession. The daikon group showed mostly long and white root phenotypes (**Supplementary Figure 1**). The main variables used to separate the two groups were the length and color of the roots. The other radish groups were not divided into seven variables. Sucrose was negatively loaded into PC1 and PC2 as a single variable (**Figure 2A**). Similar results were identified when analyzing the sixty three radish samples, based on the mean values (**Supplementary Figure 2C**). Root length was positively correlated with the weight and fructose content of roots in PC1 (**Figure 2A**). Therefore, we changed the grouping criteria from radish varieties to root color phenotype and tried PCA using four variables, color, weight, length, and fructose content (**Supplementary Figure 3** and **Figure 2B**). PC1 and PC2 accounted for 73.58% of the variables. Interestingly, white radish and colored radish were clearly distinguishable. Root length and fructose content were identified as variables associated with white radishes (**Figure 2B** and **Supplementary Figure 2D**). Box plot analysis was performed to verify the differences in the root weight, root length, and fructose content in relation to the root color. The weight of the white radish was not significantly different from that of the other colored groups. The length and fructose content of white radish were significantly different from that of the brown and pink radish. Green radish roots were similar to that of white radish in terms of weight, length, and fructose content. The roots of white radish were significantly longer and had higher fructose content, compared to that of brown and pink radish (**Figure 2C**). Correlation coefficient (*R*) analysis supported these results. The total sugar content showed a positive *R* score with hexose content (**Figures 3A,B**). The fructose content showed a positive *R* score with weight and length, and a negative *R* score with the color of roots (**Figures 3A,C**). Root diameter did not show a significant *R* score with sugar content (**Figure 3A**). Root color showed a negative *R* score with the root length. Glucose and sucrose content did not show significant *R* scores for root phenotypes (**Figures 3A,D**). The fructose-to-glucose ratio (FGR) was used to analyze the distribution pattern of hexose in radish roots. Sucrose was the dominant sugar only in IT-8 and JP-69 (**Figure 4A**). The FGR value was equal to or significantly less than one in most of the accessions. Only seven accessions statistically exceeded the FRG value of one (**Figure 4B**). These results indicate that glucose is the main sugar and that fructose content is associated with the phenotypic characteristics of radish roots, such as weight, length, and color.

Expression Analysis of Genes Involved in Sucrose Metabolism in Radish Roots

To identify the genes related to sucrose metabolism in radish roots, we selected seven radish accessions (**Figure 5A**). JP-61, IT-15, RA-82, JP-64, and RA-92 had high hexose and low sucrose

[1]https://ccb.jhu.edu/software/hisat2/index.shtml

[2]https://pypi.org/project/HTSeq

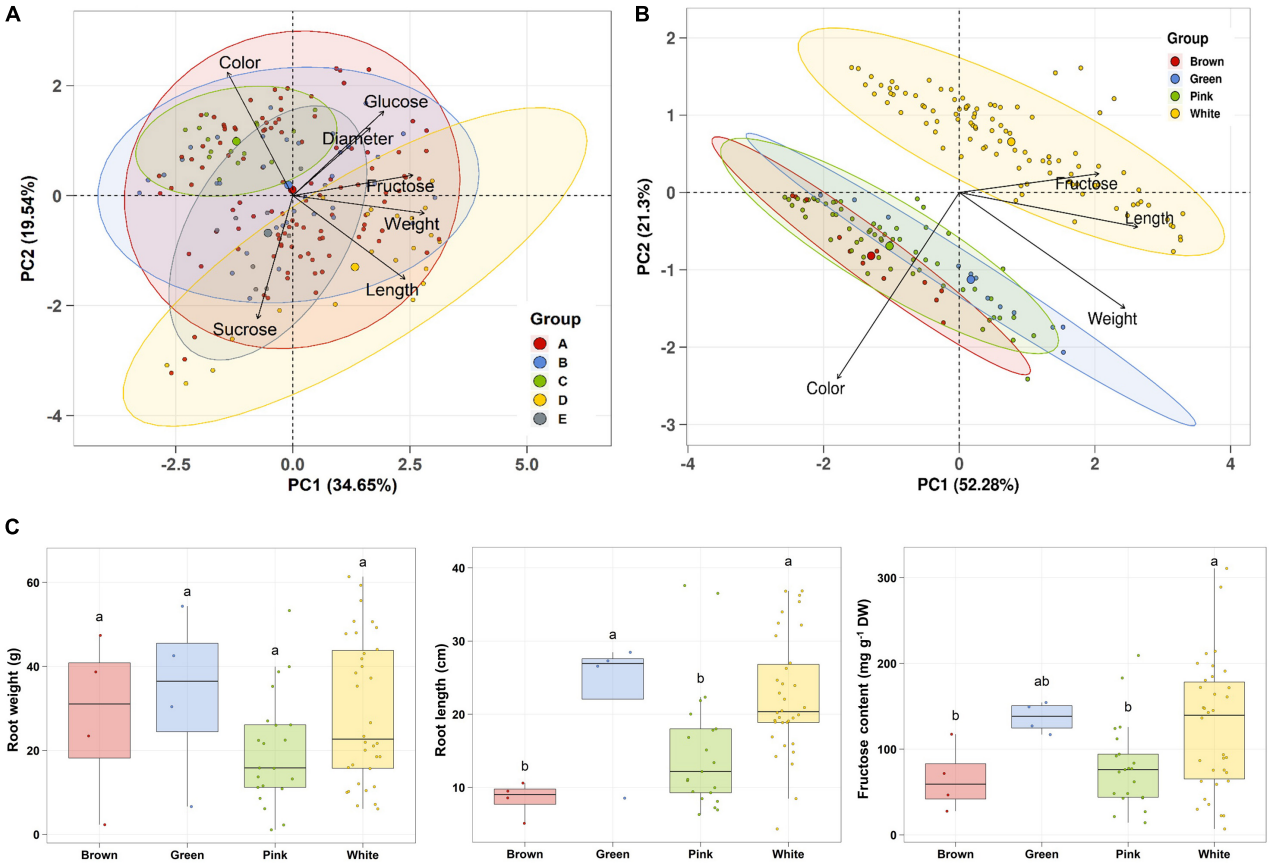

FIGURE 2 | Association analysis between sugar content and root morphological characteristics. Data visualization performed using R program. **(A)** PCA plot based on five radish groups. A, *Raphanus sativus* var. *sativus*; B, *Raphanus sativus* convar. *sativus* (Radish group); C, *Raphanus sativus* convar. *sativus* (Small radish group); D, *Raphanus sativus* var. *longipinnatus* L. H. Bailey (Daikon Group); E, *Raphanus* sp. with *Raphanus sativus* convar. *caudatus* (L.f.) Pistrick. **(B)** PCA plot based on root color. **(C)** Box plot analysis. Anova and Tukey Honest Significance Difference (HSD) test was used to evaluate the differences between the groups. Other letters in the plot indicate significant differences at the $p < 0.05$ level.

content. RA-74 had similar hexose and sucrose contents. IT-8 had a significantly higher sucrose content compared to the hexose content and it had the highest sucrose content and was an extreme outlier among the sixty three radish accessions (**Supplementary Figure 2A** and **Supplementary Table 1**). The phenotypic characteristics of the seven radish roots are shown in **Figure 5C**. Correlation analysis between the sugar content and root phenotypic characteristics was conducted using 21 radish samples (three individual samples from seven accessions). Hexose had a positive *R* score for total sugar content, and fructose showed a positive *R* score for the weight and length of roots. Sucrose content did not show a significant *R* score with any of the phenotypic characteristics (**Supplementary Figure 4**).

We conducted RNA-seq analysis of the radish accessions. The sequencing and mapping results were presented in **Supplementary Table 2**. Eighty one genes involved in sucrose metabolism were identified in radish roots. These genes encoded for 10 main enzymes, SUSY, CWINV, CINV, FK, HK, UDPase, PGI, PGM, SPS, and SPP (**Supplementary Table 3**). Two SUSY1-encoding genes (*RSG05117* and *RSG18209*), one CWINV3-encoding gene (*RSG17864*), two CINV-encoding genes (*RSG32129* and *RSG26046*), two FK1-encoding genes (*RSG13222* and *RSG34089*), two HK1-encoding genes (*RSG19301* and *RSG43310*), one UGPase-encoding gene (*RSG31848*), two PGI-encoding genes (*RSG20307* and *RSG14173*), two PGM-encoding genes (*RSG15383* and *RSG26796*), one SPS1-encoding gene (*RSG05158*), and one SPP2-encoding gene (*RSG23194*) showed relatively higher expression, compared to that of their ortholog genes (**Supplementary Figures 5A,B**). In particular, the *RSG05117* gene encoding SUSY1 showed remarkably high expression among that of all the sucrose metabolism genes identified (**Supplementary Figure 5A**). These 16 genes are considered responsible for sucrose metabolism in radish roots.

Correlation Analysis Between the Sugar Content and Sucrose Metabolism Genes in Radish Roots

We performed a correlation analysis between the 16 major genes involved in sucrose metabolism and the sugar content in the seven radish accessions. The sucrose content of the IT-8 accession was significantly higher than that of the other six

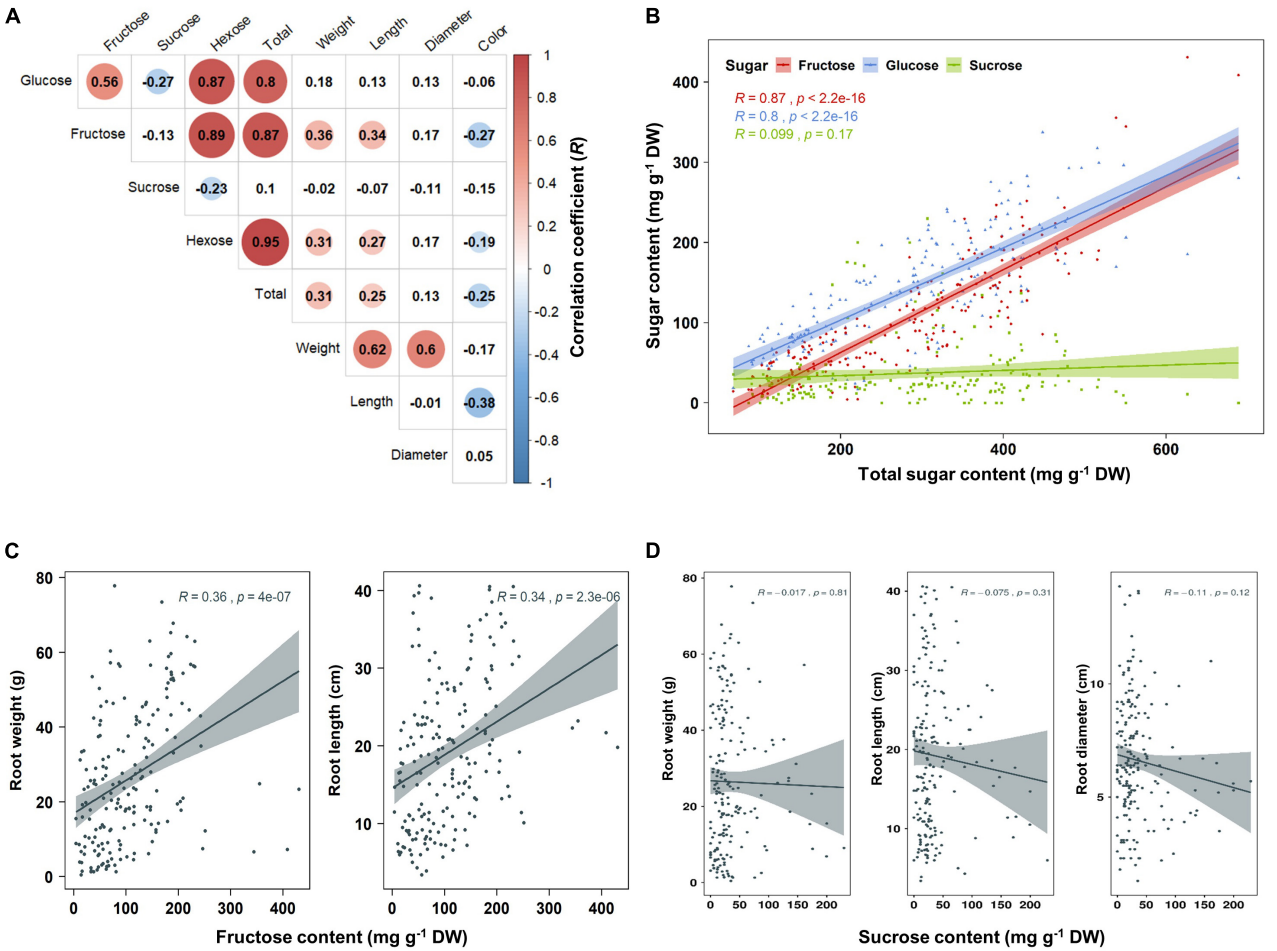

FIGURE 3 | Analysis of Pearson's correlation coefficient (*R*) between sugar content and root phenotypes. Data visualization performed using R program. **(A)** Heat map of *R* score. The *R* scores with $p < 0.01$ are indicated by color. Red and blue circles represent positive and negative *R* scores, respectively. **(B)** Correlation between total sugar content and individual sugar content. **(C)** Correlation between fructose content and root phenotypes. **(D)** Correlation between sucrose content and root phenotypes.

accessions; however, the expression of genes involved in sucrose metabolism was not specific for IT-8 among the tested accessions (**Figures 5B,D**). Expression of the SUSY1-encoding gene *RSG05117* in IT-8 was comparable to that of IT-15, RA-92, and RA-74. Another SUSY1-encoding gene *RSG18209* was similarly expressed in the tested accessions except JP-61 (**Figure 5D**). The sucrose content did not show any significant correlation with the expression of the sucrose metabolism genes among the tested accessions (**Supplementary Figure 6**). Sucrose content could be influenced by the expression of sugar transporters; and therefore, we investigated the expression levels of 85 genes encoding sugar transporters in the radish roots (**Supplementary Table 4**). Four SUC-encoding genes *RSG21948*, *RSG49762*, *RSG35389*, and *RSG51374*, five SWEET-encoding genes *RSG33430*, *RSG25697*, *RSG35586*, *RSG11173*, and *RSG45880*, two TMT-encoding genes *RSG15186* and *RSG04190*, and an STP1-encoding gene *RSG00099* were relatively highly expressed, compared to that of their paralog genes (**Supplementary Figures 7A,B**). However, sucrose content did not show a significant correlation with the expression levels of any of the sugar transporters (**Supplementary Figure 7C**, upper). These results indicate that the sucrose content in radish roots was not influenced by the expression levels of genes involved in sucrose metabolism, including the sucrose transporters. The sucrose content of the IT-8 was an extreme outlier; and therefore, we performed a correlation analysis after excluding IT-8 (**Figure 6A**). Sucrose content was significantly correlated with the CWINV3-encoding gene, *RSG17864* (**Figure 6B**). The fructose content showed a negative *R* score with the expression levels of the SUSY1-encoding gene *RSG05117* and the FK1-encoding gene *RSG34089* (**Figure 7A**). Furthermore, these genes had a positive *R* score for each other (**Figure 7B**). Similar results were observed for the paralog genes *RSG18209* and *RSG13222*, which encode SUSY1 and FK1, respectively (**Figure 7C**). In addition, the two FK1-encoding genes showed positive *R* scores with the PGI-encoding gene *RSG14173* (**Figure 7D**). These results suggest that the genes encoding SUSY1 and FK1 work together in radish roots and that of fructose produced by SUSY1 is sequentially metabolized by FK1 and PGI.

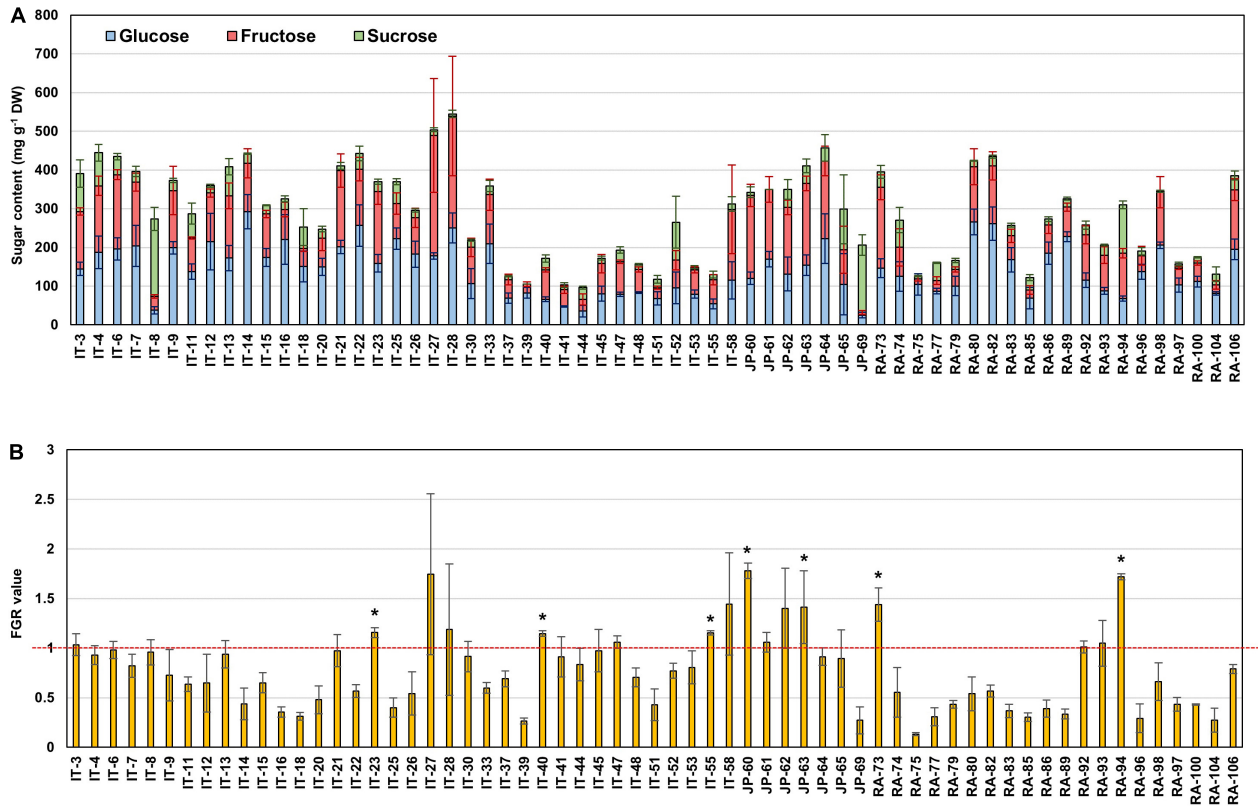

FIGURE 4 | The sugar ratio in each radish root. **(A)** Distribution of glucose, fructose, and sucrose in each radish root. **(B)** Fructose to glucose ratio (FGR). The asterisks indicate that the FGR value statistically exceeds 1 by *t*-test ($p < 0.05$).

Predominant Expression of Cellulose Biosynthetic Genes in Radish Roots

Two SUSY1-encoding genes were highly expressed in JP-61, where the sucrose content was undetectable (**Figures 5B,D**). Sugar was detected only in the soluble compartment in our study; and therefore, we hypothesized that SUSY could act in the insoluble regions such as the membrane pool. SUSY is directly associated with the synthesis of cellulose and callose in the plasma membrane and is involved in starch biosynthesis in the cytoplasm (Amor et al., 1995); and therefore, we identified seven genes involved in starch synthesis, 23 genes involved in callose synthesis, and 15 genes responsible for cellulose synthesis (**Supplementary Table 5**). In the tested accessions, the genes encoding CESA are highly expressed. Genes encoding CESA1, 3, 5, and 6 showed distinctly higher expression levels (**Figure 8A**). The integrated expression values of these genes were significantly higher than that of SS and CALS (**Figure 8B**). CESA1, CESA3, CESA5, and CESA6 are subunits of the cellulose synthase complex (CSC), involved in primary cell wall formation (Endler and Persson, 2011; Liepman and Cavalier, 2012; Verbančič et al., 2018). CESAs that function in secondary cell wall synthesis were expressed at low levels (**Figure 8C**). These results suggest that SUSY could act on the insoluble membrane, regardless of the sucrose content in the soluble regions of the cell and that it is involved in the primary cell wall synthesis of radish roots.

DISCUSSION

Sugar for Plant Development

Sugar is essential for plant growth and development, and it can act as a signaling molecule and regulator of gene expression. Sucrose, glucose, fructose, and UDP-G are detected as signals in specific metabolic pathways and developmental responses in plants (Eveland and Jackson, 2012). In this study, correlation analysis showed that the color and length of radish roots were negatively correlated. Most of the pink and brown radish had roots that were shorter than that of the white radish accessions (**Figure 2C**). The color traits of these roots were likely caused by anthocyanin and lignin deposition. Sugars promote anthocyanin accumulation in radish hypocotyls; the supply of exogenous sucrose causes rapid and distinct anthocyanin accumulation in the radish hypocotyls compared to that of the control (Hara et al., 2003). Supply of sucrose promoted lateral root formation in anthocyanin-accumulated hypocotyls. Sucrose is a signal for anthocyanin biosynthesis and the morphological development of the hypocotyl; this is applicable to the radish hypocotyl (Hara et al., 2003). Growth and lignin synthesis showed a significant negative correlation in the hybrid forest tree population. Sucrose could be a major regulator of lignin synthesis. The negative correlation between growth and lignin deposition is caused by the competition for

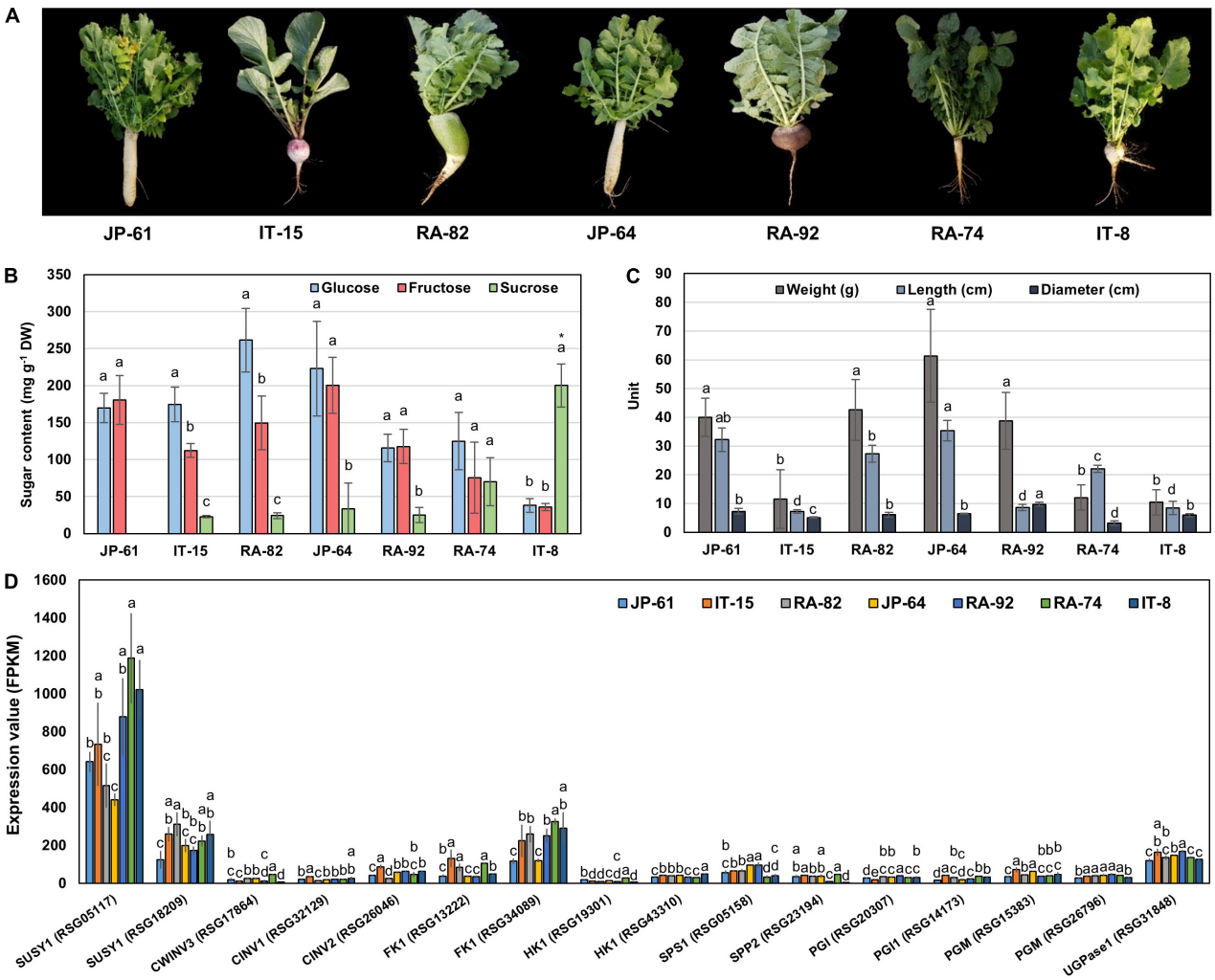

FIGURE 5 | Information of phenotypes, sugar content, and genes expression involved in sucrose metabolism in seven radish roots. The error bars represent the standard deviation of three repeated data. **(A)** Phenotypic images. **(B)** Individual sugar content. Anova and Tukey HSD were performed to reveal the differences of individual sugar content in each accession. Other letters above the bar graph indicate significant differences at the $p < 0.05$ level. **(C)** Measurement of the morphological characteristics. Other letters above the bar graph indicate significant differences at the $p < 0.05$ level in phenotypic characteristics between each radish accession. **(D)** Expression results of genes involved in sucrose metabolism. Anova and Tukey HSD were used to evaluate the differences between the sucrose metabolism genes expressed in each accession. The letters above the bar graph indicate significant differences at the $p < 0.05$ level.

carbon allocation between the cellulose and lignin synthesis pathways (Novaes et al., 2010). The anthocyanin and lignin biosynthetic pathways are closely linked in plants. They are two major pathways in phenylpropanoid metabolism and share the substrate ρ-coumaroyl CoA (Hara et al., 2004; Peng et al., 2008). Distinct anthocyanin accumulation occurs under nitrogen (N) limitation, which is the ability to adapt to N limitation in Arabidopsis (Peng et al., 2008). The Arabidopsis *NLA* (nitrogen limitation adaptation) mutant did not accumulate anthocyanin in the N limitation, instead accumulating significant lignin. The authors concluded that the phenylpropanoid metabolic flux was converted from anthocyanin to lignin synthesis in the *NLA* mutant under the N limitation (Peng et al., 2008). Therefore, plant development could be affected by the sucrose signals applied to metabolic pathways other than that for plant growth. It is possible that the short morphological characteristics of the colored radish roots are partially related to anthocyanin and lignin biosynthesis. A negative correlation between root length and color of radish has also been reported in other study (Yi et al., 2016).

The fructose content showed a significant positive *R* score with root length (**Figure 3A**). These results can be explained based on the sink capacity of the roots. Increasing the sink capacity lowers the local concentration of sucrose in sink organs, which makes it possible to unload more sucrose from the source organ into the sink organ across a concentration gradient through the phloem (Rouhier and Usuda, 2001; Mitsui et al., 2015; Fugate et al., 2019; Stein and Granot, 2019). Therefore, the resulting fructose by sucrose degradation could accumulate in the large sink organs. Hexoses promote organ growth and proliferation

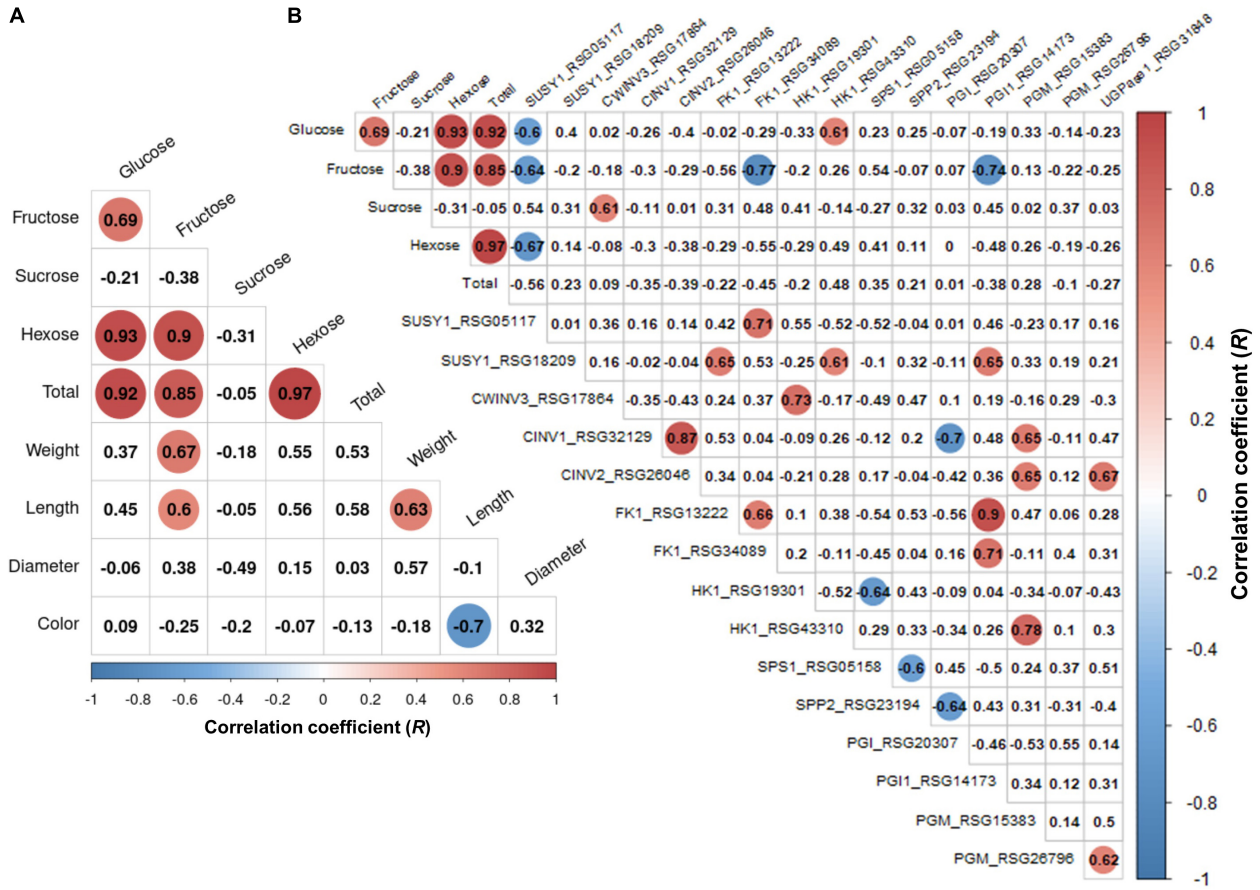

FIGURE 6 | Analysis of Pearson's correlation coefficient (*R*) among the sugar content, root phenotypes, and expression level of sucrose metabolism genes in the six radish accessions. The outlier accession IT-8 was excluded. Data visualization was performed using R program. The *R* scores with $p < 0.01$ are indicated by color. Red and blue circles represent positive and negative *R* scores, respectively. **(A)** Heat map of *R* score between sugar content and root phenotypes. **(B)** Heat map of *R* score between total sugar content and expression level of genes involved in sucrose metabolism.

in plants (Eveland and Jackson, 2012). A positive correlation between the local hexose concentration and root elongation was reported in Arabidopsis. It has been suggested that the structural properties of roots can be significantly affected by carbon availability in plant, which may be caused by local hexose concentration (Freixes et al., 2002).

Sucrose Content in Radish Roots

The hexose content was very high, whereas the sucrose content was approximately 8.5% in the sixty three radish accessions (**Supplementary Figure 2A**). A distinctly high sucrose content was identified in two accessions, IT-8 and JP-69, which is possibly a transient phenomenon during the growth process. We could not identify any molecular mechanisms underlying sucrose accumulation in the IT-8 roots at the transcriptional level. In addition, the sucrose content in IT-8 and JP-69 was not high, compared to the hexose content in our previous study, using the same radish accessions. In particular, the sucrose content of IT-8 was only approximately 5.8% of the total sugar content. However, the overall sucrose content was very low, and glucose was the main sugar among the 82 radish accessions (Seo et al., 2018). These results suggest that sucrose is not the main sugar and is mostly metabolized in radish roots.

The sucrose content of the IT-8 roots was unique among the sixty three radish accessions. The initial approach of this study was to identify a specific molecular mechanism that influences the high sucrose content in IT-8 roots. Invertases, SPS, and SPP are responsible for the storage and re-synthesis of sucrose in sugar cane stalk, and SUSYs are involved in the storage of sucrose in sugar beet roots (Giaquinta, 1979; Wang et al., 2013; Fugate et al., 2019). SUC1 and SUC2 are responsible for apoplastic phloem unloading and the cellular uptake of sucrose into sink cells (Wang et al., 2016; Julius et al., 2017). Clade III SWEETs are efficient sucrose transporters (Eom et al., 2015; Julius et al., 2017). SUC4 and TMT are sucrose transporters located in the tonoplast (Eom et al., 2015; Jung et al., 2015; Julius et al., 2017). BvTMT2.1, the sugar beet tonoplast monosaccharide transporter, plays a role as a specific transporter for sucrose uptake in the tonoplast; and therefore, it was included in the TST groups (Hedrich et al., 2015; Jung et al., 2015). The expression of these genes is strongly correlated with the accumulation of sucrose in plants (Julius et al., 2017). However, the expression of these genes was not specific

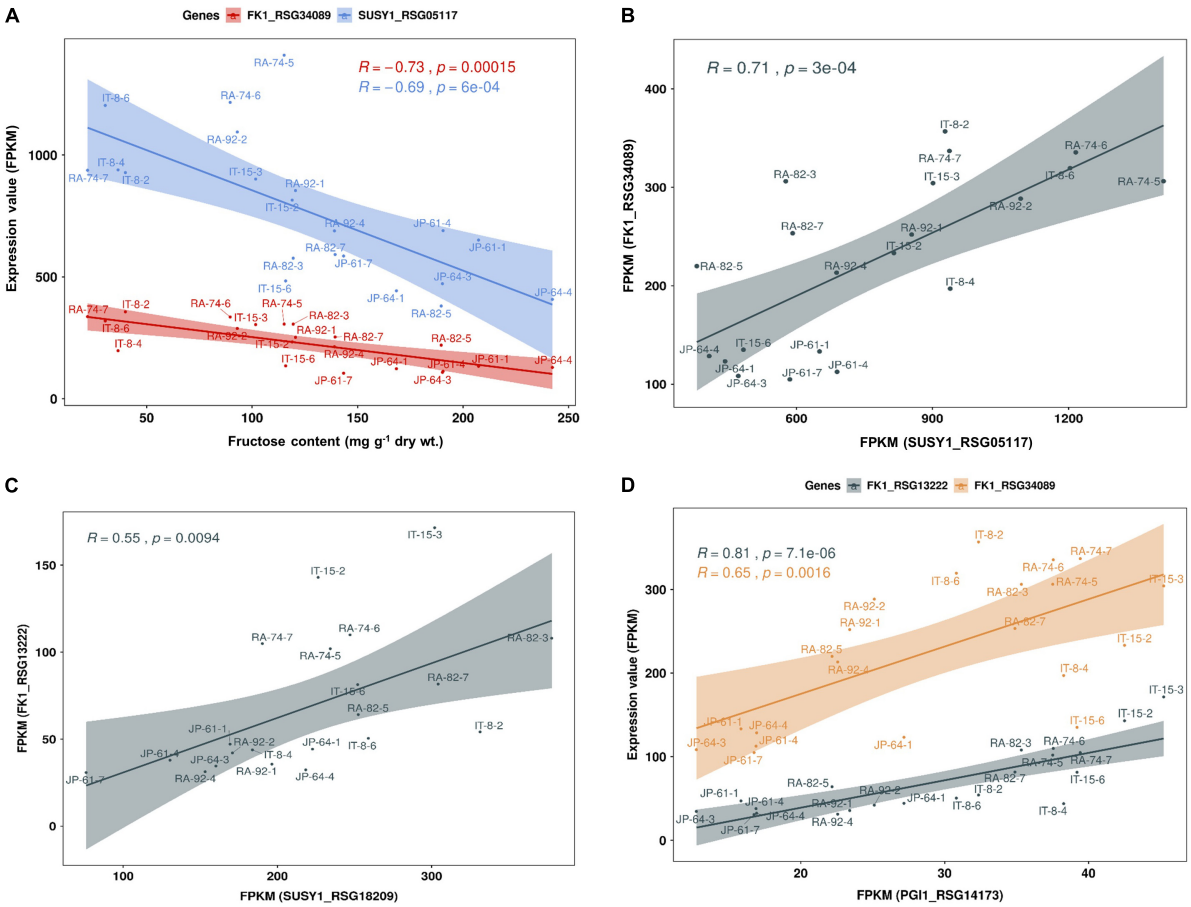

FIGURE 7 | Scatter plot of Pearson's correlation coefficient (*R*) between fructose content and expression level of genes involved in sucrose metabolism in seven radish roots. Data visualization performed using R program. **(A)** The fructose content has a negative correlation with the expression levels of SUSY1-encoding gene *RSG05117* and FK1-encoding gene *RSG34089*. **(B)** Expression level of *RSG05117* and *RSG34089* shows a positive correlation and **(C)** similar results are observed among their paralog genes, *RSG18209* and *RSG13222*. **(D)** Expression levels of the two FK1-encoding genes show a positive correlation with that of PGI1-encoding gene, *RSG14173*.

to the IT-8 roots (**Figure 5** and **Supplementary Figure 7**). These results supported our hypothesis that the high sucrose content in the roots of IT-8 could be transient.

Sucrose Transport Pathway in Radish Roots

A positive *R* score between the gene *RSG17864* encoding CWINV and the sucrose content, and the distinct expression of the SUC1-encoding genes *RSG49762* and *RSG21948* and STP1-encoding gene *RSG00099*, among the sugar transporters, could provide information on the transport pathway of sucrose in radish roots (**Figure 6B** and **Supplementary Figure 7**). Sucrose degradation by CWINV in the apoplast and the cellular uptake by the hexose transporters constitute the apoplasmic pathway, which is essential for the apoplastic phloem unloading of sucrose by SUC1 transporters (Julius et al., 2017). In this study, the expression levels of two SUC1-encoding genes showed a positive *R* score when compared to that of the STP1-encoding gene (**Supplementary Figure 7D**). These results suggest that sucrose transport from leaves to roots is majorly mediated by the apoplasmic pathway in radish. However, the high sucrose content in the IT-8 roots cannot be explained by the apoplastic pathway. A positive *R* score between the sucrose content and the CWINV-encoding gene was achieved when IT-8 was excluded (**Supplementary Figure 6**). Sucrose transport can also occur via the symplastic pathway via plasmodesmata (Giaquinta, 1979; Fugate et al., 2019) and this pathway is considered the most important for the sink organs in plants (Verbančič et al., 2018). Therefore, the symplastic pathway could be partially involved in the high sucrose content of IT-8 roots.

Membrane-Associated Sucrose Synthases and Cellulose Synthesis in Radish Roots

The high expression levels of SUSY1-encoding genes in JP-61 roots suggest that SUSY can act independently in the insoluble regions of cells (**Figures 5B,D**). SUSY exists in both soluble and insoluble forms, and the latter is mainly membrane-bound

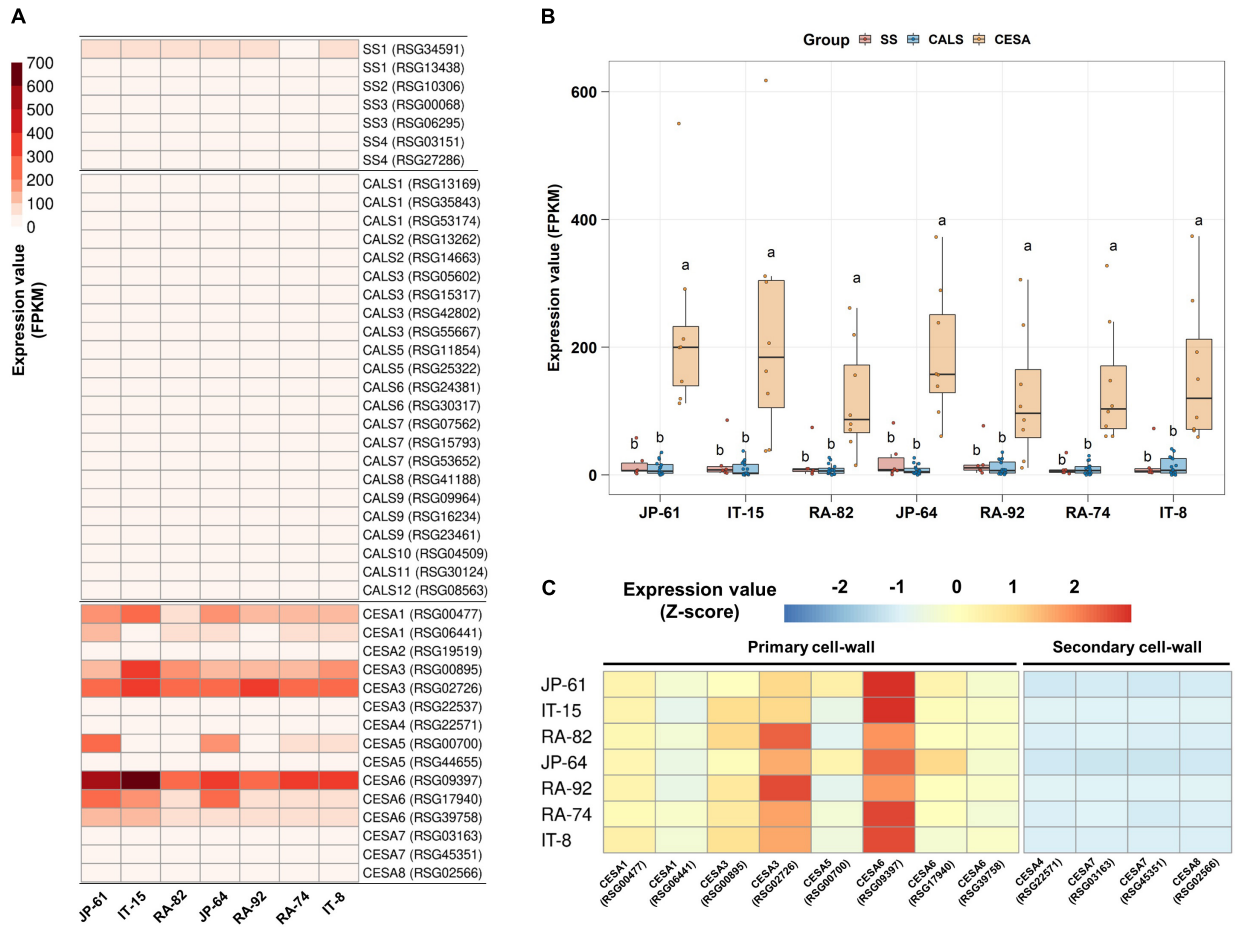

FIGURE 8 | Expression analysis of starch and cell wall synthesis related-genes in the seven radish roots. Data visualization performed using R program. **(A)** Analysis of heat map using FPKM. **(B)** Box plot analysis of genes involved in the synthesis of starch, callose, and primary cell wall. Genes below 2 FPKM were excluded among the tested accessions. Anova and Tukey HSD were used to reveal the differences between the integrated expression of the genes involved in this biosynthesis in each accession. Other letters in the plot indicate significant differences at $p < 0.05$. **(C)** Relative expression analysis of genes involved in the synthesis of primary and secondary cell walls. Expression values of individual genes in each accession were calculated using the Z-score.

(Coleman et al., 2009). SUSY1 protein was detected in the insoluble material of Arabidopsis (Barratt et al., 2009). SUSY antibodies cross-react in membrane fractions of *Zea mays*, *Oriza sativa*, and *Nicotiana tabacum* (Persia et al., 2008). The resulting UDP-G by SUSY is a precursor for the synthesis of callose and cellulose; and therefore, SUSY is directly responsible for cell wall synthesis in the membrane pool. There is an association between SUSY and the membranes during the cell wall synthesis in plants (Bieniawska et al., 2007; Endler and Persson, 2011; Rende et al., 2017; Verbančič et al., 2018). SUSY is active in the cell wall of tobacco pollen tubes and is involved in the synthesis of cellulose and callose (Persia et al., 2008). More than half of the total SUSY is tightly associated with the plasma membrane in cotton fibers, and these play a role in the direct transfer of carbon to CSC or CALS (Amor et al., 1995; Stein and Granot, 2019). The overexpression of SUSY enhanced cellulose synthesis in cotton, and in a spontaneously recessive shrunken kernel maize mutant (shrunken1); the lack of SUSY activity decreased the cell wall thickness during endosperm development in transgenic poplar plants (Endler and Persson, 2011; Rende et al., 2017). The SUSY overexpressing transgenic hybrid poplar (*Populus alba* × *grandidentata*) exhibited an increase in the cellulose content from 2 to 6% (Coleman et al., 2009). Membrane-associated SUSY plays a role in inducing carbon flow during cell wall synthesis (Baroja-Fernández et al., 2012). In this study, high expression levels of CESA-encoding genes were identified in seven radish roots, which indicated that SUSY could act in the membrane pool and was closely related to cellulose synthesis.

Alternative Pathway for Cellulose Synthesis in Radish Roots

SUSY plays an important role in cellulose synthesis; however, it is still unclear whether SUSY is essential for cellulose synthesis. Hybrid aspen (*Populus tremula* × *tremuloides*), which showed only 4% SUSY activity compared to that in the wild type, has normal cellulose biosynthesis (Rende et al., 2017). In Arabidopsis,

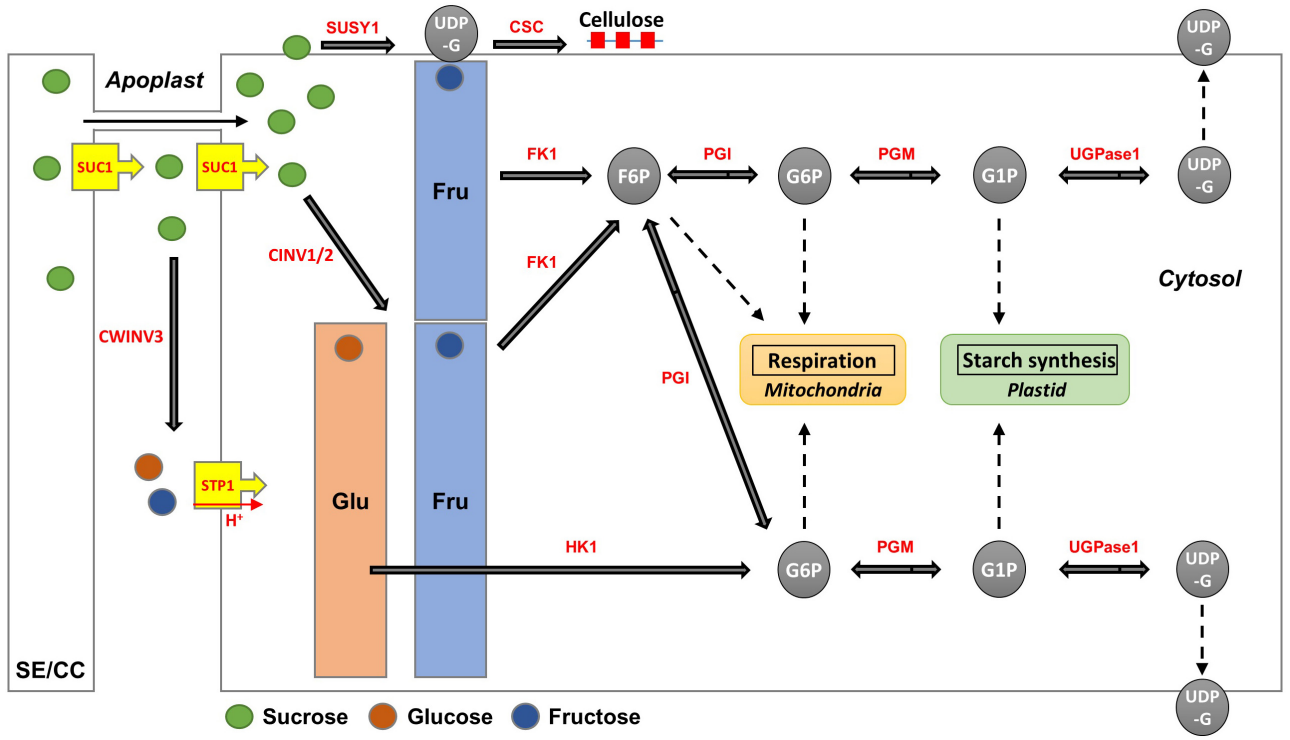

FIGURE 9 | Putative schematic diagram of hexose accumulation and sucrose metabolism in radish roots. The major enzymes (red color) are encoded by the following genes: SUC1 encoding *RSG21948* and *RSG49762*, CWINV3 encoding *RSG17864*, STP1 encoding *RSG00099*, CINV encoding *RSG32129* and *RSG26046*, SUSY1 encoding *RSG05117* and *RSG17864*, FK1 encoding *RSG13222* and *RSG34089*, HK1 encoding *RSG19301* and *RSG43310*, PGI encoding *RSG20307* and *RSG14173*, PGM encoding *RSG15383* and *RSG26796*, and UGPase encoding *RSG31848*. CSC for primary cell wall formation is constructed by CESAs encoding *RSG00477*, *RSG06441*, *RSG00895*, *RSG02726*, *RSG00700*, *RSG09397*, *RSG17940*, and *RSG39758*.

the SUSY1/SUSY2/SUSY3/SUSY4 quadruple mutant, excluding SUSY5 and SUSY6, which are specifically related to callose synthesis in phloem sieve elements, are morphologically normal and there is no difference in cellulose content, compared to that in the wild type (Bieniawska et al., 2007; Barratt et al., 2009). The remained SUSY activity in this quadruple mutant is controversial (Baroja-Fernández et al., 2012); however, Barratt et al., 2009 suggested that SUSY is not essential for cellulose synthesis, and an alternative pathway could completely supply UDP-G for cellulose synthesis, therefore, replacing the deficiency in SUSY activity (Barratt et al., 2009). An alternative pathway for UDP-G production in sucrose metabolism is achieved through CINV and UGPase (Verbančič et al., 2018). Unlike the SUSY quadruple mutant, double mutants of CINV1 and CINV2 show significant inhibition of root and shoot growth, starch loss in the root cap, and changes in sugar levels, in Arabidopsis (Barratt et al., 2009). Abnormal cellulose biosynthesis and a decrease in UDP-G production were identified in this Arabidopsis mutant (Barnes and Anderson, 2018). In a CINV mutant of *Lotus japonicas*, the growth was seriously affected; inhibition of CINV in hybrid aspen reduced the level of UDP-G and reduced the crystalline cellulose content of woody tissue (Rende et al., 2017; Verbančič et al., 2018). UGPase is a key enzyme that produces UDP-G for carbohydrate metabolism via an alternative pathway (Kleczkowski et al., 2004). An Arabidopsis UGPase1/UGPase2 double mutant showed a growth defect and decreased levels of CESA transcripts (Endler and Persson, 2011). These results imply that CINV and UGPase are more important than SUSY in supplying UDP-G for cellulose synthesis in plants. However, our study showed a strong relationship between cellulose synthesis and the transcription of SUSY1. Genes encoding CINV and UGPase showed low expression compared to that of the two SUSY1-encoding genes, while CESA-encoding genes, involved in cellulose synthesis, were expressed at remarkably high levels, compared with that of callose and starch synthases (**Supplementary Figure 5** and **Figure 8**). The *CINV* gene is highly expressed in 7-day-old radish roots, compared to that of the two *SUSY1* genes; however, the expression decreased in the 14-day-old radish roots. The two *SUSY1* genes were highly expressed, compared to that of the *CINV* gene in 14-day-old radish roots; and the strong expression of the two *SUSY1* genes was maintained during the development of radish roots (Mitsui et al., 2015). *CINV* seems to play an important role in the early stages of root development for UDP-G supply, and this role is likely to be replaced by *SUSY1* in radish roots. Sucrose catabolism by SUSY typically consumes less ATP than that by invertases, which is a reversible mechanism that allows feedback regulation. Therefore, this mechanism is advantageous in terms of energy conservation (Barratt et al., 2009).

Sugar-Sensing in Radish Roots

When sucrose is degraded by SUSY, the resulting fructose causes an increase in the concentration of fructose in the cytoplasm. High fructose concentrations inhibit SUSY and FK activities in plants (Granot et al., 2013; Stein and Granot, 2018). Inhibition of these genes by high fructose concentration could play a role in diverting carbon into metabolic pathways other than cytoplasmic glycolysis (Stein and Granot, 2018); however, this phenomenon needs to be explained in terms of photosynthetic regulation through hexose sugar sensing. Sugars, including glucose and fructose, could be used as substrates for HK, and they inhibit the expression of genes involved in photosynthesis, such as Rubisco and chlorophyll A/B binding protein (Rolland et al., 2002; Granot et al., 2013). Tomato mutants that inhibit FK activity in petioles and stems accumulate less sugar in the stem, because of the reduced sugar transportation from the leaves (Stein et al., 2016). In this study, fructose content was negatively correlated with the expression levels of SUSY1, FK1, and PGI-encoding genes (**Figure 6B**). The high fructose concentration in the cytoplasm could have inhibited the photosynthetic activity of the source leaves, therefore limiting the sucrose transport to sink roots. Therefore, the expression of genes encoding SUSY1, FK1, and PGI was reduced in radish roots. Sugar sensing is also caused by glucose levels (Rolland et al., 2002; Eveland and Jackson, 2012; Granot et al., 2013). In this study, the glucose content showed a negative *R* score with the expression levels of the SUC1-encoding genes, which suggests that the high concentration of glucose in the cytoplasm limits the apoplastic phloem unloading of sucrose, by inhibiting the expression of SUC1 (**Supplementary Figure 7C**).

Hexose Accumulation and Fructose Metabolism in Radish Roots

The apoplasmic pathway can lead to a high hexose concentration in the cytoplasm (Julius et al., 2017). CINV is an essential enzyme for plant growth (Barratt et al., 2009; Barnes and Anderson, 2018). Bieniawska et al. (2007) hypothesized that all sucrose in the roots would be ultimately mobilized by invertases (Bieniawska et al., 2007). These suggest the importance of invertases for hexose accumulation and plant growth. In radish roots, the high hexose content is probably caused by invertases. Considering that hexose accumulation in the cytoplasm could be caused by invertases, the fructose produced by SUSY could be recognized as excess fructose. This hypothesis is supported by the fact that SUSY and FK work together (Stein and Granot, 2018), and our results corroborate this (**Figures 7B,C**). Additionally, positive *R* scores were found among the genes encoding FK and PGI (**Figure 7D**). Therefore, it is believed that most of the fructose produced by SUSY activity is phosphorylated in radish roots. In this process, the fructose produced by invertases could also be phosphorylated by FK1, which could explain why the fructose content in the cytoplasm is lower than the glucose content in most radish accessions (**Figure 4**). The invertases are less active than SUSY; however, the invertase pathway can supply carbon to all parts of sucrose metabolism through HK, PGM, and UGPase (Bieniawska et al., 2007). The less prominent activity of these genes is probably because SUSY is more efficient at carbon partitioning. In summary, we present a putative schematic diagram linking sugar content and sucrose metabolism in radish roots (**Figure 9**).

In conclusion, glucose is the dominant sugar in the radish roots. Fructose content correlated with the length, weight, and color phenotypes of roots. Two SUSY-encoding genes are highly expressed and are believed to be involved in cellulose synthesis. A high hexose content was possibly achieved via the apoplastic pathway. The significant *R* scores between the genes encoding SUSY and FK suggest that most of the fructose resulting from SUSY is phosphorylated. Sucrose was metabolized rather than stored, and cellulose was the main carbon sink in the radish roots. Additional molecular genetic studies are required to determine the correlation between phenotypic characteristic and gene expression. We believe that, these results might improve the overall understanding of sucrose metabolism in plants and provide information on important genes for developing new radish varieties.

DATA AVAILABILITY STATEMENT

The original contributions presented in the study are publicly available. This data can be found here: NCBI repository, accession number: PRJNA650223 (https://www.ncbi.nlm.nih.gov/bioproject/650223).

AUTHOR CONTRIBUTIONS

SML and S-JK contributed to the conception and design of the study. JSK provided the material for the study and contributed to the revision of the manuscript. M-SS collected materials and classified resources. SYW contributed to the review of the manuscript. J-NK wrote the first draft of the manuscript. All authors contributed to manuscript revision, read, and approved the submitted version.

FUNDING

This research was supported by the "National Institute of Agricultural Sciences" (Project Nos. PJ0125152019 and PJ0150352020), Rural Development Administration, Republic of Korea.

ACKNOWLEDGMENTS

We would like to thank Editage (www.editage.co.kr) for English language editing.

SUPPLEMENTARY MATERIAL

The Supplementary Material for this article can be found online at: https://www.frontiersin.org/articles/10.3389/fpls.2021.716782/full#supplementary-material

REFERENCES

Amor, Y., Haigler, C. H., Johnson, S., Wainscott, M., and Delmer, D. P. (1995). A membrane-associated form of sucrose synthase and its potential role in synthesis of cellulose and callose in plants. *Proc. Natl. Acad. Sci. U.S.A.* 92, 9353–9357. doi: 10.1073/pnas.92.20.9353

Barnes, W. J., and Anderson, C. T. (2018). Cytosolic invertases contribute to cellulose biosynthesis and influence carbon partitioning in seedlings of *Arabidopsis thaliana*. *Plant J.* 94, 956–974. doi: 10.1111/tpj.13909

Baroja-Fernández, E., Muñoz, F. J., Li, J., Bahaji, A., Almagro, G., Montero, M., et al. (2012). Sucrose synthase activity in the sus1/sus2/sus3/sus4 *Arabidopsis* mutant is sufficient to support normal cellulose and starch production. *Proc. Natl. Acad. Sci. U.S.A.* 109, 321–326. doi: 10.1073/pnas.1117099109

Barratt, D. P., Derbyshire, P., Findlay, K., Pike, M., Wellner, N., Lunn, J., et al. (2009). Normal growth of *Arabidopsis* requires cytosolic invertase but not sucrose synthase. *Proc. Natl. Acad. Sci. U.S.A.* 106, 13124–13129. doi: 10.1073/pnas.0900689106

Bieniawska, Z., Paul Barratt, D., Garlick, A. P., Thole, V., Kruger, N. J., Martin, C., et al. (2007). Analysis of the sucrose synthase gene family in *Arabidopsis*. *Plant J.* 49, 810–828. doi: 10.1111/j.1365-313X.2006.03011.x

Büttner, M. (2007). The monosaccharide transporter (-like) gene family in *Arabidopsis*. *FEBS Lett.* 581, 2318–2324. doi: 10.1016/j.febslet.2007.03.016

Chen, L. Q. (2014). SWEET sugar transporters for phloem transport and pathogen nutrition. *New Phytol.* 201, 1150–1155. doi: 10.1111/nph.12445

Coleman, H. D., Yan, J., and Mansfield, S. D. (2009). Sucrose synthase affects carbon partitioning to increase cellulose production and altered cell wall ultrastructure. *Proc. Natl. Acad. Sci. U.S.A.* 106, 13118–13123. doi: 10.1073/pnas.0900188106

Endler, A., and Persson, S. (2011). Cellulose synthases and synthesis in *Arabidopsis*. *Mol. Plant*. 4, 199–211. doi: 10.1093/mp/ssq079

Eom, J.-S., Chen, L.-Q., Sosso, D., Julius, B. T., Lin, I., Qu, X.-Q., et al. (2015). SWEETs, transporters for intracellular and intercellular sugar translocation. *Curr. Opin. Plant Biol.* 25, 53–62. doi: 10.1016/j.pbi.2015.04.005

Eveland, A. L., and Jackson, D. P. (2012). Sugars, signalling, and plant development. *J. Exp. Bot.* 63, 3367–3377. doi: 10.1093/jxb/err379

Freixes, S., Thibaud, M. C., Tardieu, F., and Muller, B. (2002). Root elongation and branching is related to local hexose concentration in *Arabidopsis thaliana* seedlings. *Plant Cell Environ.* 25, 1357–1366.

Fugate, K. K., Eide, J. D., Martins, D. N., Grusak, M. A., Deckard, E. L., and Finger, F. L. (2019). Colocalization of sucrose synthase expression and sucrose storage in the sugarbeet taproot indicates a potential role for sucrose catabolism in sucrose accumulation. *J. Plant Physiol.* 240:153016. doi: 10.1016/j.jplph.2019.153016

Giaquinta, R. T. (1979). Sucrose translocation and storage in the sugar beet. *Plant Physiol.* 63, 828–832. doi: 10.1104/pp.63.5.828

Granot, D., David-Schwartz, R., and Kelly, G. (2013). Hexose kinases and their role in sugar-sensing and plant development. *Front. Plant Sci.* 4:44. doi: 10.3389/fpls.2013.00044

Hara, M., Oki, K., Hoshino, K., and Kuboi, T. (2003). Enhancement of anthocyanin biosynthesis by sugar in radish (*Raphanus sativus*) hypocotyl. *Plant Sci.* 164, 259–265. doi: 10.1016/S0168-9452(02)00408-9

Hara, M., Oki, K., Hoshino, K., and Kuboi, T. (2004). Effects of sucrose on anthocyanin production in hypocotyl of two radish (*Raphanus sativus*) varieties. *Plant Biotechnol. J.* 21, 401–405.

Hedrich, R., Sauer, N., and Neuhaus, H. E. (2015). Sugar transport across the plant vacuolar membrane: nature and regulation of carrier proteins. *Curr. Opin. Plant Biol.* 25, 63–70. doi: 10.1016/j.pbi.2015.04.008

International Board for Plant Genetic Resources, and Commission of the European Communities (1990). *Descriptors for Brassica and Raphanus*. Rome: Bioversity International.

Julius, B. T., Leach, K. A., Tran, T. M., Mertz, R. A., and Braun, D. M. (2017). Sugar transporters in plants: new insights and discoveries. *Plant Cell Physiol.* 58, 1442–1460. doi: 10.1093/pcp/pcx090

Jung, B., Ludewig, F., Schulz, A., Meißner, G., Wöstefeld, N., Flügge, U.-I., et al. (2015). Identification of the transporter responsible for sucrose accumulation in sugar beet taproots. *Nat. Plants* 1:14001. doi: 10.1038/NPLANTS.2014.1

Kang, J.-N., Won, S. Y., Seo, M.-S., Lee, J., Lee, S. M., Kwon, S.-J., et al. (2020). Induction of glucoraphasatin biosynthesis genes by MYB29 in radish (*Raphanus sativus L.*) roots. *Int. J. Mol. Sci.* 21:5721. doi: 10.3390/ijms21165721

Kleczkowski, L. A., Geisler, M., Ciereszko, I., and Johansson, H. (2004). UDP-glucose pyrophosphorylase. An old protein with new tricks. *Plant Physiol.* 134, 912–918. doi: 10.1104/pp.103.036053

Liepman, A. H., and Cavalier, D. (2012). The cellulose synthase-like A and cellulose synthase-like C families: recent advances and future perspectives. *Front. Plant Sci.* 3:109. doi: 10.3389/fpls.2012.00109

McCormick, A., Watt, D., and Cramer, M. (2009). Supply and demand: sink regulation of sugar accumulation in sugarcane. *J. Exp. Bot.* 60, 357–364. doi: 10.1093/jxb/ern310

Mitsui, Y., Shimomura, M., Komatsu, K., Namiki, N., Shibata-Hatta, M., Imai, M., et al. (2015). The radish genome and comprehensive gene expression profile of tuberous root formation and development. *Sci. Rep.* 5:10835. doi: 10.1038/srep10835

Noronha, H., Silva, A., Dai, Z., Gallusci, P., Rombolà, A. D., Delrot, S., et al. (2018). A molecular perspective on starch metabolism in woody tissues. *Planta* 248, 559–568. doi: 10.1007/s00425-018-2954-2

Novaes, E., Kirst, M., Chiang, V., Winter-Sederoff, H., and Sederoff, R. (2010). Lignin and biomass: a negative correlation for wood formation and lignin content in trees. *Plant Physiol.* 154, 555–561. doi: 10.1104/pp.110.161281

Peng, M., Hudson, D., Schofield, A., Tsao, R., Yang, R., Gu, H., et al. (2008). Adaptation of *Arabidopsis* to nitrogen limitation involves induction of anthocyanin synthesis which is controlled by the NLA gene. *J. Exp. Bot* 59, 2933–2944.

Persia, D., Cai, G., Del Casino, C., Faleri, C., Willemse, M. T., and Cresti, M. (2008). Sucrose synthase is associated with the cell wall of tobacco pollen tubes. *Plant Physiol.* 147, 1603–1618. doi: 10.1104/pp.108.115956

Rende, U., Wang, W., Gandla, M. L., Jönsson, L. J., and Niittylä, T. (2017). Cytosolic invertase contributes to the supply of substrate for cellulose biosynthesis in developing wood. *New Phytol.* 214, 796–807. doi: 10.1111/nph.14392

Rolland, F., Moore, B., and Sheen, J. (2002). Sugar sensing and signaling in plants. *Plant Cell* 14, S185–S205. doi: 10.1105/tpc.010455

Rouhier, H., and Usuda, H. (2001). Spatial and temporal distribution of sucrose synthase in the radish hypocotyl in relation to thickening growth. *Plant Cell Physiol.* 42, 583–593. doi: 10.1093/pcp/pce071

Seo, M.-S., Chung, J.-H., Park, B.-S., and Kim, J. S. (2018). Analysis of sugars content by genotypes in 82 radish (*Raphanus sativus L.*). *Korean J. Plant Res.* 31, 453–465. doi: 10.7732/kjpr.2018.31.5.453

Stein, O., Damari-Weissler, H., Secchi, F., Rachamilevitch, S., German, M. A., Yeselson, Y., et al. (2016). The tomato plastidic fructokinase Sl FRK 3 plays a role in xylem development. *New Phytol.* 209, 1484–1495. doi: 10.1111/nph.13705

Stein, O., and Granot, D. (2018). Plant fructokinases: evolutionary, developmental, and metabolic aspects in sink tissues. *Front. Plant Sci.* 9:339. doi: 10.3389/fpls.2018.00339

Stein, O., and Granot, D. (2019). An overview of sucrose synthases in plants. *Front. Plant Sci.* 10:95. doi: 10.3389/fpls.2019.00095

Stokes, M. E., Chattopadhyay, A., Wilkins, O., Nambara, E., and Campbell, M. M. (2013). Interplay between sucrose and folate modulates auxin signaling in *Arabidopsis*. *Plant Physiol.* 162, 1552–1565. doi: 10.1104/pp.113.215095

Verbančič, J., Lunn, J. E., Stitt, M., and Persson, S. (2018). Carbon supply and the regulation of cell wall synthesis. *Mol. Plant* 11, 75–94. doi: 10.1016/j.molp.2017.10.004

Wang, J., Nayak, S., Koch, K., and Ming, R. (2013). Carbon partitioning in sugarcane (*Saccharum species*). *Front. Plant Sci.* 4:201. doi: 10.3389/fpls.2013.00201

Wang, W., Zhou, H., Ma, B., Owiti, A., Korban, S. S., and Han, Y. (2016). Divergent evolutionary pattern of sugar transporter genes is associated with the difference

in sugar accumulation between grasses and eudicots. *Sci. Rep.* 6:29153. doi: 10.1038/srep29153

Xiong, Y., McCormack, M., Li, L., Hall, Q., Xiang, C., and Sheen, J. (2013). Glucose–TOR signalling reprograms the transcriptome and activates meristems. *Nature* 496, 181–186. doi: 10.1038/nature12030

Yi, G., Lim, S., Chae, W. B., Park, J. E., Park, H. R., Lee, E. J., et al. (2016). Root glucosinolate profiles for screening of radish (Raphanus sativus L.) genetic resources. *J. Agric. Food Chem.* 64, 61–70.

Yu, R., Xu, L., Zhang, W., Wang, Y., Luo, X., Wang, R., et al. (2016). De novo taproot transcriptome sequencing and analysis of major genes involved in sucrose metabolism in radish (*Raphanus sativus L.*). *Front. Plant Sci.* 7:585. doi: 10.3389/fpls.2016.00585

Zhang, K., Wu, Z., Tang, D., Luo, K., Lu, H., Liu, Y., et al. (2017). Comparative transcriptome analysis reveals critical function of sucrose metabolism related-enzymes in starch accumulation in the storage root of sweet potato. *Front. Plant Sci.* 8:914. doi: 10.3389/fpls.2017.00914

Conflict of Interest: The authors declare that the research was conducted in the absence of any commercial or financial relationships that could be construed as a potential conflict of interest.

frontiers in Plant Science

ORIGINAL RESEARCH
published: 22 December 2021
doi: 10.3389/fpls.2021.758933

Proteogenic Dipeptides Are Characterized by Diel Fluctuations and Target of Rapamycin Complex-Signaling Dependency in the Model Plant *Arabidopsis thaliana*

Maria Juliana Calderan-Rodrigues[1†], Marcin Luzarowski[1†], Carolina Cassano Monte-Bello[1], Romina I. Minen[2], Boris M. Zühlke[1,3], Zoran Nikoloski[1,3], Aleksandra Skirycz[1,2] and Camila Caldana[1*]*

[1] Max Planck Institute of Molecular Plant Physiology, Potsdam, Germany, [2] Boyce Thompson Institute, Ithaca, NY, United States, [3] Institute for Biochemistry and Biology, University of Potsdam, Potsdam, Germany

OPEN ACCESS

Edited by:
Deyu Xie,
North Carolina State University,
United States

Reviewed by:
Jacob Oliver Brunkard,
University of California, Berkeley,
United States
Homero Reyes De La Cruz,
Universidad Michoacana de San Nicolás de Hidalgo, Mexico

***Correspondence:**
Camila Caldana
caldana@mpimp-golm.mpg.de
Aleksandra Skirycz
as4258@cornell.edu

[†] These authors have contributed equally to this work

Specialty section:
This article was submitted to Plant Metabolism and Chemodiversity, a section of the journal Frontiers in Plant Science

Received: 15 August 2021
Accepted: 11 November 2021
Published: 22 December 2021

Citation:
Calderan-Rodrigues MJ, Luzarowski M, Monte-Bello CC, Minen RI, Zühlke BM, Nikoloski Z, Skirycz A and Caldana C (2021) Proteogenic Dipeptides Are Characterized by Diel Fluctuations and Target of Rapamycin Complex-Signaling Dependency in the Model Plant Arabidopsis thaliana. Front. Plant Sci. 12:758933. doi: 10.3389/fpls.2021.758933

As autotrophic organisms, plants capture light energy to convert carbon dioxide into ATP, nicotinamide adenine dinucleotide phosphate (NADPH), and sugars, which are essential for the biosynthesis of building blocks, storage, and growth. At night, metabolism and growth can be sustained by mobilizing carbon (C) reserves. In response to changing environmental conditions, such as light-dark cycles, the small-molecule regulation of enzymatic activities is critical for reprogramming cellular metabolism. We have recently demonstrated that proteogenic dipeptides, protein degradation products, act as metabolic switches at the interface of proteostasis and central metabolism in both plants and yeast. Dipeptides accumulate in response to the environmental changes and act *via* direct binding and regulation of critical enzymatic activities, enabling C flux distribution. Here, we provide evidence pointing to the involvement of dipeptides in the metabolic rewiring characteristics for the day-night cycle in plants. Specifically, we measured the abundance of 13 amino acids and 179 dipeptides over short- (SD) and long-day (LD) diel cycles, each with different light intensities. Of the measured dipeptides, 38 and eight were characterized by day-night oscillation in SD and LD, respectively, reaching maximum accumulation at the end of the day and then gradually falling in the night. Not only the number of dipeptides, but also the amplitude of the oscillation was higher in SD compared with LD conditions. Notably, rhythmic dipeptides were enriched in the glucogenic amino acids that can be converted into glucose. Considering the known role of Target of Rapamycin (TOR) signaling in regulating both autophagy and metabolism, we subsequently investigated whether diurnal fluctuations of dipeptides levels are dependent on the TOR Complex (TORC). The *Raptor1b* mutant (*raptor1b*), known for the substantial reduction of TOR kinase activity, was characterized by the augmented accumulation of dipeptides, which is especially pronounced under LD conditions. We were particularly intrigued by the group of 16 dipeptides, which, based on their oscillation under SD conditions and accumulation

in *raptor1b*, can be associated with limited C availability or photoperiod. By mining existing protein-metabolite interaction data, we delineated putative protein interactors for a representative dipeptide Pro-Gln. The obtained list included enzymes of C and amino acid metabolism, which are also linked to the TORC-mediated metabolic network. Based on the obtained results, we speculate that the diurnal accumulation of dipeptides contributes to its metabolic adaptation in response to changes in C availability. We hypothesize that dipeptides would act as alternative respiratory substrates and by directly modulating the activity of the focal enzymes.

Keywords: dipeptide, diel cycle, metabolism, TOR signaling, protein-metabolite interactions, carbon limitation, amino acid

INTRODUCTION

In a wide range of organisms, photoperiod length influences several vital events such as growth rate, reproduction, disease progression, and migration. The coordination of these internal events with the predictable photoperiod changes can optimize the use of resources, such as food availability and environmental conditions (Dardente et al., 2014). In plants, the length of light and night periods affect the following: biomass accumulation and growth (Nozue et al., 2007; Khoeyi et al., 2012; Doust, 2017), flowering (Garner and Allard, 1920; Yanovsky and Kay, 2002; Salazar et al., 2009), and cell wall composition and C allocation (Sulpice et al., 2014; Mengin et al., 2017; Alves et al., 2019). The adaptation to variation in light exposure is a competitive asset that allows plants to be tuned with foreseeable environmental changes following seasonal transitions. Moreover, plant development under different photoperiods establishes distinct internal dynamics by adjusting the metabolism to available sunlight (Seaton et al., 2018). This is particularly relevant for plants from high latitudes, as the growing season is getting longer due to climate changes, and thus, adaptation to the dynamic environment can be crucial in sustaining productivity [reviewed by Piao et al. (2019)].

Plants rely on the light supply to capture energy to convert carbon dioxide into ATP, nicotinamide adenine dinucleotide phosphate (NADPH), and sugars, which are essential for the biosynthesis of building blocks, cell proliferation, biomass accumulation, and reproductive fitness. In long photoperiods (LD) (16 h light/8 h dark), Arabidopsis transcript and protein levels match accelerated growth and have a faster transition to flowering, in comparison to short days (SD) (8 h light/16 h dark) (Baerenfaller et al., 2015). At night, plant growth is supplied by C skeletons released from the mobilization of transient starch that is synthesized during the light period (Smith and Stitt, 2007). Reasonably, the rates of C allocation into starch during the day are faster and its mobilization during the night is slower in SD condition, allowing this polysaccharide to last until the next light period (Sulpice et al., 2014; Mengin et al., 2017). The diel pattern of starch turnover optimizes growth under C limitation, in which, almost all of these compounds accumulated during the day were used to supply growth while avoiding C starvation, protein catabolism, and growth impairment caused by a premature C exhaustion at night (Moraes et al., 2019 and references therein). Starch accumulation pattern is more dependent on the duration of the light period rather than light intensity since shorter periods of light allocate a higher proportion of photosynthate into starch, whereas when irradiance fluctuated, this change was milder. The higher rate of starch accumulation in SD to sustain metabolism and growth at the longer nights leaves less C available for growth in the light period (Mengin et al., 2017), characterizing this photoperiod to display a smaller proportion of C that is available for growth compared with LD. Thus, when we mention C limitation or C restriction throughout the text related to our experiments, they are considered in terms of C mobilization to fuel growth rather than the photosynthetic rate. Both the decreased extent of diurnal turnover of C reserves and the transcriptional daytime changes in LD suggested that this photoperiod does not need tight energy management as SD (Baerenfaller et al., 2015). In addition to starch, autophagy also contributes in generating energy during longer night periods of SD under diurnal low light intensity, thus providing an alternative energy supply source as amino acids from protein catabolism (Izumi et al., 2013). Accordingly, transcripts and metabolic data related to autophagy increased during the dark even when the photoperiod comprised 14 h light, and had further augmented in the extended night (Usadel et al., 2008). Moreover, under conditions of starvation, like the one faced by the starchless *phosphoglucomutase* mutant (*pgm*) grown under SD, the rates of protein degradation increased rapidly from 4 h night onward, establishing a connection between C availability and protein degradation (Ishihara et al., 2015). Further, small Arabidopsis accessions cultivated in SD had presented higher ribosome synthesis while large accessions showed evidence of even protein degradation at night, indicating that the C-efficiency of growth would be decreased due to a higher energy cost in small accessions (Ishihara et al., 2017).

The "Target of Rapamycin" (TOR) kinase is an evolutionarily conserved key component in the network-regulating energy sensing into growth-mediated processes. The balance control between anabolism (e.g., biosynthesis of protein, lipids, and nucleotides) and catabolism (e.g., autophagy) in response to environmental cues are among the main functions of this pathway (Liu and Sabatini, 2020). The TOR complex (TORC) controls a plethora of metabolic pathways integrating energy status, like C and nitrogen (N) balance into biosynthetic growth in photosynthetic organisms (Caldana et al., 2013, 2019;

Dobrenel et al., 2016; Jüppner et al., 2018; Monte-Bello et al., 2018; Mubeen et al., 2019; da Silva et al., 2021). TOR stimulates cell proliferation through light and its derived signals such as sugars and hormones (Pfeiffer et al., 2016; Li et al., 2017; Mohammed et al., 2018). As in other organisms, plant TORC is an autophagy repressor by inhibiting AuTophaGy (ATG) genes (Liu and Bassham, 2010) and possibly binding to the autophagy initiators ATG1-ATG13 (Van Leene et al., 2019). When purine levels are reduced, TOR activity is decreased into Arabidopsis T2 family endoribonuclease RNS2 (*rns2-2*) mutant, which in turn activates autophagy, suggesting that TOR mediates this catabolic process by responding to the levels of nucleotides to restore homeostasis (Kazibwe et al., 2020). As a consequence, the autophagy-induced recycling of nutrients can reactivate the TOR pathway, while nucleotides promote TOR activity (Busche et al., 2021).

In most eukaryotes, the TOR kinase is assembled into two distinct protein complexes, known as TORC1 and TORC2, which shared the same catalytic subunit TOR kinase and the regulatory subunit Lethal with Sec Thirteen8 (LST8). Their precise substrate recruitment and the physiological and biochemical distinction are mainly attributed to the regulatory subunits, the Regulatory-associated protein of TOR (RAPTOR) and Rapamycin-insensitive companion of mammalian target of rapamycin (RICTOR) in TORC1 and TORC2, respectively. In mammals, RAPTOR was identified as a mediator of the mTOR activity *in vivo* (Hara et al., 2002), then forming a nutrient-sensitive complex. Under poor nutrient conditions, RAPTOR and mTOR tight interaction destabilizes the complex and leads to reduced kinase activity (Kim et al., 2002). In plants, only TORC1 components have been so far identified (Menand et al., 2002; Mahfouz et al., 2006; Agredano-Moreno et al., 2007; Maegawa et al., 2015). However, the lack of viability or lethality of *tor* mutants (Menand et al., 2002; Ren et al., 2011) hampered research on the TOR pathway-mediated regulation in plants. To better understand TOR roles in plant development, the *raptor1b* T-DNA KO lines that displayed a strong reduction of TOR kinase activity, which were determined by assaying the ribosomal protein kinase 6 (S6K) activity (Salem et al., 2018), have been previously characterized. As other mutants from the complex (Moreau et al., 2012), *raptor1b* plants presented impaired development under LD photoperiod, such as massive changes in central C and N metabolism, increased levels of starch, free amino acids, and induced autophagy (Salem et al., 2017, 2018).

The small-molecule regulation of enzymatic activities is critical for the reprogramming of cellular metabolism in response to the changing environments across life kingdoms. Amino acids were proven to be activators of the TOR pathway-mediated impact on respiratory levels at night in plants (O'Leary et al., 2020), aside from restoring TOR activity under nitrogen starvation (Liu et al., 2021). Interestingly, the feeding of leukemia stem cells with specific dipeptides affects mTOR activity and nutrient signaling (Naka et al., 2015). Moreover, cyclodipeptides released by bacteria activated the TOR pathway and increased growth in plants (Corona-Sánchez et al., 2019; González-López et al., 2021). Recent system-wide characterization of the protein-protein-metabolite complexes in the model plant *Arabidopsis thaliana* provided evidence supporting the role of proteinogenic dipeptides in the regulation of enzymatic activities and C flux distribution (Veyel et al., 2017, 2018). For instance, an acidic dipeptide Tyr-Asp inhibits the activity of a key glycolytic enzyme glyceraldehyde 3-phosphate dehydrogenase, and as consequence, redirects glycolytic triose-phosphates toward the pentose phosphate pathway (PPP) and NADPH production (Moreno et al., 2021). Importantly, Tyr-Asp supplementation improved tobacco and Arabidopsis growth performance measured under oxidative stress conditions. Consistent with their role in metabolic adaptation to stress, acidic dipeptides, such as Tyr-Asp, accumulated in response to heat, dark, and microbial infection (Strehmel et al., 2017), and this observed accumulation is autophagy-dependent (Thirumalaikumar et al., 2020). Moreover, Glyceraldehyde 3-phosphate dehydrogenase (GAPDH) is not the sole glycolytic enzyme affected by dipeptides. For example, the inhibition of Arabidopsis phosphoenolpyruvate carboxykinase activity by the group of branched-chain amino acid (BCAA) containing dipeptides, but not by Tyr-Asp, points to a multisite regulation of glycolytic/gluconeogenic pathway by dipeptides. Proteolysis is the main source of dipeptides biogenesis, and autophagy has been addressed as the mechanism through which dipeptides are generated in plants under heat stress (Thirumalaikumar et al., 2020).

The emerging role of dipeptides as important players in shifting C metabolism has prompted us to investigate whether changes in photoperiod, light intensity, and thus C supply, would affect the accumulation of these signaling molecules along the diel cycle in *A. thaliana*. We found that a higher number of dipeptides have their levels oscillating under SD (8 h light/16 h dark, 20°C/16°C, 180 μmol m^{-2} s^{-1}) than LD (16 h light, 8 h dark, 20°C/16°C, 120 μmol m^{-2} s^{-1}). To get further insights into the role of these dipeptides in rewiring metabolism under SD, we took the advantage of the mutant involved in energy sensing, *raptor1b*, which presents a photoperiod-condition phenotype. The greater the C availability the stronger is the metabolic phenotype (Deprost et al., 2007; Moreau et al., 2012; Salem et al., 2018), at the same time that de-repress autophagy machinery (Salem et al., 2018). As expected, when compared with Col-0, *raptor1b* presents a larger number of dipeptides with altered levels under LD. By focusing on dipeptides that present an oscillating pattern along the diel cycle in Col-0 only under SD conditions, and always enhanced levels in *raptor1b*, we have identified a group of 16 dipeptides that can be possibly associated with C-restricted supply. By mining existing protein-metabolite interaction data (Zühlke et al., 2021), we delineated putative protein interactors for a representative dipeptide Pro-Gln. The obtained list included enzymes of C and amino acid metabolism, which are also linked to the TORC-mediated metabolic network. If taken together, our data strengthen published findings (Thirumalaikumar et al., 2020; Luzarowski et al., 2021; Moreno et al., 2021), supporting the role of dipeptides in rewiring metabolism under nutrient restrictions, which needs to be further explored.

MATERIALS AND METHODS

Plant Material and Growth Conditions

Plants of *Arabidopsis thaliana Columbia-0* (Col-0) and *rb10* (*raptor1b* T-DNA KO line; SALK_101990) were grown in soil in a controlled environment chamber in SD (8 h light/16 h dark, 20°C/16°C, 180 μmol m^{-2} s^{-1}) and LD (16 h light, 8 h dark, 20°C/16°C, 120 μmol m^{-2} s^{-1}) photoperiods under a relative humidity of 75% (see **Figure 1** for details on experimental design). After 30 days of growth, whole rosettes were harvested every 4 h from Zeitgeber time (ZT) 0 and additional time points were added during the light- dark transitions (ZT 1, 2, 23, and 1 h before the start of the dark phase, i.e., 7 or 15, depending on the photoperiod) and were immediately frozen in liquid nitrogen. Frozen plant tissue was ground into a fine powder and stored at −80°C until use. Five biological replicates consisted of pools were composed of 15 or 5 plants harvested for SD and LD, respectively.

For the enzymatic measurements (see section "Enzymatic Activity Assay"), *A. thaliana* Col-0 plants were grown under a 12 h light/12 h dark diel cycle in a chamber at 23°C and with a light intensity of 100 μmol m^2 s^{-1}. Rosette leaves from 4-week-old plants were harvested 2 h into light or 2 h into dark, and rapidly frozen with liquid nitrogen. Plant material was ground into a fine powder and stored at −80°C until use.

Metabolite Analysis

Metabolites were extracted from 50 mg of fresh rosette material following the method described by Giavalisco et al. (2011), with modifications. A volume of 1 mL of the precooled methyl-tert-butyl-ether (MTBE) extraction mixture (−20°C) was added to the homogenized tissues. Subsequently, the tubes were then homogenized using vortex and incubated in a shaker (100 rpm, 10 min, 4°C), followed by 10 min of sonication. This extraction allows the separation between the polar and apolar phases. For this separation, 500 μL of the methanol: water (1:3/v:v) mixture was added to each tube and the samples were mixed in the vortex (5 min). The samples were centrifuged (20,000 *g*, 10 min, 4°C), harvested, concentrated (SpeedVac), and stored at −80°C until liquid chromatography-mass spectrometry (LC-MS) analysis. Two volumes of the polar phase were used for liquid chromatography (LC) analyses.

The dried aqueous phase was solubilized in 200 μL of high-performance LC (HPLC)-grade water and sonicated for 5 min using an ultrasonication bath. Samples were centrifuged for 10 min at 20,800 *g*, RT. The supernatant was transferred to the UPLC glass vial. A 3 μl of polar metabolite extract was separated using an ultra-performance LC (UPLC) equipped with an HSS T3 C18 reversed-phase column at a 400 μl/min flow rate. Mass spectra were acquired using an Exactive mass spectrometer in positive ionization mode (Giavalisco et al., 2011). Mobile phase solutions were prepared as follows: buffer A (0.1% formic acid in H2O) and buffer B (0.1% formic acid in ACN). The following gradients were used for metabolite separation: 1 min 1% LC-MS mobile phase buffer B, 11 min linear gradient from 1 to 40% buffer B, 13 min linear gradient from 40% to 70% buffer B, then 15 min linear gradient from 70 to 99% buffer B, and held a 99% buffer B concentration until 16 min. Starting from 17 min, a linear gradient from 99 to 1% buffer B was used. The column was re-equilibrated for 3 min with 1% buffer B before the next measurement was performed. Mass spectra were acquired using the following settings: mass range from 100 to 1,500 *m/z*, resolution set to 25,000, loading time restricted to 100 ms, AGC target set to $1e^6$, capillary voltage to 3 kV with a sheath gas flow, and auxiliary gas value of 60 and 20, respectively. The capillary temperature was set to 250°C and skimmer voltage to 25 V.

Data Processing

Data were processed using Expressionist Refiner MS 14.0.5 (Genedata AG, Basel, Switzerland) as previously described (Veyel et al., 2017; Sokolowska et al., 2019). Minor changes were applied to the workflow: chromatogram alignment (RT search interval 0.5 min) and peak detection (minimum peak size 0.03 min, gap/peak ratio 50%, smoothing window 5 points, center computation by intensity-weighted method with the threshold at 70%, boundary determination using inflection points). Detailed instructions for using the software can be found in prior work (Sokolowska et al., 2019).

The processing of 95 and 105 samples, collected from both SD and LD conditions, resulted in the detection of 135,294 and 245,041 peaks (mass features), respectively. Subsequently, mass features were filtered for these with intensity above 10,000 presents in at least 32 and 29% of the samples at SD and LD photoperiods, respectively. Intensities of remaining mass features were medianly normalized and annotated using the in-house reference compound library as described below.

Annotation

Mass features described by RT and m/z were matched to in-house libraries of authentic reference compounds, allowing a 0.005 Da mass and dynamic retention time deviation (maximum 0.2 min). This enabled the identification of 130 and 168 metabolites in SD and LD conditions, respectively (**Supplementary Datasets 1–4**). In both **Supplementary Datasets 1, 3**, there were 110 common metabolites detected.

Generation of Heatmaps

Intensities of 110 metabolites found in SD and LD conditions were $\log_2$-transformed and the missing values (0) were replaced by NA. Metabolites whose intensities were significantly affected during the experiment were determined using one-way ANOVA, followed by Bonferroni's correction for multiple comparisons (adjusted $P < 0.05$) (**Supplementary Tables 1**, **2**). Subsequently, the mean intensity of three to five biological replicates was scaled using the "scale" function in R. Scaled, the mean intensity of metabolites significantly affected during the experiment in wild type (WT), and *raptor1b* mutant were shown in **Figure 2** and in **Supplementary Figures 1–3**.

Two-way ANOVA, followed by Bonferroni's correction for multiple comparisons (adjusted $P < 0.05$) were used to determine metabolites that are significantly affected by time, gene deletion, or both factors (**Supplementary Table 3**). Next, the mean intensity of three to five biological replicates was calculated for each time point (**Supplementary Tables 4**, **5**). Finally, intensity

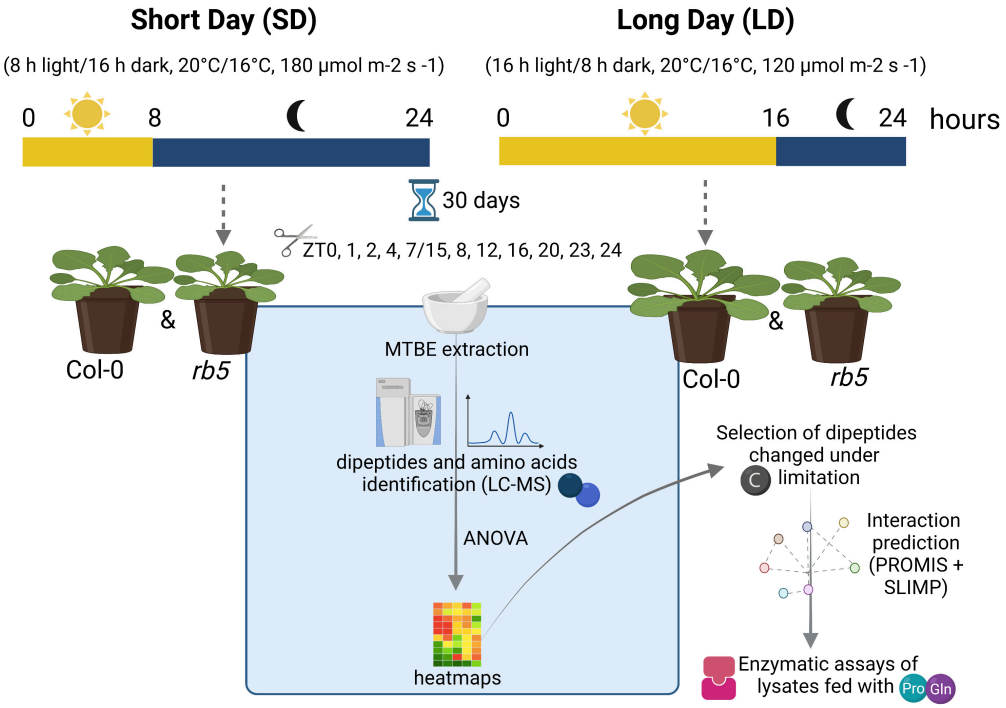

FIGURE 1 | Overview of the experimental design. *rb5* is the abbreviated form for *raptor1b*. Created with BioRender.com.

fold change was calculated between *raptor1b* and Col-0 plants (**Figure 3** and **Supplementary Figures 4A,B**).

Heatmaps were generated using the "pheatmap" package. The R-packages used for data processing, analysis and visualization were mentioned in the GitHub repository[1]. The heatmaps are presented in two different ways: (i) (A) grouping common dipeptides, whose level was affected in both photoperiods, and the ones either affected solely in (B) SD or (C) LD condition alone (**Figures 2**, **3**; **Supplementary Figure 2**); K-means clustering was performed with k = 3, and (ii) clustering the oscillating dipeptides by computing Euclidean distance between the rows. Clustering was performed using the complete method (**Supplementary Figures 1A,B, 3, 4**). Thus, the data presented in **Figure 2** correlate with **Supplementary Figure 1**, **Figure 3**, and **Supplementary Figure 4** are compatible, and **Supplementary Figure 2** corresponds to **Supplementary Figure 3**.

Interactome Analysis

Pro-Gln interactors were retrieved from SLIMP (Zühlke et al., 2021). Protein-protein interactions were imported from STRING (Szklarczyk et al., 2016; **Supplementary Table 6**), and used to build the interaction network of the Pro-Gln interactors into Cytoscape (Shannon et al., 2003; **Supplementary Table 7**).

Enzymatic Activity Assay

Soluble proteins were extracted from 20 mg of Arabidopsis material by addition of 10 mg (w/v) polyvinylpolypyrrolidone and 1 mL ice-cold extraction buffer, shaken vigorously and incubated 5 min in ice. The extraction buffer was composed of 50 mM HEPES/KOH, pH 7.5, 10 mM $MgCl_2$, 1 mM EDTA, 1 mM EGTA, 1 mM benzamidine, 1 mM ε-aminocaproic acid, 0.25% (w/v) BSA, 10 µM leupeptin, 0.5 mM DTT, 0.1% (v/v) Triton X-100, 20% (v/v) glycerol, and 1 mM phenylmethylsulfonyl fluoride. The lysate was centrifuged for 10 min at 14,000 *g* and 4°C (Gibon et al., 2004).

The mitochondrial isocitrate dehydrogenase (ICDHP) activity was measured in conditions adapted from Sadka et al. (2000). The standard reaction media contained both 100 mM Tris–HCl pH 7.5, 10 mM $MgCl_2$, 0.25 mM $NADP^+$, and 2 mM D,L-isocitrate. Glyceraldehyde-3-phosphate dehydrogenase (GAPC), glucose-6-phosphate dehydrogenase (G6PDH), and 6-phosphogluconate dehydrogenase (6PGDH) were assayed as described by Rius et al. (2006), with minor modifications. The GAPC assay premix consisted of 50 mM Tricine-KOH pH 8.5, 4 mM NAD^+, 1.2 mM fructose 1,6-bisphosphate (FBP), 10 mM sodium arsenate, and 1 U/ml aldolase from rabbit muscle (Sigma). G6PDH and 6PGDH assay mixture was composed by 100 mM Tris–HCl pH 8.0, 10 mM $MgCl_2$, 0.5 mM EDTA, 5 mM DTT, 0.25 mM $NADP^+$, and 1 mM G6P or 6PG, respectively. All measurements were performed in a final volume of 50 µl at 25°C under control (mock) conditions or with the addition of 100 µM Pro, Gln, or with the dipeptide Pro-Gln. One unit of enzyme activity (U) is defined as the amount of enzyme catalyzing the formation of 1 µmol of NAD(P)H per min under the above-described conditions.

[1]https://zenodo.org/badge/latestdoi/393474100

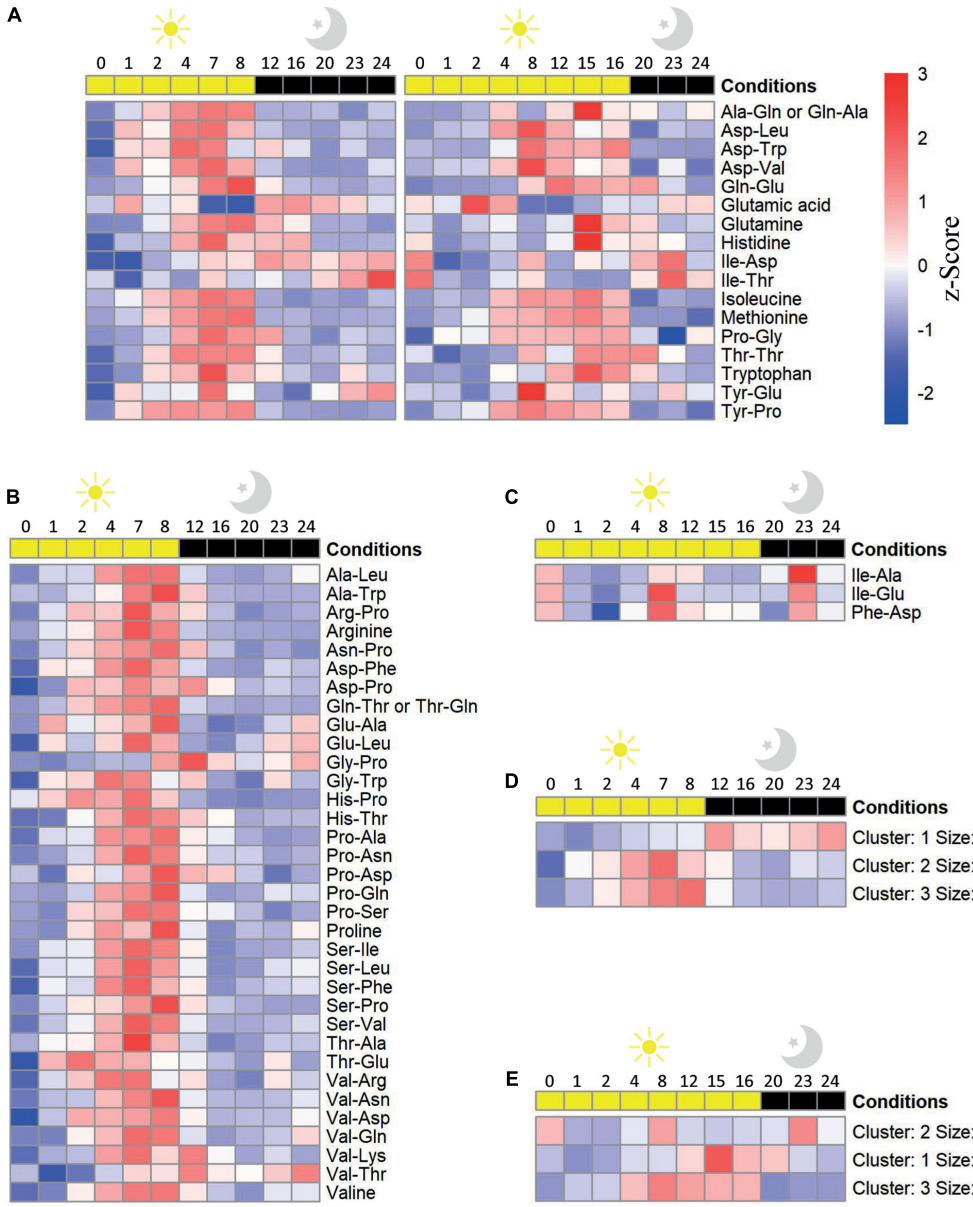

FIGURE 2 | Oscillation of amino acid and dipeptide levels in *Arabidopsis thaliana* Col-0 plants throughout a diel cycle (24 h). Dipeptides and amino acid levels that were significantly (adjusted *P* value ≤ 0.05) affected throughout a diel cycle at **(A)** short- (SD) and long day (LD), **(B)** solely at SD, and **(C)** solely at LD conditions are illustrated as a heatmap. Metabolites were ordered alphabetically. Shown is scaled abundance. K-means clustering of the metabolites levels at **(D)** SD and **(E)** LD was performed with $k = 3$. *n* biological replicates = 3–5.

RESULTS

Amino Acid and Dipeptide Levels Oscillate Throughout a Diel Cycle

The accumulation of dipeptides in response to environmental cues and their roles as signals rewiring the metabolism (Liu and Christians, 1994; Naka et al., 2015; Strehmel et al., 2017; Doppler et al., 2019) prompted us to investigate whether the accumulation of dipeptides is dependent on the photoperiod. For this aim, we assessed the profile of dipeptides in *A. thaliana* plants cultivated for 30 days under SD and LD photoperiods, which are two contrasting conditions in terms of light and dark periods. In this analysis, we also included the profile of 13 amino acids to understand whether there is any correlation between the composition of dipeptide and the accumulation of the amino acids. To identify the pattern of the small molecules which correlates to the changes in the diel cycle, we performed a K-means clustering analysis (**Figure 2**).

A total of 11 dipeptides and six amino acids displayed an oscillation pattern along the diel cycle in both conditions,

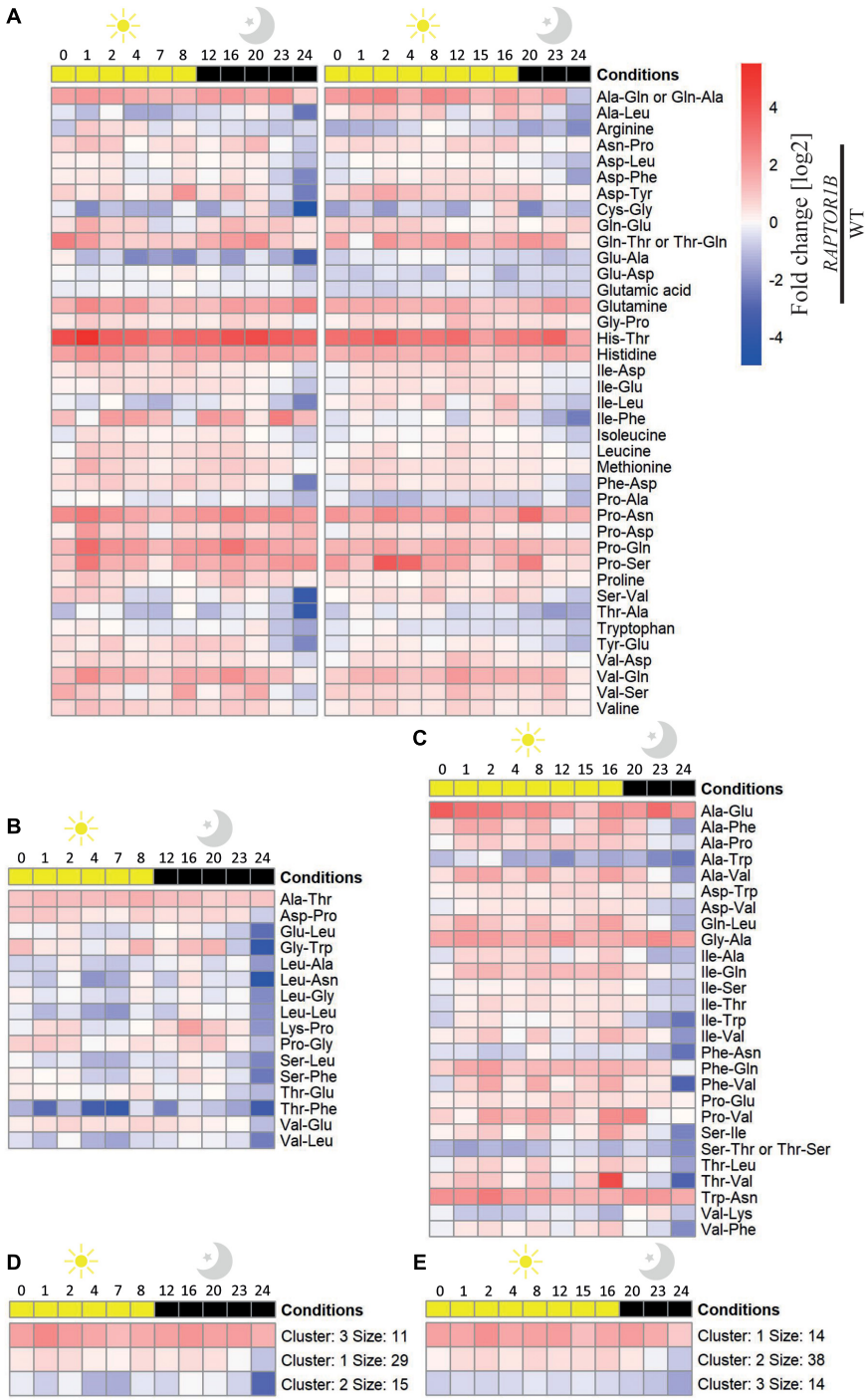

FIGURE 3 | Fold change values of the oscillating amino acid and dipeptide levels in *A. thaliana raptor1b* over Col-0 plants throughout a diel cycle (24 h). Fold change [$\log_2$] of the dipeptides and amino acid levels significantly (adjusted *P*-value $\leq$ 0.05) affected throughout a diel cycle at **(A)** SD and LD, **(B)** solely at SD, and **(C)** solely at LD conditions are illustrated as a heatmap. Metabolites were ordered alphabetically. K-means clustering of the levels of the metabolites at **(D)** SD and **(E)** LD was performed with $k = 3$. *n* biological replicates = 3–5.

predominantly increasing during the day while decreasing at night. Majority of these compounds peak from the middle of the light period onward (ZT 4 and 8, in SD and LD, respectively) (**Figure 2A**), matching the augmented time of light exposure.

In LD condition, far less proteogenic dipeptides showed significant oscillation along the diel cycle (**Figures 2A,C**) and this trend was not related to the total amount of identified dipeptides in the two growth conditions (see "Materials and Methods"

section). Regarding small molecules accumulation, three main clusters were identified: (i) with overall decreased levels along the diel cycle with two peaks of increase at the middle of the day and night (cluster 2); (ii) early (ZT4, cluster 3), and (iii) late (ZT8, cluster 1) accumulation in the light followed by a reduction in the dark (**Figure 2E**). Dipeptides from clusters 1 and 3 were mostly composed of non-aromatic amino acids containing linear aliphatic side chains, with exception of Val and Leu in the C-terminus. On the other hand, four out of the seven dipeptides from Cluster 2 present Ile at the N-terminus.

Reasonably, under the SD photoperiod, a higher number of dipeptides presented changes in their levels along the diel cycle in SD compared with LD (**Figure 2**). In the SD photoperiod, nine amino acids and 42 dipeptides had their levels significantly affected during the diel cycle considering the sum of molecules altered in both photoperiods and the ones solely oscillating under SD (**Figures 2A,B**). The vast majority of these compounds (38 dipeptides and 8 amino acids) (**Figure 2D**) enhanced their levels in response to light, reaching a maximum level at the end of the day and then gradually decreasing during the night. Such pattern was grouped into two clusters, 2 and 3, which mainly differ in the timing of the response. These dipeptides are mostly composed of the glucogenic amino acids Asp, Pro, Ser, and Val at the N-terminus, whereas at the C-terminus, only Pro was overrepresented. Despite being part of cluster 2, the Glu-containing dipeptides Glu-Ala, Glu-Leu, and Tyr-Glu displayed a discrete increase at night. Cluster 1 included only 4 dipeptides and Glu, presenting augmented levels predominantly at dark. Out of the 4 dipeptides from Cluster 1, only two, Gly-Pro and Val-Thr, were specific with SD condition.

A reasonable number of dipeptides from samples harvested at 0 and 24 h present differential levels in these time points (**Figures 2**, **3**). Indeed, we expected similar behavior of the molecules within compatible time points following a 24 h cycle. To test whether the observed dipeptides accumulation follows the 24 h cycle, we compared the level of these molecules in these two time points. For about 68 to 80% of the molecules that show diurnal changes in the accumulation in either or both SD and LD conditions, the levels, even if not identical, are not significantly different (P-value $>$ 005). It is important to note that due to the size of experiments, harvesting the material takes minutes, and hence time 0 h may not be exactly identical to the 24 h, which could contribute to a level of discrepancy. In the future, it will be interesting to follow dipeptide levels across multiple days to estimate the amplitude and frequency of the oscillations accurately.

Mutation in the Substrate Recruiter of TOR Complex Increases Dipeptide Levels in LD Condition

To further explore the role of these dipeptides, we consequently performed a similar experiment using the mutant RAPTOR1B, *raptor1b*, which is the regulatory unit of the TORCI, known to sense energy and nutrient status to control protein synthesis and autophagy (Salem et al., 2018). TORC mutants have much more marked phenotypic changes under LD conditions (Deprost et al., 2007; Moreau et al., 2012; Salem et al., 2018), at the same time that de-repress autophagy machinery. Therefore, the induced autophagy characteristic of *raptor1b* under LD condition (Salem et al., 2018) places this mutant as a good candidate to validate the hypothesis that these dipeptide levels are dependent on autophagy to rewire the metabolism according to the diel cycle.

Similar to the Col-0, there was a higher number of dipeptides and amino acids oscillating in SD compared to LD in *raptor1b* (**Supplementary Figures 2A–E, 3A,B**). However, when the levels of these dipeptides were compared relative to the ones in Col-0, two main trends were observed. First, the oscillation pattern of these compounds was almost abolished along the diel cycle in both photoperiods, if the fold change was considered (**Figures 3A–E**). Second, there was a larger number of dipeptides presenting significant changes in *raptor1b* compared with Col-0 in LD (**Figures 3A,C**), supporting the stronger metabolic phenotype observed in *raptor1b* under this photoperiod (Salem et al., 2018). Interestingly, majority of these dipeptides were accumulated along the diel cycle in both photoperiods. However, the magnitude of these changes was, in general, more pronounced in longer photoperiods. Only 21 and 36% dipeptides with significant differences in Col-0 and *raptor1b* presented continuously reduced levels in LD and SD, respectively (**Figure 3A**). To identify candidates that would respond to limited C availability in an autophagy-dependent manner, we focused on the dipeptides presenting oscillating levels in Col-0 only under SD conditions, whereas in *raptor1b* the response should always be altered in relation to the WT (**Figures 2B**, **3A**). This analysis pointed to alterations in the levels of the amino acids Arg, Pro, and Val and 16 dipeptides. Interestingly, seven dipeptides contained Pro (Gly-Pro, Pro-Ser, Asn-Pro, Pro-Ala, Pro-Asn, Pro-Asp, Pro-Gln), whereas four were composed by the BCAAs Val (Ser-Val, Val-Asp, Val-Gln) and Leu (Ala-Leu). Except for Gly-Pro, the levels of these compounds increase during the day and decrease at night in Col-0 under SD conditions (**Figure 2B**).

Putative Pro-Gln Interactors Include Multiple Enzymes for the Central Carbon and Amino Acid Metabolism

By using PROMIS, a biochemical approach that relies on the co-fractionation-mass spectrometry (CF-MS) of proteins and associated small-molecule ligands in the cellular lysate (Veyel et al., 2017, 2018; Luzarowski et al., 2021), we demonstrated that dipeptides are present in the protein complexes. However, the main limitation of CF-MS is that every metabolite usually co-elutes with hundreds of different proteins. By combining PROMIS with orthogonal small-molecule centric approaches, such as affinity purification and thermal proteome profiling, we identified and verified protein targets for selected dipeptides. We became particularly intrigued by the protein-metabolite interactions between proteinogenic dipeptides and the enzymes of central C metabolism. The mechanistic characterization of the interaction between different dipeptides and proteins revealed that Tyr-Asp and BCAA-containing dipeptides displayed an inhibitory effect on distinct proteins,

attesting the multisite regulation of C metabolism by different dipeptides (Moreno et al., 2021).

To test whether the sixteen dipeptides delineated by our analysis (**Figures 2B**, **3A**) are also involved in rewiring metabolism under C restricted conditions, we looked for the enzymes of central C and amino acid metabolism among their putative protein interactors. We first queried the STITCH (Kuhn et al., 2008) and BRENDA (Jeske et al., 2019) databases for known interactors for the 16 dipeptides, but we found none. As a result, we then exploited a recent set of predicted protein-metabolite interactions obtained by combining three different PROMIS experiments with supervised machine learning prediction of the interactors (SLIMP) (Zühlke et al., 2021). SLIMP helps to distinguish between true and coincidental interactors by looking for co-elution across the multiple separations. Out of the sixteen selected dipeptides, seven are involved in the predictions of protein-metabolite interactions by SLIMP, including one of the six Pro containing dipeptides, the Pro-Gln. The list of the predicted Pro-Gln interactors comprised 124 proteins, of which some were involved in the TOR pathway and critical metabolic enzymes (**Figure 4A**; **Supplementary Tables 6**, **7**). We mined these 124 proteins to identify those involved in C metabolism. In addition to the GAPC 1 and 2, which we previously showed to be regulated by the dipeptide Tyr-Asp (Moreno et al., 2021), the list comprised two cytosolic isoforms of G6PDH, 5, and 6, and all the three Arabidopsis isoforms of 6PGDH (**Figures 4A,B**; **Supplementary Table 6**). Furthermore, the list of predicted Pro-Gln interactors contained enzymes related to the tricarboxylic acid cycle (TCA cycle) activity, as peroxisomal citrate synthases (CSY2 and CSY3) and ICDHP (**Figure 4**; **Supplementary Table 6**). Finally, the Pro-Gln interaction network is comprised of two enzymes of BCAA biosynthesis 2: isopropylmalate synthase (IMS1) and ketol-acid reductoisomerase (ILV5) (**Supplementary Table 6**). To follow-up on the interaction data, we measured enzymatic activity of the GAPC, G6PDH, 6PGDH, and ICDHP in the lysate prepared from the Arabidopsis plants grown under 12 h/12 h regime, harvested either 2 h into the light or 2 h into the dark and supplemented with either 100 μM Pro-Gln, Pro or Gln. In contrast to the previously published effect of Tyr-Asp on GAPC or Ala-Ile on PEPCK activity (Moreno et al., 2021), we measured no difference for the tested enzyme-ligand combinations (**Supplementary Figures 5A–D**). Thus, in our experimental conditions, Pro-Gln did not show a biologically relevant role in the regulation of the activity of these four enzymes associated with C metabolism.

DISCUSSION

The length of light and dark cycles in a day affects not only the rates of transcription (Baerenfaller et al., 2015) and translation (Sulpice et al., 2014) but also several metabolic processes (Seaton et al., 2018), including the diurnal turnover of C reserves, which ultimately impacted growth (Baerenfaller et al., 2015). Since SD and LD have an opposite duration of light and dark periods, we evaluated how these conditions would influence the collection of dipeptides in Arabidopsis.

Due to the light-dependent accumulation pattern of the 11 dipeptides in both photoperiods, their oscillation is not strictly related to the control of C-dependent metabolism. Most of the dipeptides with augmented levels at night were composed of glucogenic BCAAs at the N-terminus, in both photoperiods (**Figure 2**). Glucogenic and ketogenic amino acids can be distinguished by their ability or inability to be used to generate glucose. The dipeptides composed of glucogenic amino acids could be mobilized and generate the C skeletons to produce pyruvate and then glucose through gluconeogenesis (Eastmond et al., 2015). As the duration of the night dramatically influences C availability for growth (Sulpice et al., 2014), these dipeptides could be interesting candidates for triggering metabolic shifts.

Under C restricted conditions imposed by longer night periods coupled with low light intensity, sugar and energy supply relies on autophagy to provide recycling metabolites and building blocks to sustain plant growth (Izumi et al., 2013). In addition, proteolysis is induced at night and considered one of the first responses when the C supply drops, provoking a change from protein synthesis to degradation to provide an alternative source of energy (Usadel et al., 2008; Ishihara et al., 2015). As 11 out of the 31 dipeptides oscillating solely under SD were previously either associated with autophagy or displayed lower levels in autophagy mutants (Thirumalaikumar et al., 2020), their oscillation under C limited supply might also result from this catabolic process. The massive increase of oscillating dipeptides in plants under SD photoperiod and the consequently reduced C mobilization compared with LD is thus suggested to be derived from induced protein degradation or autophagy, as these processes can take part in the biogenesis of small molecules (Thirumalaikumar et al., 2020), a hypothesis that remains to be tested. Besides the role of amino acids in protein synthesis, they are also required for signaling processes and can aid to balance the plant energy homeostasis under C deprivation. SD forces the metabolism to match reduced C mobilization with decreased C utilization, favoring C partitioning for respiration and maintenance to detriment of growth (Stitt and Zeeman, 2012). Along the time, several adaptations to SD such as C allocation, protein turnover and central metabolism allow the plant to continuously grow but at an extremely reduced rate due to C limitation (Smith and Stitt, 2007). Besides the differences of C supply related to the duration of the night, our experimental design does not exclude the effects of light intensity and photoperiod themselves in the dipeptides profile. The distinct light intensities were chosen to allow the comparison of plants at similar developmental stages and to reduce the gap in terms of daily light integral (DLI) between the two photoperiods. Accordingly, some dipeptides accumulated in high light conditions (LD, 300 compared with 150 μ $\mu E.m^{-2}.sec^{-1}$) (Thirumalaikumar et al., 2020), but from the 31 dipeptides oscillating only in SD (the photoperiod condition with the highest light intensity in the present study), only five of them match this data (Thr-Glu, Val-Asp, Ala-Trp, Gly-Pro). Moreover, the combined increased Glu and Glu-containing dipeptides at the same time points in the dark might indicate altered N metabolism (Hildebrandt et al., 2015) along the day under limited C supplied for growth (SD), although dipeptides regulatory roles

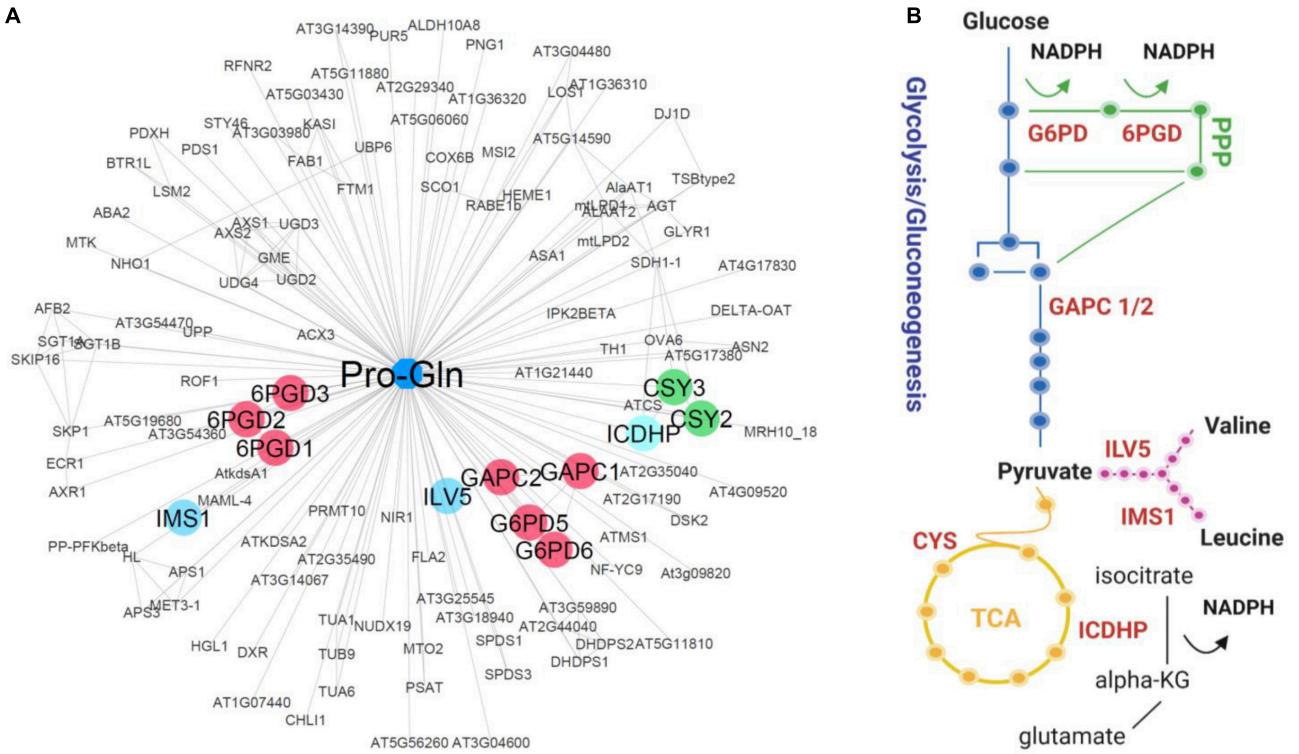

FIGURE 4 | Pro-Gln/protein interaction network. **(A)** Pro-Gln interactors were predicted by SLIMP (Zühlke et al., 2021) with a score above 0.5. Protein-protein interactions were imported from STRING (Szklarczyk et al., 2016) based on the experimental and database evidence. Edge length is inversely proportional to either a STRING (PPI) or SLIMP (PMI) score. The network was created using Cytoscape (Shannon et al., 2003). Indicated proteins were selected based on their functions in C and amino acid metabolism. **(B)** Schematic representation of the metabolic pathways was created using Biorender.com.

have shown to be diverse than the amino acid itself (Moreno et al., 2021).

The more relaxed energy management in LD photoperiod (Baerenfaller et al., 2015) might be associated with the decreased number of oscillating peptides compared to SD. A considerable number of the dipeptides oscillating under LD presented BCAA either at N- or at the C-terminus, mostly found in Cluster 2 (**Figure 2**). Interestingly, genes from the BCAA degradation pathways are upregulated during the night, when this catabolic activity is required to fulfill energy demand (Caldana et al., 2011; Peng et al., 2015) and what could have been in line with the night peak characteristic from this Cluster.

Plants facing contrasting C availability presented specific but integrated sugar signaling pathways. One example is the TOR/SnRK1 hub; high C availability relies on TOR, whilst low C supply requires SnRK1 to mediate metabolic responses (Wingler, 2018). TOR connects nutrients, inner inputs, and environmental signals to control several aspects of C metabolism (Dobrenel et al., 2013). In line with that, the most marked phenotype of *raptor1b* plants under high C availability strengthens the role of TOR as a fundamental adaptor to C supply. Despite the increasing evidence linking the TORC pathway to the integration of metabolic signals, energy status, and hormones in a wide range of plant growth-mediated processes (Moreau et al., 2012; Caldana et al., 2013; Xiong et al., 2013; Pfeiffer et al., 2016; Zhang et al., 2016; Dong et al., 2017; Li et al., 2017; Mohammed et al., 2018; Salem et al., 2018), little is known about its mode of action and the key players in controlling cellular homeostasis in a condition-dependent manner. The downregulation of TORC in plants activates autophagy, which derives from the generation of autophagosomes, enhanced expression of *ATG* genes, and their phosphorylation [reviewed by Mugume et al. (2020)], aside from nucleotides depletion (Kazibwe et al., 2020). The role of TOR as a repressor of autophagy (Pu et al., 2017), this process suggested to generate proteogenic dipeptides (Thirumalaikumar et al., 2020), makes *raptor1b* a suitable model to study the regulatory interplay among light, C availability, TOR, and small molecules. Compared with Col-0 *A. thaliana*, the increased number of altered dipeptides from the *raptor1b* plants grown under LD (**Figure 3**) might be linked to the de-activated autophagy in this mutant. Autophagy is repressed by TOR and activated by SnRK1, both proteins regulated by the nutrient availability in plants (Pu et al., 2017). Under nutrient deprivation, such as C shortage imposed by extended darkness period, TOR is inhibited *via* RAPTOR by SnRK1, thus releasing the repression of autophagy which will the outcome in recycling building blocks to relieve plant metabolism (Nukarinen et al., 2016; Soto-Burgos and Bassham, 2017). Not surprisingly, there was a larger number of dipeptides significantly increasing in *raptor1b* under LD conditions compared with Col-0. Since all the 16 dipeptides

found to respond either to the reduced proportion of C available to growth imposed by SD conditions or the suppression of RAPTOR1B were glucogenic, it is reasonable to speculate that they could be involved in generating glucose to bypass possible C limitations. Out of these selected dipeptides, six and five presented Pro or BCAA at the N- or C-terminal. The generation of some of these dipeptides could be a product of autophagy, given that from the 16 selected dipeptides, 6 (Asp-Phe, Glu-Ala, Pro-Ala, Pro-Ser, Val-Gln, and Val-Asp) were either associated with increased autophagy transcripts or displayed reduced levels in autophagy mutants (Thirumalaikumar et al., 2020).

Regardless of the condition, Pro levels itself increased in *raptor1b* compared with Col-0 plants, which is a characteristic output of TORC inhibition (Moreau et al., 2012; Caldana et al., 2013; Salem et al., 2017; da Silva et al., 2021). This increment is even more pronounced when plants are transferred to a condition of augmented C supply (Moreau et al., 2012), matching the higher magnitude of phenotypic changes in *raptor1b* plants under LD (Salem et al., 2018). Pro accumulation is well known to occur under various stress conditions, probably playing an osmoprotective role (Verbruggen and Hermans, 2008). More recently, a new role for Pro in stimulating leaf nighttime O_2 consumption rate under the control of the TOR pathway has emerged in a TOR-dependent context (O'Leary et al., 2020). The higher levels of some amino acids may require TORC to restrict respiratory catabolism preventing nutrient depletion. To overcome C deprivation conditions, such as long nights, the use of amino acids and fatty acids as respiratory substrates in plants can be a strategy to grant survival. Therefore, we favor the interpretation that the altered levels of Pro or Pro-containing dipeptides in *raptor1b* compared to Col-0 Arabidopsis might indicate that the mutants induce respiratory catabolism to feed C into the respiratory system; a hypothesis that demands further investigation to be proved. In addition to their role as putative respiratory substrates, we speculate that dipeptides would bind and regulate the activity of proteins. Nevertheless, as the TOR pathway integrates light and nutrient signals [reviewed by Wu et al. (2018)], besides the differences in C supply regarding SD and LD conditions, we cannot rule out the effects of both light intensity and duration on the alteration of these dipeptides' levels in *raptor1b*.

Herein, we mined the SLIMP dataset for targets of a representative Pro-containing dipeptide, which we identified to be possibly related to C restriction. Dipeptides can influence the function of proteins and determined processes. Uptake of the dipeptide Gly-Sar can mediate mTOR activity in leukemia stem cells (Naka et al., 2015). Interestingly, several bacterial Pro-containing cyclodipeptides were proven to activate the TOR signaling pathway increasing growth in plants (Corona-Sánchez et al., 2019; González-López et al., 2021), including cyclodipeptides versions of Pro-Phe, which oscillated only in *raptor1b* (**Supplementary Figures 2**, **3**) and Pro-Val, whose level was increased in the mutant compared to Col-0 under LD (**Figure 3**; **Supplementary Figure 4**). Among the 124 proteins identified as putative Pro-Gln interactors, we retrieved four related to the TOR pathway, besides several enzymes involved in C metabolism, such as glycolysis, gluconeogenesis, TCA cycle, and PPP (**Figure 4**). Threonine synthase (TS) and Tubulin alpha-6 (TUA6) are proteins coeluting with Pro-Gln that have been previously shown to physically interact with RAPTOR1B in protein-protein interaction assays (Van Leene et al., 2019). As we were interested in searching for proteins related to C metabolism, GAPC, G6PDH, 6PGDH, CSY2, CSY3, ICDHP, IMS1, and ILV5 were highlighted from this list. The G6PDH and 6PGDH are enzymes of the PPP downstream of glucose-6-phosphate that have an interplay with the TOR pathway in other organisms (Wagle et al., 1998; Tsouko et al., 2014). While CSY2 and CSY3 are required for fatty acid respiration (Pracharoenwattana et al., 2005), ICDHP catalyzes the conversion between isocitrate and 2-oxoglutarate (2OG). Analogously to G6PDH and 6PGDH, ICDHP is an NADP-dehydrogenase and contributes to cellular NADPH production (Leterrier et al., 2012). Interestingly, the IMS1 mutant *rol17* showed reduced sensitivity to the TOR inhibitor AZD8055, establishing a yet undepicted connection between this protein and the TOR network to adjust metabolic homeostasis (Schaufelberger et al., 2019). During C starvation, BCAAs support electron provision to electron-transfer flavoprotein/electron-transfer flavoprotein: ubiquinone oxidoreductase (ETF/ETFQO) complex, sustaining mitochondrial respiration under C starvation conditions (Araújo et al., 2010). Taken together, Pro-Gln interactors pointed out a role in providing alternative substrates for sustaining respiration under C limited conditions.

As no differential activity could be retrieved when Pro-Gln was added in the plant lysates (**Supplementary Figure 5**), we could not validate the role of this dipeptide in modulating the activities of GAPC, G6PDH, 6PGDH, and ICDHP. However, we cannot exclude that these results are dependent on the experimental conditions, such as the choice of the starting material, which might demand other players or might be inhibited in the specific conditions of the assay. Moreover, the obtained results do not exclude the binding, as not all interactional events will necessarily result in altered enzymatic activity. Future work will concentrate on the functional validation of these putative targets, which may be obtained by recombinant production and purification of these proteins to assay the enzymatic activity with no interferents.

DATA AVAILABILITY STATEMENT

The original contributions presented in the study are included in the article/**Supplementary Material**, further inquiries can be directed to the corresponding authors.

AUTHOR CONTRIBUTIONS

ML analyzed the mass spectrometry data and generated the Figures. MJC-R, ML, CC, and AS interpreted the data, wrote the manuscript, and revised it. CCM-B and RIM designed and performed the experiments, BZ generated SLIMP dataset using PROMIS data provided by the group of AS under supervision of ZN. AS and CC designed and supervised the experiments and the manuscript revision.

FUNDING

This work was supported by the Max Planck Society.

SUPPLEMENTARY MATERIAL

The Supplementary Material for this article can be found online at: https://www.frontiersin.org/articles/10.3389/fpls.2021.758933/full#supplementary-material

Supplementary Figure 1 | Oscillation of amino acid and dipeptide levels in *A. thaliana* Col-0 plants throughout a diel cycle (24 h). Dipeptides and amino acid levels that were significantly (adjusted *P*-value $\leq$ 0.05) affected throughout a diel cycle at **(A)** SD and **(B)** LD conditions are illustrated as a heatmap. Shown is scaled abundance. Euclidean distance was computed between the rows and row-wise clustering was performed using the complete method. *n* biological replicates = 3–5.

Supplementary Figure 2 | Oscillation of amino acid and dipeptide levels in *A. thaliana raptor1b* plants throughout a diel cycle (24 h). Dipeptides and amino acid levels that were significantly (adjusted *P* value $\leq$ 0.05) affected throughout a diel cycle at **(A)** SD and LD, **(B)** solely at SD, and **(C)** solely at LD conditions are illustrated as a heatmap. Metabolites were ordered alphabetically. Shown is scaled abundance. Kmeans clustering of the metabolites levels at **(D)** SD and **(E)** LD was performed with k = 3. *n* biological replicates = 3–5.

Supplementary Figure 3 | Oscillation of amino acid and dipeptide levels in *A. thaliana raptor1b* plants throughout a diel cycle (24 h). Dipeptides and amino acid levels that were significantly (adjusted *P*-value $\leq$ 0.05) affected throughout a diel cycle at **(A)** SD and **(B)** LD conditions are illustrated as a heatmap. Shown is scaled abundance. Euclidean distance was computed between the rows and row-wise clustering was performed using the complete method. *n* biological replicates = 3–5.

Supplementary Figure 4 | Fold change values of the oscillating amino acid and dipeptide levels in *A. thaliana raptor1b* over Col-0 plants throughout a diel cycle (24 h). Fold change [$\log_2$] of the dipeptides and amino acid levels significantly (adjusted *P*-value $\leq$ 0.05) affected throughout a diel cycle at **(A)** SD and **(B)** LD conditions are illustrated as a heatmap. Euclidean distance was computed between the rows and row-wise clustering was performed using the complete method.

Supplementary Figure 5 | Enzymatic activity measurements of Pro-Gln putative protein interactors. **(A)** ICDHP, **(B)** GAPC, **(C)** G6PDH, and **(D)** 6PGDH activity measurements under control conditions (mock) or with the addition of 100 μM Pro, Gln, or Pro-Gln. Enzymatic assays were performed on plant lysates harvested 2 h into the day (white bars) and 2 h into the dark (gray bars). Data are the mean of at least two independent data sets ± standard error.

Supplementary Table 1 | One-way analysis of variance (ANOVA) followed by Bonferroni's correction for multiple comparisons (.adj) of the intensities from the identified dipeptides and amino acids in Col-0 *A. thaliana* along a diel cycle under SD and LD conditions. The main effect of time (0–24 h) was analyzed under SD and LD conditions. Only the dipeptides showing significant *P*-values ($P < 0.05$) are presented. *n* biological replicates = 3–5.

Supplementary Table 2 | One-way ANOVA followed by Bonferroni's correction for multiple comparisons (.adj) of the intensities from the identified dipeptides and amino acids in *raptor1b A. thaliana* along a diel cycle under SD and LD conditions. The main effect of time (0–24 h) was analyzed under SD and LD conditions. Only the dipeptides showing significant *P*-values ($P < 0.05$) are presented. *n* biological replicates = 3–5.

Supplementary Table 3 | Two-way ANOVA followed by Bonferroni's correction for multiple comparisons (.adj) of the intensities from the identified dipeptides and amino acids. The main effects of time (0–24 h), *raptor1b* genotype (over Col-0), or both factors were analyzed under SD and LD conditions. Significant *P*-values are highlighted in red ($P < 0.05$). *n* biological replicates = 3–5.

Supplementary Table 4 | Statistical summary of the measured amino acids and dipeptides in Col-0 and *raptor1b A. thaliana* under SD. *n* biological replicates = 3–5.

Supplementary Table 5 | Statistical summary of the measured amino acids and dipeptides in Col-0 and *raptor1b A. thaliana* under LD. *n* biological replicates = 3–5.

Supplementary Table 6 | Pro-Gln protein interactors retrieved from SLIMP (Zühlke et al., 2021), used for STRING (Szklarczyk et al., 2016) protein-protein interaction analysis. Targets mentioned in the text are highlighted in red letters.

Supplementary Table 7 | Parameters used in Cytoscape (Shannon et al., 2003) to build the interaction network of the Pro-Gln interactors retrieved from SLIMP (Zühlke et al., 2021) in Cytoscape. Protein-protein interactions were imported from STRING (Szklarczyk et al., 2016) based on the experimental and database evidence.

Supplementary Dataset 1 | Liquid chromatography-mass spectrometry (LC-MS) measurements of amino acids and dipeptides from the methyl-tert-butyl-ether (MTBE) -extraction in Col-0 and *raptor1b A. thaliana* along a diel cycle under SD condition. Values are normalized as described in the "Materials and Methods" section. *n* biological replicates = 3–5.

Supplementary Dataset 2 | LC-MS measurements of the polar fraction from the MTBE-extraction in Col-0 and *raptor1b A. thaliana* along a diel cycle under SD condition. Raw chromatograms were processed using Expressionist Refiner MS as described in the "Materials and Methods" section. *n* biological replicates = 3–5.

Supplementary Dataset 3 | LC-MS measurements of amino acids and dipeptides from the MTBE-extraction in Col-0 and *raptor1b A. thaliana* along a diel cycle under LD condition. Values are normalized as described in the "Materials and Methods" section. *n* biological replicates = 3–5.

Supplementary Dataset 4 | LC-MS measurements of polar fraction from the MTBE-extraction in Col-0 and *raptor1b A. thaliana* along a diel cycle under LD condition. Raw chromatograms were processed using Expressionist Refiner MS as described in the "Materials and Methods" section. *n* biological replicates = 3–5.

REFERENCES

Agredano-Moreno, L. T., Reyes de la Cruz, H., Martínez-Castilla, L. P., and Sánchez de Jiménez, E. (2007). Distinctive expression and functional regulation of the maize (*Zea mays* L.) TOR kinase ortholog. *Mol. BioSyst.* 3, 794–794. doi: 10.1039/b705803a

Alves, L. C., Llerena, J. P. P., Mazzafera, P., and Vicentini, R. (2019). Diel oscillations in cell wall components and soluble sugars as a response to short-day in sugarcane (*Saccharum* sp.). *BMC Plant Biol.* 19:215. doi: 10.1186/s12870-019-1837-4

Araújo, W. L., Ishizaki, K., Nunes-Nesi, A., Larson, T. R., Tohge, T., Krahnert, I., et al. (2010). Identification of the 2-hydroxyglutarate and isovaleryl-CoA dehydrogenases as alternative electron donors linking lysine catabolism to the electron transport chain of Arabidopsis mitochondria. *Plant Cell* 22, 1549–1563. doi: 10.1105/tpc.110.075630

Baerenfaller, K., Massonnet, C., Hennig, L., Russenberger, D., Sulpice, R., Walsh, S., et al. (2015). A long photoperiod relaxes energy management in *Arabidopsis* leaf six. *Curr. Plant Biol.* 2, 34–45. doi: 10.1016/J.CPB.2015.07.001

Busche, M., Scarpin, M. R., Hnasko, R., and Brunkard, J. O. (2021). TOR coordinates nucleotide availability with ribosome biogenesis in plants. *Plant Cell* 33, 1615–1632. doi: 10.1093/plcell/koab043

Caldana, C., Degenkolbe, T., Cuadros-Inostroza, A., Klie, S., Sulpice, R., Leisse, A., et al. (2011). High-density kinetic analysis of the metabolomic and transcriptomic response of *Arabidopsis* to eight environmental conditions. *Plant J.* 67, 869–884. doi: 10.1111/j.1365-313X.2011.04640.x

Caldana, C., Li, Y., Leisse, A., Zhang, Y., Bartholomaeus, L., Fernie, A. R., et al. (2013). Systemic analysis of inducible target of rapamycin mutants reveal a general metabolic switch controlling growth in *Arabidopsis thaliana*. *Plant J.* 73, 897–909. doi: 10.1111/tpj.12080

Caldana, C., Martins, M. C. M., Mubeen, U., and Urrea-Castellanos, R. (2019). The magic "hammer" of TOR: the multiple faces of a single pathway in the metabolic regulation of plant growth and development. *J. Exp. Bot.* 70, 2217–2225. doi: 10.1093/jxb/ery459

Corona-Sánchez, I., Peña-Uribe, C. A., González-López, O., Villegas, J., Campos-Garcia, J., and de la Cruz, H. R. (2019). Cyclodipeptides from *Pseudomonas aeruginosa* modulate the maize (*Zea mays* L.) root system and promote S6 ribosomal protein kinase activation. *PeerJ* 7:e7494. doi: 10.7717/peerj.7494

da Silva, V. C. H., Martins, M. C. M., Calderan-Rodrigues, M. J., Artins, A., Monte Bello, C. C., Gupta, S., et al. (2021). Shedding light on the dynamic role of the "Target of Rapamycin" kinase in the fast-growing C4 species *Setaria viridis*, a suitable model for biomass crops. *Front. Plant Sci.* 12:637508. doi: 10.3389/fpls.2021.637508

Dardente, H., Hazlerigg, D. G., and Ebling, F. J. (2014). Thyroid hormone and seasonal rhythmicity. *Front. Endocrinol.* 26:19. doi: 10.3389/fendo.2014.00019

Deprost, D., Yao, L., Sormani, R., Moreau, M., Leterreux, G., Nicolai, M., et al. (2007). The Arabidopsis TOR kinase links plant growth, yield, stress resistance and mRNA translation. *EMBO Rep.* 8, 864–870. doi: 10.1038/sj.embor.7401043

Dobrenel, T., Caldana, C., Hanson, J., Robaglia, C., Vincentz, M., Veit, B., et al. (2016). TOR signaling and nutrient sensing. *Ann. Rev. Plant Biol.* 67, 261–285. doi: 10.1146/annurev-arplant-043014-114648

Dobrenel, T., Marchive, C., Azzopardi, M., Clément, G., Moreau, M., Sormani, R., et al. (2013). Sugar metabolism and the plant target of rapamycin kinase: a sweet operaTOR? *Front. Plant Sci.* 4:93. doi: 10.3389/fpls.2013.00093

Dong, Y., Silbermann, M., Speiser, A., Forieri, I., Linster, E., Poschet, G., et al. (2017). Sulfur availability regulates plant growth *via* glucose-TOR signaling. *Nat. Commun.* 8:1174. doi: 10.1038/s41467-017-01224-w

Doppler, M., Kluger, B., Bueschl, C., Steiner, B., Buerstmayr, H., Lemmens, M., et al. (2019). Stable isotope-assisted plant metabolomics: investigation of phenylalanine-related metabolic response in wheat upon treatment with the Fusarium Virulence Factor deoxynivalenol. *Front Plant Sci.* 10:1137. doi: 10.3389/fpls.2019.01137

Doust, A. N. (2017). "The effect of photoperiod on flowering time, plant architecture, and biomass in Setaria in the genetics and genomics of Setaria," in *Plant Genetics and Genomics: Crops and Models*, eds A. N. Doust and X. M. Diao (New York, NY: Springer-Verlag), 19.

Eastmond, P. J., Astley, H. M., Parsley, K., Aubry, S., Williams, B. P., and Menard, G. N. (2015). *Arabidopsis* uses two gluconeogenic gateways for organic acids to fuel seedling establishment. *Nat. Commun.* 6:6659. doi: 10.1038/ncomms7659

Garner, W. W., and Allard, H. A. (1920). Effect of the relative length of day and night and other factors of the environment on growth and reproduction in plants. *J. Agric Res.* 18, 553–606. doi: 10.1175/1520-0493192048<415b:EOTRLO<2.0.CO;2

Giavalisco, P., Li, Y., Matthes, A., Eckhardt, A., Hubberten, H.-M., Hesse, H., et al. (2011). Elemental formula annotation of polar and lipophilic metabolites using 13 C, 15 N and 34 S isotope labelling, in combination with high-resolution mass spectrometry. *Plant J.* 68, 364–376. doi: 10.1111/j.1365-313X.2011.04682.x

Gibon, Y., Blaesing, O. E., Hannemann, J., Carillo, P., Höhne, M., Hendriks, J. H. M., et al. (2004). A robot-based platform to measure multiple enzyme activities in *Arabidopsis* using a set of cycling assays: comparison of changes of enzyme activities and transcript levels during diurnal cycles and in prolonged darkness. *Plant Cell* 16, 3304–3325. doi: 10.1105/tpc.104.025973

González-López, O., Palacios-Nava, B. B., Peña-Uribe, C. A., Campos-García, J., López-Bucio, J., García-Pineda, E., et al. (2021). Growth promotion in *Arabidopsis thaliana* by bacterial cyclodipeptides involves the TOR/S6K pathway activation. *J. Plant Physiol.* 257:153343. doi: 10.1016/j.jplph.2020.153343

Hara, K., Maruki, Y., Long, X., Yoshino, K.-i., Oshiro, N., Hidayat, S., et al. (2002). Raptor, a binding partner of target of rapamycin (TOR), mediates TOR action. *Cell* 110, 177–189. doi: 10.1016/s0092-8674(02)00833-4

Hildebrandt, T. M., Nunes Nesi, A., Araújo, W. L., and Braun, H. P. (2015). Amino acid catabolism in plants. *Mol. Plant*. 8, 1563–1579. doi: 10.1016/j.molp.2015.09.005

Ishihara, H., Moraes, T. A., Pyl, E.-T., Schulze, W. S., Obata, T., Scheffel, A., et al. (2017). Growth rate correlates negatively with protein turnover in *Arabidopsis* accessions. *Plant J.* 91, 416–429. doi: 10.1111/tpj.13576

Ishihara, H., Obata, T., Sulpice, R., Fernie, A. R., and Stitt, M. (2015). Quantifying protein synthesis and degradation in *Arabidopsis* by dynamic $^{13}CO_2$ labeling and analysis of enrichment in individual amino acids in their free pools and in protein. *Plant Phys.* 168, 74–93. doi: 10.1104/pp.15.00209

Izumi, M., Hidema, J., Makino, A., and Ishida, H. (2013). Autophagy contributes to nighttime energy availability for growth in *Arabidopsis*. *Plant Physiol.* 161, 1682–1693. doi: 10.1104/pp.113.215632

Jeske, L., Placzek, S., Schomburg, I., Chang, A., and Schomburg, D. (2019). BRENDA in 2019: a European ELIXIR core data resource. *Nucleic Acids Res.* 47, D542–D549. doi: 10.1093/nar/gky1048

Jüppner, J., Mubeen, U., Leisse, A., Caldana, C., Wiszniewski, A., Steinhauser, D., et al. (2018). The target of rapamycin kinase affects biomass accumulation and cell cycle progression by altering carbon/nitrogen balance in synchronized *Chlamydomonas reinhardtii* cells. *Plant J.* 93, 355–376. doi: 10.1111/tpj.13787

Kazibwe, Z., Soto-Burgos, J., MacIntosh, G. C., and Bassham, D. C. (2020). TOR mediates the autophagy response to altered nucleotide homeostasis in an RNase mutant. *J. Exp. Bot*. 71, 6907–6920. doi: 10.1093/jxb/eraa410

Khoeyi, Z. A., Seyfabadi, J., and Ramezanpur, Z. (2012). Effect of light intensity and photoperiod on biomass and fatty acids. *Aquacult. Int.* 20, 41–49. doi: 10.1007/s10499-011-9440-1

Kim, D.-H., Sarbassov, D. D., Ali, S. M., King, J. E., Latek, R. R., Erdjument-Bromage, H., et al. (2002). mTOR interacts with raptor to form a nutrient-sensitive complex that signals to the cell growth machinery. *Cell* 110, 163–175. doi: 10.1016/s0092-8674(02)00808-5

Kuhn, M., von Mering, C., Campillos, M., Jensen, L. J., and Bork, P. (2008). STITCH: interaction networks of chemicals and proteins. *Nucleic Acids Res.* 36, D684–D688. doi: 10.1093/nar/gkm795

Leterrier, M., Juan, B., Barroso, J. B., Valderrama, R., Palma, J. M., and Corpas, F. J. (2012). NADP-dependent isocitrate dehydrogenase from *Arabidopsis* roots contributes in the mechanism of defence against the nitro-oxidative stress induced by salinity. *Sci. World J.* 2:694740. doi: 10.1100/2012/694740

Li, X., Cai, W., Liu, Y., Li, H., Fu, L., Liu, Z., et al. (2017). Differential TOR activation and cell proliferation in *Arabidopsis* root and shoot apexes. *Proc. Natl. Acad. Sci. U.S.A.* 114, 2765–2770. doi: 10.1073/pnas.1618782114

Liu, D. L. Y., and Christians, N. E. (1994). Isolation and identification of root-inhibiting compounds from corn gluten hydrolysate. *J. Plant Growth Regul.* 13, 227–230. doi: 10.1007/BF00226041

Liu, G. Y., and Sabatini, D. M. (2020). mTOR at the nexus of nutrition, growth, ageing and disease. *Nat. Rev. Mol. Cell Biol.* 21, 183–203. doi: 10.1038/s41580-019-0199-y

Liu, Y., and Bassham, D. C. (2010). TOR is a negative regulator of autophagy in *Arabidopsis thaliana*. *PLoS One* 5:e11883. doi: 10.1371/journal.pone.0011883

Liu, Y., Duan, X., Zhao, X., Ding, W., Wang, Y., and Xiong, Y. (2021). Diverse nitrogen signals activate convergent ROP2-TOR signaling in *Arabidopsis*. *Dev Cell* 56, 1283–1295. doi: 10.1016/j.devcel.2021.03.022

Luzarowski, M., Vicente, R., Kiselev, A., Wagner, M., Schlossarek, D., Erban, A., et al. (2021). Global mapping of protein–metabolite interactions in *Saccharomyces cerevisiae* reveals that Ser-Leu dipeptide regulates phosphoglycerate kinase activity. *Commun. Biol.* 4:181. doi: 10.1038/s42003-021-01684-3

Maegawa, K., Takii, R., Ushimaru, T., and Kozaki, A. (2015). Evolutionary conservation of TORC1 components, TOR, Raptor, and LST8, between rice and yeast. *Mol. Genet. Genom.* 290, 2019–2030. doi: 10.1007/s00438-015-1056-0

Mahfouz, M. M., Kim, S., Delauney, A. J., and Verma, D. P. S. (2006). Arabidopsis TARGET OF RAPAMYCIN interacts with RAPTOR, which regulates the activity of S6 Kinase in response to osmotic stress signals. *Plant Cell* 18, 477–490. doi: 10.1105/tpc.105.035931

Menand, B., Desnos, T., Nussaume, L., Berger, F., Bouchez, D., Meyer, C., et al. (2002). Expression and disruption of the *Arabidopsis* TOR (Target of Rapamycin) gene. *Proc. Natl. Acad. Sci. U.S.A.* 99, 6422–6427. doi: 10.1073/pnas.092141899

Mengin, V., Pyl, E.-T., Moraes, T. A., Sulpice, R., Krohn, N., Encke, B., et al. (2017). Photosynthate partitioning to starch in *Arabidopsis thaliana* is insensitive to light intensity but sensitive to photoperiod due to a restriction on growth in the

light in short photoperiods. *Plant Cell Environ.* 40, 2608–2627. doi: 10.1111/pce.13000

Mohammed, B., Bilooei, S. F., Doczi, R., Grove, E., Railo, S., Palme, K., et al. (2018). Converging light, energy and hormonal signaling control meristem activity, leaf initiation, and growth. *Plant Physiol.* 176, 1365–1381. doi: 10.1104/pp.17.01730

Monte-Bello, C. C., Araujo, E. F., Martins, M. C. M., Mafra, V., da Silva, V. C. H., Celente, V., et al. (2018). A flexible low cost hydroponic system for assessing plant responses to small molecules in sterile conditions. *JOVE* 138:57800. doi: 10.3791/57800

Moraes, T. A., Mengin, V., Annunziata, M. G., Encke, B., Krohn, N., Höhne, M., et al. (2019). Response of the circadian clock and diel starch turnover to one day of low light or low CO_2. *Plant Physiol.* 179, 1457–1478. doi: 10.1104/pp.18.01418

Moreau, M., Azzopardi, M., Clément, G., Dobrenel, T., Marchive, C., Renne, C., et al. (2012). Mutations in the Arabidopsis homolog of LST8/GßL, a partner of the Target of Rapamycin kinase, impair plant growth, flowering, and metabolic adaptation to long days. *Plant Cell* 24, 463–481. doi: 10.1105/tpc.111.091306

Moreno, J. C., Rojas, B. E., Vicente, R., Gorka, M., Matz, T., Chodasiewicz, M., et al. (2021). Tyr-Asp inhibition of glyceraldehyde 3-phosphate dehydrogenase affects plant redox metabolism. *EMBO J.* 40:e106800. doi: 10.15252/embj.2020106800

Mubeen, U., Giavalisco, P., and Caldana, C. (2019). TOR inhibition interrupts the metabolic homeostasis by shifting the carbon-nitrogen balance in *Chlamydomonas reinhardtii*. *Plant Signal Behav.* 14, 1670595–1670595. doi: 10.1080/15592324.2019.1670595

Mugume, Y., Kazibwe, Z., and Bassham, D. (2020). Target of rapamycin in control of autophagy: puppet master and signal integrator. *IJMS* 21:8259. doi: 10.3390/ijms21218259

Naka, K., Jomen, Y., Ishihara, K., Kim, J., Ishimoto, T., Bae, E. J., et al. (2015). Dipeptide species regulate p38MAPKSmad3 signalling to maintain chronic myelogenous leukaemia stem cells. *Nat. Commun.* 6:8039. doi: 10.1038/ncomms9039

Nozue, K., Covington, M. F., Duek, P. D., Lorrain, S., Fankhauser, C., and Harmer, S. L. (2007). Rhythmic growth explained by coincidence between internal and external cues. *Nature* 448, 358–361. doi: 10.1038/nature05946

Nukarinen, E., Nägele, T., Pedrotti, L., Wurzinger, B., Mair, A., Landgraf, R., et al. (2016). Quantitative phosphoproteomics reveals the role of the AMPK plant ortholog SnRK1 as a metabolic master regulator under energy deprivation. *Sci. Rep.* 6:31697. doi: 10.1038/srep31697

O'Leary, B. M., Oh, G. G. K., Lee, C. P., and Millar, A. H. (2020). Metabolite regulatory interactions control plant respiratory metabolism via target of rapamycin (TOR) kinase activation. *Plant Cell* 32, 666–682. doi: 10.1105/tpc.19.00157

Peng, C., Uygun, S., Shiu, S. H., and Last, R. L. (2015). The impact of the branched-chain ketoacid dehydrogenase complex on amino acid homeostasis in *Arabidopsis*. *Plant Physiol.* 169, 1807–1820. doi: 10.1104/pp.15.00461

Pfeiffer, A., Janocha, D., Dong, Y., Medzihradszky, A., Schöne, S., Daum, G., et al. (2016). Integration of light and metabolic signals for stem cell activation at the shoot apical meristem. *eLife* 5:17023. doi: 10.7554/eLife.17023

Piao, S., Wang, X., Park, T., Chen, C., Lian, X., and He, Y. (2019). Characteristics, drivers and feedbacks of global greening. *Nat. Rev. Earth Environ.* 1, 14–27. doi: 10.1038/s43017-019-0001-x.pdf

Pracharoenwattana, I., Cornah, J. E., and Smith, S. M. (2005). Arabidopsis peroxisomal citrate synthase is required for fatty acid respiration and seed germination. *Plant Cell* 17, 2037–2048. doi: 10.1105/tpc.105.031856

Pu, Y., Luo, X., and Bassham, D. C. (2017). TOR-dependent and -independent pathways regulate autophagy in *Arabidopsis thaliana*. *Front. Plant Sci.* 8:1204. doi: 10.3389/fpls.2017.01204

Ren, M., Qiu, S., Venglat, P., Xiang, D., Feng, L., Selvaraj, G., et al. (2011). Target of rapamycin regulates development and ribosomal RNA expression through kinase domain in *Arabidopsis*. *Plant Physiol.* 155, 1367–1382. doi: 10.1104/pp.110.169045

Rius, S. P., Casati, P., Iglesias, A. A., and Gomez-Casati, D. F. (2006). Characterization of an *Arabidopsis thaliana* mutant lacking a cytosolic non-phosphorylating glyceraldehyde-3-phosphate dehydrogenase. *Plant Mol. Biol.* 61, 945–957. doi: 10.1007/s11103-006-0060-5

Sadka, A., Dahan, E., Or, E., and Cohen, L. (2000). $NADP^+$-isocitrate dehydrogenase gene expression and isozyme activity during citrus fruit development. *Plant Sci.* 158, 173–181. doi: 10.1016/s0168-9452(00)00328-9

Salazar, J. D., Saithong, T., Brown, P. E., Foreman, J., Locke, J. C. W., Halliday, K. J., et al. (2009). Prediction of photoperiodic regulators from quantitative gene circuit models. *Cell* 139, 1170–1179. doi: 10.1016/j.cell.2009.11.029

Salem, M. A., Li, Y., Bajdzienko, K., Fisahn, J., Watanabe, M., Hoefgen, R., et al. (2018). RAPTOR controls developmental growth transitions by altering the hormonal and metabolic balance. *Plant Physiol.* 177, 565–593. doi: 10.1104/pp.17.01711

Salem, M. A., Li, Y., Wiszniewski, A., and Giavalisco, P. (2017). Regulatory-associated protein of TOR (RAPTOR) alters the hormonal and metabolic composition of *Arabidopsis* seeds, controlling seed morphology, viability and germination potential. *Plant J* 92, 525–545. doi: 10.1111/tpj.13667

Schaufelberger, M., Galbier, F., Herger, A., Francisco, R. B., Roffler, S., and Clement, G. (2019). Mutations in the *Arabidopsis ROL17/isopropylmalate synthase 1* locus alter amino acid content, modify the TOR network, and suppress the root hair cell development mutant *lrx1*. *J. Exp. Bot.* 70, 2313–2323. doi: 10.1093/jxb/ery463

Seaton, D. D., Graf, A., Baerenfaller, K., Stitt, M., Millar, A. J., and Gruissem, W. (2018). Photoperiodic control of the *Arabidopsis* proteome reveals a translational coincidence mechanism. *Mol. Syst. Biol.* 14:e7962. doi: 10.15252/msb.20177962

Shannon, P., Markiel, A., Ozier, O., Baliga, N. S., Wang, J. T., Ramage, D., et al. (2003). Cytoscape: a software environment for integrated models of biomolecular interaction networks. *Genome Res.* 13, 2498–2504. doi: 10.1101/gr.1239303

Smith, A. M., and Stitt, M. (2007). Coordination of carbon supply and plant growth. *Plant Cell Environ.* 30, 1126–1149. doi: 10.1111/j.1365-3040.2007.01708.x

Sokolowska, E. W., Schlossarek, D., Luzarowski, M., and Skirycz, A. (2019). PROMIS: global analysis of PROtein-metabolite interactions. *Curr. Protoc. Plant Biol.* 4:e20101. doi: 10.1002/cppb.20101

Soto-Burgos, J., and Bassham, D. C. (2017). SnRK1 activates autophagy *via* the TOR signaling pathway in *Arabidopsis thaliana*. *PLoS One* 12:e0182591. doi: 10.1371/journal.pone.0182591

Stitt, M., and Zeeman, S. C. (2012). Starch turnover: pathways, regulation and role in growth. *Curr. Opin. Plant Biol.* 15, 282–292. doi: 10.1016/j.pbi.2012.03.016

Strehmel, N., Hoehenwarter, W., Mönchgesang, S., Majovsky, P., Krüger, S., Scheel, D., et al. (2017). Stress-related mitogen-activated protein kinases stimulate the accumulation of small molecules and proteins in *Arabidopsis thaliana* root exudates. *Front. Plant Sci.* 21:1292. doi: 10.3389/fpls.2017.01292

Sulpice, R., Flis, A., Ivakov, A. A., Apelt, F., Krohn, N., Encke, B., et al. (2014). Arabidopsis coordinates the diurnal regulation of carbon allocation and growth across a wide range of photoperiods. *Mol. Plant* 7, 137–155. doi: 10.1093/mp/sst127

Szklarczyk, D., Morris, J. H., Cook, H., Kuhn, M., Wyder, S., Simonovic, M., et al. (2016). The STRING database in 2017: quality-controlled protein–protein association networks, made broadly accessible. *Nuclic Acids Res.* 45, D362–D368. doi: 10.1093/nar/gkw937

Thirumalaikumar, V. P., Wagner, M., Balazadeh, S., and Skirycz, A. (2020). Autophagy is responsible for the accumulation of proteogenic dipeptides in response to heat stress in *Arabidopsis thaliana*. *FEBS J.* 288, 281–292. doi: 10.1111/febs.15336

Tsouko, E., Khan, A. S., White, M. A., Han, J. J., Shi, Y., Merchant, F. A., et al. (2014). Regulation of the pentose phosphate pathway by an androgen receptor-mTOR-mediated mechanism and its role in prostate cancer cell growth. *Oncogenesis* 3:e103. doi: 10.1038/oncsis.2014.18

Usadel, B., Bläsing, O. E., Gibon, Y., Retzlaff, K., Höhne, M., Günther, M., et al. (2008). Global Transcript levels respond to small changes of the carbon status during progressive exhaustion of carbohydrates in *Arabidopsis* rosettes. *Plant Phys* 146, 1834–1861. doi: 10.1104/pp.107.115592

Van Leene, J., Han, C., Gadeyne, A., Eeckhout, D., Matthijs, C., Cannoot, B., et al. (2019). Capturing the phosphorylation and protein interaction landscape of the plant TOR kinase. *Nat. Plants* 5, 316–327. doi: 10.1038/s41477-019-0378-z

Verbruggen, N., and Hermans, C. (2008). Proline accumulation in plants: a review. *Amino Acids* 35, 753–759. doi: 10.1007/s00726-008-0061-6

Veyel, D., Kierszniowska, S., Kosmacz, M., Sokolowska, E. M., Michaelis, A., Luzarowski, M., et al. (2017). System-wide detection of protein-small molecule complexes suggests extensive metabolite regulation in plants. *Sci. Rep.* 7:42387. doi: 10.1038/srep42387

Veyel, D., Sokolowska, E. M., Moreno, J. C., Kierszniowska, S., Cichon, J., Wojciechowska, I., et al. (2018). PROMIS, global analysis of PROtein–metabolite interactions using size separation in *Arabidopsis thaliana*. *J. Biol. Chem.* 293, 12440–12453. doi: 10.1074/jbc.ra118.003351

Wagle, A., Jivraj, S., Garlock, G. L., and Stapleton, S. R. (1998). Insulin regulation of glucose-6-phosphate dehydrogenase gene expression is rapamycin-sensitive and requires phosphatidylinositol 3-Kinase. *J. Biol. Chem.* 273, 14968–14974. doi: 10.1074/jbc.273.24.14968

Wingler, A. (2018). Transitioning to the next phase: the role of sugar signaling throughout the plant life cycle. *Plant Physiol.* 176, 1075–1084. doi: 10.1104/pp.17.01229

Wu, Y., Shi, L., Fu, L., Liu, Y., Xiong, Y., and Sheen, J. (2018). Integration of nutrient, energy, light, and hormone signaling *via* TOR in plants. *J. Exp. Bot.* 70, 2227–2238. doi: 10.1093/jxb/erz028

Xiong, Y., McCormack, M., Li, L., Hall, Q., Xiang, C., and Sheen, J. (2013). Glucose-TOR signalling reprograms the transcriptome and activates meristems. *Nature* 496, 181–186. doi: 10.1038/nature12030

Yanovsky, M. J., and Kay, S. A. (2002). Molecular basis of seasonal time measurement in *Arabidopsis*. *Nature* 419, 308–312. doi: 10.1038/nature00996

Zhang, Z., Zhu, J.-Y., Roh, J., Marchive, C., Kim, S.-K., Meyer, C., et al. (2016). TOR signaling promotes accumulation of BZR1 to balance growth with carbon availability in *Arabidopsis*. *Curr. Biol.* 26, 1854–1860. doi: 10.1016/j.cub.2016.05.005

Zühlke, B. M., Sokolowska, E. M., Luzarowski, M., Schlossarek, D., Chodasiewicz, M., Leniak, E., et al. (2021). SLIMP: supervised learning of metabolite-protein interactions from co-fractionation mass spectrometry data. *bioRxiv* [Preprint]. doi: 10.1101/2021.06.16.448636

Conflict of Interest: The authors declare that the research was conducted in the absence of any commercial or financial relationships that could be construed as a potential conflict of interest.

Publisher's Note: All claims expressed in this article are solely those of the authors and do not necessarily represent those of their affiliated organizations, or those of the publisher, the editors and the reviewers. Any product that may be evaluated in this article, or claim that may be made by its manufacturer, is not guaranteed or endorsed by the publisher.

frontiers in Plant Science

REVIEW
published: 11 January 2022
doi: 10.3389/fpls.2021.781508

Turning the Knobs: The Impact of Post-translational Modifications on Carbon Metabolism

Cleverson C. Matiolli†, Rafael Cavém Soares†, Hugo L. S. Alves and Isabel A. Abreu**

Instituto de Tecnologia Química e Biológica António Xavier (ITQB NOVA), Universidade Nova de Lisboa, Oeiras, Portugal

Plants rely on the carbon fixed by photosynthesis into sugars to grow and reproduce. However, plants often face non-ideal conditions caused by biotic and abiotic stresses. These constraints impose challenges to managing sugars, the most valuable plant asset. Hence, the precise management of sugars is crucial to avoid starvation under adverse conditions and sustain growth. This review explores the role of post-translational modifications (PTMs) in the modulation of carbon metabolism. PTMs consist of chemical modifications of proteins that change protein properties, including protein-protein interaction preferences, enzymatic activity, stability, and subcellular localization. We provide a holistic view of how PTMs tune resource distribution among different physiological processes to optimize plant fitness.

Keywords: carbon metabolism, photosynthesis, starch, stress, PTMs, sink-source, sugar sensing

OPEN ACCESS

Edited by:
Maria Grazia Annunziata, University of Potsdam, Germany

Reviewed by:
Greg B. Moorhead, University of Calgary, Canada
Borjana Arsova, Helmholtz Association of German Research Centres (HZ), Germany

****Correspondence:***
Cleverson C. Matiolli
matiolli@itqb.unl.pt
Isabel A. Abreu
abreu@itqb.unl.pt

† These authors have contributed equally to this work

Specialty section:
This article was submitted to Plant Metabolism and Chemodiversity, a section of the journal Frontiers in Plant Science

Received: *22 September 2021*
Accepted: *15 December 2021*
Published: *11 January 2022*

Citation:
Matiolli CC, Soares RC, Alves HLS and Abreu IA (2022) Turning the Knobs: The Impact of Post-translational Modifications on Carbon Metabolism. Front. Plant Sci. 12:781508. doi: 10.3389/fpls.2021.781508

INTRODUCTION

Plants are sessile autotrophs that thrive in ever-changing environments. These changes can be predictable, such as the daily oscillations in light and temperature or unexpected pathogen infection, flooding, and desiccation. To survive and reproduce successfully, plants must quickly adjust their metabolic activities and growth and development to overcome environmental challenges.

An essential asset of a plant's life is the energy stored in the chemical bonds of sugars. During the day, plants capture the energy carried by the light to fix atmospheric carbon dioxide (CO_2) into photosynthates. The fixed carbon is partitioned between sucrose, which is transported throughout the plant to feed sink tissues, and transitory leaf starch, the latter consumed during the night to sustain metabolic activities (Webb and Satake, 2015; Mathan et al., 2021). Notably, sugar and energy levels must be tightly regulated to avoid energy starvation and its detrimental effects on plant fitness.

Plants deploy extensive crosstalk between carbon metabolism and other physiological processes to coordinate growth and stress responses. Several genetic and physiological studies highlight the interaction between sugar and hormone signaling (Rolland and Sheen, 2005; Rolland et al., 2006), showing that the genetic programs organizing the production and consumption of carbohydrates are vastly complex. The balance between growth and stress tolerance is a central issue in plant fitness: plants demand carbon and energy to overcome, or at least tolerate, the environmental challenges. On the other hand, these resources are needed for growth and reproduction. More profound knowledge of the control of carbon metabolism will allow the manipulation of carbon fluxes in the plant.

Post-translational modifications (PTMs) of proteins are essential tools of the plant regulatory toolbox to regulate carbon metabolism by enabling fast, often reversible, adjustments of target

protein properties. PTMs are Nature's solution for the transduction of perceived developmental and environmental signals. They increase the proteome complexity to achieve an efficient multi-signal integration and robustness of the responses, allowing the timing of metabolism in front of parallel cues. Additionally, different PTMs can target the same protein, sometimes the same amino acid residue, or have multiple inputs in different signaling pathway components, which dramatically increases the number of proteome combinations to accommodate fine-tuned responses (reviewed in Vu et al., 2018).

The sheer complexity of the regulation of carbon acquisition and utilization by plants is quite challenging to unveil. Despite this, the precise control of metabolic carbon fluxes is an appealing strategy to improve crop yield. There are plenty of detailed reviews discussing the role of PTMs in regulating carbon metabolism in plants. They cover in detail most of the aspects of carbon and energy-sensing (Ramon et al., 2008; Baena-González and Hanson, 2017; Margalha et al., 2019), carbon fixation (Houtz et al., 2008; Grabsztunowicz et al., 2017), starch metabolism (Kötting et al., 2010; Abt and Zeeman, 2020), and general effects of PTMs on plant metabolism (Friso and Van Wijk, 2015). However, discoveries in these research fields are frequent because a large community is engaged in dissecting carbon pathways in plants. Thus, in the present review, we provide a holistic update on the effects of PTMs in carbon metabolism. We discuss relevant updates on the carbon flow from the fixation of atmospheric CO_2 into sugars to hexose breakdown by glycolysis. We sought to cover some critical aspects of this extensive issue in plant physiology by approaching the role of PTMs in carbon metabolism: sensing; fixation; storage and remobilization; transport, and cytosolic glycolysis.

SENSING CARBON AND ENERGY: THE EUKARYOTIC CONSERVED MASTERS OF CARBON FLUX CONTROL

The utilization of carbon and energy is tightly regulated to avoid the detrimental effects of starvation (Moraes et al., 2019; Viana et al., 2021). The adequate management of sugar status, which represents the amount of carbon and energy readily available in the system, requires cellular mechanisms to detect sugar levels. These sensing mechanisms are integrated into stress-responsive regulatory networks, allowing crosstalk between developmental and environmental signals to coordinate plant metabolism and growth. Additionally, monitoring the sugar availability in different plant parts is key to determining the (re)distribution of sugars throughout the organism. In the last two decades, the role of three eukaryotic conserved kinases in maintaining carbon-energy-nutrient homeostasis has become apparent. These are the SUCROSE NON-FERMENTING RELATED KINASE1 (SnRK1) and TARGET OF RAPAMYCIN (TOR), which are pivotal protein kinases regulating carbon and nitrogen metabolism, and the hexose-phosphorylation enzyme HEXOKINASE1 (HXK1). The concerted action of these three kinases promotes carbon-energy-nutrient homeostasis, which is crucial to ensure plant fitness in changing environments (**Figure 1**).

The energy-sensing kinase SnRK1 is a central hub integrating stress responses with carbon and energy metabolism in plants (**Figure 1**; Wurzinger et al., 2018; Margalha et al., 2019; Alves et al., 2021). Dropping sugar and energy levels activates SnRK1, which in turn phosphorylates enzymes and transcription factors to reprogram the metabolism (Baena-González et al., 2007; Mair et al., 2015; Nietzsche et al., 2016). Rising SnRK1 activity favors catabolism rather than anabolism, thus repressing growth and activating energy recovery from alternative carbon sources (Baena-González et al., 2007; Nukarinen et al., 2016; Pedrotti et al., 2018). For instance, SnRK1 phosphorylates and inactivates SUCROSE PHOSPHATE SYNTHASE (SPS), NITRATE REDUCTASE (NR), and FRUCTOSE-2,6-BIPHOSPHATASE (F2KP) (**Figure 1**) [overviewed in Nägele and Weckwerth (2014)]. The inactivation of these enzymes by SnRK1 aims to redirect carbon from anabolism, such as sucrose synthesis and export, to catabolic energy-generating pathways. Additionally, the regulation of NR activity by SnRK1 is a possible point of crosstalk for carbon and nitrogen metabolism.

A great deal of SnRK1 complex regulation is that it accommodates multiple environmental and metabolic signals. The complex regulation is thought to be achieved through an array of possible configurations of SnRK1 complex subunits in addition to upstream PTMs or allosteric regulations. Briefly, SnRK1 is a trimeric protein complex containing one catalytic (α-subunit) and two regulatory β- and γ-subunits (Crepin and Rolland, 2019). However, how the subunits interact to manage the diverse set of signal inputs received by the trimeric complex is still poorly understood. SnRK1 is inhibited by trehalose-6-phosphate (T6P), which communicates the sucrose levels in the plant (sucrose-T6P nexus; reviewed in Baena-González and Lunn, 2020). Interestingly, a recent report demonstrates that the SnRK1 α-subunit alone shows independent catalytic activity when dissociated from its regulatory subunits. Upon energy limitation, i.e., a drop in sugar levels and ATP:ADP ratio, the catalytic SnRK1α subunit dissociates from the membrane-bound β-subunits. After the dissociation from the β-subunit, the SnRK1 catalytic α-subunit translocates to the nucleus to regulate gene expression through the phosphorylation of low-energy responsive transcription factors (TFs) (**Figure 1**; Ramon et al., 2019). The transcriptional reprogramming triggered by SnRK1 is partially mediated by the C/S1-group of bZIP transcription factors (Baena-González et al., 2007; Matiolli et al., 2011; Viana et al., 2021). The phosphorylation of bZIP63 by SnRK1 is followed by rearranging the heterodimerization of bZIP63 with the C/S1-group of bZIPs (Mair et al., 2015). The resulting bZIP63-S1 heterodimers promote the expression of catabolism-associated genes to recover energy from alternative sources, such as amino acids, to sustain respiration and enhance survival. Additionally, both SnRK1 and bZIP63 mediate the entrainment of the Arabidopsis circadian oscillator by sugars (Frank et al., 2018), which is thought to synchronize plant metabolism to daily external cues (**Figure 1**). The influence of SnRK1 and bZIP63 on the circadian oscillator might be essential to modulate starch degradation and plant growth (Viana et al., 2021).

SnRK1 also modulates the activity of other transcription factors regulating genes associated with carbon and energy

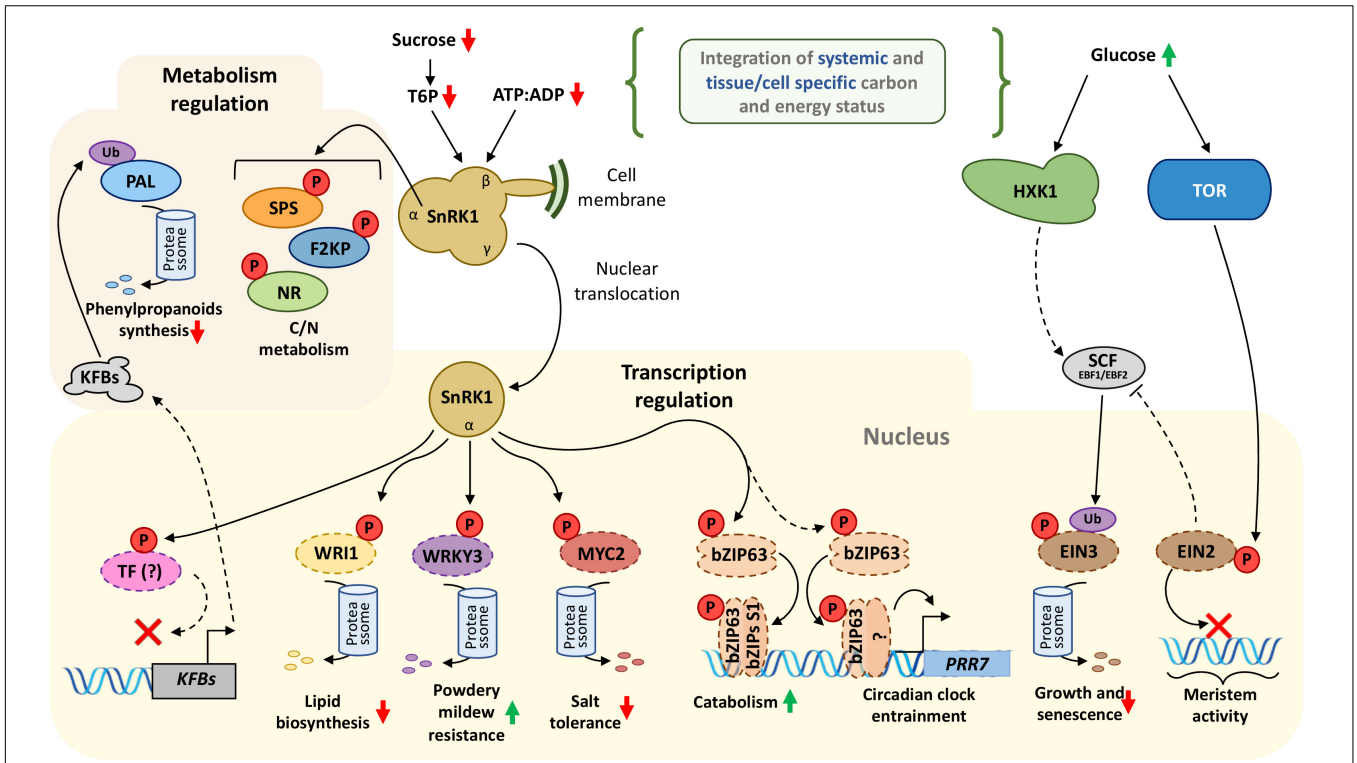

FIGURE 1 | The evolutionary conserved carbon and energy-sensing in plants. Sugars and energy levels are detected by SnRK1 and TOR sensors, which in turn phosphorylate enzymes and transcription factors (TFs) to shift the balance between anabolic and catabolic processes to attain metabolic homeostasis. The hexose-phosphorylating enzyme HXK1 has catalysis-independent sugar sensing activity, which regulates ethylene signaling and the gene expression of photosynthesis-related genes. Sugar levels modulate SnRK1 activity (see the article for details on the sucrose-T6P nexus regulating SnRK1 activity) and ATP:ADP ratio. SnRK1 phosphorylates enzymes involved in carbon and nitrogen metabolism – such as SPS, F2KP, and NR – to coordinate the metabolic demands of growth and stress responses. SnRK1 phosphorylates and destabilizes several TFs – namely WRI1, WRKY3, and MYC2 – to adjust the physiological responses to a plethora of internal and external cues (e.g., carbon and energy starvation; biotic and abiotic stresses). The phosphorylation of the sugar-responsive circadian clock regulator bZIP63 by SnRK1 modifies its dimerization pattern with C/S1-bZIPs group, activating the transcription of genes associated with catabolism to supply metabolic demands. Additionally, bZIP63 entrains the circadian clock in response to sugars by inducing *PRR7* transcription, possibly relying on SnRK1 signaling. SnRK1 likely targets a still unidentified TF to modulate the expression of specific KFBs, which are E3-ubiquitin ligases containing Kelch motifs. These KFBs ubiquitinate and target the PAL enzyme to degradation, decreasing the phenylpropanoids biosynthesis. EIN3, an ethylene-responsive TF, appears to be at the interface of the molecular responses to both energy deficit and availability. EIN3 stability is putatively modulated by SnRK1 and HXK1, which respond to antagonistic signals: dropping or rising sugar levels, respectively. SnRK1 directly phosphorylates EIN3 to destabilize it. Glucose availability perceived by HXK1 indirectly triggers EIN3 degradation, a process that could involve $SCF^{EBF1/2}$-mediated EIN3 ubiquitination. TOR prevents the nuclear translocation of EIN2, which in turn inhibits EBF1/2 translation and thus EIN3 degradation, highlighting a potential role of EINs in the crosstalk between hormonal and energy/nutrient signaling. Interestingly, phosphorylation and ubiquitination seem to be fundamental PTMs that translate the energy and stress signals perceived by SnRK1, HXK1, and TOR. Ellipses and other rounded shapes = proteins (dashed lines: transcription factors (TFs), solid lines: enzymes). Phosphorylation (P); ubiquitination (Ub). Connectors ending with arrows = activation; connectors ending with bars = repression. Solid connectors = demonstrated pathways; dashed connectors = hypothetic pathways. Green upward arrows = induction; red downward arrows = repression.

metabolism. For instance, SnRK1 phosphorylates the AP2-type TF WRINKLED1 (WRI1) to trigger its degradation by the 26S proteasome, which in turn represses lipid biosynthesis when the cellular sugar level is low (Zhai et al., 2017). SnRK1 phosphorylation also triggers the degradation of the basic helix-loop-helix (bHLH) MYC2 to antagonize salt tolerance (Im et al., 2014). In barley, SnRK1 phosphorylates WRKY3 to enhance the resistance to powdery mildew (Han et al., 2020), possibly modulating carbon homeostasis to optimize growth-defense balance (**Figure 1**). Phenylpropanoid synthesis is a strong sink for fixed carbon in plants, synthesizing lignin and secondary metabolites for defense. When activated by energy starvation, SnRK1 represses the accumulation of phenylpropanoids by downregulating the transcription of a set of KELCH DOMAIN-CONTAINING F-BOX (KFB) proteins. These KFB proteins ubiquitinate the PHENYLALANINE AMMONIA-LYASE (PAL) and assign it for degradation (**Figure 1**). The transcription of KFB genes by SnRK1 could be mediated by SnRK1-dependent phosphorylation of still unidentified transcription factors (Wang et al., 2021). The evidence suggests a clear relationship between phosphorylation and ubiquitination, two of the most common PTMs in plants, prompting us to uncover how these two PTMs crosstalk to integrate different signals.

Efficient environmental and metabolic signal integration requires multi-level interaction between different signaling pathways. For instance, SnRK1 shares targets, including carbon

and nitrogen metabolic enzymes, with several calcium-dependent protein kinases (CDPKs) (reviewed in Alves et al., 2021). Interestingly, SnRK1 and HXK1 signaling pathways converge in the regulation of the ETHYLENE INSENSITIVE3 (EIN3) transcription factor protein stability (Moore et al., 2003; Yanagisawa et al., 2003; Kim et al., 2017). Ethylene is a gaseous hormone that regulates growth and senescence, two critical physiological processes inextricably bound to the carbon and energy economy. While glucose availability induces EIN3 degradation mediated by HXK1 glucose sensing-activity, SnRK1 directly phosphorylates EIN3 to enable its degradation (**Figure 1**). The proteolysis of EIN3 triggered by HXK1-mediated glucose sensing and SnRK1 direct phosphorylation is likely mediated by the $SCF^{EBF1/EBF2}$ complexes containing the F-box proteins EIN3-binding F-box1 or 2 (EBF1/EBF2) that ubiquitinate the transcription factor EIN3 (Gagne et al., 2004). Phosphorylation and degradation of EIN3 slow down leaf senescence, suggesting a fine-tunning mechanism to regulate developmental aging of photosynthetic tissues according to carbon status. Interestingly, phosphorylation of ETHYLENE INSENSITIVE2 (EIN2) by TOR prevents its nuclear localization (Fu et al., 2021) and partially mediates the glucose-activated gene expression reprogramming orchestrated by TOR to regulate meristem activity (Xiong et al., 2013). The putative increase of the EIN2 pool outside the nucleus might enhance its role as a repressor of EBF1/2 translation (Li et al., 2015), thus inhibiting EIN3 degradation. The crosstalk between SnRK1, TOR, and HXK1 to modulate ethylene signaling in response to carbon status is a clear example of the multi-level regulation of critical developmental signaling pathways by PTMs.

TOR is responsible for monitoring resource availability to activate metabolic processes associated with biosynthesis and growth. Thus, TOR and SnRK1 have antagonistic effects on plant energy and carbon metabolism. While SnRK1 is activated by energy and carbon deprivation, TOR is activated by carbon and nutrient availability to promote translation and meristem activation in response to sugars and amino acids (Xiong et al., 2013; Cao P. et al., 2019; Liu et al., 2021). In plants, TOR acts in a protein complex composed of two more regulatory proteins: RAPTOR1B and LST8 (Dobrenel et al., 2016). The SnRK1 α-subunit interacts with RAPTOR1B in the cytoplasm of plant cells and phosphorylates RAPTOR1B *in vitro* (Nukarinen et al., 2016), resembling the regulatory crosstalk observed in yeast and mammals for the ortholog counterparts of the plant SnRK1 and RAPTOR1B. The regulatory crosstalk between SnRK1 and TOR pathways is thought to balance anabolism and catabolism to maintain carbon and nutrient homeostasis. For instance, TOR inhibition disrupts the carbon/nitrogen (C/N) balance under carbon limitation in *Chlamydomonas reinhardtii* (Mubeen et al., 2019).

The regulator of G-protein signaling1 (RGS1) is a transmembrane protein localized in the plasma membrane that senses D-glucose (Chen and Jones, 2004), coordinating cell proliferation and hypocotyl elongation in response to glucose (Chen et al., 2003). There are fewer studies analyzing the function of RGS1 in sugar sensing and carbon metabolism regulation, but recent evidence links RGS1 to plant immunity. Plant immunity can be a taxing physiological process in plants. On one side, pathogens try to hijack carbon, energy, and nutrients from the host plant. On the other side, the plant deploys both evasive and attacking strategies to fend off the invaders. The primary response to biotic stress relies on detecting microbe-associated molecular patterns (MAMPs) by specific cell membrane receptors. Liang et al. (2018) showed that RGS1 maintains the flagellin receptor FLAGELLIN-SENSITIVE2 (FLS2) in an inactive form by forming a protein complex (Liang et al., 2018). Upon detecting bacterial flagellin or its conserved peptide flg22, RGS1 is phosphorylated by FLS2-bound kinase BRASSINOSTEROID INSENSITIVE 1-associated receptor kinase 1 (BAK1) to promote the release of FLS2 and subsequent downstream activation of cytoplasmic kinases. One can hypothesize that this mechanism may act as a rheostat balancing glucose availability with the costly defense activation.

CARBON FIXATION: PHOTOSYNTHESIS

Chloroplasts are power generators of plant cells: they convert the energy carried by light into the chemical energy of covalent bonds of sugars. These sugars can be stored as semi-crystalline starch granules, the "battery" keeping the plant metabolism running in the absence of light or transported from photosynthetic tissues (source) in the form of sucrose to non-photosynthetic or young tissues (sink). The light energy is captured by the light-harvesting complex (LHC) to produce reducing power in the form of NADPH and create a proton gradient between the thylakoid lumen and the chloroplast stroma. The proton gradient is then converted into ATP by the ATP-synthase embedded in the thylakoid membrane. The NADPH and ATP are used in the series of carbon-fixing reactions inside the chloroplast. The light input also triggers redox signaling by allowing the reduction of disulfide bridges in chloroplastic proteins through the ferredoxin/thioredoxin (Fd/Trx) system and NADP-dependent thioredoxin reductase C (NTRC) (Nikkanen and Rintamäki, 2019). The reducing power stored in the thioredoxins is used to reduce enzymes of the Calvin-Benson cycle (CBC) (reviewed in Selinski and Scheibe, 2019). Notably, the Fd/Trx and NTRC-mediated reduction-signaling pathways complement each other during light conditions, and they also can communicate among them. The Fd/Trx system affects NTRC substrate availability by balancing the chloroplastic NADPH/ATP ratio through ferredoxin-NADP reductase and the reduction-activation of NADP-malate dehydrogenase (NADP-MDH) (Ceccarelli et al., 2004; Lemaire et al., 2005; Yokochi et al., 2021). Thioredoxin also affects ATP synthesis directly through the reduction-activation of chloroplast ATP synthase (Schumann et al., 1985). NADP-MDH synthesizes malate from oxaloacetate, which is easily transported and readily used as an indirect source of reducing equivalents or for ATP synthesis. The regulation of the redox state of enzymes associated with carbon fixation and starch metabolism is one of the most relevant PTMs modulating carbon metabolism (**Figure 2**).

Photosynthetic carbon fixation starts when atmospheric CO_2 is assimilated into 3-phosphoglycerate (3PG) in a

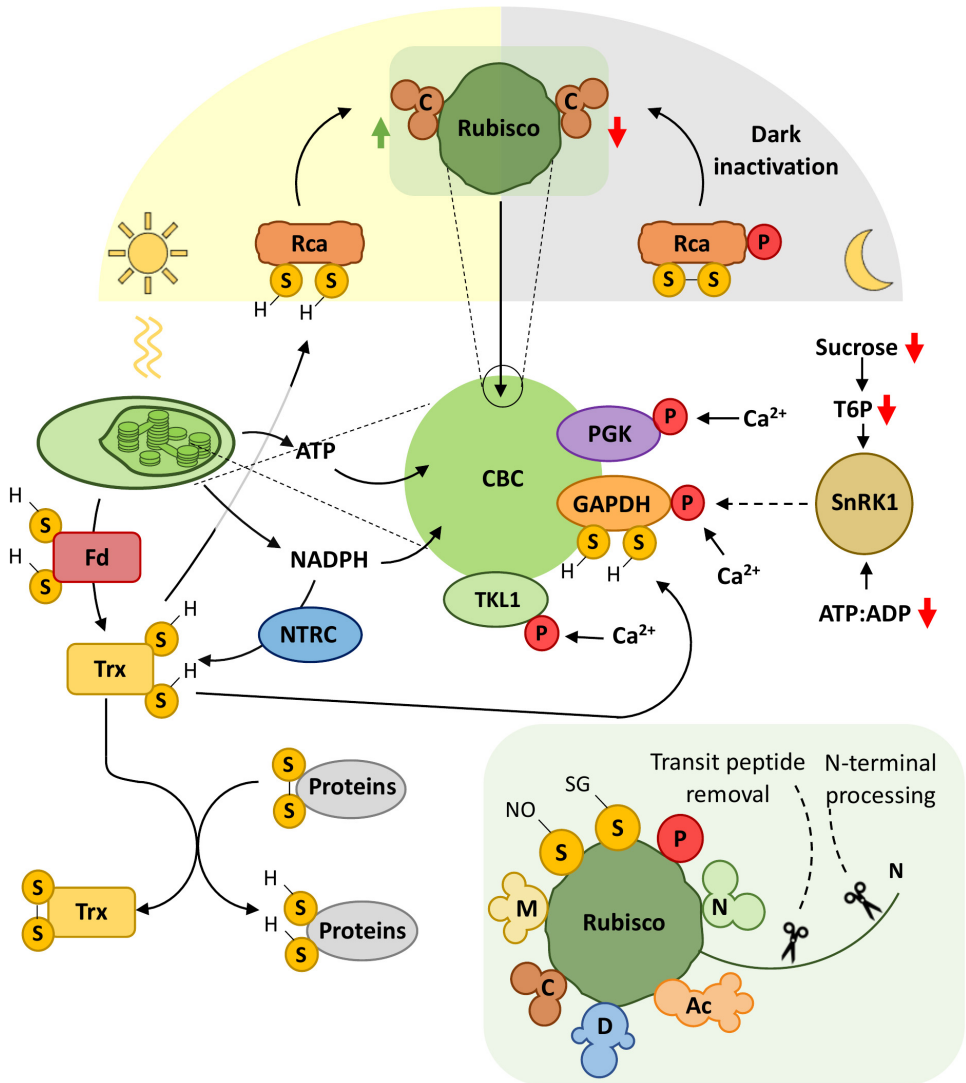

FIGURE 2 | PTMs modulate carbon fixation. The carbon assimilation in plants is heavily regulated to allow its adjustment to a plethora of incoming signals from metabolism and the external environment. The figure depicts the photosynthetic carbon fixation through the Calvin-Benson cycle (CBC) and Rubisco activity, coupled to the Fd/Trx and NTRC complexes and ATP formation. The major signals modulating the CBC activity are light/dark transitions, redox status, sugar availability, Ca^{2+} levels, and ATP:ADP ratio. Light powers photosynthesis to generate energy (ATP) and reducing power in the form of NADPH. NTRC uses NADPH as a substrate to reduce Trx, in a mechanism not necessarily dependent on light. Importantly, NADPH allows the communication between the Fd/Trx and NTRC complexes. Trx sulfhydryl groups reduce several proteins, including CBC enzymes, to regulate their activity. One crucial example is Rca, whose reduction state directly affects Rubisco activity. During the day, reduced Rca removes inhibitory RuBP and facilitates Rubisco carbamylation to enhance its carboxylase activity. During the night, oxidized and phosphorylated Rca cannot reactivate Rubisco, shutting down photosynthesis. The activity of other CBC enzymes, such as PGK, TKL1, and GAPDH, is modulated via Ca^{2+}-dependent phosphorylation, which highlights the integration of developmental signals and environmental stresses into photosynthesis regulation. GAPDH is a putative *in vivo* direct target of SnRK1 and is also modulated by the redox state through Trx. The SnRK1-Trx regulation of GAPDH activity may act as a central hub in the CBC to adjust carbon and energy metabolic fluxes accordingly to tissue-specific and/or developmental demands. Inset figure: Rubisco is regulated by a myriad of PTMs, highlighting its central role in carbon fixation. Phosphorylation (P), tyrosine nitration (N), lysine methylation (M), acetylation (Ac), sulfhydryl groups (S-H), disulfide bridge (S-S), nitrosylation (S-NO), glutathionylation (S-SG), deformylation (D), carbamylation (C). Connectors ending with arrows = activation; connectors ending with bars = repression. Solid connectors = demonstrated pathways; dashed connectors = hypothetic pathways. Green upward arrows = induction; red downward arrows = repression.

reaction catalyzed by Ribulose-1,5-bisphosphate (RuBP) carboxylase/oxygenase (Rubisco). As a central enzyme in carbon fixation, Rubisco is heavily regulated by various PTMs, namely: phosphorylation, tyrosine nitration, acetylation, lysine methylation, nitrosylation and glutathionylation, N-terminal processing, deformylation, transit peptide removal, and carbamylation (reviewed in Grabsztunowicz et al., 2017; **Figure 2**). The reactivation of Rubisco by the carbamylation of the lysine in the Rubisco active site relies on the regulation of the chaperone Rubisco activase (Rca) by both the redox state

and ATP/ADP ratio in the chloroplast (Carmo-Silva et al., 2015). The Fd/Trx system reduces Rca disulfide bridges, resulting in increased Rca activity (Zhang and Portis, 1999). Activated Rca continuously remodels inhibited active sites of Rubisco by removing inhibitory RuBP to enhance photosynthetic activity (Carmo-Silva et al., 2015; Perdomo et al., 2021; **Figure 2**). Moreover, Rca dark-dependent inactivation is putatively regulated by Thr78 and Ser172 phosphorylation (Boex-Fontvieille et al., 2014). Rca phosphorylation relocates it to the thylakoid membrane, where Rca protects the chloroplast Serine/threonine-protein kinase (Stt7) from proteolysis. Stt7 participates in balancing excitation energy between photosystem I and II for photosynthetic yield optimization (Lemeille et al., 2010). The phosphoproteome of the *Chlamydomonas* mutant *stt7* revealed three groups of thylakoid membrane proteins regulated by phosphorylation: (i) Stt7-dependent (composed mostly of LHCII proteins); (ii) redox-dependent (independently of Stt7); and (iii) redox-independent (Lemeille et al., 2010).

Besides Rubisco, other CBC enzymes are regulated by phosphorylation. PHOSPHOGLYCERATE KINASE (PGK), GLYCERALDEHYDE 3-PHOSPHATE DEHYDROGENASE (GAPDH), and TRANSKELOTASE1 (TKL1) are phosphorylated in a Ca^{2+}-dependent manner (Reiland et al., 2009; Piattoni et al., 2017), suggesting that the activity of these enzymes is modulated by internal and external cues triggering cellular [Ca^{2+}] changes, such as developmental signals and environmental stresses. Interestingly, GAPDH is phosphorylated by the SnRK1 *in vitro*, and its activation mechanism also requires redox regulation (Holtgrefe et al., 2008; Piattoni et al., 2017; Schneider et al., 2018; **Figure 2**). A sugar-derived signal might affect this process because tissues with different carbon reserves present different SnRK1 activities and phospho-GAPDH profiles (Piattoni et al., 2017). GAPDH seems to act as a central hub for regulating energy supply and balancing carbon and energy metabolic fluxes (Schneider et al., 2018).

CARBON STORAGE AND REMOBILIZATION: STARCH METABOLISM AND AUTOPHAGY

A share of the photoassimilates is stored as starch during the day. The partitioning of photoassimilates is heavily regulated to accommodate current cellular metabolic activities and storage for later use and the likely occurrence of environmental fluctuations in light and carbon utilization demand to fight stress. For instance, transitory starch synthesis and degradation can coincide during long-day or low-light end-of-day conditions (Fernandez et al., 2017) or during stress (Thalmann and Santelia, 2017). Various enzymes control starch synthesis and degradation, and some take part in both processes (reviewed in Kötting et al., 2010). Additionally, several starch metabolic enzymes have differential spatio-temporal expression patterns (Qu et al., 2018). All these factors point to a complex and concerted regulation of starch enzymes' activity with temporal and spatial parameters.

The major transitory starch synthesis pathway starts with the conversion of glucose-6-phosphate (G6P) to glucose-1-phosphate (G1P) by the plastidial protein PHOSPHOGLUCOMUTASE1 (PGM1), an enzyme that catalyzes the interconversion G6P ↔ G1P (Caspar et al., 1985). While the conversion of G6P to G1P is an essential step of starch synthesis, the generation of G6P from G1P can feed glucose to glycolysis or to anabolic reactions during starch degradation. Arabidopsis mutants lacking a functional PGM1 enzyme accumulate around 1% of the starch of a wild type plant, severely impairing C-net fixation throughout the diel cycle and growth (Usadel et al., 2008). PGM1 is S-nitrosylated in multiple sites (Hu et al., 2015), leading to the hypothesis that PGM1 activity could be modulated by nitric oxide (NO) levels. Interestingly, high NO levels inhibit starch accumulation in Arabidopsis (Zhang et al., 2017). It could be interesting to investigate if PGM1 S-nitrosylation plays a role in the regulation of starch synthesis. Additionally, a quantitative phosphoproteomic analysis of the Arabidopsis ABA-insensitive triple mutant *snrk2.2/2.3/2.6* revealed that PGM1 could be phosphorylated in response to ABA (Wang et al., 2013), resulting in the putative modulation of photosynthetic carbon flow into or from starch in response to abiotic stress.

Redox-regulation and phosphorylation are the prevailing PTMs modulating starch metabolism (**Figure 3**). ADP-glucose (ADPGlc) synthesis by ADP-glucose pyrophosphorylase (AGPase) is a key regulatory node for directing carbon to starch granule formation according to the plastid redox state (Michalska et al., 2009). The AGPase is a heterotetrameric holoenzyme composed of two small catalytic (APS) and two large (APL) subunits. They are arranged in two pairs APS-APL heterodimers linked by a disulfide-bridge between the two APS subunits (Geigenberger et al., 2005; Hädrich et al., 2012). The AGPase connects photosynthesis to starch metabolism through the Fd/Trx system and the NADP-dependent thioredoxin reductase C (NTRC) (Hendriks et al., 2003; Skryhan et al., 2018). The AGPase heterotetramer is activated *in vitro* by thioredoxin *f/m* and NTRC when the disulfide bridge formed by the APS subunits' Cys82 residues is reduced (Michalska et al., 2009; Geigenberger, 2011). NTRC has also been shown to modulate AGPase activity *in vivo* and regulate the AGPase independently of light via NADPH generated by sugar catabolism (Michalska et al., 2009). The AGPase redox state, and thus starch synthesis, is also modulated by SnRK1 (**Figure 3**). Redox activation of other starch biosynthetic enzymes was also observed *in vitro* for starch synthases (SS), branching (SBE), and debranching enzymes (DBE), such as the Arabidopsis SS1, SS3, SBE2, and the spinach pullulanase (Schindler et al., 2001; Glaring et al., 2012). Overexpression of SnRK1 in Arabidopsis decreases the amount of AGPase in the active reduced state (Geigenberger et al., 2005; Jossier et al., 2009). Interestingly, the artificial increase of T6P through the overexpression of TREHALOSE PHOSPHATE SYNTHASE1 (TPS1) also leads to the accumulation of AGPase in a monomeric state (Kolbe et al., 2005). The increase of AGPase in the monomeric state could be reproduced by sucrose but not glucose, suggesting that the process may obey the sucrose-T6P nexus (Baena-González and Lunn, 2020; Peixoto et al., 2021). The increase in sucrose levels leads to increased T6P accumulation, a process that might be regulated by SnRK1

(Peixoto et al., 2021), which in turn, feedback regulates carbon partitioning between sucrose and starch. Further analysis considering the diel fluctuation in the sink and source tissues on the regulation of SnRK1 and T6P in starch metabolism is needed to clarify this pathway.

Starch granule formation is catalyzed by SS, SBE, and debranching enzymes (DBE), as depicted in **Figure 3**. To initiate the synthesis of insoluble glucan composed of amylose and amylopectin polymers, SSs transfer the glucosyl-moiety of ADPGlc to the acceptor molecule α-1,4-D-glucan, performing α-1,4 linkage (glucan elongation). SBEs perform transglycosylation of α-1,4 linkages to α-1,6 branch points between the same or different α-1,4-D-glucans molecules (glucan branching). DBEs, which cleave α-1,6- linkages, are thought to curate the glucan branching points to allow correct granule formation. Increasing evidence supports the regulation of starch granule formation-associated enzymes through phosphorylation. The Arabidopsis SS2 is phosphorylated at the end of the dark period, at the region S63/65, which holds the canonical binding motif of Casein Kinase II (CKII) (Reiland et al., 2009; Patterson et al., 2018). Although the functional relevance of this phosphorylation is unclear, chloroplastic CKII also phosphorylates other starch biosynthetic enzymes such as fibrillin and SBE2.1 *in vitro* (Schönberg et al., 2014). Fibrillin interacts with SS4, allowing the complex to associate with specific thylakoid regions where starch granules formation may initiate (Gámez-Arjona et al., 2014; Schönberg et al., 2014). Phosphorylation also affects complex formation between SSs, SBEs, and other proteins, which may increase starch polymerization efficiency (Tetlow et al., 2004, 2008; Liu et al., 2012; Mehrpouyan et al., 2021). Barley SS and SBEs have been found to interact with 14-3-3 proteins, which can form dimers and bind to phosphorylated client proteins (**Figure 3**; Alexander and Morris, 2006). Thus, 14-3-3 proteins may act as a scaffold for the formation of starch metabolic enzyme complexes. In wheat, phosphorylation activates SBEIIa and SBEIIb in chloroplasts and amyloplasts, respectively, while dephosphorylation decreases their activities (Tetlow et al., 2004).

The GLUCAN WATER DIKINASE (GWD) phosphorylates the C6 position of glucose moieties in starch granules, opening its structure and consequently increasing the accessibility of β-amylases (BAMs) to the polymer (**Figure 3**), allowing efficient starch degradation (Reimann et al., 2004; Ritte et al., 2006; Edner et al., 2007). The redox state of GWD strongly affects its activity *in vitro*, being rendered almost totally inactive after being oxidized while its reduction could revert this effect (Mikkelsen et al., 2005). The major product of leaf starch breakdown is maltose, a reaction catalyzed by BAMs (Weise et al., 2005). In Arabidopsis, the degradation of starch into maltose is catalyzed by β-AMYLASE1 (BAM1) and β-AMYLASE3 (BAM3), a process in which the latter plays a major role in transitory leaf starch degradation. Knockout *bam3* mutant plants show stunted growth and strong starch-excess phenotype, while *bam1* has slightly higher starch accumulation at the end of the night compared to wild type plants. Importantly, knocking out BAM3 exacerbates the latter phenotype (Caspar et al., 1991; Fulton et al., 2008), suggesting that they operate cooperatively to convert starch into maltose. The redox-regulated BAM1 is the only BAM enzyme activated in reducing conditions *in vitro*, especially by thioredoxin *f* and NTRC (Sparla et al., 2006; Valerio et al., 2011). Interestingly, BAM1, but not BAM3, is associated with a diurnal starch breakdown in osmotically stressed mesophyll and guard cells for osmolytes production to open the stomata in the morning (Valerio et al., 2011). The N-terminal of BAM1 (Ser31) is phosphorylated in a TOR-dependent manner (**Figure 3**; Van Leene et al., 2019). How this phosphorylation influences BAM1 activity is still unknown, but it is reasonable to hypothesize that the TOR-mediated phosphorylation could activate BAM1 to remobilize carbon from starch to growth and to open the stomata.

BAM1 and α-AMYLASE3 (AMY3) act synergistically to promote stomatal opening in the light and under osmotic stress. The AREB/ABF-SnRK2 kinase-signaling pathway increases the activity of BAM1 in response to ABA treatment by enhancing BAM1 transcription (Thalmann et al., 2016). In the same work, the authors showed that the *amy3 bam1* double mutant has impaired root growth, suggesting that this ABA-regulatory pathway adjusts carbon utilization from starch to meet both growth and stress tolerance demands. AMY3 was found to interact with SCE1 in a large-scale screening for proteins interacting with SUMOylation machinery (Elrouby and Coupland, 2010), suggesting that AMY3 might be regulated by SUMOylation (**Figure 3**). The degradation of starch by BAMs releases maltose that is transported to the cytosol through the maltose transporter MALTOSE EXCESS1 (MEX1) (Niittylä et al., 2004). MEX1 localized in the chloroplast envelope and was found to be phosphorylated at Ser76 in a large-scale phosphoproteomic assay (**Figure 3**; Nakagami et al., 2010). It could be interesting to investigate if the phosphorylation of Ser76 regulates MEX1 transport activity in response to the cellular carbon status. The maltose exported from the chloroplast is processed by the maltotriose-metabolizing enzyme DISPROPORTIONATING ENZYME2 (DPE2) to generate glucose for glycolysis and sucrose synthesis for export during the night. A quick search for Arabidopsis DPE2 PTMs using the PTM-Viewer webtool[1] revealed that DPE2 undergoes multiple modifications, including acetylation, ubiquitination, and phosphorylation (**Figure 3**). Further investigation of these PTMs, as well as its effectors, may shed light on the regulation of carbon flux from the chloroplast to the cytosol for glycolysis and sucrose synthesis.

Autophagy is an evolutionary conserved catabolic process encompassing both selective and non-selective degradation of cytosolic material. It recycles carbon, nitrogen, and energy to sustain respiration, growth, and reproduction. In plants, the attack of condemned proteins and organelles by lytic enzymes takes place in vacuolar autophagic bodies that are originated either by the engulfment of cytosolic material through tonoplast invagination (i.e., microautophagy) or by the vacuolar fusion with the autophagosome carrying proteins, organelles, and large portions of the cytosol (i.e., macroautophagy, hereafter autophagy) (Li and Vierstra, 2012). Autophagy plays a vital role in plants by keeping adequate energy and nutrient levels throughout development, particularly upon exposure to adverse environmental conditions (Thompson et al., 2005;

[1]https://www.psb.ugent.be/webtools/ptm-viewer

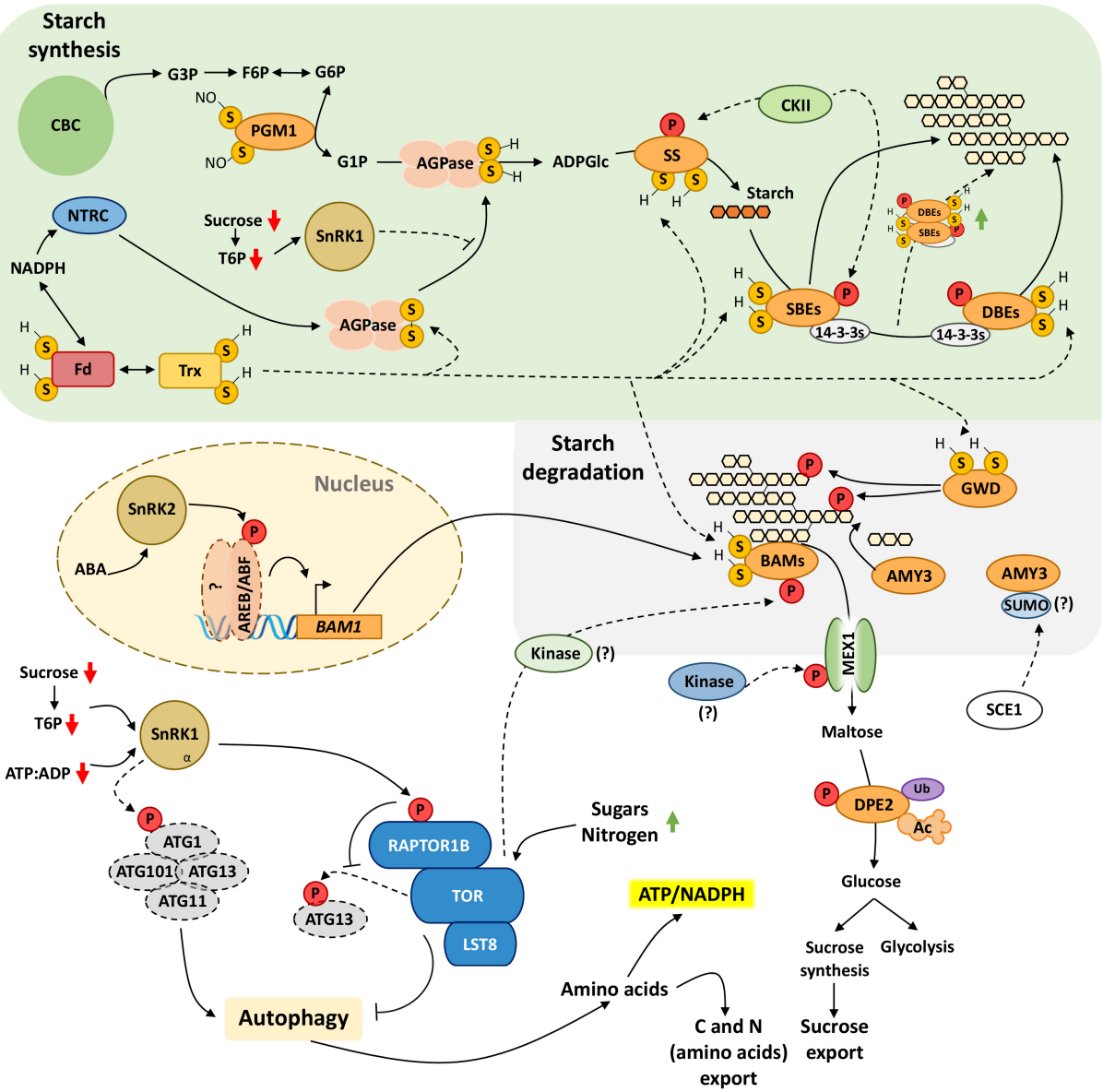

FIGURE 3 | Cellular redox status and phosphorylation control critical steps of starch metabolism. PTMs serve for tight, transient control of enzymes involved in starch metabolism to meet the energy demands associated with daily growth and stress responses. NTRC uses the NADPH to reduce and activate AGPase. Trx can also reduce AGPase *in vitro*, but the *in vivo* evidence is still lacking. Here, we hypothesize that Trx could also regulate the redox state of other enzymes associated with starch metabolism. AGPase might also integrate systemic and tissue-specific signals conveying the carbon status, putatively through the sucrose-T6P nexus and SnRK1 regulatory axis. AGPase synthesizes the substrate of starch polymerization, ADP-Glucose (ADP-Glc), which enters the starch synthesis pathway performed by a set of enzymes that elongates and control the branching of starch polymer (e.g., SS, SBEs, and DBEs). The phosphorylation of these enzymes seems to generally enhance their activity, possibly through the formation of metabolic enzyme complexes. The binding of 14-3-3 proteins to SBEs and DBEs might also promote enzyme complex formation to increase starch polymerization efficiency. Redox regulation is also necessary for starch degradation as the reduced GWD phosphorylates starch to open its structure and increase starch availability to amylases. Beta-amylases (BAMs) catalyze starch breakdown into maltose, and this crucial step might integrate hormonal (ABA) and nutrient signals through SnRK2-AREB/ABF pathway and TOR. While SnRK2 enhances *BAM1* expression, TOR-dependent BAM1 phosphorylation might enhance its activity. The physiological relevance of several PTMs of proteins involved in starch degradation, such as alpha-amylase AMY3, maltose export from chloroplast (MEX1), and conversion to glucose (DPE2), is yet to be clarified. Nonetheless, protein disulfide reduction and phosphorylation seem to be essential PTMs regulating starch synthesis/degradation dynamics. Upon C-starvation, SnRK1 promotes autophagy processes through ATG1 phosphorylation, activating the ATG1 kinase complex (ATG1, AGT13, ATG101, and ATG11). SnRK1 also phosphorylates RAPTOR1B and disrupts the TOR kinase complex that inhibits the ATG1 complex. The SnRK1-TOR axis regulates starch degradation and autophagy to promote energy and nutritional homeostasis at the cellular and systemic levels. Phosphorylation (P), ubiquitination (Ub), acetylation (Ac), sulfhydryl groups (S-H), disulfide bridge (S-S), nitrosylation (S-NO). Connectors ending with arrows = activation; connectors ending with bars = repression. Solid connectors = demonstrated pathways; dashed connectors = hypothetic pathways. Green upward arrows = induction; red downward arrows = repression. Starch is represented by many linked glucose moieties, while fewer linked glucose moieties represent starch degradation products.

Izumi et al., 2013; Michaeli et al., 2016). The AUTOPHAGY RELATED1 (ATG1) kinase complex is composed of four subunits (ATG1/ATG13/ATG11/ATG101) (**Figure 3**) and initiates the autophagic process by phosphorylating proteins and targeting them for destruction (Kijanska and Peter, 2013). Nutrient deficiency and environmental stresses activate SnRK1, which promotes autophagy to remobilize resources needed to sustain respiration and cope with stress. Part of this regulation is thought to be achieved through the repression of the TOR complex. SnRK1 catalytic α-subunit interacts with the TOR complex regulatory subunit RAPTOR1B and phosphorylates it *in vitro* (Nukarinen et al., 2016). On the other hand, ATG13, a member of the ATG1 kinase complex, is phosphorylated in multiple sites in a TOR-dependent manner (Van Leene et al., 2019). Thus, RAPTOR1B phosphorylation by SnRK1 is likely to alleviate the repression of the ATG1 kinase complex exerted by the TOR complex activity (**Figure 3**). SnRK1 can also regulate autophagy through direct or indirect phosphorylation of ATG1 protein in the ATG1 kinase complex (Chen et al., 2017). Recently, Huang et al. (2019) proposed that SnRK1 regulates autophagy through two distinct pathways: short-term C-starvation triggers the phosphorylation of ATG1 protein, while long-term C-starvation signal is conveyed by ATG1-independent signaling pathway to activate the ATG1 kinase complex (Huang et al., 2019).

Autophagy and starch degradation seem to act synergistically during the night to optimize growth because double mutants impaired in both processes have enhanced dwarf phenotype compared to the single mutants (Izumi et al., 2013; **Figure 3**). SnRK1 may act as a hub coordinating starch degradation and autophagy to supply energy and nutrients required by growth and stress responses. We discussed before that TOR inhibition disrupts the carbon/nitrogen (C/N) balance under carbon limitation caused by extended darkness in *Chlamydomonas reinhardtii* (Mubeen et al., 2019). Moreover, extended darkness leads to carbon starvation due to the exhaustion of the transitory starch accumulated for the duration of the night. Thus, the additive effect of starch degradation and autophagy on growth likely involves the coordination of SnRK1 and TOR pathways, ensuring the availability of energy and amino acids for translation. Altogether, the SnRK1-TOR regulatory axis dynamically modulates starch and autophagy remobilization to optimize resource utilization under nutrient and carbon-energy stress.

As we see, recycling carbon and energy is essential in stress responses and plant development. It is becoming clear that ubiquitination, and its interaction with phosphorylation, plays a large role in sugar sensing in the early stages of Arabidopsis development. Loss-of-function mutants of RING-H2 E3 ligase *SUGAR-INSENSITIVE3* (*SIS3*) are hypersensitive to sucrose-mediated repression of cotyledon expansion and true leaves formation (Huang et al., 2010), but the molecular mechanism is still unclear since upstream regulators and SIS3 ubiquitination targets are still unknown. ATL15 is RING-H2 E3 ligase, which belongs to the family Arabidopsis Tóxicos en Levadura (ATL) that possess a characteristic N-terminal transmembrane domain that also regulates Arabidopsis development in response to sugars. The *ATL15* transcript is repressed by sugars, and the *atl15* knockout mutant is hypersensitive to high glucose concentrations during early seedling development (Aoyama et al., 2017). Starch levels are also lower in seedlings of *atl15* grown in high glucose concentrations, suggesting that *ATL15* could affect carbon partitioning. Further experiments under physiological conditions, i.e., older plants grown in soil and under equinoctial conditions, are needed to establish ATL15 as a regulator of carbon fluxes. Another ATL family member, ATL8, is induced by sugar starvation and interacts with STARCH SYNTHASE4 (SS4) in the split-ubiquitin assay (Luo et al., 2019). The results suggest that ATL8 could also be involved in starch metabolism. However, protein-protein interaction assays in plant cells are needed to demonstrate the co-localization of these proteins.

CARBON TRANSPORT AND PARTITIONING: THE SUGAR FLOW FROM SOURCE TO SINK

Understanding the mechanisms by which plants allocate resources to different processes in a sink-source context is fundamental to improving and domesticating crops. For example, during seed development and filling, the plant destinates substantial amounts of carbon, nitrogen, and other essential elements to the seed. The resources stored in the seeds are required for the first stages of seedling development when photosynthesis and nutrient uptake are not an option yet. The nutrient-rich seeds are extensively used in human/animal feeding and in a variety of technological applications. Thus, seed quality is a major plant trait for crop improvement. To balance the relative amounts of starch and proteins in the seeds, plants constantly monitor the carbon/nitrogen ratio (C/N status), seeking its homeostasis.

In this context, the central energy and carbon status sensor SnRK1 has emerged as a potential molecular target to optimize crop yield. Besides its fundamental role in adjusting plant metabolism to cope with low energy stress (LES), SnRK1 also controls the C/N balance, and thus starch/protein ratio, in maize seeds. A recent report showed that daily rhythms of sucrose concentration direct carbon and nitrogen accumulation in maize seeds through ZmSnRK1 (Li et al., 2020; **Figure 4A**). When sucrose levels are low, ZmSnRK1 phosphorylates the E3 ubiquitin ligase ZmRFWD3 and targets it for degradation. On the other hand, sufficient sucrose inhibits ZmSnRK1, allowing ZmRFWD3 protein accumulation. ZmRFWD3 ubiquitinates the bZIP transcription factor Opaque2 (O2), a major regulator of balanced C/N accumulation in maize seeds, increasing its nuclear localization during daytime by enhancing its interaction with importin1, the α-subunit of Importin-1 (Li et al., 2020). The cytonuclear distribution of O2 in maize endosperm follows a diurnal pattern that correlates with both sucrose and ZmRFWD3 levels, leading to enhanced transcription of zein genes during daytime. The loss-of-function *zmrfwd3* mutant has disrupted diurnal cytoplasmic O2 localization pattern and slight changes in seed C/N ratio due to decreased zeins and increased starch amounts. Li et al. (2020) work connects circadian rhythms of sugar status to the sink-source relationship and C/N ratio in

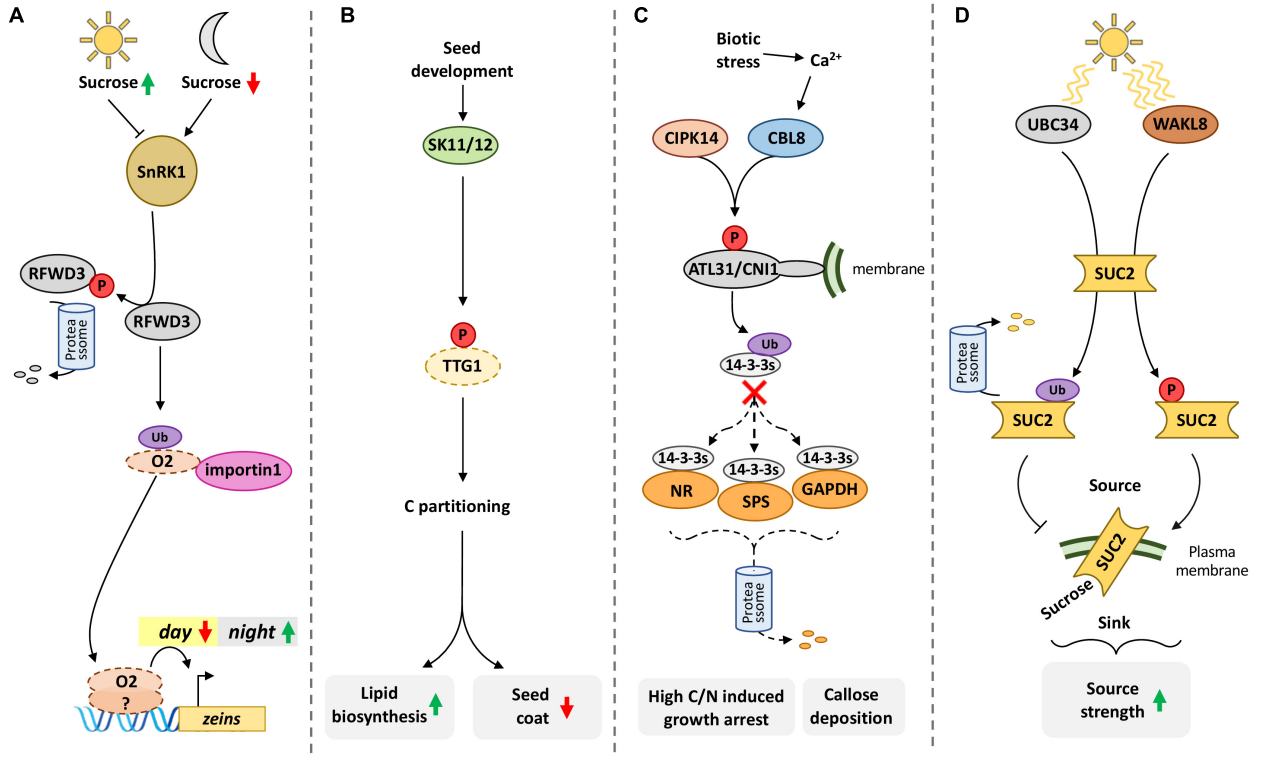

FIGURE 4 | PTMs orchestrate the source-sink relationship. Integrating phosphorylation (red circles) and ubiquitination (purple ellipses) of specific enzymes and TFs is pivotal to controlling carbon fluxes throughout the plant. **(A)** SnRK1 integrates metabolic information to control carbon/nitrogen (C/N) balance in maize seeds. During the night, low sucrose availability in the endosperm activates SnRK1, which in turn phosphorylates the E3 ubiquitin ligase RFWD3 to trigger its ubiquitination and subsequent proteasomal degradation. Conversely, high sucrose availability during daytime inhibits SnRK1 and, consequently, stabilizes RFWD3. RFWD3 ubiquitinates the basic leucine zipper (bZIP) O2 transcription factor, promoting O2 interaction with importin1, the α-subunit of Importin-1, to enhance O2 nuclear localization and activate the expression of *zein* genes. The activation of *zein* genes enhances storage protein accumulation in maize seeds to balance their C/N status. **(B)** Phosphorylation of TTG1 by SK11/12 modulates TTG1 protein-protein interaction patterns, shifting seed metabolism between lipid biosynthesis and the production of mucilage pigments in the seed coat. **(C)** CIPK14 and CBL8 act synergistically to phosphorylate ATL31/CNI1, which in turn ubiquitinates 14-3-3s proteins. 14-3-3s degradation might destabilize SPSs, NR, and GAPDH, shifting C/N metabolism and possibly modulating growth according to C/N balance. This mechanism could also modulate carbon flow to biotic responses by adjusting callose deposition, a costly metabolic process, and a strong carbon sink. **(D)** The SUC2 sucrose transport activity is modulated by light intensity by the concerted action of UBC34 and WAKL8. While the E3 ubiquitin-conjugating enzyme UBC34 ubiquitinates and targets SUC2 for degradation under normal light, the phosphorylation of SUC2 by the wall-associated kinase WAKL8 enhances SUC2 activity in response to high light. SUC2 increased activity promotes sucrose transport from source to sink tissues to optimize growth under favorable conditions. This mechanism emphasizes how ubiquitination and phosphorylation integrate to adjust carbon homeostasis and source-sink relationships. Phosphorylation (P), ubiquitination (Ub). Connectors ending with arrows = activation; connectors ending with bars = repression. Solid connectors = demonstrated pathway; dashed connectors = hypothetic pathway. Green upward arrows = induction; red downward arrows = repression.

maize seeds. The regulation of ZmSnRK1 by sucrose in maize seeds is likely to be mediated by T6P. Thus, SnRK1 may have a dual, but coordinated, function: manage cellular metabolism in response to cellular energy charge and modulate carbon and nitrogen fluxes throughout the plant. In Arabidopsis, the phosphorylation of TRANSPARENT TESTA GLABRA1 (TTG1) by SHAGGY-like kinases 11/12 (SK11/12) direct carbon flux to lipid biosynthesis and reduce the amount of carbon destinated to the seed coat, modulating the carbon partitioning between zygotic and maternal sinks (Li et al., 2018; **Figure 4B**).

The correct balance of C/N metabolism is essential to maximize plant fitness. The CBL-INTERACTING KINASE14 (CIPK14) acts together with CALCINEURIN B-LIKE8 (CBL8) to phosphorylate the RING-H2 ubiquitin ligase ARABIDOPSIS TOXICOS EN LEVADURA31/CARBON/NITROGEN INSENSITIVE1 (ATL31/CNI1) in a Ca^{2+}-dependent manner (Yasuda et al., 2017). Transgenic Arabidopsis overexpressing ATL31/CNI1 is hyposensitive to the seedling growth arrest caused by high C/N ratio (Sato et al., 2009). The ATL31/CNI1 localization in membranes, possibly in the plasma membrane but not excluding other membrane organelles, is necessary for its role in C/N-mediated growth arrest. Phosphorylated ATL31/CNI1 binds to and ubiquitinates 14-3-3 proteins *in vitro*, suggesting that high C/N ratio induced ATL31/CNI1 phosphorylation is required for 14-3-3 repression under nutritional stress (Yasuda et al., 2017). The 14-3-3 proteins are known to regulate the stability of key enzymes involved in carbon and nitrogen metabolism. In sugar-starved Arabidopsis cells, the loss of 14-3-3 binding to SUCROSE PHOSPHATE SYNTHASE (SPS), NITRATE REDUCTASE (NR), and GLYCERALDEHYDE-

3-PHOSPHATE DEHYDROGENASE (GAPDH) is accompanied by the degradation of these critical metabolic enzymes (Cotelle, 2000; **Figure 4C**). Interestingly, the overexpression of ATL31 leads to accelerated callose deposition, a strong carbon sink, in response to powdery mildew penetration (Maekawa et al., 2014). Additionally, the tomato ATL31 ortholog might be involved in modulating starch degradation and the priming of callose deposition upon mycorrhizal inoculation (Sanmartín et al., 2021). One can hypothesize that the degradation of 14-3-3 proteins by ATL31 could lead to a metabolic shift of carbon utilization in response to biotic interactions.

The sucrose transporter SUC2 is a major proton-sucrose symporter responsible for loading the sucrose in the apoplast of source organs to the phloem for transport to sink tissues. The UBIQUITIN-CONJUGATING ENZYME 34 (UBC34) is an atypical E2-conjugating enzyme that ubiquitinates SUC2 in Arabidopsis, triggering SUC2 turnover in a light-dependent manner (Xu et al., 2020). In the same work, the authors also uncovered that SUC2 phosphorylation by the WALL-ASSOCIATED KINASE LIKE 8 (WAKL8) increases its activity in response to high light. The antagonistic relationship between UBC34 and WAKL8 in the regulation of SUC2 activity is highlighted by the phenotypes of the respective mutants: *ubc34* mutants show increased phloem loading and biomass accumulation while these parameters are reduced in *wakl8* (**Figure 4D**). Thus, ubiquitination and phosphorylation are dynamically integrated to adjust the activity of key proteins associated with carbon homeostasis.

CARBON UTILIZATION IN ENERGY METABOLISM: GLYCOLYSIS

The management of photoassimilates through interconversion of different sugars, sugar phosphates, and starch allows effective balancing of carbon and energy fluxes between tissues and organs during the diel cycle. The glucose breakdown through glycolysis generates ATP, NADH, and organic acid pyruvate. The pyruvate is further oxidized through the tricarboxylic acid (TCA) pathway in the mitochondria for further energy and reducing power production. In this section, we discuss the regulation of cytosolic glycolysis by PTMs.

The hexose-phosphorylating enzyme HXK1 possesses a glucose-sensing activity that is independent of its catalytic activity (Moore et al., 2003). HXK1 localizes in the nucleus upon glucose binding and mediates the repression of photosynthesis-related genes (Cho et al., 2006). Despite its central role in regulating carbon metabolism, we still have little knowledge of the regulation of HXK1 by PTMs. A recent report showed that the Arabidopsis HXK1 could be phosphorylated at S184 and S186 (Mergner et al., 2020). These phosphorylation sites are in the vicinity of the serine S177, which by homology can be the residue responsible for the phosphoryl transfer during catalysis. The substitution S177A in Arabidopsis renders a catalytically inactive HXK1 that still can sense glucose (Moore et al., 2003). Moreover, S177 corresponds to the S158 in the yeast Hxk2 (Feng et al., 2015), which was shown to facilitate phosphoryl transfer during glucose phosphorylation (Arora et al., 1991; Feng et al., 2015) and is necessary for catalysis (Heidrich et al., 1997). The kinetic analysis of HXK1 S184 and S186 phospho-mimic and phospho-null isoforms is necessary to establish putative roles of these residues phosphorylation in the HXK1 catalytic activity. Furthermore, previous *in vitro* proteome-wide screening seeking for SUMOylation targets identified the SUMOylation of Arabidopsis HXK1 (Elrouby and Coupland, 2010). This was later reinforced by phylogenetic analysis of HXK1, suggesting the existence of conserved SUMOylation motifs in plant hexokinases (Castro et al., 2020), and by HXK1 interaction with SUMO CONJUGATING ENZYME1 (SCE1) (Elrouby and Coupland, 2010). However, the *in vivo* occurrence and the possible physiological significance of HXK1 SUMOylation in plants remains to be investigated.

The next step of glycolysis involves the isomerization of G6P to fructose-6-phosphate (F6P) catalyzed by the moonlighting enzyme phosphoglucose isomerase (PGI). To this day, there are no reports of PTMs regulating PGI activity or subcellular localization in plants. Also, no PTMs of PHOSPHOFRUCTOKINASE1 (PFK1), the enzyme catalyzing the phosphorylation of F6P to produce fructose-1,6-bisphosphate (F1,6P), were identified to this date. The FRUCTOSE-1,6-BISPHOSPHATASE/FRUCTOSE INSENSITIVE 1 (FBPase/FINS1) dephosphorylates F1,6P, generating F6P for sucrose synthesis (Cho and Yoo, 2011). FINS1 was found to be ubiquitinated in a ubiquitinome assay using Arabidopsis cell-suspension cultures (Walton et al., 2016), suggesting that the ubiquitin-proteasome system (UPS) might regulate the FINS1 protein accumulation. FINS1 acetylation was also identified in another wide screening in Arabidopsis (Liu et al., 2018). One could hypothesize that FINS1 acetylation could potentially communicate the acetyl-CoA levels to reduce carbon flux through oxidative phosphorylation (Shi and Tu, 2015). Besides the role of FINS1 in modulating the distribution of fructose between respiration and sucrose synthesis, *FINS1* was also identified in a screening for fructose-insensitive mutants in Arabidopsis. The *fins1* mutant shows reduced photosynthetic rates, enhanced starch accumulation, and lower sucrose levels during the day (Rojas-González et al., 2015). Like HXK1, the FINS1 sugar-sensing ability is independent of its catalytic activity (Cho and Yoo, 2011; **Figure 5**).

Reactive oxygen species (ROS) and reactive nitrogen species (RNS) can regulate redox PTMs (e.g., carbonylation, glutathionylation, sulfhydryl oxidations, nitration, S-nitrosylation, and nitro-alkylation) and hold a crucial role during stress signaling (Turkan, 2018; Aranda-Caño et al., 2019; Ventimiglia and Mutus, 2020). The glycolytic enzyme GAPDH converts glyceraldehyde-3-phosphate (G3P) to 1,3-bisphosphoglycerate (1,3BPG), which can then be subsequently metabolized to 3-phosphoglycerate (3PG) and then to pyruvate for entering in the TCA cycle. Nitric oxide (NO) is a potent redox signaling molecule that leads to the formation of S-nitrosoglutathione and to protein S-nitrosylation. GAPDH, which might act as a NO sensor, is inactivated by S-glutathionylation and S-nitrosylation in the active site Cys159 (Hara et al., 2006; Holtgrefe et al., 2008; Schneider et al., 2018).

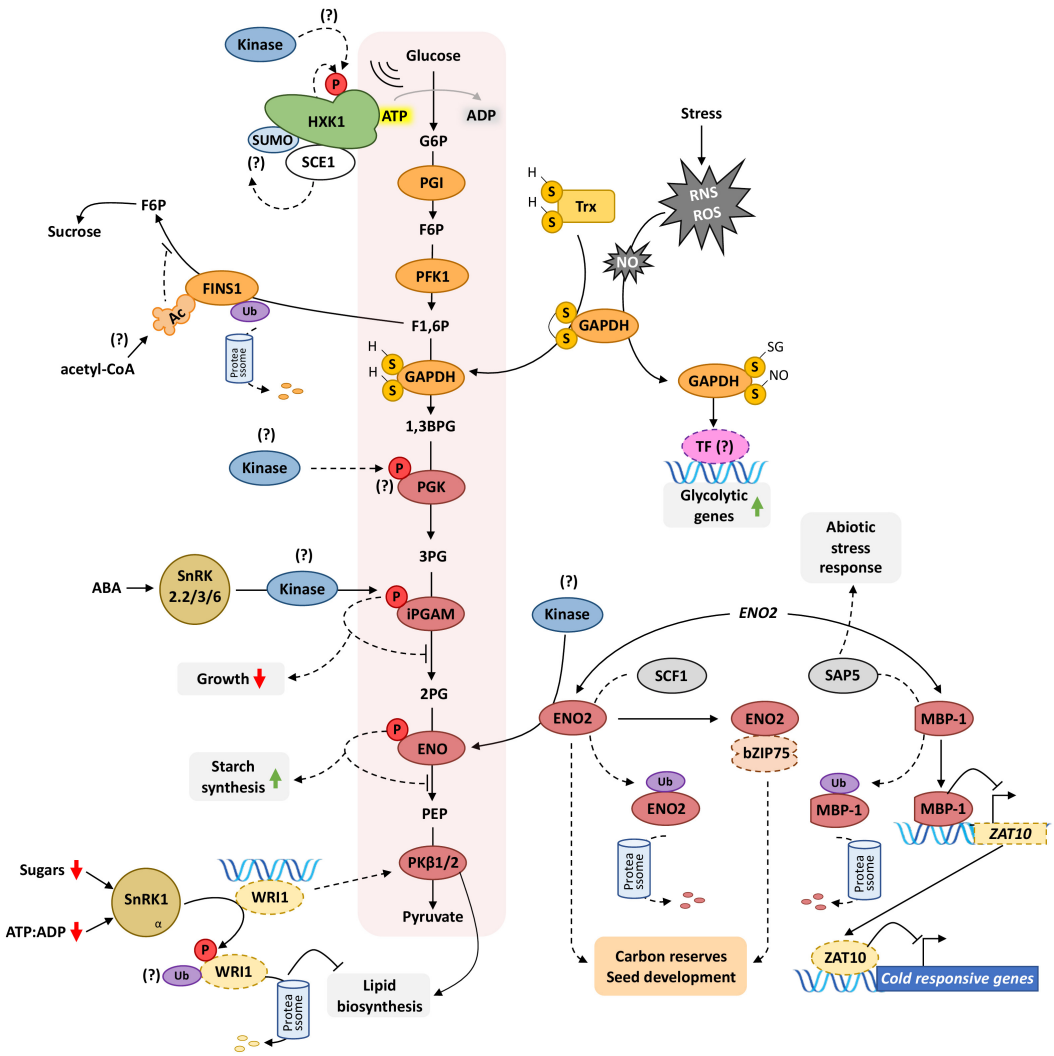

FIGURE 5 | PTMs modulate carbon flow through glycolysis. Glycolysis is a highly conserved linear sugar catabolic pathway leading to the generation of ATP, NADPH, pyruvate, and metabolic intermediates for macromolecules biosynthesis. Thus, the elucidation of the PTMs targeting glycolytic enzymes is pivotal to understanding carbon and energy allocation in plants. HXK1, a hexose-phosphorylating enzyme mediating glucose entry in the glycolysis catabolic pathway, is phosphorylated near its active site, which could impact its glucose-sensing or catalytic activities. It is still unclear if the phosphorylation results from the activity of an upstream kinase targeting HXK1 or autophosphorylation. HXK1 also has a predicted SUMOylation site and interacts with the SUMO-conjugating enzyme SCE1, further supporting its putative SUMOylation. FINS1 redirect F1,6P from glycolysis to sucrose synthesis, possibly integrating metabolic information through acetyl-CoA mediated acetylation. FINS1 is ubiquitinated *in vivo* and possibly targeted for degradation to direct carbon toward glycolytic catabolism. The reduction of GAPDH mediated by reduced Trx increases its activity. Additionally, oxidative stress increases NO accumulation and triggers GAPDH S-glutathionylation and S-nitrosylation to promote the upregulation of glycolytic genes over GAPDH glycolytic activity. PGK is phosphorylated *in vivo*, but the upstream kinase and the physiological consequences of the phosphorylation are still unknown. The iPGAM phosphorylation relies on ABA signaling and SnRK2.2/3/6 action, which could promote growth arrest by diminishing glycolytic flux. The *ENO2* transcript can be translated to ENO2, which converts 2PG to PEP, or to MBP-1, lacking the ENO2 N-terminal region. MBP-1 inhibits the ZAT10 transcription to repress the ZAT10-mediated cold responses. SCF1 and SAP5 might ubiquitinate ENO2 and MBP-1, respectively, to control their accumulation. ENO2 interacts with bZIP75 to regulate carbon reserves during seed development. Here again, phosphorylation and ubiquitination seem to have a crucial role in regulating glycolysis to distribute C accordingly to metabolic and stress signals efficiently. The transcription factor WRI1, which modulates the transcription of PKβ1/2, is destabilized by SnRK1 direct phosphorylation, which may trigger the ubiquitination and degradation of WRI1 to regulate lipid biosynthesis. Ellipses and other rounded shapes = proteins (dashed lines: transcription factors (TFs), solid lines: enzymes). Phosphorylation (P), acetylation (Ac), sulfhydryl groups (S-H), disulfide bridge (S-S), ubiquitination (Ub), nitric oxide (NO), reactive oxygen species (ROS), reactive nitrogen species (RNS). Connectors ending with arrows = activation; connectors ending with bars = repression. Solid connectors = demonstrated pathways; dashed connectors = hypothetic pathways. Green upward arrows = induction; red downward arrows = repression. The consumption or the generation of ATP and NADPH by glycolysis were omitted for simplicity.

GAPDH also interacts *in vivo* with thioredoxin-*h*3, which might revert GAPDH oxidative modifications. This might allow redox-dependent regulation of GAPDH to alter subcellular localization and subsequently its function, empowering it as a moonlighting protein. Moonlighting proteins show more than one physiologically relevant function (Jeffery, 2018). While

oxidized GAPDH would locate in the nucleus to perform moonlighting functions (e.g., transcriptional activation of glycolytic genes during oxidative stress), Thx-mediated reduction of GAPDH would increase the GAPDH pool both in the cytosol and associate it with the mitochondria membrane to optimize the glycolytic flux (**Figure 5**; Schneider et al., 2018). Notably, an increasing number of glycolytic enzymes have been described to be S-glutathionylated, such as aldolase, A4-GAPDH, and cytosolic triosephosphate isomerase, which results in the latter's inactivation (**Figure 5**; Ito et al., 2003; Michelet et al., 2005).

The PHOSPHOGLYCERATE KINASE (PGK) generates one ATP by transferring one phosphate from 1,3-bisphosphoglycerate (1,3BPG) to ADP, catalyzing the second step of the glycolysis sub-pathway that generates pyruvate from G3P. PGK is phosphorylated in the Ser201 (Van Leene et al., 2019), but the upstream kinase(s) and the stimulus that triggers the phosphorylation remain to be investigated. The next step of the pathway converting G6P to pyruvate involves the isomerization of 3-phosphoglycerate (3PG) to 2-phosphoglycerate (2PG) catalyzed by 2,3-BIPHOSPHOGLYCERATE-independent PHOSPHOGLYCERATE MUTASE (iPGAM). The Arabidopsis double mutant *ipgam1 ipgam2* has impaired stomatal movements in response to blue light, ABA, and low CO_2 (Zhao and Assmann, 2011). Both vegetative and reproductive growths are severely impaired in *ipgam1 ipgam2*. Interestingly, ABA induces the phosphorylation of iPGAM1 Ser17 in an *SnRK2.2/2.3/2.6*-dependent manner (Wang et al., 2013). These findings suggest that iPGAM1 ABA-induced phosphorylation could repress its activity to repress growth.

The next step of glycolysis is converting 2PG to phosphoenolpyruvate (PEP) catalyzed by the enolase (ENO2 and ENO3 in Arabidopsis). Interestingly, the Arabidopsis *ENO2* locus encodes two alternative translation products starting at distinct translational start sites. The full-length protein (48 kDa) encodes the glycolytic enzyme enolase that catalyzes PEP production in the cytoplasm, while the alternative translation product MBP-1-like protein (AtMBP-1 = 37 kDa) localizes in the nucleus acting as a transcriptional regulator (Kang et al., 2013). AtMBP-1 represses the transcription of the zinc finger TF ZAT10 through direct binding to the promoter to repress cold response (Hojoung et al., 2002). AtMBP-1 also regulates the expression of ABA-signaling genes and is ubiquitinated by the E3 ubiquitin ligase STRESS-ASSOCIATED PROTEIN5 (SAP5), a positive regulator of abiotic stress responses (Kang et al., 2011, 2013). The Arabidopsis mutant *eno2* has altered starch and glucose levels in vegetative tissues and reduced seed size and weight. The reduced seed weight could be due to the impairment of cell proliferation, which could be caused by the lower cytokinin levels and/or the altered sugar status found in the mutant (Liu et al., 2020). In the same work, the authors found that ENO2 interacts with the bZIP75 transcription factor instead of AtMBP-1. ENO2 is phosphorylated at Ser56 (Roitinger et al., 2015) and Ser275 (Nakagami et al., 2010) in Arabidopsis, but the effects on the enolase activity and the physiological outcomes are still unknown. ENO2 also interacts with the SUMOylation enzyme SCE1, suggesting that it could also be SUMOylated (Elrouby and Coupland, 2010). In maize, the enolase ZmENO1 is phosphorylated in developing seeds in the eukaryotic conserved phosphorylation site Ser43. The phosphorylation is likely to modulate enzyme activity since the phosphomimetic isoform (Ser43Asp) shows decreased enolase activity *in vitro* (Cao H. et al., 2019). The phosphorylation of ZmENO1 positively correlates with starch accumulation in seeds (Cao H. et al., 2019).

The enzyme pyruvate kinase (PK) transfers a phosphate group from PEP to ADP, generating one pyruvate and one ATP. There are 14 loci encoding putative PKs in Arabidopsis; four of each are plastidial (Wulfert et al., 2020). Two plastidial PKs, namely PKβ1 and PKβ2, regulate the carbon flow to lipid biosynthesis in Arabidopsis seeds (Andre et al., 2007; Baud et al., 2007). Interestingly, the seed phenotype of *pkβ1 pkβ2* double mutant resembles the wrinkled phenotype of the WRINKLED1 mutant *wri1*, being the transcription of both PKβ1 and PKβ2 induced by WRI1 (Baud et al., 2007). Since SnRK1 negatively regulates the WRI1 stability through phosphorylation, the SnRK1-WRI1 pathway is likely conveying carbon status information to allocate carbon in Arabidopsis seeds correctly. SnRK1 seems critical for carbon partitioning in reproductive tissues of Angiosperms since maize ZmSnRK1 modulates the C/N status in seeds, as previously discussed (Li et al., 2020; **Figure 4**).

FUTURE PERSPECTIVES

Post-translational modifications greatly expand the plant proteome configurations by adding control layers beyond transcription-translation and allosteric regulatory mechanisms. The PTMs also allow dynamic and reversible changes in protein activity and subcellular localization, enabling plant adaptation to environmental changes in a resource-wise manner. New techniques and increasing computational power are now enabling high throughput and precise identification of PTMs.

However, there are still bottlenecks dampening the identification of the physiological significance of PTMs. The effects of PTMs on protein activity or localization must be analyzed through *in vitro* and reverse genetic approaches, usually one modification at a time. Additionally, the complexity of carbon metabolism in plants, which pervades many cellular organelles at the subcellular level and in long-distance transport and communication at the systemic level, makes it harder to get a comprehensive picture of the effects of PTMs on carbon fluxes. The development of high throughput gene-editing technologies coupled with rapid automated phenotyping platforms could solve this issue in a mid- to long-term timescale. PTM sites identified through *in vivo* large-scale proteomic analysis could guide gene editing to modify the modified target amino acid residue precisely, followed by an automated phenotypic screen of dozens, maybe hundreds, of lines. However, further optimization of gene editing methods for plants allowing the substitution of specific amino acids is required for large-scale screenings. Measurements of photosynthetic capacity or growth rates are already performed at large scales. Cheaper and automated sample

processing and analysis are also quintessential to analyzing the effects of these PTMs on plant physiology. The wide array of metabolites (e.g., sugars, phosphate-sugars, and secondary metabolite intermediates) composing the path of carbon fluxes in the plant must be consistently and precisely measured, particularly those with low accumulation such as T6P.

The data collected in such high throughput proteomics-gene editing-phenotyping-"omics" pipelines using model plants, such as Arabidopsis and rice, can be fed into kinetics' mathematical modeling (Nägele and Weckwerth, 2014) or machine learning algorithms. Machine learning can boost predictive models to identify both putative PTMs of new proteins and their physiological effects on the organism (Greener et al., 2022). Ensemble models using multiple machine learning algorithms might be deployed to analyze different parameters affecting plant metabolism. For example, deep learning algorithms (e.g., AlphaFold) could be used to predict changes in protein structure and enzyme activity induced by PTMs. The predicted changes in enzyme activity could be concatenated with machine learning models assessing the changes in metabolic fluxes, composing an ensemble model that could estimate the accumulation of reaction products. These trained models can be used to predict PTMs and their physiological consequences in less-studied species and crops with complex genome organization or long-life cycles, such as sugarcane and many trees, respectively. Mathematical modeling of the interaction between the circadian clock on sugar and starch metabolism exemplifies how computation can reveal clues on physiological outputs (Pokhilko et al., 2014; Webb and Satake, 2015). However, these models essentially consider the transcription-translational feedback regulations of the genes involved. Enhanced proteomic and metabolomic analysis capabilities will enable better models, which will speed up the discovery of new phenomena and improvement of crops in the climate change scenario.

AUTHOR CONTRIBUTIONS

All authors listed have made a substantial, direct, and intellectual contribution to the work, and approved it for publication.

FUNDING

We acknowledge the Portuguese Fundação para a Ciência e a Tecnologia (FCT) for a fellowship for HA (PD/BD/147218/2019) and for a contract for CM (PTDC/BIA-FBT/31211/2017). This work was supported by the PTDC/BIA-FBT/31211/2017 and also by the FCT research fund GREEN-it "Bioresources4Sustainability" (UIDB/04551/2020). The funding sources were not involved in analyses, interpretation of data, writing, or in the decision to submit this manuscript. Proteome Regulation in Plants Lab: HA, CM, RS, and IA.

REFERENCES

Abt, M. R., and Zeeman, S. C. (2020). Evolutionary innovations in starch metabolism. *Curr. Opin. Plant Biol.* 55, 109–117. doi: 10.1016/j.pbi.2020.03.001

Alexander, R. D., and Morris, P. C. (2006). A proteomic analysis of 14-3-3 binding proteins from developing barley grains. *Proteomics* 6, 1886–1896. doi: 10.1002/pmic.200500548

Alves, H. L. S., Matiolli, C. C., Soares, R. C., Almadanim, M. C., Oliveira, M. M., and Abreu, I. A. (2021). Carbon/nitrogen metabolism and stress response networks – calcium-dependent protein kinases as the missing link? *J. Exp. Bot.* 72, 4190–4201. doi: 10.1093/jxb/erab136

Andre, C., Froehlich, J. E., Moll, M. R., and Benning, C. (2007). A heteromeric plastidic pyruvate kinase complex involved in seed oil biosynthesis in *Arabidopsis*. *Plant Cell* 19, 2006–2022. doi: 10.1105/tpc.106.048629

Aoyama, S., Terada, S., Sanagi, M., Hasegawa, Y., Lu, Y., Morita, Y., et al. (2017). Membrane-localized ubiquitin ligase ATL15 functions in sugar-responsive growth regulation in *Arabidopsis*. *Biochem. Biophys. Res. Commun.* 491, 33–39. doi: 10.1016/j.bbrc.2017.07.028

Aranda-Caño, L., Sánchez-Calvo, B., Begara-Morales, J. C., Chaki, M., Mata-Pérez, C., Padilla, M. N., et al. (2019). Post-translational modification of proteins mediated by nitro-fatty acids in plants: nitroalkylation. *Plants* 8:82. doi: 10.3390/plants8040082

Arora, K. K., Filburn, C. R., and Pedersen, P. L. (1991). Glucose phosphorylation. Site-directed mutations which impair the catalytic function of hexokinase. *J. Biol. Chem.* 266, 5359–5362. doi: 10.1016/s0021-9258(19)67600-3

Baena-González, E., and Hanson, J. (2017). Shaping plant development through the SnRK1–TOR metabolic regulators. *Curr. Opin. Plant Biol.* 35, 152–157. doi: 10.1016/j.pbi.2016.12.004

Baena-González, E., and Lunn, J. E. (2020). SnRK1 and trehalose 6-phosphate – two ancient pathways converge to regulate plant metabolism and growth. *Curr. Opin. Plant Biol.* 55, 52–59. doi: 10.1016/j.pbi.2020.01.010

Baena-González, E., Rolland, F., Thevelein, J. M., and Sheen, J. (2007). A central integrator of transcription networks in plant stress and energy signalling. *Nature* 448, 938–942. doi: 10.1038/nature06069

Baud, S., Wuillème, S., Dubreucq, B., De Almeida, A., Vuagnat, C., Lepiniec, L., et al. (2007). Function of plastidial pyruvate kinases in seeds of *Arabidopsis thaliana*. *Plant J.* 52, 405–419. doi: 10.1111/j.1365-313X.2007.03232.x

Boex-Fontvieille, E., Daventure, M., Jossier, M., Hodges, M., Zivy, M., and Tcherkez, G. (2014). Phosphorylation pattern of Rubisco activase in *Arabidopsis* leaves. *Plant Biol.* 16, 550–557. doi: 10.1111/plb.12100

Cao, H., Zhou, Y., Chang, Y., Zhang, X., Li, C., and Ren, D. (2019). Comparative phosphoproteomic analysis of developing maize seeds suggests a pivotal role for enolase in promoting starch synthesis. *Plant Sci.* 289:110243. doi: 10.1016/j.plantsci.2019.110243

Cao, P., Kim, S. J., Xing, A., Schenck, C. A., Liu, L., Jiang, N., et al. (2019). Homeostasis of branched-chain amino acids is critical for the activity of TOR signaling in *Arabidopsis*. *eLife* 8:e50747. doi: 10.7554/eLife.50747

Carmo-Silva, E., Scales, J. C., Madgwick, P. J., and Parry, M. A. J. (2015). Optimizing Rubisco and its regulation for greater resource use efficiency. *Plant Cell Environ.* 38, 1817–1832. doi: 10.1111/pce.12425

Caspar, T., Huber, S. C., and Somerville, C. (1985). Alterations in growth, photosynthesis, and respiration in a starchless mutant of *Arabidopsis thaliana* (L.) deficient in chloroplast phosphoglucomutase activity. *Plant Physiol.* 79, 11–17. doi: 10.1104/pp.79.1.11

Caspar, T., Lin, T. P., Kakefuda, G., Benbow, L., Preiss, J., and Somerville, C. (1991). Mutants of *Arabidopsis* with altered regulation of starch degradation. *Plant Physiol.* 95, 1181–1188. doi: 10.1104/pp.95.4.1181

Castro, P. H., Freitas, S., and Azevedo, H. (2020). Plant hexokinase phylogenetic analysis highlights a possible regulation by the posttranslational modifier SUMO. *Micro Biol.* 2020, 0–4. doi: 10.17912/micropub.biology.000260

Ceccarelli, E. A., Arakaki, A. K., Cortez, N., and Carrillo, N. (2004). Functional plasticity and catalytic efficiency in plant and bacterial ferredoxin-NADP(H) reductases. *Biochim. Biophys. Acta Proteins Proteomics* 1698, 155–165. doi: 10.1016/j.bbapap.2003.12.005

Chen, J. G., and Jones, A. M. (2004). AtRGS1 function in *Arabidopsis thaliana*. *Methods Enzmol.* 389, 338–350. doi: 10.1016/S0076-6879(04)89020-7

Chen, J. G., Willard, F. S., Huang, J., Liang, J., Chasse, S. A., Jones, A. M., et al. (2003). A seven-transmembrane RGS protein that modulates plant cell proliferation. *Science* 301, 1728–1731. doi: 10.1126/science.1087790

Chen, L., Su, Z. Z., Huang, L., Xia, F. N., Qi, H., Xie, L. J., et al. (2017). The AMP-activated protein kinase KIN10 is involved in the regulation of autophagy in *Arabidopsis*. *Front. Plant Sci.* 8:1201. doi: 10.3389/fpls.2017.01201

Cho, Y. H., and Yoo, S. D. (2011). Signaling role of fructose mediated by FINS1/FBP in *Arabidopsis thaliana*. *PLoS Genet.* 7:e1001263. doi: 10.1371/journal.pgen.1001263

Cho, Y. H., Yoo, S. D., and Sheen, J. (2006). Regulatory functions of nuclear hexokinase1 complex in glucose signaling. *Cell* 127, 579–589. doi: 10.1016/j.cell.2006.09.028

Cotelle, V. (2000). 14-3-3s regulate global cleavage of their diverse binding partners in sugar-starved *Arabidopsis* cells. *EMBO J.* 19, 2869–2876. doi: 10.1093/emboj/19.12.2869

Crepin, N., and Rolland, F. (2019). SnRK1 activation, signaling, and networking for energy homeostasis. *Curr. Opin. Plant Biol.* 51, 29–36. doi: 10.1016/j.pbi.2019.03.006

Dobrenel, T., Caldana, C., Hanson, J., Robaglia, C., Vincentz, M., Veit, B., et al. (2016). TOR signaling and nutrient sensing. *Annu. Rev. Plant Biol.* 67, 261–285. doi: 10.1146/annurev-arplant-043014-114648

Edner, C., Li, J., Albrecht, T., Mahlow, S., Hejazi, M., Hussain, H., et al. (2007). Glucan, water dikinase activity stimulates breakdown of starch granules by plastidial β-amylases. *Plant Physiol.* 145, 17–28. doi: 10.1104/pp.107.104224

Elrouby, N., and Coupland, G. (2010). Proteome-wide screens for small ubiquitin-like modifier (SUMO) substrates identify *Arabidopsis* proteins implicated in diverse biological processes. *Proc. Natl. Acad. Sci. U.S.A.* 107, 17415–17420. doi: 10.1073/pnas.1005452107

Feng, J., Zhao, S., Chen, X., Wang, W., Dong, W., Chen, J., et al. (2015). Biochemical and structural study of *Arabidopsis* hexokinase 1. *Acta Crystallogr. Sect. D Biol. Crystallogr.* 71, 367–375. doi: 10.1107/S1399004714026091

Fernandez, O., Ishihara, H., George, G. M., Mengin, V., Flis, A., Sumner, D., et al. (2017). Leaf starch turnover occurs in long days and in falling light at the end of the day. *Plant Physiol.* 174, 2199–2212. doi: 10.1104/pp.17.00601

Frank, A., Matiolli, C. C., Viana, A. J. C., Hearn, T. J., Kusakina, J., Belbin, F. E., et al. (2018). Circadian entrainment in *Arabidopsis* by the sugar-responsive transcription factor bZIP63. *Curr. Biol.* 28, 2597.e6–2606.e6. doi: 10.1016/j.cub.2018.05.092

Friso, G., and Van Wijk, K. J. (2015). Posttranslational protein modifications in plant metabolism. *Plant Physiol.* 169, 1469–1487. doi: 10.1104/pp.15.01378

Fu, L., Liu, Y., Qin, G., Wu, P., Zi, H., Xu, Z., et al. (2021). The TOR–EIN2 axis mediates nuclear signalling to modulate plant growth. *Nature* 591, 288–292. doi: 10.1038/s41586-021-03310-y

Fulton, D. C., Stettler, M., Mettler, T., Vaughan, C. K., Li, J., Francisco, P., et al. (2008). β-Amylase4, a noncatalytic protein required for starch breakdown, acts upstream of three active β-amylases in *Arabidopsis* chloroplasts. *Plant Cell* 20, 1040–1058. doi: 10.1105/tpc.107.056507

Gagne, J. M., Smalle, J., Gingerich, D. J., Walker, J. M., Yoo, S. D., Yanagisawa, S., et al. (2004). *Arabidopsis* EIN3-binding F-box 1 and 2 form ubiquitin-protein ligases that repress ethylene action and promote growth by directing EIN3 degradation. *Proc. Natl. Acad. Sci. U.S.A.* 101, 6803–6808. doi: 10.1073/pnas.0401698101

Gámez-Arjona, F. M., Raynaud, S., Ragel, P., and Mérida, Á (2014). Starch synthase 4 is located in the thylakoid membrane and interacts with plastoglobule-associated proteins in *Arabidopsis*. *Plant J.* 80, 305–316. doi: 10.1111/tpj.12633

Geigenberger, P. (2011). Regulation of starch biosynthesis in response to a fluctuating environment. *Plant Physiol.* 155, 1566–1577. doi: 10.1104/pp.110.170399

Geigenberger, P., Kolbe, A., and Tiessen, A. (2005). Redox regulation of carbon storage and partitioning in response to light and sugars. *J. Exp. Bot.* 56, 1469–1479. doi: 10.1093/jxb/eri178

Glaring, M. A., Skryhan, K., Kötting, O., Zeeman, S. C., and Blennow, A. (2012). Comprehensive survey of redox sensitive starch metabolising enzymes in *Arabidopsis thaliana*. *Plant Physiol. Biochem. PPB* 58, 89–97. doi: 10.1016/j.plaphy.2012.06.017

Grabsztunowicz, M., Koskela, M. M., and Mulo, P. (2017). Post-translational modifications in regulation of chloroplast function: recent advances. *Front. Plant Sci.* 8:240. doi: 10.3389/fpls.2017.00240

Greener, J. G., Kandathil, S. M., Moffat, L., and Jones, D. T. (2022). A guide to machine learning for biologists. *Nat. Rev. Mol. Cell Biol.* 23, 40–55. doi: 10.1038/s41580-021-00407-0

Hädrich, N., Hendriks, J. H. M., Kötting, O., Arrivault, S., Feil, R., Zeeman, S. C., et al. (2012). Mutagenesis of cysteine 81 prevents dimerization of the APS1 subunit of ADP-glucose pyrophosphorylase and alters diurnal starch turnover in *Arabidopsis thaliana* leaves. *Plant J.* 70, 231–242. doi: 10.1111/j.1365-313X.2011.04860.x

Han, X., Zhang, L., Zhao, L., Xue, P., Qi, T., Zhang, C., et al. (2020). SnRK1 phosphorylates and destabilizes WRKY3 to enhance barley immunity to powdery mildew. *Plant Commun.* 1:100083. doi: 10.1016/j.xplc.2020.100083

Hara, M. R., Cascio, M. B., and Sawa, A. (2006). GAPDH as a sensor of NO stress. *Biochim. Biophys. Acta Mol. Basis Dis.* 1762, 502–509. doi: 10.1016/j.bbadis.2006.01.012

Heidrich, K., Otto, A., Behlke, J., Rush, J., Wenzel, K. W., and Kriegel, T. (1997). Autophosphorylation-inactivation site of hexokinase 2 in *Saccharomyces cerevisiae*. *Biochemistry* 36, 1960–1964. doi: 10.1021/bi9623643

Hendriks, J. H. M., Kolbe, A., Gibon, Y., Stitt, M., and Geigenberger, P. (2003). ADP-glucose pyrophosphorylase is activated by posttranslational redox-modification in response to light and to sugars in leaves of *Arabidopsis* and other plant species. *Plant Physiol.* 133, 838–849. doi: 10.1104/pp.103.024513

Hojoung, L., Guo, Y., Ohta, M., Xiong, L., Stevenson, B., and Zhu, J. K. (2002). LOS2, a genetic locus required for cold-responsive gene transcription encodes a bi-functional enolase. *EMBO J.* 21, 2692–2702. doi: 10.1093/emboj/21.11.2692

Holtgrefe, S., Gohlke, J., Starmann, J., Druce, S., Klocke, S., Altmann, B., et al. (2008). Regulation of plant cytosolic glyceraldehyde 3-phosphate dehydrogenase isoforms by thiol modifications. *Physiol. Plant.* 133, 211–228. doi: 10.1111/j.1399-3054.2008.01066.x

Houtz, R. L., Magnani, R., Nayak, N. R., and Dirk, L. M. A. (2008). Co- and post-translational modifications in Rubisco: unanswered questions. *J. Exp. Bot.* 59, 1635–1645. doi: 10.1093/jxb/erm360

Hu, J., Huang, X., Chen, L., Sun, X., Lu, C., Zhang, L., et al. (2015). Site-specific nitrosoproteomic identification of endogenously S-nitrosylated proteins in *Arabidopsis*. *Plant Physiol.* 167, 1731–1746. doi: 10.1104/pp.15.00026

Huang, X., Zheng, C., Liu, F., Yang, C., Zheng, P., Lu, X., et al. (2019). Genetic analyses of the *Arabidopsis* ATG1 kinase complex reveal both kinase-dependent and independent autophagic routes during fixed-carbon starvation. *Plant Cell* 31, 2973–2995. doi: 10.1105/tpc.19.00066

Huang, Y., Li, C. Y., Pattison, D. L., Gray, W. M., Park, S., and Gibson, S. I. (2010). Sugar-Insensitive3, A ring E3 ligase, is a new player in plant sugar response. *Plant Physiol.* 152, 1889–1900. doi: 10.1104/pp.109.150573

Im, J. H., Cho, Y. H., Kim, G. D., Kang, G. H., Hong, J. W., and Yoo, S. D. (2014). Inverse modulation of the energy sensor Snf1-related protein kinase 1 on hypoxia adaptation and salt stress tolerance in *Arabidopsis thaliana*. *Plant Cell Environ.* 37, 2303–2312. doi: 10.1111/pce.12375

Ito, H., Iwabuchi, M., and Ogawa, K. (2003). The sugar-metabolic enzymes aldolase and triose-phosphate isomerase are targets of glutathionylation in *Arabidopsis thaliana*: detection using biotinylated glutathione. *Plant Cell Physiol.* 44, 655–660. doi: 10.1093/pcp/pcg098

Izumi, M., Hidema, J., Makino, A., and Ishida, H. (2013). Autophagy contributes to nighttime energy availability for growth in *Arabidopsis*. *Plant Physiol.* 161, 1682–1693. doi: 10.1104/pp.113.215632

Jeffery, C. J. (2018). Protein moonlighting: what is it, and why is it important? *Philos. Trans. R. Soc. Lond. B Biol. Sci.* 373, 1–19. doi: 10.1098/rstb.2016.0523

Jossier, M., Bouly, J. P., Meimoun, P., Arjmand, A., Lessard, P., Hawley, S., et al. (2009). SnRK1 (SNF1-related kinase 1) has a central role in sugar and ABA signalling in *Arabidopsis thaliana*. *Plant J.* 59, 316–328. doi: 10.1111/j.1365-313X.2009.03871.x

Kang, M., Abdelmageed, H., Lee, S., Reichert, A., Mysore, K. S., and Allen, R. D. (2013). AtMBP-1, an alternative translation product of LOS2, affects abscisic acid responses and is modulated by the E3 ubiquitin ligase AtSAP5. *Plant J.* 76, 481–493. doi: 10.1111/tpj.12312

Kang, M., Fokar, M., Abdelmageed, H., and Allen, R. D. (2011). *Arabidopsis* SAP5 functions as a positive regulator of stress responses and exhibits E3 ubiquitin ligase activity. *Plant Mol. Biol.* 75, 451–466. doi: 10.1007/s11103-011-9748-2

Kijanska, M., and Peter, M. (2013). Atg1 kinase regulates early and late steps during autophagy. *Autophagy* 9, 249–251. doi: 10.4161/auto.22584

Kim, G. D., Cho, Y. H., and Yoo, S. D. (2017). Regulatory functions of cellular energy sensor SNF1-related kinase1 for leaf senescence delay through ETHYLENE- INSENSITIVE3 repression. *Sci. Rep.* 7, 1–13. doi: 10.1038/s41598-017-03506-1

Kolbe, A., Tiessen, A., Schluepmann, H., Paul, M., Ulrich, S., and Geigenberger, P. (2005). Trehalose 6-phosphate regulates starch synthesis via posttranslational redox activation of ADP-glucose pyrophosphorylase. *Proc. Natl. Acad. Sci. U.S.A.* 102, 11118–11123. doi: 10.1073/pnas.0503410102

Kötting, O., Kossmann, J., Zeeman, S. C., and Lloyd, J. R. (2010). Regulation of starch metabolism: the age of enlightenment? *Curr. Opin. Plant Biol.* 13, 320–328. doi: 10.1016/j.pbi.2010.01.003

Lemaire, S. D., Quesada, A., Merchan, F., Corral, J. M., Igeno, M. I., Keryer, E., et al. (2005). NADP-malate dehydrogenase from unicellular green alga *Chlamydomonas reinhardtii*. A first step toward redox regulation? *Plant Physiol.* 137, 514–521. doi: 10.1104/pp.104.052670

Lemeille, S., Turkina, M. V., Vener, A. V., and Rochaix, J. D. (2010). Stt7-dependent phosphorylation during state transitions in the green alga *Chlamydomonas reinhardtii*. *Mol. Cell. Proteomics* 9, 1281–1295. doi: 10.1074/mcp.M000020-MCP201

Li, C., Qi, W., Liang, Z., Yang, X., Ma, Z., and Song, R. (2020). A SnRK1-ZmRFWD3-Opaque2 signaling axis regulates diurnal nitrogen accumulation in maize seeds. *Plant Cell* 32, 2823–2841. doi: 10.1105/TPC.20.00352

Li, C., Zhang, B., Chen, B., Ji, L., and Yu, H. (2018). Site-specific phosphorylation of TRANSPARENT TESTA GLABRA1 mediates carbon partitioning in *Arabidopsis* seeds. *Nat. Commun.* 9, 1–13. doi: 10.1038/s41467-018-03013-5

Li, F., and Vierstra, R. D. (2012). Autophagy: a multifaceted intracellular system for bulk and selective recycling. *Trends Plant Sci.* 17, 526–537. doi: 10.1016/j.tplants.2012.05.006

Li, W., Ma, M., Feng, Y., Li, H., Wang, Y., Ma, Y., et al. (2015). EIN2-directed translational regulation of ethylene signaling in *Arabidopsis*. *Cell* 163, 670–683. doi: 10.1016/j.cell.2015.09.037

Liang, X., Ma, M., Zhou, Z., Wang, J., Yang, X., Rao, S., et al. (2018). Ligand-triggered de-repression of *Arabidopsis* heterotrimeric G proteins coupled to immune receptor kinases. *Cell Res.* 28, 529–543. doi: 10.1038/s41422-018-0027-5

Liu, F., Ahmed, Z., Lee, E. A., Donner, E., Liu, Q., Ahmed, R., et al. (2012). Allelic variants of the amylose extender mutation of maize demonstrate phenotypic variation in starch structure resulting from modified protein–protein interactions. *J. Exp. Bot.* 63, 1167–1183. doi: 10.1093/jxb/err341

Liu, S., Yu, F., Yang, Z., Wang, T., Xiong, H., Chang, C., et al. (2018). Establishment of dimethyl labeling-based quantitative acetylproteomics in *Arabidopsis*. *Mol. Cell. Proteomics* 17, 1010–1027. doi: 10.1074/mcp.RA117.000530

Liu, Y., Duan, X., Zhao, X., Ding, W., Wang, Y., and Xiong, Y. (2021). Diverse nitrogen signals activate convergent ROP2-TOR signaling in *Arabidopsis*. *Dev. Cell* 56, 1283–1295. doi: 10.1016/j.devcel.2021.03.022

Liu, Z., Zheng, L., Pu, L., Ma, X., Wang, X., Wu, Y., et al. (2020). ENO2 affects the seed size and weight by adjusting cytokinin content and forming ENO2-bZIP75 complex in *Arabidopsis thaliana*. *Front. Plant Sci.* 11:574316. doi: 10.3389/fpls.2020.574316

Luo, Y., Aoyama, S., Fukao, Y., Chiba, Y., Sato, T., and Yamaguchi, J. (2019). Involvement of the membrane-localized ubiquitin ligase ATL8 in sugar starvation response in *Arabidopsis*. *Plant Biotechnol.* 36, 107–112. doi: 10.5511/plantbiotechnology.19.0328a

Maekawa, S., Inada, N., Yasuda, S., Fukao, Y., Fujiwara, M., Sato, T., et al. (2014). The carbon/nitrogen regulator *Arabidopsis* TOXICOS EN LEVADURA31 controls papilla formation in response to powdery mildew fungi penetration by interacting with SYNTAXIN OF PLANTS121 in *Arabidopsis*. *Plant Physiol.* 164, 879–887. doi: 10.1104/pp.113.230995

Mair, A., Wurzinger, B., Simeunovic, A., Nägele, T., Weckwerth, W., Teige, M., et al. (2015). SnRK1-triggered switch of bZIP63 dimerization mediates the low-energy response in plants. *eLife* 4:e05828. doi: 10.7554/eLife.05828

Margalha, L., Confraria, A., and Baena-González, E. (2019). SnRK1 and TOR: modulating growth–defense trade-offs in plant stress responses. *J. Exp. Bot.* 70, 2261–2274. doi: 10.1093/jxb/erz066

Mathan, J., Singh, A., and Ranjan, A. (2021). Sucrose transport and metabolism control carbon partitioning between stem and grain in rice. *J. Exp. Bot.* 72, 4355–4372. doi: 10.1093/jxb/erab066

Matiolli, C. C., Tomaz, J. P., Duarte, G. T., Prado, F. M., Del Bem, L. E. V., Silveira, A. B., et al. (2011). The *Arabidopsis* bZIP gene AtbZIP63 is a sensitive integrator of transient abscisic acid and glucose signals. *Plant Physiol.* 157, 692–705. doi: 10.1104/pp.111.181743

Mehrpouyan, S., Menon, U., Tetlow, I. J., and Emes, M. J. (2021). Protein phosphorylation regulates maize endosperm starch synthase IIa activity and protein–protein interactions. *Plant J.* 105, 1098–1112. doi: 10.1111/tpj.15094

Mergner, J., Frejno, M., List, M., Papacek, M., Chen, X., Chaudhary, A., et al. (2020). Mass-spectrometry-based draft of the *Arabidopsis* proteome. *Nature* 579, 409–414. doi: 10.1038/s41586-020-2094-2

Michaeli, S., Galili, G., Genschik, P., Fernie, A. R., and Avin-Wittenberg, T. (2016). Autophagy in plants - What's new on the menu? *Trends Plant Sci.* 21, 134–144. doi: 10.1016/j.tplants.2015.10.008

Michalska, J., Zauber, H., Buchanan, B. B., Cejudo, F. J., and Geigenberger, P. (2009). NTRC links built-in thioredoxin to light and sucrose in regulating starch synthesis in chloroplasts and amyloplasts. *Proc. Natl. Acad. Sci. U.S.A.* 106, 9908–9913. doi: 10.1073/pnas.0903559106

Michelet, L., Zaffagnini, M., Marchand, C., Collin, V., Decottignies, P., Tsan, P., et al. (2005). Glutathionylation of chloroplast thioredoxin f is a redox signaling mechanism in plants. *Proc. Natl. Acad. Sci. U.S.A.* 102, 16478–16483. doi: 10.1073/pnas.0507498102

Mikkelsen, R., Mutenda, K. E., Mant, A., Schürmann, P., and Blennow, A. (2005). α-Glucan, water dikinase (GWD): a plastidic enzyme with redox-regulated and coordinated catalytic activity and binding affinity. *Proc. Natl. Acad. Sci. U.S.A.* 102, 1785–1790. doi: 10.1073/pnas.0406674102

Moore, B., Zhou, L., Rolland, F., Hall, Q., Cheng, W. H., Liu, Y. X., et al. (2003). Role of the *Arabidopsis* glucose sensor HXK1 in nutrient, light, and hormonal signaling. *Science* 300, 332–336. doi: 10.1126/science.1080585

Moraes, T. A., Mengin, V., Annunziata, M. G., Encke, B., Krohn, N., Höhne, M., et al. (2019). Response of the circadian clock and diel starch turnover to one day of low light or low CO2. *Plant Physiol.* 179, 1457–1478. doi: 10.1104/pp.18.01418

Mubeen, U., Giavalisco, P., and Caldana, C. (2019). TOR inhibition interrupts the metabolic homeostasis by shifting the carbon-nitrogen balance in *Chlamydomonas reinhardtii*. *Plant Signal. Behav.* 14:1670595. doi: 10.1080/15592324.2019.1670595

Nägele, T., and Weckwerth, W. (2014). Mathematical modeling reveals that metabolic feedback regulation of SnRK1 and hexokinase is sufficient to control sugar homeostasis from energy depletion to full recovery. *Front. Plant Sci.* 5:365. doi: 10.3389/fpls.2014.00365

Nakagami, H., Sugiyama, N., Mochida, K., Daudi, A., Yoshida, Y., Toyoda, T., et al. (2010). Large-scale comparative phosphoproteomics identifies conserved phosphorylation sites in plants. *Plant Physiol.* 153, 1161–1174. doi: 10.1104/pp.110.157347

Nietzsche, M., Landgraf, R., Tohge, T., and Börnke, F. (2016). A protein–protein interaction network linking the energy-sensor kinase SnRK1 to multiple signaling pathways in *Arabidopsis thaliana*. *Curr. Plant Biol.* 5, 36–44. doi: 10.1016/j.cpb.2015.10.004

Niittylä, T., Messerli, G., Trevisan, M., Chen, J., Smith, A. M., and Zeeman, S. C. (2004). A previously unknown maltose transporter essential for starch degradation in leaves. *Science* 303, 87–89. doi: 10.1126/science.1091811

Nikkanen, L., and Rintamäki, E. (2019). Chloroplast thioredoxin systems dynamically regulate photosynthesis in plants. *Biochem. J.* 476, 1159–1172. doi: 10.1042/BCJ20180707

Nukarinen, E., Ngele, T., Pedrotti, L., Wurzinger, B., Mair, A., Landgraf, R., et al. (2016). Quantitative phosphoproteomics reveals the role of the AMPK plant ortholog SnRK1 as a metabolic master regulator under energy deprivation. *Sci. Rep.* 6, 1–19. doi: 10.1038/srep31697

Patterson, J. A., Tetlow, I. J., and Emes, M. J. (2018). Bioinformatic and in vitro analyses of *Arabidopsis* starch synthase 2 reveal post-translational regulatory mechanisms. *Front. Plant Sci.* 9:1338. doi: 10.3389/fpls.2018.01338

Pedrotti, L., Weiste, C., Nägele, T., Wolf, E., Lorenzin, F., Dietrich, K., et al. (2018). Snf1-RELATED KINASE1-controlled C/S1-bZIP signaling activates alternative mitochondrial metabolic pathways to ensure plant survival in extended darkness. *Plant Cell* 30, 495–509. doi: 10.1105/tpc.17.00414

Peixoto, B., Moraes, T. A., Mengin, V., Margalha, L., Vicente, R., Feil, R., et al. (2021). Impact of the SnRK1 protein kinase on sucrose homeostasis and the transcriptome during the diel cycle. *Plant Physiol.* 187, 1357–1373. doi: 10.1093/plphys/kiab350

Perdomo, J. A., Buchner, P., and Carmo-Silva, E. (2021). The relative abundance of wheat Rubisco activase isoforms is post-transcriptionally regulated. *Photosynth. Res.* 148, 47–56. doi: 10.1007/s11120-021-00830-6

Piattoni, C. V., Ferrero, D. M. L., Dellaferrera, I., Vegetti, A., and Iglesias, A. (2017). Cytosolic glyceraldehyde-3-phosphate dehydrogenase is phosphorylated during seed development. *Front. Plant Sci.* 8:522. doi: 10.3389/fpls.2017.00522

Pokhilko, A., Flis, A., Sulpice, R., Stitt, M., and Ebenhöh, O. (2014). Adjustment of carbon fluxes to light conditions regulates the daily turnover of starch in plants: a computational model. *Mol. Biosyst.* 10, 613–627. doi: 10.1039/c3mb70459a

Qu, J., Xu, S., Zhang, Z., Chen, G., Zhong, Y., Liu, L., et al. (2018). Evolutionary, structural and expression analysis of core genes involved in starch synthesis. *Sci. Rep.* 8, 1–16. doi: 10.1038/s41598-018-30411-y

Ramon, M., Dang, T. V. T., Broeckx, T., Hulsmans, S., Crepin, N., Sheen, J., et al. (2019). Default activation and nuclear translocation of the plant cellular energy sensor SnRK1 regulate metabolic stress responses and development. *Plant Cell* 31, 1614–1632. doi: 10.1105/tpc.18.00500

Ramon, M., Rolland, F., and Sheen, J. (2008). Sugar sensing and signaling. *Arabidopsis Book* 6:e0117. doi: 10.1199/tab.0117

Reiland, S., Messerli, G., Baerenfaller, K., Gerrits, B., Endler, A., Grossmann, J., et al. (2009). Large-scale *Arabidopsis* phosphoproteome profiling reveals novel chloroplast kinase substrates and phosphorylation networks. *Plant Physiol.* 150, 889–903. doi: 10.1104/pp.109.138677

Reimann, R., Hippler, M., Machelett, B., and Appenroth, K. J. (2004). Light induces phosphorylation of glucan water dikinase, which precedes starch degradation in turions of the duckweed *Spirodela polyrhiza*. *Plant Physiol.* 135, 121–128. doi: 10.1104/pp.103.036236

Ritte, G., Heydenreich, M., Mahlow, S., Haebel, S., Kötting, O., and Steup, M. (2006). Phosphorylation of C6- and C3-positions of glucosyl residues in starch is catalysed by distinct dikinases. *FEBS Lett.* 580, 4872–4876. doi: 10.1016/j.febslet.2006.07.085

Roitinger, E., Hofer, M., Köcher, T., Pichler, P., Novatchkova, M., Yang, J., et al. (2015). Quantitative phosphoproteomics of the ataxia telangiectasia-mutated (ATM) and ataxia telangiectasia-mutated and Rad3-related (ATR) dependent DNA damage response in *Arabidopsis thaliana*. *Mol. Cell. Proteomics* 14, 556–571. doi: 10.1074/mcp.M114.040352

Rojas-González, J. A., Soto-Súarez, M., García-Díaz, Á, Romero-Puertas, M. C., Sandalio, L. M., Mérida, Á, et al. (2015). Disruption of both chloroplastic and cytosolic FBPase genes results in a dwarf phenotype and important starch and metabolite changes in *Arabidopsis thaliana*. *J. Exp. Bot.* 66, 2673–2689. doi: 10.1093/jxb/erv062

Rolland, F., Baena-Gonzalez, E., and Sheen, J. (2006). Sugar sensing and signaling in plants: conserved and novel mechanisms. *Annu. Rev. Plant Biol.* 57, 675–709. doi: 10.1146/annurev.arplant.57.032905.105441

Rolland, F., and Sheen, J. (2005). Sugar sensing and signalling networks in plants. *Biochem. Soc. Trans.* 33, 269–271. doi: 10.1042/BST0330269

Sanmartín, N., Pastor, V., Pastor-Fernández, J., Flors, V., Pozo, M. J., and Sánchez-Bel, P. (2021). Role and mechanisms of callose priming in mycorrhiza-induced resistance. *J. Exp. Bot.* 71, 2769–2781. doi: 10.1093/JXB/ERAA030

Sato, T., Maekawa, S., Yasuda, S., Sonoda, Y., Katoh, E., Ichikawa, T., et al. (2009). CNI1/ATL31, a RING-type ubiquitin ligase that functions in the carbon/nitrogen response for growth phase transition in *Arabidopsis* seedlings. *Plant J.* 60, 852–864. doi: 10.1111/j.1365-313X.2009.04006.x

Schindler, I., Renz, A., Schmid, F. X., and Beck, E. (2001). Activation of spinach pullulanase by reduction results in a decrease in the number of isomeric forms. *Biochim. Biophys. Acta* 1548, 175–186. doi: 10.1016/s0167-4838(01)00228-x

Schneider, M., Knuesting, J., Birkholz, O., Heinisch, J. J., and Scheibe, R. (2018). Cytosolic GAPDH as a redox-dependent regulator of energy metabolism. *BMC Plant Biol.* 18:184. doi: 10.1186/s12870-018-1390-6

Schönberg, A., Bergner, E., Helm, S., Agne, B., Dünschede, B., Schünemann, D., et al. (2014). The peptide microarray "chlorophos1.0" identifies new phosphorylation targets of plastid casein kinase II (pCKII) in *Arabidopsis thaliana*. *PLoS One* 9:e0108344. doi: 10.1371/journal.pone.0108344

Schumann, J., Richter, M. L., and McCarty, R. E. (1985). Partial proteolysis as a probe of the conformation of the gamma subunit in activated soluble and membrane-bound chloroplast coupling factor 1. *J. Biol. Chem.* 260, 11817–11823. doi: 10.1016/s0021-9258(17)39104-4

Selinski, J., and Scheibe, R. (2019). Malate valves: old shuttles with new perspectives. *Plant Biol.* 21, 21–30. doi: 10.1111/plb.12869

Shi, L., and Tu, B. P. (2015). Acetyl-CoA and the regulation of metabolism: mechanisms and consequences. *Curr. Opin. Cell Biol.* 33, 125–131. doi: 10.1016/j.ceb.2015.02.003

Skryhan, K., Gurrieri, L., Sparla, F., Trost, P., and Blennow, A. (2018). Redox regulation of starch metabolism. *Front. Plant Sci.* 9:1344. doi: 10.3389/fpls.2018.01344

Sparla, F., Costa, A., Lo Schiavo, F., Pupillo, P., and Trost, P. (2006). Redox regulation of a novel plastid-targeted β-amylase of *Arabidopsis*. *Plant Physiol.* 141, 840–850. doi: 10.1104/pp.106.079186

Tetlow, I. J., Beisel, K. G., Cameron, S., Makhmoudova, A., Liu, F., Bresolin, N. S., et al. (2008). Analysis of protein complexes in wheat amyloplasts reveals functional interactions among starch biosynthetic enzymes. *Plant Physiol.* 146, 1878–1891. doi: 10.1104/pp.108.116244

Tetlow, I. J., Wait, R., Lu, Z., Akkasaeng, R., Bowsher, C. G., Esposito, S., et al. (2004). Protein phosphorylation in amyloplasts regulates starch branching enzyme activity and protein–protein interactions. *Plant Cell* 16, 694–708. doi: 10.1105/tpc.017400

Thalmann, M., Pazmino, D., Seung, D., Horrer, D., Nigro, A., Meier, T., et al. (2016). Regulation of leaf starch degradation by abscisic acid is important for osmotic stress tolerance in plants. *Plant Cell* 28, 1860–1878. doi: 10.1105/tpc.16.00143

Thalmann, M., and Santelia, D. (2017). Starch as a determinant of plant fitness under abiotic stress. *New Phytol.* 214, 943–951. doi: 10.1111/nph.14491

Thompson, A. R., Doelling, J. H., Suttangkakul, A., and Vierstra, R. D. (2005). Autophagic nutrient recycling in *Arabidopsis* directed by the ATG8 and ATG12 conjugation pathways. *Plant Physiol.* 138, 2097–2110. doi: 10.1104/pp.105.060673

Turkan, I. (2018). ROS and RNS: key signalling molecules in plants. *J. Exp. Bot.* 69, 3313–3315. doi: 10.1093/jxb/ery198

Usadel, B., Bläsing, O. E., Gibon, Y., Retzlaff, K., Höhne, M., Günther, M., et al. (2008). Global transcript levels respond to small changes of the carbon status during progressive exhaustion of carbohydrates in *Arabidopsis* rosettes. *Plant Physiol.* 146, 1834–1861. doi: 10.1104/pp.107.115592

Valerio, C., Costa, A., Marri, L., Issakidis-Bourguet, E., Pupillo, P., Trost, P., et al. (2011). Thioredoxin-regulated β-amylase (BAM1) triggers diurnal starch degradation in guard cells, and in mesophyll cells under osmotic stress. *J. Exp. Bot.* 62, 545–555. doi: 10.1093/jxb/erq288

Van Leene, J., Han, C., Gadeyne, A., Eeckhout, D., Matthijs, C., Cannoot, B., et al. (2019). Capturing the phosphorylation and protein interaction landscape of the plant TOR kinase. *Nat. Plants* 5, 316–327. doi: 10.1038/s41477-019-0378-z

Ventimiglia, L., and Mutus, B. (2020). The physiological implications of s-nitrosoglutathione reductase (Gsnor) activity mediating no signalling in plant root structures. *Antioxidants* 9, 1–11. doi: 10.3390/antiox9121206

Viana, A. J. C., Matiolli, C. C., Newman, D. W., Vieira, J. G. P., Duarte, G. T., Martins, M. C. M., et al. (2021). The sugar-responsive circadian clock regulator bZIP63 modulates plant growth. *New Phytol.* 231, 1875–1889. doi: 10.1111/nph.17518

Vu, L. D., Gevaert, K., and De Smet, I. (2018). Protein language: post-translational modifications talking to each other. *Trends Plant Sci.* 23, 1068–1080. doi: 10.1016/j.tplants.2018.09.004

Walton, A., Stes, E., Cybulski, N., Bel, M., Iñigo, S., Durand, A. N., et al. (2016). It's time for some "site"-seeing: novel tools to monitor the ubiquitin landscape in *Arabidopsis thaliana*. *Plant Cell* 28, 6–16. doi: 10.1105/tpc.15.00878

Wang, B., Zhao, X., Zhao, Y., Shanklin, J., Zhao, Q., and Liu, C. J. (2021). *Arabidopsis* SnRK1 negatively regulates phenylpropanoid metabolism via Kelch domain-containing F-box proteins. *New Phytol.* 229, 3345–3359. doi: 10.1111/nph.17121

Wang, P., Xue, L., Batelli, G., Lee, S., Hou, Y. J., Van Oosten, M. J., et al. (2013). Quantitative phosphoproteomics identifies SnRK2 protein kinase substrates and reveals the effectors of abscisic acid action. *Proc. Natl. Acad. Sci. U.S.A.* 110, 11205–11210. doi: 10.1073/pnas.1308974110

Webb, A. A. R., and Satake, A. (2015). Understanding circadian regulation of carbohydrate metabolism in *Arabidopsis* using mathematical models. *Plant Cell Physiol.* 56, 586–593. doi: 10.1093/pcp/pcv033

Weise, S. E., Kim, K. S., Stewart, R. P., and Sharkey, T. D. (2005). B-maltose is the metabolically active anomer of maltose during transitory starch degradation. *Plant Physiol.* 137, 756–761. doi: 10.1104/pp.104.055996

Wulfert, S., Schilasky, S., and Krueger, S. (2020). Transcriptional and biochemical characterization of cytosolic pyruvate kinases in *Arabidopsis thaliana*. *Plants* 9:353. doi: 10.3390/plants9030353

Wurzinger, B., Nukarinen, E., Nägele, T., Weckwerth, W., and Teige, M. (2018). The SnRK1 kinase as central mediator of energy signaling between different organelles. *Plant Physiol.* 176, 1085–1094. doi: 10.1104/pp.17.01404

Xiong, Y., McCormack, M., Li, L., Hall, Q., Xiang, C., and Sheen, J. (2013). Glucose-TOR signalling reprograms the transcriptome and activates meristems. *Nature* 496, 181–186. doi: 10.1038/nature12030

Xu, Q., Yin, S., Ma, Y., Song, M., Song, Y., Mu, S., et al. (2020). Carbon export from leaves is controlled via ubiquitination and phosphorylation of sucrose transporter SUC2. *Proc. Natl. Acad. Sci. U.S.A.* 117, 6223–6230. doi: 10.1073/pnas.1912754117

Yanagisawa, S., Yoo, S. D., and Sheen, J. (2003). Differential regulation of EIN3 stability by glucose and ethylene signalling in plants. *Nature* 425, 521–525. doi: 10.1038/nature01984

Yasuda, S., Aoyama, S., Hasegawa, Y., Sato, T., and Yamaguchi, J. (2017). *Arabidopsis* CBL-interacting protein kinases regulate carbon/nitrogen-nutrient response by phosphorylating ubiquitin ligase ATL31. *Mol. Plant* 10, 605–618. doi: 10.1016/j.molp.2017.01.005

Yokochi, Y., Yoshida, K., Hahn, F., Miyagi, A., Wakabayashi, K. I., Kawai-Yamada, M., et al. (2021). Redox regulation of NADP-malate dehydrogenase is vital for land plants under fluctuating light environment. *Proc. Natl. Acad. Sci. U.S.A.* 118, 1–12. doi: 10.1073/pnas.2016903118

Zhai, Z., Liu, H., and Shanklin, J. (2017). Phosphorylation of WRINKLED1 by KIN10 results in its proteasomal degradation, providing a link between energy homeostasis and lipid biosynthesis. *Plant Cell* 29, 871–889. doi: 10.1105/tpc.17.00019

Zhang, N., and Portis, A. R. (1999). Mechanism of light regulation of Rubisco: a specific role for the larger rubisco activase isoform involving reductive activation by thioredoxin-f. *Proc. Natl. Acad. Sci. U.S.A.* 96, 9438–9443. doi: 10.1073/pnas.96.16.9438

Zhang, Z. W., Luo, S., Zhang, G. C., Feng, L. Y., Zheng, C., Zhou, Y. H., et al. (2017). Nitric oxide induces monosaccharide accumulation through enzyme S-nitrosylation. *Plant Cell Environ.* 40, 1834–1848. doi: 10.1111/pce.12989

Zhao, Z., and Assmann, S. M. (2011). The glycolytic enzyme, phosphoglycerate mutase, has critical roles in stomatal movement, vegetative growth, and pollen production in *Arabidopsis thaliana*. *J. Exp. Bot.* 62, 5179–5189. doi: 10.1093/jxb/err223

Conflict of Interest: The authors declare that the research was conducted in the absence of any commercial or financial relationships that could be construed as a potential conflict of interest.

Publisher's Note: All claims expressed in this article are solely those of the authors and do not necessarily represent those of their affiliated organizations, or those of the publisher, the editors and the reviewers. Any product that may be evaluated in this article, or claim that may be made by its manufacturer, is not guaranteed or endorsed by the publisher.

frontiers in Plant Science

ORIGINAL RESEARCH
published: 31 January 2022
doi: 10.3389/fpls.2021.758526

The Role of Sugar Transporter CsSWEET7a in Apoplasmic Phloem Unloading in Receptacle and Nectary During Cucumber Anthesis

*Yaxin Li†‡, Huan Liu‡, Xuehui Yao‡, Lulu Sun and Xiaolei Sui**

Beijing Key Laboratory of Growth and Developmental Regulation for Protected Vegetable Crops, College of Horticulture, China Agricultural University, Beijing, China

OPEN ACCESS

Edited by:
Rubén Vicente, Universidade Nova de Lisboa, Portugal

Reviewed by:
Clay Carter, University of Minnesota Twin Cities, United States
Maria Grazia Annunziata, University of Potsdam, Germany

***Correspondence:**
Xiaolei Sui
suixiaolei@cau.edu.cn

†Present address:
Yaxin Li, Department of Plant Biology, School of Integrative Biology, University of Illinois at Urbana-Champaign, Urbana, IL, United States

‡These authors have contributed equally to this work

Specialty section:
This article was submitted to Plant Metabolism and Chemodiversity, a section of the journal Frontiers in Plant Science

Received: *14 August 2021*
Accepted: *31 December 2021*
Published: *31 January 2022*

Citation:
Li Y, Liu H, Yao X, Sun L and Sui X (2022) The Role of Sugar Transporter CsSWEET7a in Apoplasmic Phloem Unloading in Receptacle and Nectary During Cucumber Anthesis. Front. Plant Sci. 12:758526. doi: 10.3389/fpls.2021.758526

During anthesis, there is an increased demand for carbohydrates due to pollen maturation and nectary secretion that warrants a systematic phloem unloading strategy for sugar partitioning. Sugar transporters are key components of the apoplasmic phloem unloading strategy and control the sugar flux needed for plant development. Currently, the phloem unloading strategy during anthesis has not been explored in cucumber, and the question of which sugar transporters are active during flower anthesis is poorly understood. In this study, a study utilizing the phloem-mobile symplasmic tracer carboxyfluorescein (CF) suggested that the phloem unloading was symplasmically isolated in the receptacle and nectary of cucumber flowers at anthesis. We also identified a hexose transporter that is highly expressed in cucumber flower, Sugar Will Eventually be Exported Transporter 7a (SWEET7a). *CsSWEET7a* was mainly expressed in receptacle and nectary tissues in both male and female flowers, where its expression level increased rapidly right before anthesis. At anthesis, the CsSWEET7a protein was specifically localized to the phloem region of the receptacle and nectary, indicating that CsSWEET7a may function in the apoplasmic phloem unloading during flower anthesis. Although cucumber mainly transports raffinose family oligosaccharides (RFOs) in the phloem, sucrose, glucose, and fructose are the major sugars in the flower receptacle and the nectary as well as in nectar at anthesis. In addition, the transcript levels of genes encoding soluble sugar hydrolases (α-*galactosidase*, *sucrose synthase*, *cytoplasmic invertase*, and *cell wall invertase*) were correlated with that of *CsSWEET7a*. These results indicated that CsSWEET7a may be involved in sugar partitioning as an exporter in the phloem of the receptacle and nectary to supply carbohydrates for flower anthesis and nectar secretion in cucumber.

Keywords: ***Cucumis sativus*** **L., hexose transporter, flowering, phloem transport, pollinator reward, SWEET protein**

INTRODUCTION

In flowering plants, the reproductive tissues require large amounts of carbohydrates for pollen maturation, nectar secretion, pollen tube generation, and seed initiation (Borghi and Fernie, 2017). Flower petals and sepals have limited capacity for photosynthesis when they are green, and this capacity further decreases before anthesis as the petal color changes (Müller et al., 2010). As a sink

organ, the flower relies heavily on the sugar produced in leaves as the energy for its development. The sugar produced in the source leaf is transferred to a sink organ through three main steps: phloem loading (Zhang and Turgeon, 2018), phloem long-distance transport (Jensen, 2018), and phloem unloading (Milne et al., 2018). During phloem unloading, sugar is unloaded from the sieve element/companion cell (SE/CC) complex into sink tissues *via* one of the two pathways: flowing into phloem parenchyma cells through plasmodesmata (symplasmic unloading) or transport through the apoplasm mediated by sugar transporters (apoplasmic unloading) (Oparka, 1990).

Within a flower, different tissues may use different unloading strategies. For example, pollen grains and pollen tubes are symplasmically isolated from surrounding tissues and utilize an apoplasmic unloading strategy (Borghi and Fernie, 2017). In *Arabidopsis*, carbohydrate movement into the anther *via* the filament uses a symplasmic unloading strategy (Imlau et al., 1999). Similarly, phloem unloading in the *Arabidopsis* petal is symplasmic (Imlau et al., 1999). However, it is not clear which phloem unloading strategies are utilized in the nectary and receptacle. In many plant species, the nectary aids reproduction through attracting pollinators by secreting nectar. The receptacle is often enlarged to support the flower and hold all flower tissues together. In cucumber (*Cucumis sativus* L.), the nectary in male flowers is button-like in appearance, usually three-lobed, and lies on the receptacle (Collison and Martin, 1975). The nectary in the female cucumber flower initiates at the junction between the base of the style and the receptacle before forming a ring-shaped structure (Bai et al., 2004). As non-photosynthetic organs, most of the nectary, as well as the secreted nectar, are dependent on phloem-derived sugars from sources (Roy et al., 2017). Phloem is reported to be the most common vascular tissue in nectary and the sugar content can reach up to 50% in phloem-rich nectary, while the sugar concentration can be as low as 8% in xylem dominant nectary (Frey-Wyssling, 1955; Roy et al., 2017). In *Arabidopsis* (Lin et al., 2014) and squash (Solhaug et al., 2019a), several steps are important for nectar secretion, including starch accumulation at the early developmental stage of nectary and subsequent starch degradation pre-anthesis, sucrose synthesis, and sucrose export. In addition, the direct transport of phloem sugar, without prior storage as starch, could also play an important role in the generation of squash nectar (Solhaug et al., 2019a). Thus, it is important to understand how carbohydrates are unloaded from phloem in the receptacle and nectary. As a model plant of unisexual floral development (Gu et al., 2011), cucumber offers a great opportunity to streamline the study of carbohydrate partitioning in flowers.

During apoplasmic unloading, transporters move sugars across membranes, with an exporter taking sugar from the SE/CC into the apoplasmic space and an energy-dependent importer taking sugar into phloem parenchyma cells (Milne et al., 2018). Sucrose transporter (SUT) and monosaccharide transporters [e.g., sugar transport protein (STP)] were reported to function at the latter step (Büttner, 2010; Borghi and Fernie, 2017), while a sugar exporter (functioning at the first step) has not been reported in flowers. Cucumber Sugar Will Eventually be Exported Transporter 7a (SWEET7a) is known to localize the companion cells in fruit vascular bundles and to export hexose to the apoplasmic space to stimulate sugar unloading in fruit (Li et al., 2021). In *Arabidopsis* pollen, AtSWEET8 and AtSWEET13 are involved in pollen maturation, and an aborted silique phenotype was observed in *sweet8* single mutant (Guan et al., 2008), while this phenotype was more severe in *sweet8;13* double mutant (Sun et al., 2013). AtSWEET9 is specifically expressed in nectary parenchyma cells and functions together with cell wall invertase (CWINV) and sucrose phosphate synthases (SPS) in nectary secretion (Lin et al., 2014). Similarly, SWEET9 homologs are involved in nectary secretion in *Brassica*, *Nicotiana*, and *Petunia hybrida* (Ge et al., 2000; Lin et al., 2014). Additionally, several SWEET homologs are expressed in flowers of *Arabidopsis* (Lin et al., 2014), cucumber (Li et al., 2017), and *Jasminum sambac* (Wang et al., 2019). Besides, SWEETs function as a uniporter, which facilitates sugar transport along substrate gradient. Specifically, Clade I/II SWEETs mainly transport hexoses and Clade III SWEETs transport sucrose, while Clade IV SWEETs are tonoplast-localized hexose transporters (Chen et al., 2015a). All SWEETs identified so far function as low-affinity sugar transporters (with measured Km values in mM range) (Chen et al., 2015b), suggesting that they tend to have important roles in regions where sugars are abundant, such as the study of AtSWEET11,12,15 in seeds (Chen et al., 2015b) and CsSWEET7a in fruit (Li et al., 2021). Taken together, we hypothesized that SWEET transporters may be involved in phloem unloading in the receptacle and nectary of cucumber flowers during anthesis.

In this study, we found that phloem unloading in cucumber receptacle and nectary at anthesis is apoplasmic. Hexose transporter *CsSWEET7a* was highly expressed in nectary and receptacle in both male and female cucumber flowers, and its expression level increased as anthesis progressed. The CsSWEET7a protein is specifically localized in the phloem of nectary and receptacle during anthesis, indicating a possible role in sugar phloem unloading at these regions. Additionally, the transcript levels of genes encoding soluble sugar hydrolases (α-*galactosidase*, *sucrose synthase*, *cytoplasmic invertase*, and *CWINV*) were correlated with that of *CsSWEET7a*, suggesting a potential synergic relationship between *CsSWEET7a* and sugar hydrolases during apoplasmic phloem unloading in cucumber nectary and receptacle at anthesis.

MATERIALS AND METHODS

Plant Material and Growth Conditions

Cucumber (*Cucumis sativus* L. "Xintaimici") plants were grown in a greenhouse under natural light conditions from late February to July at China Agricultural University in Beijing. In brief, cucumber seeds were germinated for 2 days at 28°C in dark in a growth chamber before being transferred to the greenhouse under standard conditions. Water management and pest control were performed as needed.

Carboxyfluorescein Diacetate Labeling

Carboxyfluorescein diacetate (CFDA) (Sigma-Aldrich, Shanghai, China) was first dissolved in acetone and then diluted to 0.5 mg ml^{-1} with water. The leaf in the same node as a male or female flower was chosen for CFDA labeling according to the study by Sui et al. (2018) with minor adjustment. The upper leaf epidermis was abraded with fine sandpaper. Then, 200 μl CFDA solution was applied, and the leaf was covered with plastic wrap to prevent evaporation. After 6-h labeling, the male and female flowers were sampled. A hand-section of nectary and receptacle samples was examined by confocal laser scanning microscopy (CLSM) (Confocal, Tokyo, Japan).

Spatial and Temporal Expression Analysis by Reverse Transcription-Quantitative PCR

For temporal expression analysis, male and female flowers were sampled at different developmental stages according to the study by Bai et al. (2004) at zeitgeber time (ZT) 4. The whole flower was sampled and dissected under a stereomicroscope (LEICA, S8APO, Germany) for receptacle and nectary samples. Three biological replicates were prepared. For gene expression analysis in different tissues, including root, stem, leaf, male and female flowers, and ovary/fruit, the samples were harvested at ZT4 of the 2-month-old cucumber plant at anthesis.

Total RNA from different tissues was extracted using the RNeasy Plant Kit (Huayueyang, Beijing, China) according to the protocol of the manufacturer. Reverse transcription was carried out using the FastQuant RT Kit (with gDNase; Tiangen, Beijing, China). Gene expression analyses were performed by reverse transcription-quantitative PCR (RT-qPCR) with the SYBR green detection protocol (TaKaRa, Japan) on an ABI 7500 Real-Time PCR Detection System (Bio-Rad, United States). The relative expression level was normalized to the housekeeping gene *Tubulin* using the $2^{-\Delta\Delta CT}$ method (Livak and Schmittgen, 2001). Primers used in this study are as shown in **Supplementary Table 1**.

Immunohistochemical Localization and Microscopy

CsSWEET7a primary antibody was described by Li et al. (2021). An alkaline phosphatase (AP)-labeled Goat Anti-Rabbit IgG was used as the secondary antibody. For immunohistochemical analyses, the receptacle and nectary samples from male and female flowers were harvested on the day of anthesis and dissected under a stereomicroscope. All samples were fixed in formaldehyde-acetic acid-ethanol (FAA) solution, followed by series dehydration, and were embedded in the wax as previously described (Wang et al., 2014). The immunohistochemical localization analysis was performed according to the study by Li et al. (2021). After the immunohistochemical reaction, samples were applied with 80% (v/v) glycerin and coverslip to keep moisture. Immunohistochemical signals were imaged under an Olympus microscope (BX53, Japan). Immunohistochemical signals of the whole receptacle and nectary tissues were observed under the 4 × objective, and the zoom-in images of vascular inside receptacle and nectary were taken under 10× or 20× objective.

Carbohydrate Extraction and Analysis

For sugar content measurement, around 0.2 g (fresh weight) receptacle, 0.05 g (fresh weight) nectary, and 30 μl nectar were sampled at ZT4 from pools of 10 flowers. Three biological replicates were taken. The receptacle and nectary were sampled under a stereomicroscope (LEICA, S8APO, Germany), and the nectar was sampled with a 10-μl pipette. Soluble sugar was extracted according to Ma et al. (2019a) with minor adjustments. In brief, the receptacle and nectary were homogenized in 200 μl 80% (v/v) ethanol in a 1.5-ml tube with a hand-held homogenizer. To the homogenate, 800 μl of 80% (v/v) ethanol was added. Samples were extracted under 80°C for 30 min. Samples were centrifuged at 12,000 × *g* for 10 min. The supernatant was transferred to a new 5-ml tube. Extractions were repeated twice, with the three supernatants combined. Supernatants were evaporated to dryness at 40°C, dissolved in 500 μl Mili-Q water, and filtered through a 0.22-mm nylon filter membrane. Nectar samples were diluted five times and filtered through a 0.22-mm nylon filter membrane. All samples were analyzed by High-Performance Liquid Chromatography (HPLC, Dao Jin RID-20A, Japan). The Shodex Asahipak NH2P-50 4E column was used as the separation column, and 70% (v/v) acetonitrile was used as the mobile phase. The flow rate was 1 ml/min, and the column temperature was 40°C.

For starch staining, medial longitudinal anatomy of male and female flower tissues was immersed in 10% I-KI staining solution for 30 min, then washed with water 2–3 times to stop the reaction, and removed the extra staining solution. The starch accumulated tissues were stained dark brown. Images were taken under a stereomicroscope (LEICA, S8APO, Germany).

Statistical Analysis

Statistical analyses in this study were performed using one−way ANOVA followed by multiple comparisons using Fisher's least significant difference method ($P-$value < 0.05) using Origin 2021b (OriginLab, Northampton, MA, United States).

RESULTS

Phloem Unloading in Flower Nectary and Receptacle Followed an Apoplasmic Pathway at Anthesis

We first observed the anatomy of male and female cucumber flowers at anthesis (**Figures 1A–D**). Images of the medial longitudinal anatomy of male flowers showed structures including sepal, petal, pedicel, receptacle, nectary, and anther (**Figure 1A**; the filament was not shown in this figure). The receptacle was located at the bottom, and the nectary was on the top center of the receptacle (**Figure 1A**, Bai et al., 2004). The transverse view of a male flower showed that the nectary initiated at the center of the receptacle and that the nectar was stored in between the nectary and receptacle (**Figure 1B**). Images

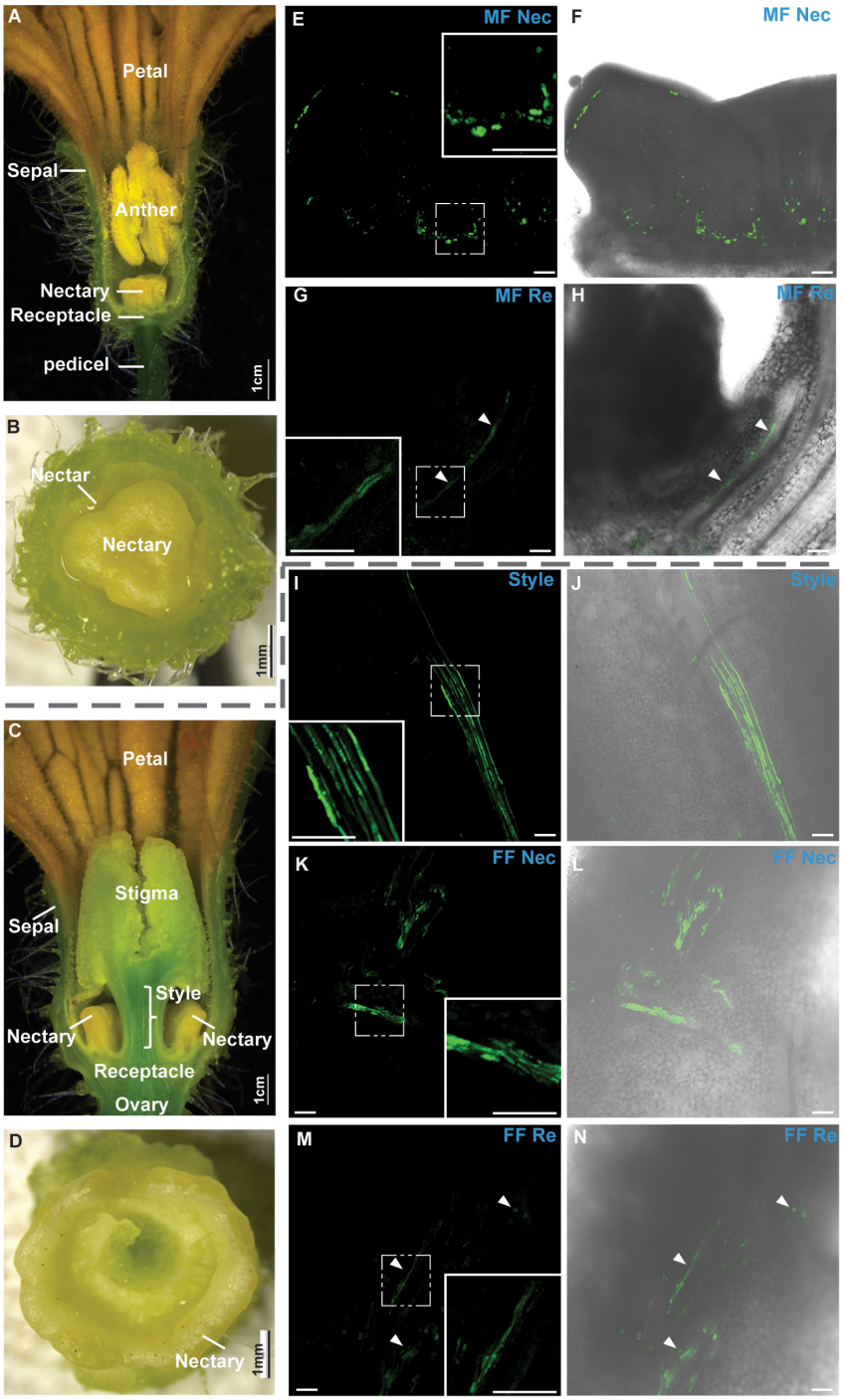

FIGURE 1 | Microscopic images of cucumber flowers at anthesis. **(A–D)** Medial longitudinal **(A,C)** and transverse anatomy images **(B,D)** of male **(A,B)** and female flowers **(C,D)** at anthesis. **(E–N)** Confocal laser scanning microscopy (CLSM) of carboxyfluorescein (CF) unloading from the phloem was shown in male **(E–H)** and female flowers **(I–N)**. CF signal was labeled in green in male and female flowers 6 h after feeding carboxyfluorescein diacetate (CFDA) at the leaf. CF signal in nectary (Nec) **(E,F)** and receptacle (Re) **(G,H)** of male flower (MF); in style **(I,J)**, nectary **(K,L)**, and receptacle **(M,N)** of the female flower (FF), respectively. The boxed insets in panels **(E,G,I,K,M)** were the close-up images. Bars in panels **(E–N)** were 100 μm. Bars in the close-up images were 50 μm. White arrows indicate the CF signal.

of the medial longitudinal anatomy of female flowers showed structures including sepal, petal, ovary, receptacle, nectary, style, and stigma (**Figure 1C**). The receptacle connected the style and the ovary, and the nectary initiated at the junctions between the style and the receptacle before developing into a ring shape structure (**Figures 1C,D**).

The membrane-permeable non-fluorescent dye CFDA, which can be deacetylated into the fluorescent CF, a membrane-impermeable fluorescent dye, was used to investigate the phloem unloading pathways in cucumber receptacle and nectary at anthesis. CF has been successfully used in multiple species and tissues for phloem transport and unloading pattern analysis (Haupt et al., 2001; Viola et al., 2001; Hu et al., 2011; Palmer et al., 2015; Sui et al., 2018). In this study, CFDA was applied to the leaf, and the CF signal was sought in the nearest male or female flower. If the plants use a symplasmic phloem unloading strategy, the CF will expand from phloem to the parenchyma cell through plasmodesmata, and a relatively uniform signal should be observed all over the tissues; if the plants undertake an apoplasmic unloading strategy, the CF will be found only in the phloem region and not dissipated to the surrounding parenchyma cells. In male flowers, the CF signal was confined in vascular regions without apparent diffusion to the surrounding tissues in the nectary (**Figures 1E,F**) or receptacle (**Figures 1G,H**). In female flowers, the CF signal was always confined to the phloem strands along the phloem pathway in the vascular bundles without apparent diffusion to the surrounding tissues in the style (**Figures 1I,J**), nectary (**Figures 1K,L**), or receptacle (**Figures 1M,N**). This indicated that phloem unloading in these tissues at anthesis was apoplasmic, and sugar transporters were probably required during this process.

CsSWEET7a Was Highly Expressed in Flower Receptacle and Nectary During Anthesis

A total of 17 SWEET genes were identified in the cucumber genome (Li et al., 2017). We surveyed the expression level of all cucumber SWEET genes in male and female flowers at anthesis using an RNA-seq dataset (PRJNA80169) from cucumber.[1] *CsSWEET1*, *CsSWEET7a*, *CsSWEET9*, and *CsSWEET17a* showed relatively higher expression levels than the other *SWEETs* in flowers at anthesis, with *CsSWEET7a* showing the highest expression among Clade I/II SWEETs (**Supplementary Figure 1A**). *CsSWEET9* of Clade III is a homolog of *Arabidopsis SWEET9*, which is expressed in nectary epidermal cells to move sucrose into nectar for secretion (Lin et al., 2014). In our previous study, CsSWEET17a of Clade IV was localized on the tonoplast (Li et al., 2017). *CsSWEET7a* was highly expressed in sink tissues (e.g., flower, root, and fruit), especially in flowers (Li et al., 2017). CsSWEET7a was reported to be localized on the plasma membrane of companion cells in cucumber fruit vasculature (Li et al., 2021), which suggests that CsSWEET7a is a promising candidate for phloem unloading in flowers. We further tested the expression pattern of *CsSWEET7a* at different developmental stages of male flowers [**Supplementary Figure 1B**; stage division as described by Bai et al. (2004) and Sun et al. (2019)]. In brief, at stage 9, microsporocytes initiate within a 1.5–2 mm length flower bud; at stage 10, anthers meiosis and nectary tissues initiate within a 3–4 mm length flower bud; at stage 11, uninuclear pollen appears, and nectary tissues form a ring within a 4–10 mm length flower bud; at stage 12, mature pollen forms, and nectary tissues fully develop in a 10–20 mm length flower bud; at stage 13, the anthesis is initiated. Our results showed that the expression level of *CsSWEET7a* slowly increased from stage 9 to stage 11 before rapidly increasing from stage 11 and peaking at anthesis (**Supplementary Figure 1B**), when flower tissues matured and prepared for anthesis, e.g., uninuclear pollen developed to mature pollen, and nectary tissues are fully developed in male flowers (Bai et al., 2004). In our previous study, the sugar level in male cucumber flowers increased from stage 9 to stage 12 (Sun et al., 2019). Thus, the increased expression level of *CsSWEET7a* in male flowers correlates well with the accumulated sugar levels and suggests that it may participate in sugar partitioning during this process.

We further examined the expression pattern of *CsSWEET7a* in different tissues in male and female flowers across flower development. *CsSWEET7a* was highly expressed in receptacle and nectary in both male (**Figure 2A**) and female flowers (**Figure 2B**). As the *CsSWEET7a* expression level increased at stage 11 in male flowers, we started to harvest receptacle and nectary samples at 3 days before anthesis (stage 11 to stage 12 samples). The expression level of *CsSWEET7a* increased from 3 days before anthesis to the day of anthesis or even 2–3 days after anthesis in receptacle and nectary of both male (**Figure 2A**) and female flowers (**Figure 2B**). This indicated that CsSWEET7a may function in receptacle and nectary regions for sugar partitioning during anthesis when the demand for sugar peaks.

CsSWEET7a Protein Was Specifically Localized in the Phloem Region in Cucumber Flowers

To investigate the function of CsSWEET7a in the receptacle and nectary of male and female flowers during anthesis, we analyzed CsSWEET7a protein localization by immunohistochemical staining (**Figures 3**, **4**). A polyclonal antibody was generated using two CsSWEET7a-specific peptides as described by Li et al. (2021). The receptacle and nectary regions of both male and female flowers at anthesis were fixed in wax for sectioning. A strong and specific immunohistochemical signal from the CsSWEET7a protein was observed in vascular tissues of receptacle and nectary both in longitudinal (**Figure 3A**) and transverse sections (**Figure 3F**) in male flowers. In close-up views, we found that CsSWEET7a was highly expressed in the phloem region of the nectary (**Figures 3B,G**) and receptacle (**Figures 3D,I**) and that no signal was observed in sections incubated with pre-immune serum (**Figures 3C,E,H,J**). Interestingly, the vascular density was higher in the receptacle than in the nectary, and more CsSWEET7a proteins were detected in the phloem tissue of the receptacle region than in the nectary region (**Figures 3A,F**). This indicates that the receptacle, which connects the pedicle and nectary, could function as a hub for carbohydrate partitioning in male flowers.

In the longitudinal sections of female flowers, a large number of vascular signatures showed immunohistochemical signals from the CsSWEET7a protein, which were strongly and specifically observed in the receptacle (**Figure 4A**), similar to

[1] http://cucurbitgenomics.org/rnaseq/home

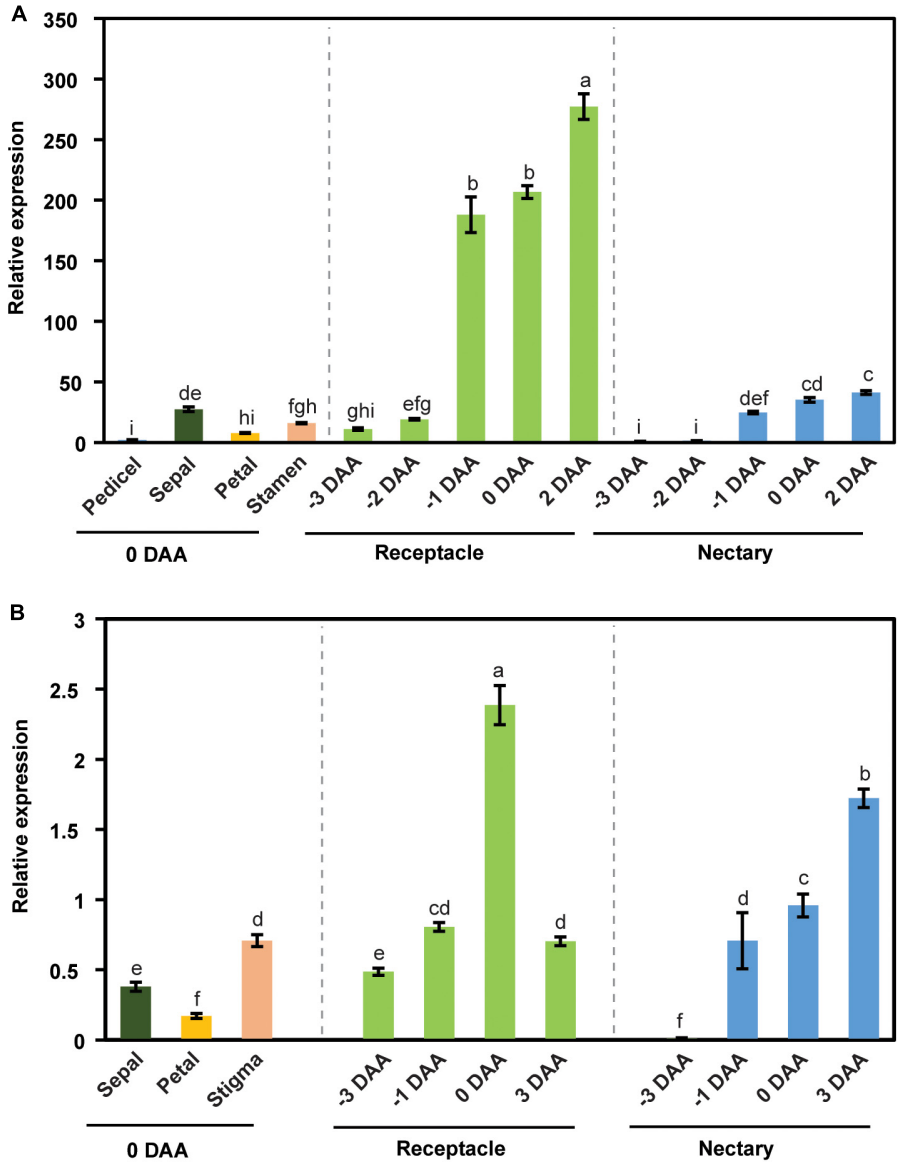

FIGURE 2 | The expression pattern of *CsSWEET7a* in male **(A)** and female flowers **(B)**. DAA, days after anthesis; −3, −2, −1 DAA, being 3, 2, and 1 day(s) before anthesis, respectively; 0 DAA, the day of anthesis; and 2 and 3 DAA, being 2 and 3 days after anthesis, respectively. Mean values ± SE of three independent biological replicates were shown. Statistical analyses were performed using one-way ANOVA followed by multiple comparisons using Fisher's LSD method (*P*-value < 0.05).

those in the male flowers. In close-up views of the receptacle, CsSWEET7a was localized to the cells at both sides of sieve elements, most likely the companion cells (**Figure 4D**). This agrees with the CsSWEET7a protein localization in fruit vascular tissues (Li et al., 2021). CsSWEET7a is also localized to the vascular tissues in the nectary (**Figures 4A,B**) and style (**Figure 4A**). In the transverse view of female flowers, CsSWEET7a protein signal was observed in vascular tissues in the receptacle as well as in nectary (**Figures 4F,G**), like what we observed in male flowers. No signals were observed in sections incubated with pre-immune serum (**Figures 4C,E,H**). Overall, CsSWEET7a protein was specifically expressed in phloem tissues in receptacle and nectary in both male and female cucumber flowers at anthesis.

Sucrose, Glucose, and Fructose Were the Major Sugars in Flower Receptacle and Nectary at Anthesis

The soluble sugar level in cucumber male flowers was reported to increase from stage 9 to stage 12 (Sun et al., 2019). Specifically, sucrose, glucose, and fructose are the major soluble sugar components, with a small amount of raffinose and stachyose in cucumber male flowers (Sun et al., 2019). To further investigate

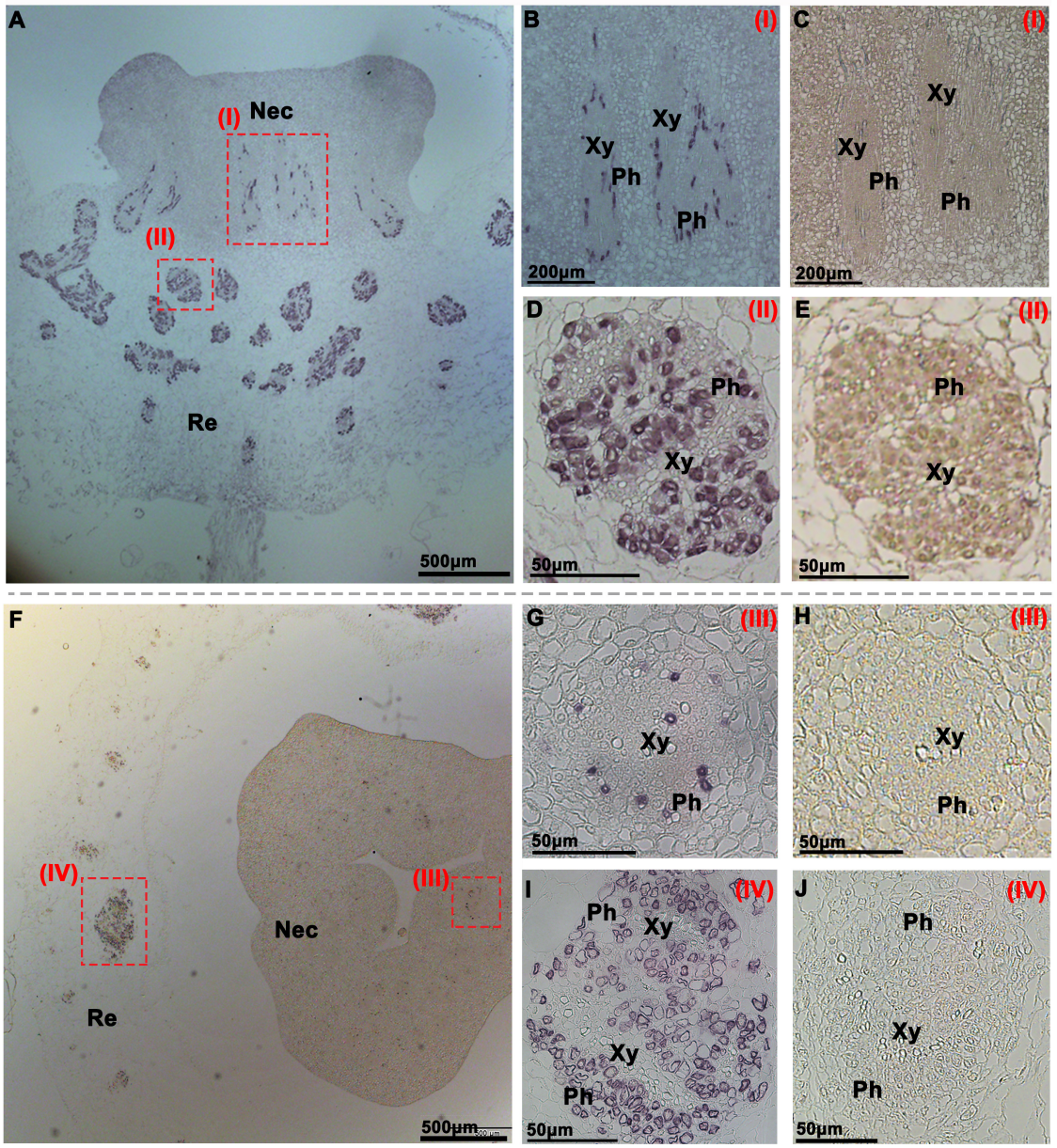

FIGURE 3 | Immunohistochemical localization of *CsSWEET7a* in male cucumber flowers. Longitudinal **(A–E)** and transverse sections **(F–J)** of male flowers with alkaline phosphatase (AP) as the second antibody. **(B,D,G,I)** The close-up of the boxes in panels **(A,F)**, respectively. **(C,E,H,J)** Sections incubated with pre-immune serum as a control. The Roman numerals in red at the top-right corner **(B–E,G–J)** correspond to the fields in panels **(A,F)**. Nec, nectary; Re, receptacle; Ph, phloem; Xy, xylem.

the sugar compositions in the receptacle, nectary, and nectar, we sampled these tissues at anthesis and extracted sugar for HPLC analysis. The results showed that nectar has the highest sugar level, followed by nectary and receptacle in both male (**Figure 5A**) and female flowers (**Figure 5B**). Moreover, sucrose, glucose, and fructose were the major soluble sugars, with only small amounts of raffinose and stachyose detected (**Figures 5A,B**). In the receptacle, nectary, and nectar of both male and female flowers, the majority of the sugar was sucrose (56–65%), followed by fructose (18–21%) and glucose (15–23%) (**Figures 5C,D**). Although the sugar compositions in the receptacle and nectary are sucrose-dominant, more than 30% hexoses are still present in the receptacle and nectary. Thus, CsSWEET7a is likely involved in the hexoses unloading, especially in the receptacle of both male and female flowers, given its strong phloem localization signals and gene expression pattern. Additionally, it has been reported that phloem-derived sugar was stored as starch in nectary before anthesis in squash (*Cucurbita pepo*), and the starch will be hydrolyzed to produce sugar for rapid energy supply during anthesis (Solhaug et al., 2019b). Thus, we examined the

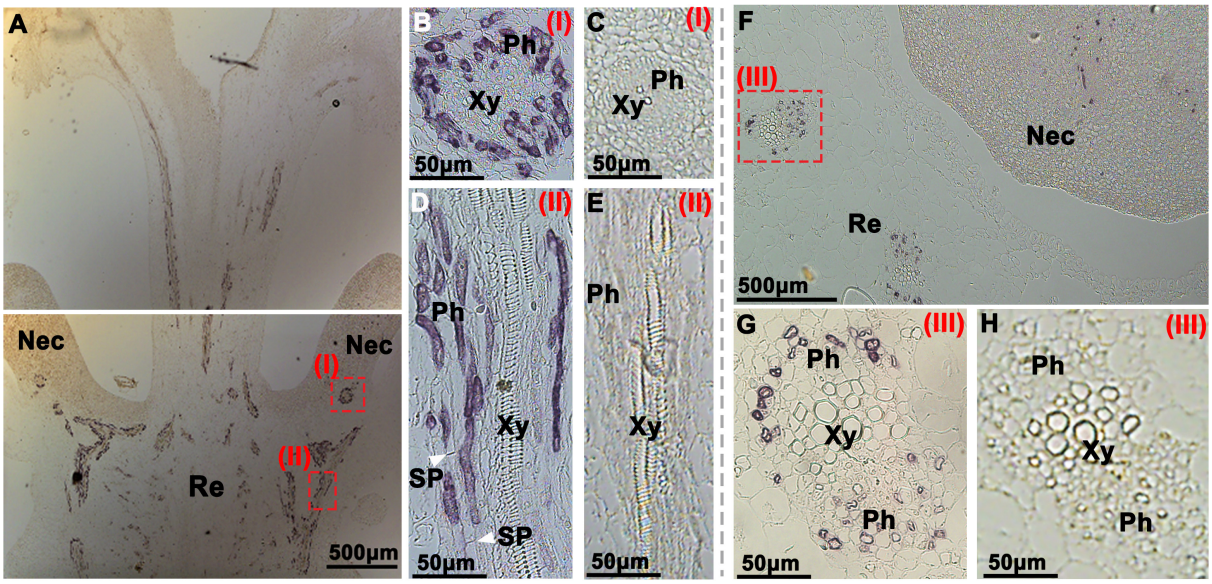

FIGURE 4 | Immunohistochemical localization of CsSWEET7a in female cucumber flowers. Longitudinal **(A–E)** and transverse sections **(F–H)** of female flowers with AP as the second antibody. **(B,D,G)** The close-up of the boxes in panels **(A,F)**, respectively. The white arrows in panel **(D)** indicate the sieve plate. **(C,E,H)** Sections were incubated with pre-immune serum as a control. Images in panels **(G,H)** were rotated 90°clockwise. The Roman numerals in red at the top-right corner **(B–E,G,H)** correspond to those fields in panels **(A,F)**. Nec, nectary; Re, receptacle; Ph, phloem; Xy, xylem; SP, sieve plate.

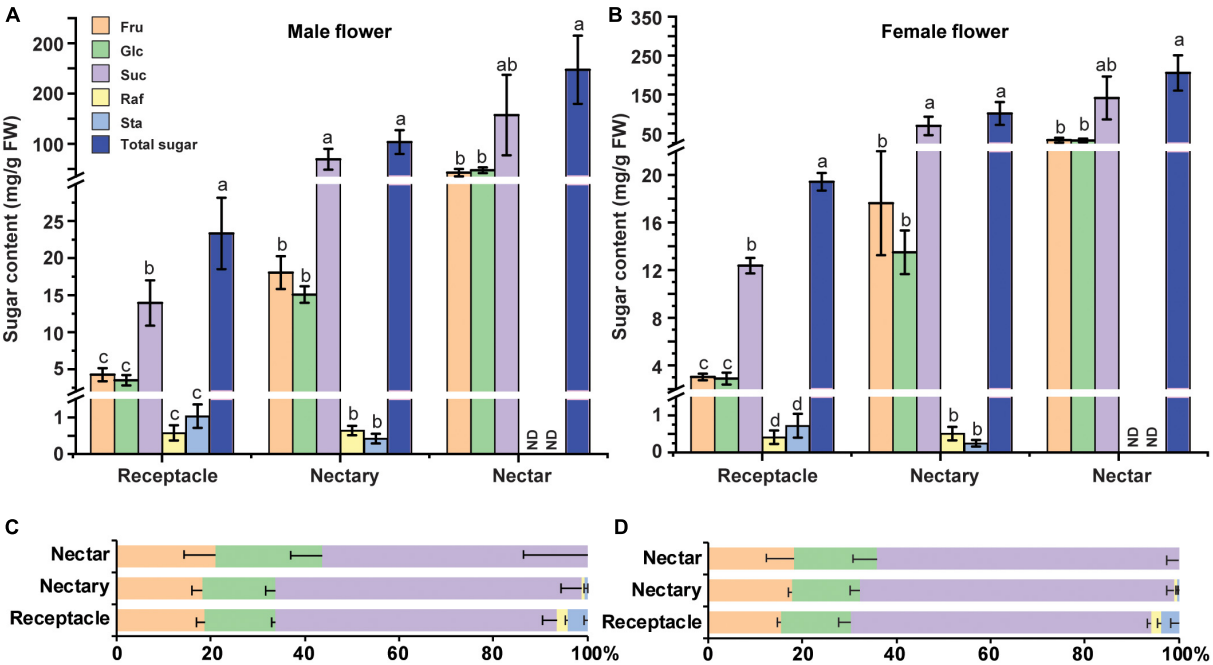

FIGURE 5 | Sugar content in male and female cucumber flowers at anthesis. Sugar content **(A,B)** and sugar distribution (%) **(C,D)** in receptacle, nectary, and nectar of male **(A,C)** and female flowers **(B,D)** at anthesis. Fru, fructose; Glc, glucose; Suc, sucrose; Raf, raffinose; Sta, stachyose; FW, fresh weight. ND, not detected. For each sample in this figure, ten flowers were collected and combined as a sample. Mean values ± SE of three independent biological replicates were shown. Statistical analyses were performed using one-way ANOVA followed by multiple comparisons using the Fisher's LSD method (*P*-value < 0.05) in each tissue.

starch accumulation before and during anthesis in cucumber flowers (from −3 DAA to 0 DAA) (**Supplementary Figure 3**). Clear starch accumulation was observed 1–3 days before anthesis (**Supplementary Figures 3A,B,D,E**) in both male and female flowers, especially in the nectary, but almost all the starch was hydrolyzed at anthesis (**Supplementary Figures 3C,F**).

Raffinose Family Oligosaccharide Metabolism Genes Are Regulated During the Anthesis Stage in the Receptacle and Nectary

Cucumber is a typical raffinose family oligosaccharide (RFO)-transporting plant, and in other words, the majority of the transporting sugar in phloem sap is stachyose and raffinose, with a small amount of sucrose. The stachyose/raffinose was first hydrolyzed by α-galactosidase to sucrose, which was further catalyzed by sucrose synthase (SUS) and/or invertase (INV) to produce hexoses, and the resulting hexoses can be exported by CsWEET7a into apoplasmic space in the cucumber fruit (Li et al., 2021). Similarly, there is only a trace amount of stachyose/raffinose in the cucumber receptacle, nectary, and nectar (**Figure 5**). Moreover, it was found that the transcript coding for many RFO/sucrose catabolism-related enzymes, such as *alkaline α-galactosidase 1* (*AGA1*), *sucrose synthase 4* (*SUS4*), *cytoplasmic invertase 1* (*CINV1*), and *cell wall invertase 4 (CWINV4)*, were highly expressed in both male and female flowers at anthesis compared with other tissues, including root, stem, and leaf (**Supplementary Figure 2**), indicating that they are most likely to be involved in active sugar hydrolysis during this period. To investigate if a similar sugar unloading strategy was undertaken at receptacle and nectary compared with that in the fruit, we further tested the expression pattern of *AGA1*, *SUS4*, *CINV1*, and *CWINV4* in receptacle and nectary at various cucumber flower developmental stages. In male (**Figures 6A,C,E,G**) and female flowers (**Figures 6B,D,F,H**), the expression levels of *AGA1*, *SUS4*, *CINV1*, and *CWINV4* peaked at anthesis in both receptacle and nectary compared with earlier developmental stages. Overall, these four sugar metabolic genes showed a similar expression pattern as *CsSWEET7a* in either receptacle or nectary of male and female flowers during anthesis (**Figure 2**), suggesting potential cooperation between sugar catabolism enzymes and sugar transporter CsSWEET7a in apoplasmic phloem unloading in cucumber receptacle and nectary.

DISCUSSION

The Significance of Apoplasmic Phloem Unloading in Flower Receptacle and Nectary at Anthesis

Plants use different unloading pathways depending on different types of sink organs, developmental stages, or changes in the environment (Milne et al., 2018; Ma et al., 2019b). Symplasmic unloading is common in meristems and in starch- or oil-storing sink organs, while apoplasmic unloading is often used in cell expansion zones and organs that accumulate soluble sugars (Oparka, 1990; Ma et al., 2019b). The use of a suitable unloading strategy can help plants save energy and adapt to environmental changes. To our knowledge, this study is the first to report that an apoplasmic phloem unloading strategy is used in the receptacle and the nectary in male and female cucumber flowers at anthesis (**Figure 1**). Compared with symplasmic unloading, which depends on both the sugar gradient (osmosis occurs along a concentration gradient) and the density of plasmodesmata, during apoplasmic unloading, sugars were exported from SE-CCs to apoplasmic space *via* an exporter, before taking up by an energy-dependent importer into phloem parenchyma cells against the concentration gradient. In flowers, a high rate of sugar import is needed during anthesis to meet the demands of pollen maturation, of nectar secretion (Borghi and Fernie, 2017), and of the increasing respiratory rate that raises the floral temperature for scent volatilization (Seymour, 1999). The soluble sugar level in male cucumber flowers increased from stage 9 to stage 11 and was maintained at the high level in stage 12 (Sun et al., 2019). If the receptacle and nectary parenchyma cells were connected to the SE/CC through a large number of plasmodesmata (symplasmic pathway), sugar might flow back symplasmically to the phloem through the connected plasmodesmata. The apoplasmic unloading mechanism seen in cucumber is common in horticultural plants, especially in the fruit (the harvestable product) where sugar can accumulate to high levels. For example, in grape berries, the phloem unloading shifts from symplasmic to apoplasmic during fruit maturation (Zhang et al., 2006). At the green fruit stage, symplasmic unloading is energy conservative. But at the mature stage, higher levels of soluble sugar accumulates in fruit to the point that the sugar content in fruit cells is higher than that in phloem sap, and sugar unloading shifts to the apoplasmic pathway (Zhang et al., 2006).

It was reported that before anthesis in squash, a species that also transports RFOs in its phloem, a massive amount of starch was stored in nectary and ready to be hydrolyzed the day before anthesis (Solhaug et al., 2019a). A similar starch accumulation pattern was observed in the cucumber nectary in our study (**Supplementary Figure 3**). Abundant starch was storied in nectary at 1–3 days before anthesis in both male and female cucumber flowers, but almost all the starch was hydrolyzed at anthesis. In *Arabidopsis*, which is a sucrose-transporting species, it might rely more on nectary starch degradation to produce nectar sugar rather than the import of phloem-derive sugars (Lin et al., 2014). But in squash, Solhaug et al. (2019a) estimated that ∼59% of the total sugar in the nectary/nectar system comes from starch, meanwhile, the imported sugar from the phloem makes up a substantial portion of total system sugar (∼41%), suggesting that phloem-derived sugar is important in nectar production at anthesis. Notably, cucumber nectary accumulates a high level of starch at pre-anthesis stages and thus maintains a constant sink status, negating a need for active apoplasmic unloading. We only carried a CF study to investigate the phloem unloading pathway at anthesis, thus the phloem unloading strategy at the early flower developmental stage in cucumber is still uncertain.

Sugar Phloem Unloading in Cucumber Flowers During Anthesis Depends on Sugar Transporters and Sugar Metabolism Enzymes

Although many SWEET transporters are expressed at anthesis (Li et al., 2017; Wang et al., 2019), their specific expression

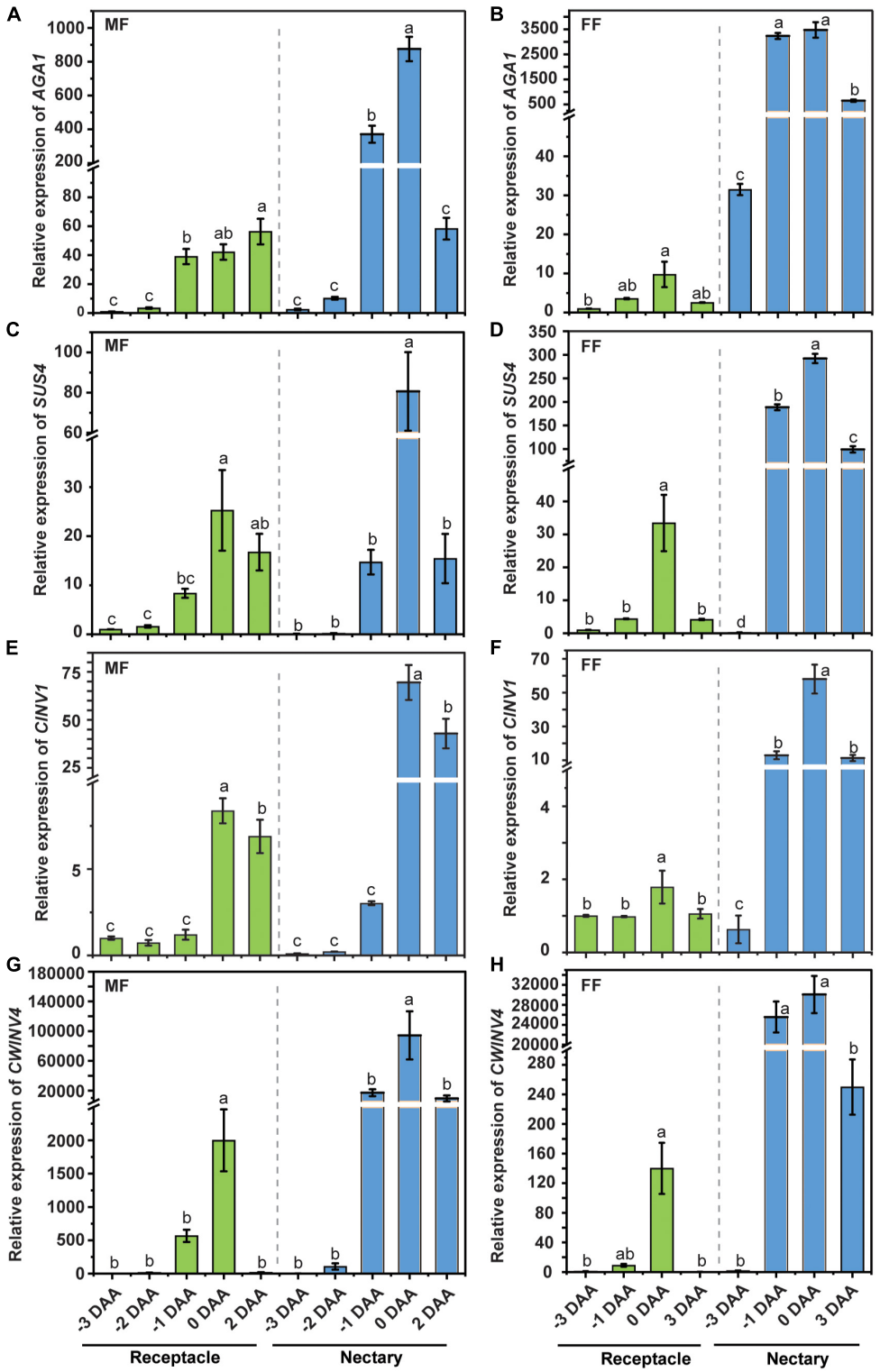

FIGURE 6 | The expression pattern of sugar metabolism enzymes in cucumber receptacle and nectary. The relative expression level of cucumber *AGA1*, *SUS4*, *CINV1*, and *CWINV4* in male **(A,C,E,G)** and female flowers **(B,D,F,H)**. DAA, days after anthesis; −3, −2, −1 DAA, being 3, 2, and 1 day(s) before anthesis, respectively; 0 DAA, the day of anthesis; and 2 and 3 DAA, being 2 and 3 days after anthesis, respectively. Mean values ± SE of three independent biological replicates were shown. Statistical analyses were performed using one-way ANOVA followed by multiple comparisons using the Fisher's LSD method (P-value < 0.05) in each tissue. Gene IDs: *AGA1* (Csa4G631570), *alkaline a-galactosidase 1*; *SUS4* (Csa5G322500), *sucrose synthase 4*; *CINV1* (Csa5G615240), *cytosol invertase 1*; *CWINV4* (Csa2G351670), *cell wall invertase 4*.

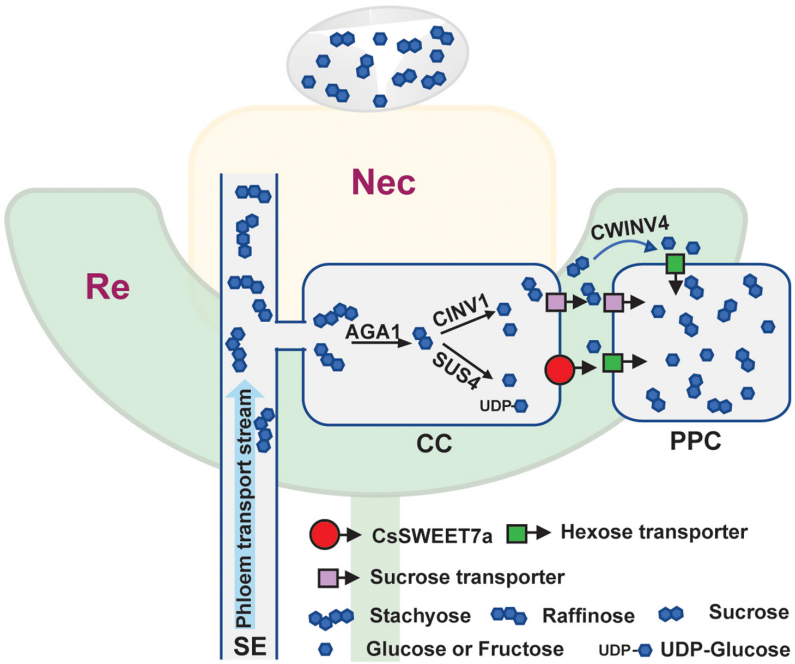

FIGURE 7 | Simplified model of CsSWEET7a function during phloem unloading in cucumber receptacle and nectary. The top light-yellow color region indicates the nectary (Nec) tissue, and the bottom light-green color region is the receptacle (Re) tissue. The droplet above the nectary represents the secreted nectar. A similar phloem unloading process is proposed in receptacle and nectary of male and female flowers. Photosynthetic sugars are transported to flower receptacles and nectary tissues *via* the phloem. As an RFOs-transporting plant, the majority of sugar in the cucumber phloem transport stream [in sieve element (SE)] is stachyose and raffinose, with a small amount of sucrose detected. The stachyose and raffinose could be broken down by α-galactosidase 1 (AGA1) to sucrose, which has three possible routes to phloem parenchyma cell (PPC): (1) sucrose is hydrolyzed by sucrose synthase 4 (SUS4) and/or cytosol invertase 1 (CINV1) to hexoses in companion cell (CC), and the resulting hexoses are exported to apoplasmic space by hexose transporter, e.g., CsSWEET7a or other SWEETs (Clade I/II which transport hexoses), before loading into PPC by hexose transporter; (2) sucrose is exported from CC to apoplasmic space by sucrose transporter, followed by hydrolyzation *via* CWINV4 to hexoses, and hexoses are taken up to PPC by hexose transporter; (3) sucrose is exported to apoplasmic space by sucrose transporter and is taken up by sucrose transporter to PPC.

pattern and functions in flowers remain unclear. In cucumber, the spatial and temporal expression analysis of *CsSWEET7a* by qRT-PCR and protein localization showed that CsSWEET7a might be involved in sugar partitioning in receptacle and nectary during anthesis. CsSWEET7a was previously reported to function as a hexose transporter in companion cells during fruit phloem unloading (Li et al., 2021). The *CsSWEET7a*-OE lines produced bigger fruit and flowers, while *CsSWEET7a*-RNAi lines had more photoassimilate trapped in the stem, resulting in smaller fruit and flowers (Li et al., 2021). In this study, CsSWEET7a protein was confirmed to be localized in the region of the phloem in the receptacle and nectary of both male and female flowers (**Figures 3**, **4**). Therefore, CsSWEET7a could serve a similar function in the receptacle and nectary for phloem unloading, as reported in cucumber fruit. However, CsSWEET1, another plasma-membrane localized hexose transporter (Li et al., 2017), and CsSWEET9, a predicted sucrose transporter, also have a relatively high expression level in flowers (**Supplementary Figure 1**). We therefore cannot exclude their role in sugar phloem unloading.

Cucumber mainly transports its sugars as RFOs, such as stachyose and raffinose, while sucrose, glucose, and fructose are primarily accumulated in cucumber young fruits (Hu et al., 2009) and flowers (**Figure 5**). Accordingly, the RFOs in the release phloem need to be broken down by AGA to sucrose. The sucrose is then hydrolyzed by SUS and/or INV to produce hexoses, which can be used for fruit development (Li et al., 2021). It suggests that cucumber sink tissues could adopt an apoplasmic phloem unloading strategy along with sugar deposition. In this study, an elevated expression of genes coding for sugar metabolism-related enzymes (**Figure 6**) as well as *CsSWEET7a* in both male and female flowers at anthesis (**Figure 2**) was observed, in support of their potential synergistic roles during RFO and sucrose hydrolyzation and phloem unloading at anthesis. Besides, a large amount of sucrose was presented in cucumber receptacle, nectary, and nectar, indicating that sucrose transporters were also required in sugar phloem unloading. It has been reported that CsSUT1 protein (sucrose transporter) is expressed in the phloem tissue in the receptacle of male cucumber flowers (Sun et al., 2019), which indicates that CsSUT1 may participate in apoplasmic unloading of sucrose in male flowers. Thus, we proposed a model (**Figure 7**) to illustrate the sugar phloem unloading strategy employed in the cucumber receptacle and nectary. The AGA1, hydrolyzes RFOs in the release phloem, and the resulting sucrose is

broken-down to hexoses by SUS4 and/or by cytoplasmic invertase CINV1. CsSWEET7a may function in companion cells to export hexoses to apoplasmic space, where hexoses can be taken up by other hexose transporters into phloem parenchyma cells. Sucrose transporters (e.g., SUTs and Clade III SWEETs that transport sucrose) and CWINV4 may also be involved in the phloem unloading process as shown in **Figure 7**.

CONCLUSION

We have provided evidence that sugar phloem unloading is symplasmically isolated in both receptacle and nectary of male and female cucumber flowers at anthesis, and the phloem-localized sugar transporter CsSWEET7a is most likely involved in this apoplasmic phloem unloading. A series of sugar metabolism enzymes including cucumber AGA1, SUS4, CINV1, and CWINV4 may have played a synergistic role in nectary and receptacle during this phloem unloading process. Our findings will provide valuable insights into the sugar partitioning strategy employed by plants to supply carbohydrates for flower anthesis and nectar secretion to reward pollinators.

DATA AVAILABILITY STATEMENT

The original contributions presented in the study are included in the article/**Supplementary Material**, further inquiries can be directed to the corresponding author.

AUTHOR CONTRIBUTIONS

XS and YL conceived the project and designed the experiments. YL, HL, and XY performed most of the experiments and analyzed the data. LS provided technical assistance to YL. YL and XS wrote the manuscript. XS agreed to serve as the author responsible for contact and ensures communication. All authors contributed to the manuscript and approved the submitted version.

FUNDING

This work was supported by the National Key Research and Development Program of China (2019YFD1000300), the National Natural Science Foundation of China (31972398), the Beijing Innovation Consortium of Agriculture Research System (BAIC01), and the China Agriculture Research System of MOF and MARA.

ACKNOWLEDGMENTS

We thank Anita K. Snyder for editing this manuscript.

SUPPLEMENTARY MATERIAL

The Supplementary Material for this article can be found online at: https://www.frontiersin.org/articles/10.3389/fpls.2021.758526/full#supplementary-material

Supplementary Figure 1 | Expression patterns of the *SWEET* gene family in cucumber flowers. **(A)** The expression pattern of the cucumber *SWEET* gene family in male (MF) and female flowers (FF). Data used in panel **(A)** came from RNA-seq data (PRJNA80169) in the cucumber database. **(B)** The relative expression level of *CsSWEET7a* from stage 9 to anthesis in male flowers. Mean values ± SE of three independent biological replicates were given. RPKM, Reads Per Kilobase per Million mapped reads.

Supplementary Figure 2 | Expression pattern of genes coding for sugar metabolism-related enzymes in cucumber. Relative expression pattern of *AGA1* **(A)**, *SUS4* **(B)**, *CINV1* **(C)**, and *CWINV4* **(D)** in root, stem, leaf, male flower, female flower, and ovary at anthesis. *AGA1* (Csa4G631570), *alkaline a-galactosidase 1*; *SUS4* (Csa5G322500), *sucrose synthase 4*; *CINV1* (Csa5G615240), *cytosol invertase 1*; *CWINV4* (Csa2G351670), *cell wall invertase 4*. Mean values ± SD of three replicates were shown. Statistical analyses were performed using one-way ANOVA followed by multiple comparisons using Fisher's LSD method (P-value < 0.05).

Supplementary Figure 3 | Starch staining in nectary of male and female cucumber flowers. Different developmental stages of male **(A–C)** and female flowers **(D–F)**. **(A,D)** is 3 days before anthesis, **(B,E)** is 1 day before anthesis, and **(C,F)** is at the day of anthesis. The white arrows in panels **(D–F)** indicate nectary. DAA, days after anthesis; MF, male flower; FF, female flower; Nec, nectary.

Supplementary Table 1 | Primers used in this study.

REFERENCES

Bai, S.-L., Peng, Y.-B., Cui, J.-X., Gu, H.-T., Xu, L.-Y., Li, Y.-Q., et al. (2004). Developmental analyses reveal early arrests of the spore-bearing parts of reproductive organs in unisexual flowers of cucumber (*Cucumis sativus* L.). *Planta* 220, 230–240. doi: 10.1007/s00425-004-1342-2

Borghi, M., and Fernie, A. R. (2017). Floral metabolism of sugars and amino acids: implications for pollinators' preferences and seed and fruit set. *Plant Physiol.* 175, 1510–1524. doi: 10.1104/pp.17.01164

Büttner, M. (2010). The Arabidopsis sugar transporter (AtSTP) family: an update. *Plant Biol.* 12, 35–41. doi: 10.1111/j.1438-8677.2010.00383.x

Chen, L.-Q., Cheung, L. S., Feng, L., Tanner, W., and Frommer, W. B. (2015a). Transport of sugars. *Annu. Rev. Biochem.* 84, 865–894. doi: 10.1146/annurev-biochem-060614-033904

Chen, L.-Q., Lin, I. W., Qu, X.-Q., Sosso, D., McFarlane, H. E., Londoño, A., et al. (2015b). A cascade of sequentially expressed sucrose transporters in the seed coat and endosperm provides nutrition for the Arabidopsis embryo. *Plant Cell* 27, 607–619. doi: 10.1105/tpc.114.134585

Collison, C. H., and Martin, E. C. (1975). A scanning electron microscope study of cucumber nectaries. *Cucumis Sativus. J. Apic. Res.* 14, 79–84. doi: 10.1080/00218839.1975.11099807

Frey-Wyssling, A. (1955). The phloem supply to the nectaries. *Acta Bot. Neerlandica* 4, 358–369. doi: 10.1111/j.1438-8677.1955.tb00337.x

Ge, Y.-X., Angenent, G. C., Wittich, P. E., Peters, J., Franken, J., Busscher, M., et al. (2000). NEC1, a novel gene, highly expressed in nectary tissue of *Petunia hybrida*. *Plant J.* 24, 725–734. doi: 10.1111/j.1365-313X.2000.00926.x

Gu, H.-T., Wang, D.-H., Li, X., He, C.-X., Xu, Z.-H., and Bai, S.-N. (2011). Characterization of an ethylene-inducible, calcium-dependent nuclease that is differentially expressed in cucumber flower development. *New Phytol.* 192, 590–600. doi: 10.1111/j.1469-8137.2011.03825.x

Guan, Y.-F., Huang, X.-Y., Zhu, J., Gao, J.-F., Zhang, H.-X., and Yang, Z.-N. (2008). RUPTURED POLLEN GRAIN1, a member of the MtN3/saliva gene

family, is crucial for exine pattern formation and cell integrity of microspores in Arabidopsis. *Plant Physiol.* 147, 852–863. doi: 10.1104/pp.108.118026

Haupt, S., Duncan, G. H., Holzberg, S., and Oparka, K. J. (2001). Evidence for symplastic phloem unloading in sink leaves of Barley. *Plant Physiol.* 125, 209–218.

Hu, L., Sun, H., Li, R., Zhang, L., Wang, S., Sui, X., et al. (2011). Phloem unloading follows an extensive apoplasmic pathway in cucumber (*Cucumis sativus* L.) fruit from anthesis to marketable maturing stage. *Plant Cell Environ.* 34, 1835–1848. doi: 10.1111/j.1365-3040.2011.02380.x

Hu, L.-P., Meng, F.-Z., Wang, S.-H., Sui, X.-L., Li, W., Wei, Y.-X., et al. (2009). Changes in carbohydrate levels and their metabolic enzymes in leaves, phloem sap and mesocarp during cucumber (*Cucumis sativus* L.) fruit development. *Sci. Hortic.* 121, 131–137. doi: 10.1016/j.scienta.2009.01.023

Imlau, A., Truernit, E., and Sauer, N. (1999). Cell-to-cell and long-distance trafficking of the green fluorescent protein in the phloem and symplastic unloading of the protein into sink tissues. *Plant Cell* 11, 309–322.

Jensen, K. H. (2018). Phloem physics: mechanisms, constraints, and perspectives. *Curr. Opin. Plant Biol.* 43, 96–100. doi: 10.1016/j.pbi.2018.03.005

Li, Y., Feng, S., Ma, S., Sui, X., and Zhang, Z. (2017). Spatiotemporal expression and substrate specificity analysis of the cucumber SWEET gene family. *Front. Plant Sci.* 2017:1855. doi: 10.3389/fpls.2017.01855

Li, Y., Liu, H., Yao, X., Wang, J., Feng, S., Sun, L., et al. (2021). Hexose transporter CsSWEET7a in cucumber mediates phloem unloading in companion cells for fruit development. *Plant Physiol.* 186, 640–654. doi: 10.1093/plphys/kiab046

Lin, I. W., Sosso, D., Chen, L.-Q., Gase, K., Kim, S.-G., Kessler, D., et al. (2014). Nectar secretion requires sucrose phosphate synthases and the sugar transporter SWEET9. *Nature* 508, 546–549. doi: 10.1038/nature13082

Livak, K. J., and Schmittgen, T. D. (2001). Analysis of relative gene expression data using real-time quantitative PCR and the $2^{-\Delta\Delta CT}$ method. *Methods* 25, 402–408. doi: 10.1006/meth.2001.1262

Ma, S., Li, Y., Li, X., Sui, X., and Zhang, Z. (2019a). Phloem unloading strategies and mechanisms in crop fruits. *J. Plant Growth Regul.* 38, 494–500. doi: 10.1007/s00344-018-9864-1

Ma, S., Sun, L., Sui, X., Li, Y., Chang, Y., Fan, J., et al. (2019b). Phloem loading in cucumber: combined symplastic and apoplastic strategies. *Plant J.* 98, 391–404. doi: 10.1111/tpj.14224

Milne, R. J., Grof, C. P., and Patrick, J. W. (2018). Mechanisms of phloem unloading: shaped by cellular pathways, their conductances and sink function. *Curr. Opin. Plant Biol.* 43, 8–15. doi: 10.1016/j.pbi.2017.11.003

Müller, G. L., Drincovich, M. F., Andreo, C. S., and Lara, M. V. (2010). Role of photosynthesis and analysis of key enzymes involved in primary metabolism throughout the lifespan of the tobacco flower. *J. Exp. Bot.* 61, 3675–3688. doi: 10.1093/jxb/erq187

Oparka, K. J. (1990). What is phloem unloading? *Plant Physiol.* 94, 393–396.

Palmer, W. M., Ru, L., Jin, Y., Patrick, J. W., and Ruan, Y.-L. (2015). Tomato ovary-to-fruit transition is characterized by a spatial shift of mRNAs for cell wall invertase and its inhibitor with the encoded proteins localized to sieve elements. *Mol. Plant* 8, 315–328. doi: 10.1016/j.molp.2014.12.019

Roy, R., Schmitt, A. J., Thomas, J. B., and Carter, C. J. (2017). Review: Nectar biology: From molecules to ecosystems. *Plant Sci.* 262, 148–164. doi: 10.1016/j.plantsci.2017.04.012

Seymour, R. S. (1999). Pattern of respiration by intact inflorescences of the thermogenic arum lily *Philodendron selloum*. *J. Exp. Bot.* 50, 845–852. doi: 10.1093/jxb/50.335.845

Solhaug, E. M., Johnson, E., and Carter, C. J. (2019a). Carbohydrate metabolism and signaling in squash nectaries and nectar throughout floral maturation. *Plant Physiol.* 180, 1930–1946. doi: 10.1104/pp.19.00470

Solhaug, E. M., Roy, R., Chatt, E. C., Klinkenberg, P. M., Mohd-Fadzil, N.-A., Hampton, M., et al. (2019b). An integrated transcriptomics and metabolomics analysis of the *Cucurbita pepo* nectary implicates key modules of primary metabolism involved in nectar synthesis and secretion. *Plant Direct* 3:e00120. doi: 10.1002/pld3.120

Sui, X., Nie, J., Li, X., Scanlon, M. J., Zhang, C., Zheng, Y., et al. (2018). Transcriptomic and functional analysis of cucumber (*Cucumis sativus* L.) fruit phloem during early development. *Plant J.* 96, 982–996. doi: 10.1111/tpj.14084

Sun, L., Sui, X., Lucas, W. J., Li, Y., Feng, S., Ma, S., et al. (2019). Down-regulation of the sucrose transporter *CsSUT1* causes male sterility by altering carbohydrate supply. *Plant Physiol.* 180, 986–997. doi: 10.1104/pp.19.00317

Sun, M.-X., Huang, X.-Y., Yang, J., Guan, Y.-F., and Yang, Z.-N. (2013). Arabidopsis RPG1 is important for primexine deposition and functions redundantly with RPG2 for plant fertility at the late reproductive stage. *Plant Reprod.* 26, 83–91. doi: 10.1007/s00497-012-0208-1

Viola, R., Roberts, A. G., Haupt, S., Gazzani, S., Hancock, R. D., Marmiroli, N., et al. (2001). Tuberization in potato involves a switch from Apoplastic to symplastic phloem unloading. *Plant Cell* 13, 385–398.

Wang, H., Sui, X., Guo, J., Wang, Z., Cheng, J., Ma, S., et al. (2014). Antisense suppression of cucumber (*Cucumis sativus* L.) sucrose synthase 3 (*CsSUS3*) reduces hypoxic stress tolerance. *Plant Cell Environ.* 37, 795–810. doi: 10.1111/pce.12200

Wang, P., Wei, P., Niu, F., Liu, X., Zhang, H., Lyu, M., et al. (2019). Cloning and functional assessments of floral-expressed SWEET transporter genes from *Jasminum sambac*. *Int. J. Mol. Sci.* 20:E4001. doi: 10.3390/ijms20164001

Zhang, C., and Turgeon, R. (2018). Mechanisms of phloem loading. *Curr. Opin. Plant Biol.* 43, 71–75. doi: 10.1016/j.pbi.2018.01.009

Zhang, X.-Y., Wang, X.-L., Wang, X.-F., Xia, G.-H., Pan, Q.-H., Fan, R.-C., et al. (2006). A shift of phloem unloading from symplasmic to apoplasmic pathway is involved in developmental onset of ripening in grape berry. *Plant Physiol.* 142, 220–232. doi: 10.1104/pp.106.081430

Conflict of Interest: The authors declare that the research was conducted in the absence of any commercial or financial relationships that could be construed as a potential conflict of interest.

Publisher's Note: All claims expressed in this article are solely those of the authors and do not necessarily represent those of their affiliated organizations, or those of the publisher, the editors and the reviewers. Any product that may be evaluated in this article, or claim that may be made by its manufacturer, is not guaranteed or endorsed by the publisher.

frontiers in Plant Science

MINI REVIEW
published: 11 February 2022
doi: 10.3389/fpls.2022.774060

How Stress Affects Your Budget—Stress Impacts on Starch Metabolism

*Camila Ribeiro[1], Mark Stitt[2] and Carlos Takeshi Hotta[3]**

[1] Centro de Tecnologia Canavieira SA, Piracicaba, Brazil, [2] Max Planck Institute for Molecular Plant Physiology, Potsdam, Germany, [3] Departamento de Bioquímica, Instituto de Química, Universidade de São Paulo, São Paulo, Brazil

Starch is a polysaccharide that is stored to be used in different timescales. Transitory starch is used during nighttime when photosynthesis is unavailable. Long-term starch is stored to support vegetative or reproductive growth, reproduction, or stress responses. Starch is not just a reserve of energy for most plants but also has many other roles, such as promoting rapid stomatal opening, making osmoprotectants, cryoprotectants, scavengers of free radicals and signals, and reverting embolised vessels. Biotic and abiotic stress vary according to their nature, strength, duration, developmental stage of the plant, time of the day, and how gradually they develop. The impact of stress on starch metabolism depends on many factors: how the stress impacts the rate of photosynthesis, the affected organs, how the stress impacts carbon allocation, and the energy requirements involved in response to stress. Under abiotic stresses, starch degradation is usually activated, but starch accumulation may also be observed when growth is inhibited more than photosynthesis. Under biotic stresses, starch is usually accumulated, but the molecular mechanisms involved are largely unknown. In this mini-review, we explore what has been learned about starch metabolism and plant stress responses and discuss the current obstacles to fully understanding their interactions.

Keywords: abiotic stress, biotic stress, starch, circadian clock, starch metabolism

OPEN ACCESS

Edited by:
Diana Santelia, ETH Zürich, Switzerland

Reviewed by:
Francisco Perez-Alfocea, Center for Edaphology and Applied Biology of Segura, Spanish National Research Council (CSIC), Spain
Roslyn Gleadow, Monash University, Australia

****Correspondence:***
Carlos Takeshi Hotta
hotta@iq.usp.br

Specialty section:
This article was submitted to Plant Metabolism and Chemodiversity, a section of the journal Frontiers in Plant Science

Received: *10 September 2021*
Accepted: *12 January 2022*
Published: *11 February 2022*

Citation:
Ribeiro C, Stitt M and Hotta CT (2022) How Stress Affects Your Budget—Stress Impacts on Starch Metabolism. Front. Plant Sci. 13:774060. doi: 10.3389/fpls.2022.774060

INTRODUCTION

Energy management is vital for plant development, and it is diversely regulated across species depending on life forms and environmental conditions. Photosynthetic reactions in leaves generate carbohydrates that can be immediately utilised as an energy source. However, part of the photosynthetic products in most plants will be stored as transitory starch during the daytime (**Figure 1A**; Stitt and Zeeman, 2012; Smith and Zeeman, 2020). During the nighttime, the starch is broken down (**Figure 1B**) to provide a source of carbon for continued sucrose synthesis and export and respiration, thus fueling the synthesis of protein and other cellular components, growth and development throughout the whole 24-h cycle (**Figure 2**; O'Leary et al., 2017; Smith and Zeeman, 2020). The rate of degradation during the nighttime is regulated so that starch is almost depleted at dawn when photosynthesis resumes and a new cycle begins (Smith and Stitt, 2007; Graf et al., 2010). The circadian rhythm highly regulates this carbon management process.

More generally, starch acts as a sugar source when photosynthesis is impaired or unavailable, not only in the nighttime but also during seed germination, tuber sprouting, tissue regeneration,

or under stress conditions (MacNeill et al., 2017; Smith and Zeeman, 2020). Starch can also have specialised roles: e.g., in the guard cells, starch can be degraded during the daytime to promote rapid stomatal opening (Valerio et al., 2011; Flütsch et al., 2020). Accordingly, starch can be stored to be used as a reserve in different timescales. Usually, transitory starch is synthesised and degraded within a day. In contrast, long-term starch is stored, often outside the source organ, to support vegetative or reproductive growth, reproduction, or stress responses (MacNeill et al., 2017).

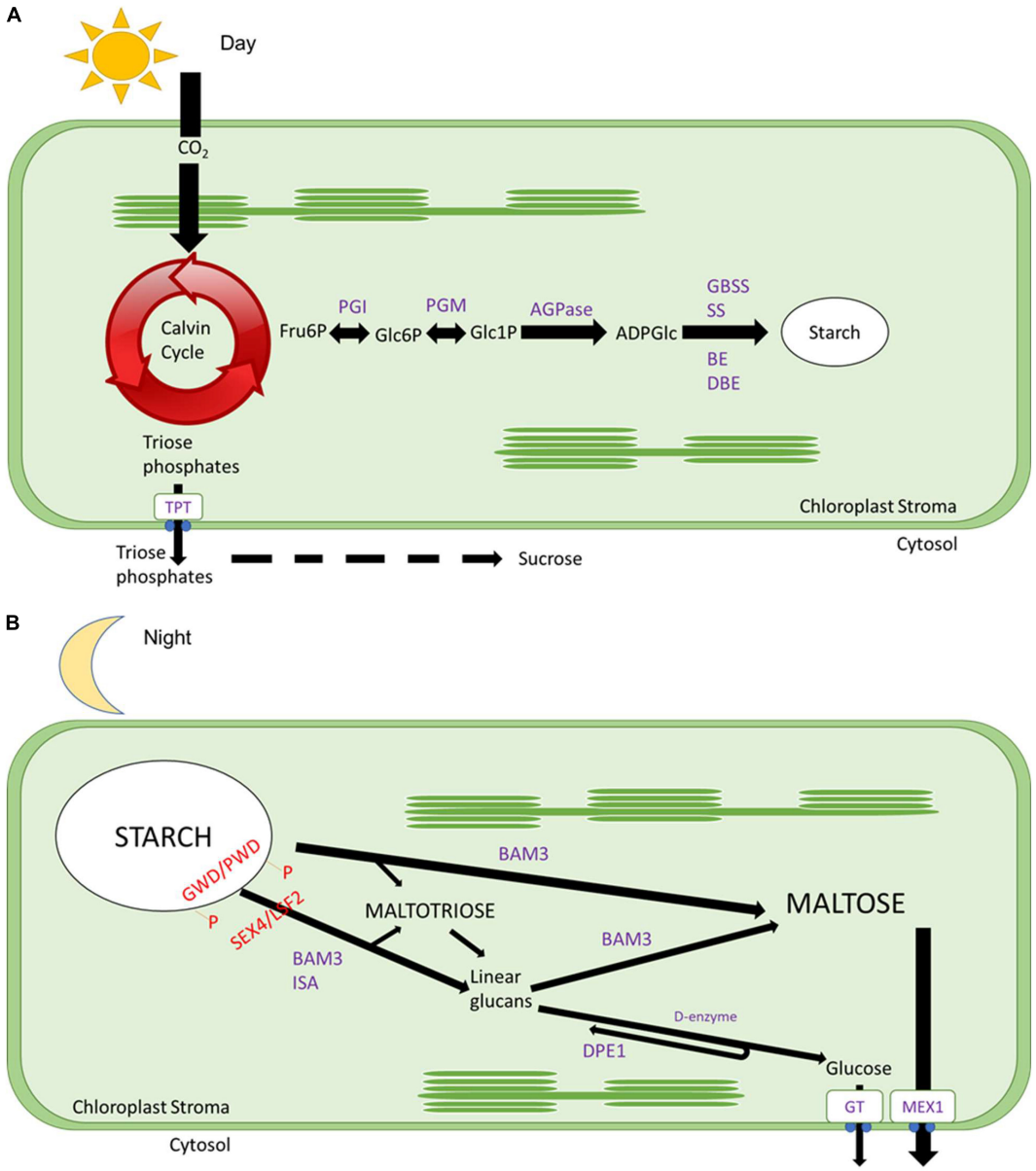

FIGURE 1 | Daily starch metabolism. **(A)** During the day, CO_2 is fixed by the Calvin cycle, and trioses phosphates will be exported out of the chloroplast to the cytosol through a triose phosphate transporter protein to be converted into sucrose. While fructose 6-phosphate will be converted into glucose 6-phosphate by phosphoglucose isomerase (PGI), then converted to glucose 1-phosphate by phosphoglucomutase (PGM), later converted to ADP glucose by ADP glucose pyrophosphorylase (AGPase), after polymerised by starch synthases (SS) and granule bound starch synthases (GBSS) and branched by branching enzymes (BE) and debranching enzymes (DBE). **(B)** During the night, the surface of the starch granule is loosed by glucan phosphorylation catalysed by glucan water dikinases (GWD), and phosphoglucan water dikinases (PDW) followed by the action of β-amylases (BAMs, especially BAM3 with a subsidiary role for BAM1, see Smith and Zeeman, 2020) and isoamylase 3 (ISA3). Starch breakdown results in the formation of maltose and maltotriose. Maltotriose is converted by disproportionation enzyme 1 (DPE1) to glucose and longer glucans that can be degraded to maltose by β-amylases. The action of BAM3, ISA3, and PDE1 requires removal of phosphate by the glucan phosphatases starch excess 4 (SEX4) and Like Sex Four 2 (LSF2). Glucose is exported to the cytosol by glucose transporter (GT), and maltose is exported out by a maltose exporter 1 (MEX) to be utilised as an energy source for nighttime reactions.

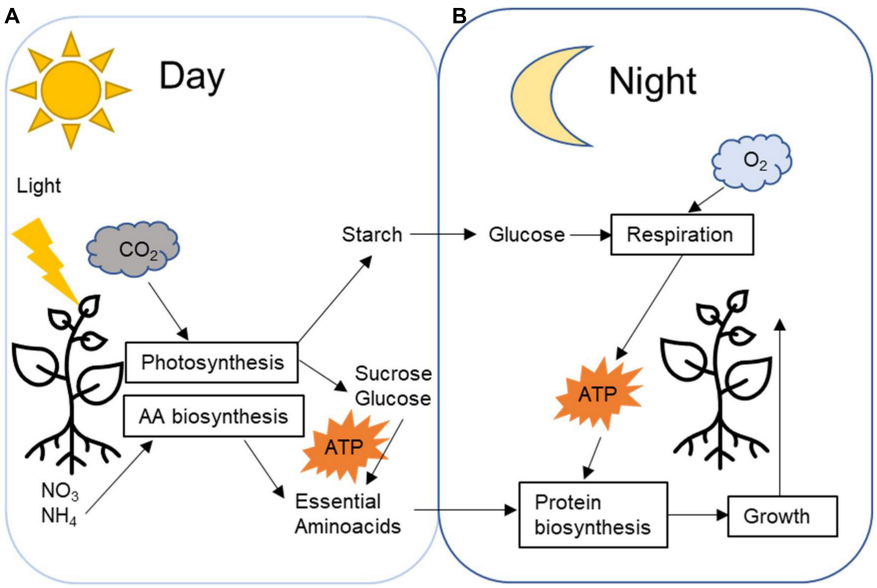

FIGURE 2 | Plant daily transitory starch carbon management processes. **(A)** During the day, CO_2 is fixed by the Calvin cycle generating sugar that will be promptly utilised as an energy source for day metabolism, such as nitrite and nitrate fixation and amino acids biosynthesis. Part of the fixed carbon is temporarily stored in the plastids as starch. **(B)** During the night, starch is broken down into glucose that respiration will generate energy for nighttime metabolism reactions, such as protein biosynthesis and plant growth.

Stress can affect carbon metabolism by affecting photosynthetic rate, carbon allocation, and night respiration. These impacts can reduce plant growth and development depending on the type of stress and affected tissue. Studies related to the effects of stress on starch metabolism have faced significant challenges because the response depends on the nature, strength and duration of the stress, how gradually it develops, and plant developmental stage and the time of the day and (Köhl, 2016). In addition, experiments on stress responses are usually not standardised, making it difficult to compare different studies. Furthermore, as transitory starch is in constant flux, experiments that measure starch at only one or a few time points may not capture complex responses on the diel rhythms. Finally, it is now clear that other degradation pathways can operate under stress conditions in the light in addition to the daily nocturnal degradation pathway.

STARCH METABOLISM AND ABIOTIC STRESS

Changes in the plant starch metabolism due to abiotic stress depend on how the stress affects growth, the relative extent of the inhibition of growth and photosynthesis, and whether modifications in C allocation support stress responses. Each of these factors depends on the type of the stress, its intensity and duration. Early stress responses require resources to provide energy and support the synthesis of new molecules to protect, restore, and acclimate the plant. As photosynthesis is frequently impaired by stress, an important role is played by carbon reallocated from starch, avoiding a significant reorganisation of metabolism (Hummel et al., 2010). Starch synthesis is decreased in water and temperature stress, mainly due to stomatal closing and lower rates of photosynthesis (Zrenner and Stitt, 1991; Thitisaksakul et al., 2012). However, there are also situations in which the stress arrests growth without affecting photosynthesis, leading to an overall increase in starch reserves (Hummel et al., 2010; de Morais et al., 2019).

As recently reviewed, transitory starch content is usually observed to decline in leaves in response to salt, drought, and cold stress (Thalmann and Santelia, 2017; Dong and Beckles, 2019), consistent with the idea that starch is synthesised at lower rates and/or is broken down more rapidly to redirect carbon for stress responses. An example of the increased degradation under stress is the stimulation of starch breakdown even under mild drought (Zrenner and Stitt, 1991) and by low temperature (Kaplan and Guy, 2004). Together, this allows carbon to be reallocated to make osmoprotectants or cryoprotectants that promote osmotic adjustment and stabilise proteins (Kempa et al., 2008; Krasensky and Jonak, 2012; Tarkowski and Van den Ende, 2015; Zanella et al., 2016); scavengers of free radicals (Couée et al., 2006; Keunen et al., 2013); and signals that refine stress responses (Rolland et al., 2006; Rook et al., 2006).

Starch degradation in response to stress may use different combinations of enzymes, while nighttime degradation uses mainly BAM3 and ISA3. Under water, stress amylase 3 (AMY3) and BAM1 are induced (Thalmann and Santelia, 2017). BAM1 can be upregulated by temperature, osmotic and salinity stress in leaf guard cells and roots (Kaplan and Guy, 2004, 2005; Kempa et al., 2008; Valerio et al., 2011). BAM1 protein is regulated by reduced thioredoxins, which are light-dependent, possibly counteracting starch synthesis during the daytime

(Valerio et al., 2011; Zanella et al., 2016). BAM1 and α-amylase 3 (AMY3) promote daytime starch degradation to support proline biosynthesis in mesophyll cells under osmotic stress (Zanella et al., 2016). In guard-cells, BAM1-dependent starch degradation promotes stomatal opening in diel rhythms in response to osmotic stress (Valerio et al., 2011).

In some experiments, plants accumulated starch in response to stress (Thalmann and Santelia, 2017). This apparent contradiction is associated with the level of stress and timing of the measurements. For example, in early stress, starch degradation may predominate as C is mobilised to support for adaptive responses; in mild drought and salt stress-responses, starch may accumulate because growth is inhibited, but photosynthesis not is proportionately affected (Hummel et al., 2010; de Morais et al., 2019). While in severe stress, such as high temperatures associated with drought during grain filling, starch degradation may predominate because carbon assimilation is heavily affected due to stomata closure or damage to the photosystems (Bahuguna et al., 2017; Dong and Beckles, 2019). As an alternative, starch accumulation under salt stress has been suggested to play a role in capturing Na^+ in its granules (Kanai et al., 2005).

The hormone abscisic acid (ABA) promotes stomatal closure under water, temperature, and osmotic stresses, lowering the internal leaf CO_2 and inhibiting photosynthesis. However, in these conditions, starch degradation in the light allows maintenance of Calvin-Benson Cycle metabolite levels and, hence, rapid flux in the Calvin-Benson cycle to generate RuBP that supports rapid oxygenation of RuBP and photorespiration (Weise et al., 2006; Sharkey, 2019; Stitt et al., 2021). Photorespiration can aid energy dissipation under stress by regenerating ADP and NADP, avoiding ROS formation and overreduction of the chloroplastidal electron transport chain, which results in photoinhibition (Kozaki and Takeba, 1996; Timm et al., 2019; Timm and Hagemann, 2020).

Starch can also be stored outside source organs as a reserve to be used in a situation of longer-term low carbon assimilation. Reproductive organs seeds or tubers can accumulate large amounts of starch to support the growth of the next generation. However, starch is often accumulated outside source leaves during vegetative growth and can play an essential role in stress responses. A noteworthy example is starch reserves in the woody tissues of the trees, in the xylem-ray parenchyma cells (Noronha et al., 2018). While little is known about the genes involved in the synthesis and degradation of starch in these tissues, starch reserves are pivotal for cold tolerance in the winter and budding in the spring (Sauter, 1988; Witt and Sauter, 1994; Noronha et al., 2018). Embolised conduits can be refilled at nighttime, but this requires much energy and solutes, provided from starch degradation, especially when the soil is dry and photosynthesis is inhibited (Zwieniecki and Holbrook, 2009). As drought stress can lead to hydraulic failure due to cavitation and conduit embolism, starch has a significant role in preventing tree deaths (McDowell et al., 2011).

Long term starch can also be stored in source organs. In *Zea mays* L. (maize, Poaceae), unlike the starch in mature zones of the leaves, starch levels in the growth zones are kept high at nighttime (Czedik-Eysenberg et al., 2016). This starch can be used to support leaf growth in the first hours when nighttime is extended, showing that this is a mechanism to buffer against stresses that limit carbon assimilation (Czedik-Eysenberg et al., 2016).

During the late reproductive phase, plants under stress may use vegetative starch reserves to guarantee the complete development of their seeds (Trouverie et al., 2006; Cuellar-Ortiz et al., 2008). In grain crops, reallocation of carbon in response to abiotic stress can also lead to grain abortion and a decrease in grain starch (Andersen et al., 2002; Mangelsen et al., 2011). The regulation of starch synthesis in seeds may differ from that in leaves. For example, AGPase stability is drastically reduced by high temperature in maize and *Hordeum vulgare* L. (barley, Poaceae), reducing grain starch (Singletary et al., 1994; Wallwork et al., 1998; Linebarger et al., 2005). In *Triticum aestivum* L. (wheat, Poaceae) and *Oryza sativa* L. (rice, Poaceae), high temperatures reduced the transcript levels of several starch synthesis genes, which are correlated with a reduction in seed size (Hurkman et al., 2003; Yamakawa and Hakata, 2010). Thus, changes in starch metabolism due to abiotic stress can also affect the quality and productivity of crops.

STARCH METABOLISM AND BIOTIC STRESS

Biotic stress can also impact starch metabolism. In contrast to most abiotic stresses, starch is accumulated, often characterised as a symptom of pathogen infection. Abnormal starch accumulation has been described in different types of plant-pathogen responses, such as *Puccinia hordei* Otth. (brown rust, Basidiomycota) infecting barley (Scholes and Farrar, 1987), *Plasmopara viticola* (Berk. and M.A. Curtis) Berl and De Toni (downy mildew, Oomycota) infecting *Vitis vinifera* L. (grapevine, Vitaceae) (Gamm et al., 2011), *Plasmodiophora brassicae* Woronin (clubroot disease, Cercozoa) infecting Brassicaceae (Ludwig-Müller and Schuller, 2008), as well as tobacco mosaic virus (mottled browning) in *Nicotiana tabaccum* L. (tobacco, Solanaceae) (Allan et al., 2001; Zhao et al., 2016).

Starch accumulation due to biotic stress has been explored in detail in *Citrus* spp. L. (Rutaceae) infected with *Candidatus* Liberibacter, which causes citrus greening or Huanglongbing (HLB), due to the economic impact of this disease in worldwide orange production (Etxeberria et al., 2009; Fan et al., 2010; Gonzalez et al., 2011). HLB is known to cause abnormal callose accumulation in citrus phloem tissues impairing source to sink flux, leading to decreased fruit production and eventually tree decay (Koh et al., 2012; Wang et al., 2017; Achor et al., 2020). Different starch biosynthetic genes were upregulated in response to HLB in leaves, such as starch synthases, granule bound starch synthase, and ADP-glucose pyrophosphorylase (Albrecht and Bowman, 2008; Martinelli et al., 2012; Mafra et al., 2013). Excessive starch accumulation in the chloroplasts is hypothesised to damage them and restrict CO_2 diffusion (Lemoine et al., 2013). It has also been proposed that excessive starch accumulation is due to the stimulated entry of carbon from the cytosol via a plastid envelope glucose-6-phosphate transporter protein

(Martinelli et al., 2012). The putative crucial role of this transport protein is supported by the lack of regulation of this gene in symptomatic fruits, where starch is not accumulated (Martinelli et al., 2012, 2013; Martinelli and Dandekar, 2017).

Curiously, HLB is associated with the induction of starch biosynthesis proteins and with the induction of α-amylase, β-amylase, and phosphoglucan dikinase in leaves (Albrecht and Bowman, 2008; Martinelli et al., 2013; Balan et al., 2018). In healthy plants, these enzymes are commonly expressed at nighttime (Graf and Smith, 2011; Lloyd and Kötting, 2016) but can be expressed more strongly to generate soluble sugars in response to stress (Doyle et al., 2007). In contrast, when quantifying sugars, an increase in maltose was identified in symptomatic leaves, with a decreased expression of MEX1 (Fan et al., 2010). Therefore, it is difficult to formulate a clear account of how HLB affects the daily rhythms of leaf starch without a full time course.

Transient expression of the truncated effector of LasΔ5315 bacteria in *Nicotiana benthamiana* Domin (Solanaceae) resulted in excessive starch accumulation and overexpression of genes related to the starch synthesis (Pitino et al., 2018). Likewise, fungal volatiles emitted by *Alternaria alternata* (Fr.) Keissl. (leaf spot, Ascomycota) induce abnormal starch accumulation in *Arabidopsis thaliana* (L.) Heynh. (Brassicaceae) and *Solanum tuberosum* L. (potato, Solanaceae) (Ezquer et al., 2010; Li et al., 2011), that is linked with induction of potato SS classes III and IV, and plastidial changes in redox status of plastidial enzymes mediated by NADP-thioredoxin reductase (Ezquer et al., 2010; Li et al., 2011).

CIRCADIAN RHYTHMS AND STRESS RESPONSES

Starch levels and gene expression are often analysed only once a day, and the actual time of day is rarely specified, with few exceptions (Quick et al., 1992; Thalmann et al., 2016). However, starch metabolism and plant stress responses typically underly rhythms with a period close to 24 h. Many related biological processes, such as photosynthesis, resistance to abiotic and biotic stresses, floral induction by photoperiodism, petal movement and floral fragrance exhibit circadian rhythms. Further, it is known that disorders in circadian function reduce plant growth and function (Dodd et al., 2005; McClung, 2019).

The circadian clock synchronises endogenous events with environmental rhythms, including responses to stress. For example, in gating, the same environmental signal may lead to different responses at different times of the day (Hotta et al., 2007; Seo and Mas, 2015). A study in Arabidopsis found 33 genes differentially expressed in dry conditions at midday, but 508 genes differentially expressed at the end of the light period, just 6 h later (Wilkins et al., 2010). In turn, responses to stress can also regulate the circadian oscillator. ABA may be part of a small regulatory loop, as the central oscillator component LATE ELONGATED HYPOCOTYL (LHY) regulates ABA biosynthesis (Adams et al., 2018), while ABA upregulates another central oscillator component, TIMING OF CAB EXPRESSION 1 (TOC1), in a clock-controlled manner (Legnaioli et al., 2009). The expression of the central oscillator *COMPONENT CIRCADIAN CLOCK ASSOCIATED 1* (*CCA1*) is affected by induction with the flg22 peptide and *P. syringae* infection, while *LHY* and *TOC1* show salicylic acid-induced increased gene expression (Lai et al., 2012; Zhang et al., 2013).

The circadian clock also regulates starch metabolism (Lu et al., 2005; Mugford et al., 2014; Seki et al., 2017; Flis et al., 2019). Such regulation avoids starvation stress at the end of the nighttime while providing abundant sucrose for maintenance and growth across different photoperiods (Flis et al., 2019). The amount of starch accumulated and its rate of mobilisation are regulated such that starch is consumed at around dawn, which the circadian clock can anticipate (Graf and Smith, 2011; Scialdone et al., 2013). Mutants of different circadian clock components fail to distribute starch mobilisations correctly, either consuming reserves too quickly, leading to late-night-time carbon deficits and transient starvation, or too slowly, leading to accumulation of starch (Eimert et al., 1995; Messerli et al., 2007; Graf and Smith, 2011; Scialdone et al., 2013; Flis et al., 2019). Thus, any circadian clock changes caused by stresses may affect the dynamics of starch rhythms.

Transcriptomic studies of Arabidopsis and sugarcane leaves showed that the transcription of genes associated with starch degradation enzymes peak at dusk and decrease at dawn (Harmer et al., 2000; Smith et al., 2004; Usadel et al., 2008; Hotta et al., 2013). However, gene expression may not correlate with protein abundance or enzyme activity. In particular, whilst many transcripts show marked oscillations, the abundance of their encoded proteins are often relatively stable across the 24 h cycle, raising questions about the biological function of these oscillations in transcript abundance (Baerenfaller et al., 2012; Ponnala et al., 2014; Graf et al., 2017). In addition to regulating expression, the circadian clock also buffers the starch metabolism against sudden fluctuations in light and temperature (Graf et al., 2010; Pyl et al., 2012; Pilkington et al., 2015; Flis et al., 2019).

There are two models to explain how rhythms in starch metabolism are generated: one that integrates starch abundance and timing information (Scialdone et al., 2013; Pokhilko et al., 2014) and one that proposes continuous regulation of the circadian clock by signals from sucrose or related metabolites (Webb and Satake, 2015; Seki et al., 2017). In addition, it has been proposed that increased rates of starch mobilisation with time in the light result in an endogenous glucose-6-phosphate oscillation (Flis et al., 2019) that serves as a buffer to regulate carbon reserves from photosynthesis at dusk. Even so, the molecular mechanisms of this control are poorly understood.

Low-carbon availability regulates the REVEILLE family, regulating many circadian clock genes (Moraes et al., 2019). Carbon starvation can also regulate the circadian clock, triggered by growth under low light or low CO_2 (Haydon et al., 2013; Frank et al., 2018). In these conditions, basic leucine zipper 63 (bZIP63) upregulates the circadian oscillator gene pseudo-response regulator 7 (*PRR7*) (Frank et al., 2018). As the circadian clock and SnRK1 regulate bZIP63, it may connect the circadian clock and sugar signalling (Mair et al., 2015; Viana et al., 2021). Mutants of *bZIP63* exhibit impaired growth under light/dark

cycles but not under constant light, possibly because starch degradation is accelerated, leading to starvation stress by the nighttime's end (Viana et al., 2021). Interestingly, *bZIP63* is also regulated by ABA (Matiolli et al., 2011). Considering that bZIP63 forms heterodimers with other family members, like bZIP1 (Kang et al., 2010), and OsZIP23 may play a similar role in rice (Kim et al., 2017), the bZIP family of transcription factors may be at the centre of three major regulatory networks.

FUTURE PROSPECTS

Starch can be an essential carbon source when photosynthesis is inhibited at night and under many stress conditions. The carbon derived from starch may help support some continued growth, but it is probably even more critical because it supports metabolic and cellular responses that ameliorate stress. While the pathways of starch degradation are pretty well-understood in source leaves, less is known about the enzymes involved in starch metabolism in sink tissues under abiotic stress. Furthermore, little is known about the interaction between starch turnover and stress responses, especially when another regulatory pathway, the circadian clock, is involved. In biotic stresses, the molecular mechanisms involved in starch accumulation are mainly unknown. In general, a better understanding of the dynamics of regulators of starch metabolism under different types of stress and at different stress intensities is needed, especially post-transcriptional regulators. A better understanding of how starch is used during different stresses could allow breeding programs or genetic engineering to generate stress-resilient plants, especially starch-based feedstocks.

AUTHOR CONTRIBUTIONS

CR, MS, and CH wrote and edited the manuscript. All authors contributed to the article and approved the submitted version.

FUNDING

This work was supported by the São Paulo Research Foundation (FAPESP) (Grant Nos. 17/50326-0 and 19/08534-0; BIOEN Program).

REFERENCES

Achor, D., Welker, S., Ben-Mahmoud, S., Wang, C., Sy, S., Dutt, M., et al. (2020). Dynamics of Candidatus Liberibacter asiaticus Movement and Sieve-Pore Plugging in Citrus Sink Cells. *Plant Physiol.* 182, 882–891. doi: 10.1104/pp.19.01391

Adams, S., Grundy, J., Veflingstad, S. R., Dyer, N. P., Hannah, M. A., Ott, S., et al. (2018). Circadian control of abscisic acid biosynthesis and signalling pathways revealed by genome-wide analysis of LHY binding targets. *New Phytol.* 220, 893–907. doi: 10.1111/nph.15415

Albrecht, U., and Bowman, K. D. (2008). Gene expression in Citrus sinensis (L.) Osbeck following infection with the bacterial pathogen Candidatus Liberibacter asiaticus causing Huanglongbing in Florida. *Plant Sci.* 175, 291–306. doi: 10.1016/j.plantsci.2008.05.001

Allan, A. C., Lapidot, M., Culver, J. N., and Fluhr, R. (2001). An Early Tobacco Mosaic Virus-Induced Oxidative Burst in Tobacco Indicates Extracellular Perception of the Virus Coat Protein. *Plant Physiol.* 126, 97–108. doi: 10.1104/pp.126.1.97

Andersen, M. N., Asch, F., Wu, Y., Jensen, C. R., Næsted, H., Mogensen, V. O., et al. (2002). Soluble Invertase Expression Is an Early Target of Drought Stress during the Critical, Abortion-Sensitive Phase of Young Ovary Development in Maize. *Plant Physiol.* 130, 591–604. doi: 10.1104/pp.005637

Baerenfaller, K., Massonnet, C., Walsh, S., Baginsky, S., Bühlmann, P., Hennig, L., et al. (2012). Systems-based analysis of Arabidopsis leaf growth reveals adaptation to water deficit. *Mol. Syst. Biol.* 8:606. doi: 10.1038/msb.2012.39

Bahuguna, R. N., Solis, C. A., Shi, W., and Jagadish, K. S. V. (2017). Post-flowering night respiration and altered sink activity account for high night temperature-induced grain yield and quality loss in rice (Oryza sativa L.). *Physiol. Plantar.* 159, 59–73. doi: 10.1111/ppl.12485

Balan, B., Ibáñez, A. M., Dandekar, A. M., Caruso, T., and Martinelli, F. (2018). Identifying Host Molecular Features Strongly Linked With Responses to Huanglongbing Disease in Citrus Leaves. *Front. Plant. Sci.* 9:277. doi: 10.3389/fpls.2018.00277

Couée, I., Sulmon, C., Gouesbet, G., and El Amrani, A. (2006). Involvement of soluble sugars in reactive oxygen species balance and responses to oxidative stress in plants. *J. Exp. Bot.* 57, 449–459. doi: 10.1093/jxb/erj027

Cuellar-Ortiz, S. M., Arrieta-Montiel, M. D. L. P., Acosta-Gallegos, J., and Covarrubias, A. A. (2008). Relationship between carbohydrate partitioning and drought resistance in common bean. *Plant Cell Environ.* 31, 1399–1409. doi: 10.1111/j.1365-3040.2008.01853.x

Czedik-Eysenberg, A., Arrivault, S., Lohse, M. A., Feil, R., Krohn, N., Encke, B., et al. (2016). The Interplay between Carbon Availability and Growth in Different Zones of the Growing Maize Leaf. *Plant Physiol.* 172, 943–967. doi: 10.1104/pp.16.00994

de Morais, M. B., Barbosa-Neto, A. G., Willadino, L., Ulisses, C., and Calsa Junior, T. (2019). Salt Stress Induces Increase in Starch Accumulation in Duckweed (Lemna aequinoctialis, Lemnaceae): biochemical and Physiological Aspects. *J. Plant Growth Regul.* 38, 683–700. doi: 10.1007/s00344-018-9882-z

Dodd, A. N., Salathia, N., Hall, A., Kevei, E., Toth, R., Nagy, F., et al. (2005). Plant circadian clocks increase photosynthesis, growth, survival, and competitive advantage. *Science* 309, 630–633. doi: 10.1126/science.1115581

Dong, S., and Beckles, D. M. (2019). Dynamic changes in the starch-sugar interconversion within plant source and sink tissues promote a better abiotic stress response. *J. Plant Physiol.* 23, 80–93. doi: 10.1016/j.jplph.2019.01.007

Doyle, E. A., Lane, A. M., Sides, J. M., Mudgett, M. B., and Monroe, J. D. (2007). An α-amylase (At4g25000) in Arabidopsis leaves is secreted and induced by biotic and abiotic stress. *Plant Cell Environ.* 30, 388–398. doi: 10.1111/j.1365-3040.2006.01624.x

Eimert, K., Wang, S. M., Lue, W. I., and Chen, J. (1995). Monogenic Recessive Mutations Causing Both Late Floral Initiation and Excess Starch Accumulation in Arabidopsis. *Plant Cell* 7, 1703–1712. doi: 10.1105/tpc.7.10.1703

Etxeberria, E., Gonzalez, P., Achor, D., and Albrigo, G. (2009). Anatomical distribution of abnormally high levels of starch in HLB-affected Valencia orange trees. *PMPP Physiol. Mol. Plant Pathol.* 74, 76–83.

Ezquer, I., Li, J., Ovecka, M., Baroja-Fernández, E., Muñoz, F. J., Montero, M., et al. (2010). Microbial Volatile Emissions Promote Accumulation of Exceptionally High Levels of Starch in Leaves in Mono- and Dicotyledonous Plants. *Plant Cell Physiol.* 51, 1674–1693. doi: 10.1093/pcp/pcq126

Fan, J., Chen, C., Brlansky, R. H., Gmitter, F. G., and Li, Z. G. (2010). Changes in carbohydrate metabolism in Citrus sinensis infected with "Candidatus Liberibacter asiaticus". *Plant Pathol.* 59, 1037–1043. doi: 10.1111/j.1365-3059.2010.02328.x

Flis, A., Mengin, V., Ivakov, A. A., Mugford, S. T., Hubberten, H. M., Encke, B., et al. (2019). Multiple circadian clock outputs regulate diel turnover of carbon and nitrogen reserves. *Plant Cell Environ.* 42, 549–573. doi: 10.1111/pce.13440

Flütsch, S., Wang, Y., Takemiya, A., Vialet-Chabrand, S. R. M., Klejchová, M., Nigro, A., et al. (2020). Guard Cell Starch Degradation Yields Glucose for Rapid Stomatal Opening in Arabidopsis[CC-BY]. *Plant Cell* 32, 2325–2344. doi: 10.1105/tpc.18.00802

Frank, A., Matiolli, C. C., Viana, A. J. C., Hearn, T. J., Kusakina, J., Belbin, F. E., et al. (2018). Circadian entrainment in Arabidopsis by the sugar-responsive transcription factor bZIP63. *Curr. Biol.* 28, 2597.e–2606.e. doi: 10.1016/j.cub.2018.05.092

Gamm, M., Héloir, M.-C., Bligny, R., Vaillant-Gaveau, N., Trouvelot, S., Alcaraz, G., et al. (2011). Changes in carbohydrate metabolism in Plasmopara viticola-infected grapevine leaves. *Mol. Plant Microbe Interact.* 24, 1061–1073. doi: 10.1094/MPMI-02-11-0040

Gonzalez, P., Reyes, J., and Etxeberria, E. (2011). Starch analysis of HLB-affected and control healthy citrus leaves reveal variations in the amylose/amylopectin ratio. *Proc. Florida State Hortic. Soc.* 124, 69–75.

Graf, A., Coman, D., Uhrig, R. G., Walsh, S., Flis, A., Stitt, M., et al. (2017). Parallel analysis of Arabidopsis circadian clock mutants reveals different scales of transcriptome and proteome regulation. *Open Biol.* 7:160333. doi: 10.1098/rsob.160333

Graf, A., Schlereth, A., Stitt, M., and Smith, A. M. (2010). Circadian control of carbohydrate availability for growth in Arabidopsis plants at night. *Proc. Natl. Acad. Sci. U. S. A.* 107, 9458–9463. doi: 10.1073/pnas.0914299107

Graf, A., and Smith, A. M. (2011). Starch and the clock: the dark side of plant productivity. *Trends Plant Sci.* 16, 169–175. doi: 10.1016/j.tplants.2010.12.003

Harmer, S. L., Hogenesch, J. B., Straume, M., Chang, H. S., Han, B., Zhu, T., et al. (2000). Orchestrated transcription of key pathways in Arabidopsis by the circadian clock. *Science* 290, 2110–2113. doi: 10.1126/science.290.5499.2110

Haydon, M. J., Mielczarek, O., Robertson, F. C., Hubbard, K. E., and Webb, A. A. (2013). Photosynthetic entrainment of the Arabidopsis thaliana circadian clock. *Nature* 502, 689–692. doi: 10.1038/nature12603

Hotta, C. T., Gardner, M. J., Hubbard, K. E., Baek, S. J., Dalchau, N., Suhita, D., et al. (2007). Modulation of environmental responses of plants by circadian clocks. *Plant Cell Environ.* 30, 333–349. doi: 10.1111/j.1365-3040.2006.01627.x

Hotta, C. T., Nishiyama, M. Y., and Souza, G. M. (2013). Circadian rhythms of sense and antisense transcription in sugarcane, a highly polyploid crop. *PLoS One* 8:e71847. doi: 10.1371/journal.pone.0071847

Hummel, I., Pantin, F., Sulpice, R., Piques, M., Rolland, G., Dauzat, M., et al. (2010). Arabidopsis plants acclimate to water deficit at low cost through changes of carbon usage: an integrated perspective using growth, metabolite, enzyme, and gene expression analysis. *Plant Physiol.* 154, 357–372. doi: 10.1104/pp.110.157008

Hurkman, W. J., McCue, K. F., Altenbach, S. B., Korn, A., Tanaka, C. K., Kothari, K. M., et al. (2003). Effect of temperature on expression of genes encoding enzymes for starch biosynthesis in developing wheat endosperm. *Plant Sci.* 164, 873–881. doi: 10.1016/S0168-9452(03)00076-1

Kanai, M., Higuchi, K., Hagihara, T., Konishi, T., Ishii, T., Fujita, N., et al. (2005). Common reed produces starch granules at the shoot base in response to salt stress. *New Phytol.* 572–580. doi: 10.1111/j.1469-8137.2007.02188.x

Kang, S. G., Price, J., Lin, P.-C., Hong, J. C., and Jang, J.-C. (2010). The Arabidopsis bZIP1 Transcription Factor Is Involved in Sugar Signaling, Protein Networking, and DNA Binding. *Mol. Plant* 3, 361–373. doi: 10.1093/mp/ssp115

Kaplan, F., and Guy, C. L. (2004). beta-Amylase induction and the protective role of maltose during temperature shock. *Plant Physiol.* 135, 1674–1684. doi: 10.1104/pp.104.040808

Kaplan, F., and Guy, C. L. (2005). RNA interference of Arabidopsis beta-amylase8 prevents maltose accumulation upon cold shock and increases sensitivity of PSII photochemical efficiency to freezing stress. *Plant J.* 44, 730–743. doi: 10.1111/j.1365-313X.2005.02565.x

Kempa, S., Krasensky, J., Santo, S. D., Kopka, J., and Jonak, C. (2008). A Central Role of Abscisic Acid in Stress-Regulated Carbohydrate Metabolism. *PLoS One* 3:e3935. doi: 10.1371/journal.pone.0003935

Keunen, E., Peshev, D., Vangronsveld, J., Ende, W. V. D., and Cuypers, A. (2013). Plant sugars are crucial players in the oxidative challenge during abiotic stress: extending the traditional concept. *Plant Cell Environ.* 36, 1242–1255. doi: 10.1111/pce.12061

Kim, S.-W., Lee, S.-K., Jeong, H.-J., An, G., Jeon, J.-S., and Jung, K.-H. (2017). Crosstalk between diurnal rhythm and water stress reveals an altered primary carbon flux into soluble sugars in drought-treated rice leaves. *Sci. Rep.* 7:8214. doi: 10.1038/s41598-017-08473-1

Koh, E.-J., Zhou, L., Williams, D. S., Park, J., Ding, N., Duan, Y.-P., et al. (2012). Callose deposition in the phloem plasmodesmata and inhibition of phloem transport in citrus leaves infected with "Candidatus Liberibacter asiaticus". *Protoplasma* 249, 687–697. doi: 10.1007/s00709-011-0312-3

Köhl, K. (2016). Metabolomics on Combined Abiotic Stress Effects in Crops. *Drought Stress Tolerance Plants* 2, 251–276. doi: 10.1007/978-3-319-32423-4_10

Kozaki, A., and Takeba, G. (1996). Photorespiration protects C3 plants from photooxidation. *Nature* 384, 557–560. doi: 10.1038/384557a0

Krasensky, J., and Jonak, C. (2012). Drought, salt, and temperature stress-induced metabolic rearrangements and regulatory networks. *J. Exp. Bot.* 63, 1593–1608. doi: 10.1093/jxb/err460.Drought

Lai, A. G., Doherty, C. J., Mueller-Roeber, B., Kay, S. A., Schippers, J. H. M., and Dijkwel, P. P. (2012). Circadian Clock-Associated 1 regulates ROS homeostasis and oxidative stress responses. *Proc. Natl. Acad. Sci. U. S. A.* 109, 17129–17134. doi: 10.1073/pnas.1209148109

Legnaioli, T., Cuevas, J., and Mas, P. (2009). TOC1 functions as a molecular switch connecting the circadian clock with plant responses to drought. *EMBO J.* 28, 3745–3757. doi: 10.1038/emboj.2009.297

Lemoine, R., Camera, S., La, Atanassova, R., Dédaldéchamp, F., Allario, T., Pourtau, N., et al. (2013). Source-to-sink transport of sugar and regulation by environmental factors. *Front. Plant Sci.* 4:272. doi: 10.3389/fpls.2013.00272

Li, J., Ezquer, I., Bahaji, A., Montero, M., Ovecka, M., Baroja-Fernández, E., et al. (2011). Microbial volatile-induced accumulation of exceptionally high levels of starch in Arabidopsis leaves is a process involving NTRC and starch synthase classes III and IV. *Mol. Plant Microbe Interact.* 24, 1165–1178. doi: 10.1094/MPMI-05-11-0112

Linebarger, C. R. L., Boehlein, S. K., Sewell, A. K., Shaw, J., and Hannah, L. C. (2005). Heat Stability of Maize Endosperm ADP-Glucose Pyrophosphorylase Is Enhanced by Insertion of a Cysteine in the N Terminus of the Small Subunit. *Plant Physiol.* 139, 1625–1634. doi: 10.1104/pp.105.067637

Lloyd, J. R., and Kötting, O. (2016). *Starch Biosynthesis and Degradation in Plants*. Chichester: John Wiley & Sons, Ltd. 1–10. doi: 10.1002/9780470015902.a0020124.pub2

Lu, Y., Gehan, J. P., and Sharkey, T. D. (2005). Daylength and circadian effects on starch degradation and maltose metabolism. *Plant Physiol.* 138, 2280–2291. doi: 10.1104/pp.105.061903

Ludwig-Müller, J., and Schuller, A. (2008). "What can we learn from clubroots: alterations in host roots and hormone homeostasis caused by Plasmodiophora brassicae" in *Sustainable Disease Management in a European Context*. eds D. B. Collinge, L. Munk, and B. M. Cooke (Dordrecht: Springer). 291–302. doi: 10.1007/978-1-4020-8780-6_8

MacNeill, G. J., Mehrpouyan, S., Minow, M. A. A., Patterson, J. A., Tetlow, I. J., and Emes, M. J. (2017). Starch as a source, starch as a sink: the bifunctional role of starch in carbon allocation. *J. Exp. Bot.* 68, 4433–4453. doi: 10.1093/jxb/erx291

Mafra, V., Martins, P. K., Francisco, C. S., Ribeiro-Alves, M., Freitas-Astúa, J., and Machado, M. A. (2013). Candidatus Liberibacter americanus induces significant reprogramming of the transcriptome of the susceptible citrus genotype. *BMC Genomics* 14:247. doi: 10.1186/1471-2164-14-247

Mair, A., Pedrotti, L., Wurzinger, B., Anrather, D., Simeunovic, A., Weiste, C., et al. (2015). SnRK1-triggered switch of bZIP63 dimerisation mediates the low-energy response in plants. *Elife* 4:e05828. doi: 10.7554/eLife.05828

Mangelsen, E., Kilian, J., Harter, K., Jansson, C., Wanke, D., and Sundberg, E. (2011). Transcriptome Analysis of High-Temperature Stress in Developing Barley Caryopses: early Stress Responses and Effects on Storage Compound Biosynthesis. *Mol. Plant* 4, 97–115. doi: 10.1093/mp/ssq058

Martinelli, F., and Dandekar, A. M. (2017). Genetic Mechanisms of the Devious Intruder Candidatus Liberibacter in Citrus. *Front. Plant Scien.* 8:904. doi: 10.3389/fpls.2017.00904

Martinelli, F., Reagan, R. L., Uratsu, S. L., Phu, M. L., Albrecht, U., Zhao, W., et al. (2013). Gene Regulatory Networks Elucidating Huanglongbing Disease Mechanisms. *PLoS One* 8:e74256. doi: 10.1371/journal.pone.0074256

Martinelli, F., Uratsu, S. L., Albrecht, U., Reagan, R. L., Phu, M. L., Britton, M., et al. (2012). Transcriptome Profiling of Citrus Fruit Response to Huanglongbing Disease. *PLoS One* 7:e38039. doi: 10.1371/journal.pone.0038039

Matiolli, C. C., Tomaz, J. P., Duarte, G. T., Prado, F. M., Del Bem, L. E. V., Silveira, A. B., et al. (2011). The Arabidopsis bZIP Gene AtbZIP63 Is a Sensitive Integrator of Transient Abscisic Acid and Glucose Signals. *Plant Physiol.* 157, 692–705. doi: 10.1104/pp.111.181743

McClung, C. R. (2019). The plant circadian oscillator. *Biology* 8:14. doi: 10.3390/biology8010014

McDowell, N. G., Beerling, D. J., Breshears, D. D., Fisher, R. A., Raffa, K. F., and Stitt, M. (2011). The interdependence of mechanisms underlying climate-driven vegetation mortality. *Trends Ecol. Evol.* 26, 523–532. doi: 10.1016/j.tree.2011.06.003

Messerli, G., Partovi Nia, V., Trevisan, M., Kolbe, A., Schauer, N., Geigenberger, P., et al. (2007). Rapid Classification of Phenotypic Mutants of Arabidopsis via Metabolite Fingerprinting. *Plant Physiol.* 143, 1484–1492. doi: 10.1104/pp.106.090795

Moraes, T. A., Mengin, V., Annunziata, M. G., Encke, B., Krohn, N., Höhne, M., et al. (2019). Response of the Circadian Clock and Diel Starch Turnover to One Day of Low Light or Low CO2. *Plant Physiol.* 179, 1457–1478. doi: 10.1104/pp.18.01418

Mugford, S. T., Fernandez, O., Brinton, J., Flis, A., Krohn, N., Encke, B., et al. (2014). Regulatory Properties of ADP Glucose Pyrophosphorylase Are Required for Adjustment of Leaf Starch Synthesis in Different Photoperiods. *Plant Physiol.* 166, 1733–47. doi: 10.1104/pp.114.247759

Noronha, H., Silva, A., Dai, Z., Gallusci, P., Rombolà, A. D., Delrot, S., et al. (2018). A molecular perspective on starch metabolism in woody tissues. *Planta* 248, 559–568. doi: 10.1007/s00425-018-2954-2

O'Leary, B. M., Lee, C. P., Atkin, O. K., Cheng, R., Brown, T. B., and Millar, A. H. (2017). Variation in Leaf Respiration Rates at Night Correlates with Carbohydrate and Amino Acid Supply. *Plant Physiol.* 174, 2261–2273. doi: 10.1104/pp.17.00610

Pilkington, S. M., Encke, B., Krohn, N., Höhne, M., Stitt, M., and Pyl, E.-T. (2015). Relationship between starch degradation and carbon demand for maintenance and growth in Arabidopsis thaliana in different irradiance and temperature regimes. *Plant Cell Environ.* 38, 157–171. doi: 10.1111/pce.12381

Pitino, M., Allen, V., and Duan, Y. (2018). Las5315 Effector Induces Extreme Starch Accumulation and Chlorosis as Ca. Liberibacter asiaticus Infection in Nicotiana benthamiana. *Front. Plant Sci.* 9:113. doi: 10.3389/fpls.2018.00113

Pokhilko, A., Flis, A., Sulpice, R., Stitt, M., and Ebenhöh, O. (2014). Adjustment of carbon fluxes to light conditions regulates the daily turnover of starch in plants: a computational model. *Mol. BioSyst.* 10, 613–627. doi: 10.1039/C3MB70459A

Ponnala, L., Wang, Y., Sun, Q., and van Wijk, K. J. (2014). Correlation of mRNA and protein abundance in the developing maise leaf. *Plant J.* 78, 424–440. doi: 10.1111/tpj.12482

Pyl, E.-T., Piques, M., Ivakov, A., Schulze, W., Ishihara, H., Stitt, M., et al. (2012). Metabolism and Growth in Arabidopsis Depend on the Daytime Temperature but Are Temperature-Compensated against Cool Nights. *Plant Cell* 24, 2443–2469. doi: 10.1105/tpc.112.097188

Quick, W. P., Chaves, M. M., Wendler, R., David, M., Rodrigues, M. L., Passaharinho, J. A., et al. (1992). The effect of water stress on photosynthetic carbon metabolism in four species grown under field conditions. *Plant Cell Environ.* 15, 25–35. doi: 10.1111/j.1365-3040.1992.tb01455.x

Rolland, F., Baena-Gonzalez, E., and Sheen, J. (2006). SUGAR SENSING AND SIGNALING IN PLANTS: conserved and Novel Mechanisms. *Annu. Rev. Plant Biol.* 57, 675–709. doi: 10.1146/annurev.arplant.57.032905.105441

Rook, F., Hadingham, S. A., Li, Y., and Bevan, M. W. (2006). Sugar and ABA response pathways and the control of gene expression. *Plant Cell Environ.* 29, 426–434. doi: 10.1111/j.1365-3040.2005.01477.x

Sauter, J. J. (1988). Temperature-induced Changes in Starch and Sugars in the Stem of Populus × canadensis «robusta». *J. Plant Physiol.* 132, 608–612. doi: 10.1016/S0176-1617(88)80263-3

Scholes, J. D., and Farrar, J. F. (1987). Development of Symptoms of Brown Rust of Barley in Relation to the Distribution of Fungal Mycelium, Starch Accumulation and Localised Changes in the Concentration of Chlorophyll. *New Phytol.* 107, 103–117. doi: 10.1111/j.1469-8137.1987.tb04885.x

Scialdone, A., Mugford, S. T., Feike, D., Skeffington, A., Borrill, P., Graf, A., et al. (2013). Arabidopsis plants perform arithmetic division to prevent starvation at night. *Elife* 2:e00669. doi: 10.7554/eLife.00669.001

Seki, M., Ohara, T., Hearn, T. J., Frank, A., da Silva, V. C. H., Caldana, C., et al. (2017). Adjustment of the Arabidopsis circadian oscillator by sugar signalling dictates the regulation of starch metabolism. *Sci. Rep.* 7:8305. doi: 10.1038/s41598-017-08325-y

Seo, P. J., and Mas, P. (2015). STRESSing the role of the plant circadian clock. *Trends Plant Sci.* 20, 230–7. doi: 10.1016/j.tplants.2015.01.001

Sharkey, T. D. (2019). Discovery of the canonical Calvin–Benson cycle. *Photosynth. Res.* 140, 235–252. doi: 10.1007/s11120-018-0600-2

Singletary, G. W., Banisadr, R., and Keeling, P. L. (1994). Heat Stress During Grain Filling in Maise: effects on Carbohydrate Storage and Metabolism. *Funct. Plant Biol.* 21, 829–841. doi: 10.1071/pp9940829

Smith, A. M., and Stitt, M. (2007). Coordination of carbon supply and plant growth. *Plant Cell Environ.* 30, 1126–1149. doi: 10.1111/j.1365-3040.2007.01708.x

Smith, A. M., and Zeeman, S. C. (2020). Starch: a Flexible, Adaptable Carbon Store Coupled to Plant Growth. *Annu. Rev. Plant. Biol.* 71, 217–245. doi: 10.1146/annurev-arplant-050718-100241

Smith, S. M., Fulton, D. C., Chia, T., Thorneycroft, D., Chapple, A., Dunstan, H., et al. (2004). Diurnal Changes in the Transcriptome Encoding Enzymes of Starch Metabolism Provide Evidence for Both Transcriptional and Posttranscriptional Regulation of Starch Metabolism in Arabidopsis Leaves. *Plant Physiol.* 136, 2687–2699. doi: 10.1104/pp.104.044347

Stitt, M., Luca Borghi, G., and Arrivault, S. (2021). Targeted metabolite profiling as a top-down approach to uncover interspecies diversity and identify key conserved operational features in the Calvin–Benson cycle. *J. Exp. Bot.* 72, 5961–5986. doi: 10.1093/jxb/erab291

Stitt, M., and Zeeman, S. C. (2012). Starch turnover: pathways, regulation and role in growth. *Curr. Opin. Plant Biol.* 15, 282–292. doi: 10.1016/j.pbi.2012.03.016

Tarkowski, ŁP., and Van den Ende, W. (2015). Cold tolerance triggered by soluble sugars: a multifaceted countermeasure. *Front. Plant Sci.* 6:203. doi: 10.3389/fpls.2015.00203

Thalmann, M., Pazmino, D., Seung, D., Horrer, D., Nigro, A., Meier, T., et al. (2016). Regulation of leaf starch degradation by abscisic acid is important for osmotic stress tolerance in plants. *Plant Cell.* 28, 1860–1878. doi: 10.1105/tpc.16.00143

Thalmann, M., and Santelia, D. (2017). Starch as a determinant of plant fitness under abiotic stress. *New Phytol.* 214, 943–951. doi: 10.1111/nph.14491

Thitisaksakul, M., Jiménez, R. C., Arias, M. C., and Beckles, D. M. (2012). Effects of environmental factors on cereal starch biosynthesis and composition. *J. Cereal Sci.* 56, 67–80. doi: 10.1016/j.jcs.2012.04.002

Timm, S., and Hagemann, M. (2020). Photorespiration—how is it regulated and how does it regulate overall plant metabolism? *J. Exp. Bot.* 71, 3955–3965. doi: 10.1093/jxb/eraa183

Timm, S., Woitschach, F., Heise, C., Hagemann, M., and Bauwe, H. (2019). Faster removal of 2-Phosphoglycolate through Photorespiration Improves Abiotic Stress Tolerance of Arabidopsis. *Plants* 8:563. doi: 10.3390/plants8120563

Trouverie, J., Prioul, J.-L., Trouverie, J., and Prioul, J.-L. (2006). Increasing leaf export and grain import capacities in maise plants under water stress. *Funct. Plant Biol.* 33, 209–218. doi: 10.1071/FP05206

Usadel, B., Bläsing, O. E., Gibon, Y., Retzlaff, K., Höhne, M., Günther, M., et al. (2008). Global Transcript Levels Respond to Small Changes of the Carbon Status during Progressive Exhaustion of Carbohydrates in Arabidopsis Rosettes. *Plant Physiol.* 146, 1834–1861. doi: 10.1104/pp.107.115592

Valerio, C., Costa, A., Marri, L., Issakidis-Bourguet, E., Pupillo, P., Trost, P., et al. (2011). Thioredoxin-regulated beta-amylase (BAM1) triggers diurnal starch degradation in guard cells, and in mesophyll cells under osmotic stress. *J. Exp. Bot.* 62, 545–555. doi: 10.1093/jxb/erq288

Viana, A. J. C., Matiolli, C. C., Newman, D. W., Vieira, J. G. P., Duarte, G. T., Martins, M. C. M., et al. (2021). The sugar-responsive circadian clock regulator bZIP63 modulates plant growth. *New Phytol.* 231, 1875–1889. doi: 10.1111/nph.17518

Wallwork, M. A. B., Logue, S. J., MacLeod, L. C., and Jenner, C. F. (1998). Effect of high temperature during grain filling on starch synthesis in the developing barley grain. *Funct. Plant Biol.* 25, 173–181. doi: 10.1071/pp97084

Wang, N., Pierson, E. A., Setubal, J. C., Xu, J., Levy, J. G., Zhang, Y., et al. (2017). The Candidatus Liberibacter–Host Interface: insights into Pathogenesis Mechanisms and Disease Control. *Annu. Rev. Phytopathol.* 55, 451–482. doi: 10.1146/annurev-phyto-080516-035513

Webb, A. A. R., and Satake, A. (2015). Understanding Circadian Regulation of Carbohydrate Metabolism in Arabidopsis Using Mathematical Models. *Plant Cell Physiol.* 56, 586–593. doi: 10.1093/pcp/pcv033

Weise, S. E., Schrader, S. M., Kleinbeck, K. R., and Sharkey, T. D. (2006). Carbon Balance and Circadian Regulation of Hydrolytic and Phosphorolytic Breakdown of Transitory Starch. *Plant Physiol.* 141, 879–886. doi: 10.1104/pp.106.081174

Wilkins, O., Bräutigam, K., and Campbell, M. M. (2010). Time of day shapes Arabidopsis drought transcriptomes. *Plant J.* 63, 715–727. doi: 10.1111/j.1365-313X.2010.04274.x

Witt, W., and Sauter, J. J. (1994). Enzymes of Starch Metabolism in Poplar Wood During Fall and Winter. *J. Plant Physiol.* 143, 625–631. doi: 10.1016/S0176-1617(11)81149-1

Yamakawa, H., and Hakata, M. (2010). Atlas of Rice Grain Filling-Related Metabolism under High Temperature: joint Analysis of Metabolome and Transcriptome Demonstrated Inhibition of Starch Accumulation and Induction of Amino Acid Accumulation. *Plant Cell Physiol.* 51, 795–809. doi: 10.1093/pcp/pcq034

Zanella, M., Borghi, G. L., Pirone, C., Thalmann, M., Pazmino, D., Costa, A., et al. (2016). β-amylase 1 (BAM1) degrades transitory starch to sustain proline biosynthesis during drought stress. *J. Exp. Bot.* 67, 1819–1826. doi: 10.1093/jxb/erv572

Zhang, Y., Persson, S., and Giavalisco, P. (2013). Differential regulation of carbon partitioning by the central growth regulator Target of Rapamycin (TOR). *Mol. Plant.* 6, 1731–1733. doi: 10.1093/mp/sst094

Zhao, J., Zhang, X., Hong, Y., Liu, Y., and Liu, Y. (2016). Chloroplast in Plant-Virus Interaction. *Front. Microbiol.* 7:1565. doi: 10.3389/fmicb.2016.01565

Zrenner, R., and Stitt, M. (1991). Comparison of the effect of rapidly and gradually developing water-stress on carbohydrate metabolism in spinach leaves. *Plant Cell Environ.* 14, 939–946. doi: 10.1111/j.1365-3040.1991.tb00963.x

Zwieniecki, M. A., and Holbrook, N. M. (2009). Confronting Maxwell's demon: biophysics of xylem embolism repair. *Trends Plant Sci.* 14, 530–534. doi: 10.1016/j.tplants.2009.07.002

Conflict of Interest: CR was employed by Centro de Tecnologia Canavieira SA.

The remaining authors declare that the research was conducted in the absence of any commercial or financial relationships that could be construed as a potential conflict of interest.

Publisher's Note: All claims expressed in this article are solely those of the authors and do not necessarily represent those of their affiliated organizations, or those of the publisher, the editors and the reviewers. Any product that may be evaluated in this article, or claim that may be made by its manufacturer, is not guaranteed or endorsed by the publisher.

frontiers | Frontiers in Plant Science

ORIGINAL RESEARCH
published: 29 April 2022
doi: 10.3389/fpls.2022.869680

Source-Sink Dynamics in Field-Grown Durum Wheat Under Contrasting Nitrogen Supplies: Key Role of Non-Foliar Organs During Grain Filling

*Raquel Martínez-Peña[1], Armin Schlereth[2], Melanie Höhne[2], Beatrice Encke[2], Rosa Morcuende[3], María Teresa Nieto-Taladriz[4], José Luis Araus[5], Nieves Aparicio[1] and Rubén Vicente[2,6]**

[1] Group of Cereals, Section of Herbaceous, Instituto Tecnológico Agrario de Castilla y León (ITACyL), Junta de Castilla y León, Valladolid, Spain, [2] Max Planck Institute of Molecular Plant Physiology, Potsdam, Germany, [3] Institute of Natural Resources and Agrobiology of Salamanca (IRNASA), Consejo Superior de Investigaciones Científicas (CSIC), Salamanca, Spain, [4] Instituto Nacional de Investigación y Tecnología Agraria y Alimentaria (INIA), Madrid, Spain, [5] Integrative Crop Ecophysiology Group, Section of Plant Physiology, Faculty of Biology, University of Barcelona, Barcelona, Spain, [6] Instituto de Tecnologia Química e Biológica António Xavier, Universidade Nova de Lisboa (ITQB NOVA), Plant Ecophysiology and Metabolism Group, Oeiras, Portugal

OPEN ACCESS

Edited by:
Sezai Ercisli,
Atatürk University, Turkey

Reviewed by:
Dejan Dodig,
Maize Research Institute Zemun Polje, Serbia
Yahia Rharrabti,
Sidi Mohamed Ben Abdellah University, Morocco

***Correspondence:**
Rubén Vicente
vicenteperez.ruben@gmail.com

Specialty section:
This article was submitted to Plant Metabolism and Chemodiversity, a section of the journal Frontiers in Plant Science

Received: 04 February 2022
Accepted: 31 March 2022
Published: 29 April 2022

Citation:
Martínez-Peña R, Schlereth A, Höhne M, Encke B, Morcuende R, Nieto-Taladriz MT, Araus JL, Aparicio N and Vicente R (2022) Source-Sink Dynamics in Field-Grown Durum Wheat Under Contrasting Nitrogen Supplies: Key Role of Non-Foliar Organs During Grain Filling. Front. Plant Sci. 13:869680. doi: 10.3389/fpls.2022.869680

The integration of high-throughput phenotyping and metabolic approaches is a suitable strategy to study the genotype-by-environment interaction and identify novel traits for crop improvement from canopy to an organ level. Our aims were to study the phenotypic and metabolic traits that are related to grain yield and quality at canopy and organ levels, with a special focus on source-sink coordination under contrasting N supplies. Four modern durum wheat varieties with contrasting grain yield were grown in field conditions under two N fertilization levels in north-eastern Spain. We evaluated canopy vegetation indices taken throughout the growing season, physiological and metabolic traits in different photosynthetic organs (flag leaf blade, sheath, peduncle, awn, glume, and lemma) at anthesis and mid-grain filling stages, and agronomic and grain quality traits at harvest. Low N supply triggered an imbalance of C and N coordination at the whole plant level, leading to a reduction of grain yield and nutrient composition. The activities of key enzymes in C and N metabolism as well as the levels of photoassimilates showed that each organ plays an important role during grain filling, some with a higher photosynthetic capacity, others for nutrient storage for later stages of grain filling, or N assimilation and recycling. Interestingly, the enzyme activities and sucrose content of the ear organs were positively associated with grain yield and quality, suggesting, together with the regression models using isotope signatures, the potential contribution of these organs during grain filling. This study highlights the use of holistic approaches to the identification of novel targets to improve grain yield and quality in C_3 cereals and the key role of non-foliar organs at late-growth stages.

Keywords: durum wheat, ear, genotypic variability, metabolism, nitrogen, phenotyping, grain yield

INTRODUCTION

Global crop production needs to double by 2050 to meet the rising population demands, nutritional requirements, and increasing biofuels consumption (Ray et al., 2013). Boosting crop yields to meet these rising demands is the ideal solution to meet this goal. Durum wheat is an economically and culturally important crops widely cultivated in the Mediterranean basin, used mainly to produce pasta and other non-baked products, as bulgur and couscous. It provides 18% of the daily intake of calories and 20% of proteins in the human diet (Royo et al., 2017). Global durum wheat production achieved around 38–40 million tons (∼5% of total wheat production) and is concentrated in Mediterranean areas, being the European Union, North Africa, and Middle East countries the primary producers and consumers (Beres et al., 2020; Xynias et al., 2020). In Spain, durum wheat was grown in 266,644 ha, producing 704,086 tons, which represented 14% and 12% of the total wheat area and production in the country, respectively (Ministry of Agriculture, Fisheries and Food of Spain, 2019; www.mapa.gob.es).

To meet future food demands, a worldwide crop yield increase of 2.4% per year is required (Ray et al., 2013), although the genetic advancement in the last decade for durum wheat has been much lower or even stagnated in different Mediterranean agro-environments (Chairi et al., 2018; Del Pozo et al., 2019). Moreover, climate change will increase the vulnerability of durum wheat production to the impact of abiotic stresses in the Mediterranean countries, where a rise in mean temperatures and lower precipitations is predicted (IPCC, 2013), which will limit grain number and further grain filling by inhibiting C fixation and N assimilation (Vicente et al., 2015, 2018b, 2019a; Medina et al., 2016). Therefore, it is of strategic importance for Mediterranean agriculture to develop new varieties with more significant production potential, better adaptation to increasingly adverse environmental conditions, and better grain quality (GQ). However, genetic advance is constrained by the lack of exploring the available genetic diversity in terms of traits to select, high-throughput phenotyping techniques to implement, and the better understanding of key molecular mechanisms behind crop adaptation to stress conditions.

Firstly, the development and implementation of high-throughput phenotyping approaches are necessary for the provision of information about the genotype-by-environment interaction and selection criteria for breeding programs, but further efforts are also needed for selection toward adaptation to abiotic stresses (Kefauver et al., 2017; Vicente et al., 2019b; Prey and Schmidhalter, 2020). Secondly, most of the breeding efforts during the last century were focused on improving wheat yields. Selection toward high-yielding cultivars has been done using a few agronomical and physiological traits (Del Pozo et al., 2016). However, other factors, such as the nutritional grain quality and pasting behavior, relevant for human diet, and industrial processing, were considered secondary (Sanchez-Garcia et al., 2015). In the Mediterranean basin, where yield gaps are high and environmental stresses may prevent progress, selection for increased adaptation to abiotic stresses is a potential strategy to support future yield progress. However, its complexity has been a challenge for crop improvement as the study of local adaptation requires multidisciplinary studies with multiple environments. Hence, the success in future breeding strategies may reside in novel holistic approaches integrating agronomy, field phenotyping, metabolism, and molecular biology in extensive wheat collections to identify attributes controlling complex traits, i.e., grain yield (GY) and GQ under various stresses (Araus et al., 2021b).

Canopy photosynthesis, understood as the photosynthesis of foliar and non-foliar photosynthetic green organs, is a key target for improving crop yield and resilience (Sanchez-Bragado et al., 2020b; Araus et al., 2021b). Traditionally, it has been thought that the key contributor for canopy photosynthesis during the grain filling stage was the flag leaf blade (the last fully developed leaf in cereals), while the reserves stored in the stems before anthesis were also involved providing C and other nutrients (Sanchez-Bragado et al., 2020b). However, it has been recently shown experimentally that the photosynthesis of non-foliar organs, including the whole ear, may significantly contribute to canopy photosynthesis and, then, GY (Gámez et al., 2020; Molero and Reynolds, 2020; Shokat et al., 2020; Araus et al., 2021b). This can be particularly relevant under abiotic stresses, e.g., water stress, but may also contribute to GY under good agronomical conditions (Sanchez-Bragado et al., 2014a,b, 2016). However, the methodologies for studying the contribution of ears or other non-foliar organs to GY are frequently intrusive or cause compensatory effects (Sanchez-Bragado et al., 2016; Rivera-Amado et al., 2020). Ears exhibit higher tolerance to limiting stress conditions compared to leaves, with minor or even insignificant negative impacts on photosynthetic and electron transport rates, and N and water status, including a higher content and expression of primary metabolism intermediates and genes, respectively (Sanchez-Bragado et al., 2014b, 2017; Vicente et al., 2018b; Vergara-Diaz et al., 2020b; Tambussi et al., 2021). Ears are the latest photosynthetic organ to develop in wheat, therefore being the youngest organ and, potentially, the last to show symptoms of senescence during the grain-filling period (Vicente et al., 2018b). Moreover, ears are, by nature, more exposed to direct sun rays and less exposed to shadows due to their apical position, with a smaller physical distance to the grain than any other organ. Awns, which are not always present in wheat varieties, seem to be a major contributor to ear photosynthesis (Sanchez-Bragado et al., 2020a). Ear bracts (glumes and lemmas) have closer contact with grains and, moreover, access to the respired CO_2 released by grains, which could be relevant in possible refixation of CO_2 (Sanchez-Bragado et al., 2020b). Regarding sheaths and peduncles, they have been associated with storage and nutrient transport functions (Scofield et al., 2009; Cimini et al., 2015). Overall, the precise pathways associated with the metabolism operating in the ears, and other non-foliar organs are still poorly understood.

N metabolism is a key factor in plant growth, with a crucial impact on GY and GQ traits, such as protein content, dough quality, and processing characteristics (Zörb et al., 2018; Wang et al., 2021). It is relevant for the wheat research to understand the N assimilation and remobilization taking place in the different green organs, especially during grain filling. For example, under

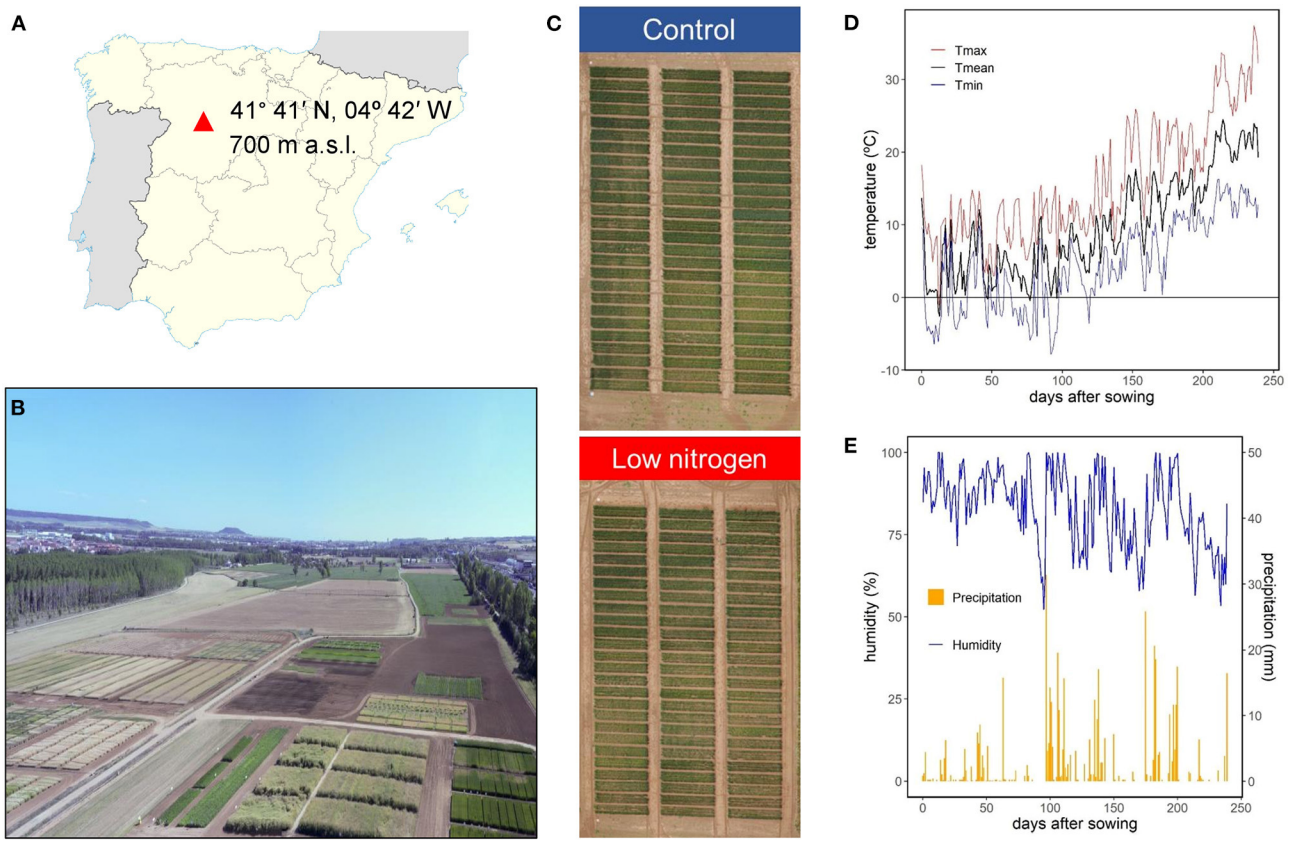

FIGURE 1 | Location **(A)** and aerial images **(B,C)** of the field trials, and daily mean (T mean), maximum (T max), and minimum (T min) temperatures **(D)**, relative humidity, and precipitation **(E)** during the crop season from November 23, 2017 to July 20, 2018 **(D)**.

water stress, the ear bracts showed active biosynthesis of organic and amino acids, which was not observed in flag leaves, thanks to a coordination between C and N metabolism, including N assimilation, photorespiratory N cycle, and tricarboxylic acid (TCA) cycle (Vergara-Diaz et al., 2020b). A preliminary study analyzing the N content and isotope composition in different parts suggested that the potential contribution of the ear, providing N to the growing grains, was around 42% (Sanchez-Bragado et al., 2017), which makes this topic of interest for addressing new avenues for crop improvement.

This study aims to perform a holistic approach, integrating agronomic, physiological, and biochemical traits to identify novel components involved in the control of complex traits in response to different N levels as a selection criterion for breeding programs. Our specific objectives are to understand (i) the phenotypic traits that are related to GY and GQ at canopy and organ levels, (ii) the potential contribution of foliar and non-foliar photosynthetic organs to developing grains and (iii) how N availability and genotypic variability modulate such factors. We evaluated a wide range of canopy vegetation indices, physiological, nutritional, and metabolic traits in green organs (flag leaf blade, sheath, peduncle, awn, glume, and lemma), and agronomic and GQ traits.

MATERIALS AND METHODS

Plant Material and Experimental Design

Four modern durum wheat [*Triticumturgidum* L. ssp. *durum* (Desf.)] varieties, widely used in the Mediterranean region, in particular in Spain, were grown during the crop season of 2017/2018, with contrasting agronomic components (e.g., yield): Euroduro, Don Ricardo, Kiko Nick, and Haristide, released in 2007, 2008, 2009, and 2015, respectively. Haristide was considered as a high-yielding variety, together with Euroduro, while Don Ricardo and, especially, Kiko Nick, were considered as low-yielding varieties (see details below). The field trials were carried out in the experimental station of Zamadueñas from the Instituto Tecnológico Agrario de Castilla y León (ITACyL), located in Valladolid, Spain (41° 41′ N, 04° 42′ W, 700 m above the sea level; **Figures 1A–C**). The climate is continental Mediterranean, and the soil is xerofluvent with sandy slit texture; the upper 0.30 m having 11.9 g kg^{-1} organic matter, 33 g kg^{-1} carbonate, 0.68 g kg^{-1} N, pH of 8.4, and electric conductivity of 0.135 dS m^{-1}. Meteorological data were collected at an automated meteorological station located in the experimental station. During the whole crop season, the average, maximum, and minimum temperatures were 9.8, 15.8, and 4.5°C, respectively, with 83% humidity and 476 mm of

accumulated precipitation (**Figures 1D,E**). The sowing, at a rate of 250 seeds m^{-2}, and the harvest, about 20–25 days after reaching physiological maturity, were performed on November 23, 2017 and July 20, 2018, respectively. Before sowing, the field trial had received a basal application of 300 kg ha^{-1} of 8-15-15 NPK fertilizer on November 22, 2017. Then, two N regimes were applied: control N supply, following the standard agronomic practices in this area, and a lower N supply (termed "low N" hereinafter; **Figure 1C**). The control N treatment was dressed with N applied at the beginning of tillering (February 20, 2018) and jointing (April 14 2018) using a dose of 150 kg ha^{-1} of calcium ammonium nitrate (CAN, 27%) and 150 kg ha^{-1} of ammonium nitrosulfate (ASN, 26%). The low N treatment was not fertilized, relying exclusively on the N available in the soil before sowing. Therefore, the control and low N treatments received a total of 105 and 24 N kg ha^{-1}, respectively. The trial was performed in an alpha-lattice design, with three replications per variety and N supply. The size of each plot was 6-m long per 1.5-m wide (9 m^2), with six rows and a space between them of 0.25 m. Weeds, insect pests, and diseases were controlled by applying of the recommenced agrochemicals to avoid yield limitations. Agronomic and GQ traits were evaluated at harvest and the phenology monitored throughout the growth cycle using the Zadoks scale (Zadoks et al., 1974). Ground-phenotypingwas performed during the crop cycle at the canopy level, while physiological and biochemical analyses were carried out in different foliar and non-foliar green organs (flag leaf blades and sheaths, peduncles, awns, glumes, and lemmas) at two specific stages; anthesis (Zadoks 65) and mid-grain filling (MGF; Zadoks 75). For these stages, the phenology of each variety was considered. Therefore, the samplings at anthesis for Kiko Nick and Don Ricardo were performed at 181 days after sowing (DAS) and for Haristide and Euroduro at 187 DAS, while at MGFEuroduro, Kiko Nick and Don Ricardo were sampled 195 DAS and, Haristide, 207 DAS.

Agronomic Components and Grain Quality Traits

At maturity, plant height (from the soil surface to the ear, excluding the awns) was evaluated. By this time, 1 week before the harvest, we had determined the number of plants per m^2 and ears per plant in two 0.5-m-length samples from the central rows of the plots. These samples were drying at 70°C for 24 h to determine the aboveground biomass. Then, the number of grains per ear, thousand grain weight (TGW), peduncle length (from the last internode to the base of the ear), and ear length (excluding the awns) were calculated in a subset of 10 main stems per plot. At the end of the experiment, the plots were harvested mechanically, and GY was determined for each one and adjusted to a 10% moisture level. Harvest index (HI) was calculated as grain weight/(grain weight + biomass). A pool of 250 g of grains per plot was collected at harvest for qualitative analyses. Protein content was determined using an Infratec 1226 Grain Analyzer (Foss Analytical, Denmark) on a dry basis. The moisture content of the grains was measured with the GrainMoistureTester PM-450 (Kett, USA). Specific weight (SW) was determined according to AACC Method 55–10. The percentage of vitreous grains (vitreousness) was determined on two lots of 100 seeds. Whole-grain flour samples were obtained after using an LM 3100 Mill (Perten Instruments AB, Sweden). Then, gluten strength was evaluated by the sodium dodecyl sulfate sedimentation (SDSS) test (Axford et al., 1978), and the yellow-color index (b*, CIE L*a*b* color system) by using a portable reflectance colorimeter (CR-310, Konica-Minolta Sensing Inc., Tokyo). Wet gluten (WG) and gluten index (GI) were determined according to the International Association for Cereal Science and Technology (ICC) Methods 155 and 158, respectively.

Canopy Vegetation Indices and Leaf Pigments

At the canopy level, we measured the normalized difference vegetation index (NDVI) by using a hand-held portable spectroradiometer (GreenSeeker, NTech Industries, USA) and RGB (red-blue-green) indices through the crop cycle as a proxy for biomass and healthy and green vegetation. RGB images were acquired by holding a 20.1-megapixel camera (Sony ILCE-QX1, Sony Corporation, Japan) attached to a Monopod VCTMP1 (Sony Corporation, Japan) at 1 m above the canopy in a zenithal plane and focusing near the center of the plot. The images were analyzed for the calculation of the vegetation indices GA (green area) and GGA (greener green area) with BreedPix software (Casadesús et al., 2007). GA and GGA are the percentage of pixels in the image (values from 0 to 1) in the hue range of 60–180° (from yellow to bluish green) and 80–180° (from yellowish-green to bluish-green), respectively (Vergara-Diaz et al., 2016). Compared to GA, GGA excludes yellowish-green tones and estimates more accurately photosynthetically active biomass (Vicente et al., 2019b). In addition, CSI (crop senescence index) was calculated according to Zaman-Allah et al. (2015) as:

$$CSI = [(GA - GGA)/GA] \times 100$$

At the leaf level, the relative contents of chlorophylls (chl), flavonols, and anthocyanins, as well as the N balance index (NBI), were measured with the leaf-clip sensor (DUALEX, Force A, France) at Zadoks 65 and 75. This portable device measures the UV absorbance of the leaf epidermis by double excitation of chlorophyll fluorescence, which allows the calculation of reflectance (chlorophyll) and fluorescence (flavonols and anthocyanins) indices, as well as the ratio between chlorophylls and flavonols as a proxy for nitrogen/carbon balance (NBI). The measurements were carried out in the middle of the flag leaf blades of five plants per plot selected randomly, and then the values were averaged per plot, being the same plants that were collected for the biochemical analyses described below. All these phenotyping measurements were done around noon (12–14 h, UTC + 1) on sunny days.

Relative Leaf Water Content and Fresh and Dry Weight

Leaf relative water content (LRWC) was determined according to Estévez-Geffriaud et al. (2020) at Zadoks 65 and 75 using the

fresh (FW), turgid (TW), and dry (DW) weights of flag leaf blades in the following equation:

$$LRWC\ (\%) = [(FW - DW)/(TW - DW)] \times 100$$

In parallel, five plants per plot were collected at Zadoks 65, 75, and 85 (soft dough) and used to calculate FW and DW of different organs (after drying in the oven at 70°C for 48 h): flag leaf blades and sheaths, peduncles, and whole ears.

Determination of the Content of Carbohydrates

Foliar and non-foliar green organs were harvested with liquid N_2 at Zadoks 65 and 75 at noon on sunny days and stored at −80°C. While blades, sheaths, and peduncles were grounded to fine powder with a mill (Mixer Mill MM300, Retsch GmbH, Germany), the awns, glumes, and lemmas were grounded manually using a mortar and pestle with liquid N_2 to allow the proper separation of the organs. First, the soluble carbohydrates glucose, fructose, sucrose, and fructans were extracted from aliquots of the green organs using serial extractions with boiling ethanol as described by Stitt et al. (1989). A water extraction step was added to solubilize the fructans. Then, the supernatants were lyophilized and resuspended in bidistilled water, while the insoluble residue was used to determine starch after incubating with amyloglucosidase and α-amylase at 37°C overnight (Morcuende et al., 2004). The different carbohydrates were analyzed in 96-well plates using a Synergy 2 multi-mode microplate reader (BioTek, Germany) with a spectrophotometric assay coupled to NADP reduction as described by Morcuende et al. (2004).

Quantification of Rubisco Large Subunit Content

Aliquots of finely powdered material from each green organ at Zadoks 65 and 75 were used for the extraction of proteins by mixing with 10 volumes of an extraction buffer that contains Tris/HCl 62.5 mM pH, 6.8; glycerol, 10% (v/v); sodium dodecyl sulfate (SDS), 2% (w/v); bromophenol blue, 0.0125% (w/v); β-mercaptoethanol, 0.05% (v/v). Then, the samples were heated at 95°C for 5 min and centrifuged at 13,000 g for 5 min. Aliquots of the supernatants were immediately subjected to SDS–polyacrylamide gel electrophoresis (SDS-PAGE) in 12.5% (w/v) polyacrylamide gels (0.75 mm of thickness), containing SDS, 0.1% (w/v), in a Mini-PROTEAN Tetra Cell system (Bio-Rad, USA). Additionally, PageRuler prestained a protein ladder (10–180 kDa, Thermo Fisher Scientific, USA), and bovine serum albumin (BSA) was used as molecular weight and concentration standards, respectively. The electrophoresis was performed at room temperature at a constant 200 V. Afterwards, the gels were stained in a solution, containing 5:4:1 (v/v/v) water–methanol–acetic acid mixture with 0.001% (w/v) Coomassie brilliant blue R-250 dye (Thermo Fisher Scientific) for 1 h, and subsequently rinsed in water to remove excess stain. The gels were scanned in a ChemiDoc MP imaging system (Bio-Rad) and the amount of Rubiscolarge subunit determined by densitometry with Image Lab software (Pérez et al., 2011; Vicente et al., 2016).

Measurement of C-N Enzyme Activities

The enzyme activities of Rubisco (initial and total), phosphoenolpyruvate carboxylase (PEPCase), glutamine synthetase (GS), ferredoxin-dependent glutamate synthase (GOGAT), and NADH-dependent glutamate dehydrogenase (GDH) were determined in green organs at Zadoks 65 and 75. Enzymes were extracted from 20-mg aliquots of finely powdered material by adding 10 mg of polyvinylpolypyrrolidone (w/v) and 1 ml of an ice-cold extraction buffer containing Hepes/KOH, 50 mM, pH 7.5, $MgCl_2$ 10 mM; (ethylenedinitrilo) tetraacetic acid (EDTA), 1 mM; ethylene-bis (oxyethylenenitrilo) tetraacetic acid (EGTA) 1 mM; benzamidine, 1 mM; ε-aminocapronic acid, 1 mM; BSA, 0.25% (w/v); leupeptin, 20 mM; 1,4-dithiothreitol, 0.5 mM; Triton X-100, 1% (v/v); glycerol, 20% (v/v); and phenylmethylsulfonyl fluoride, 1 mM. After centrifugation at 14,000 g and 4°C for 10 min, appropriate dilutions of the supernatants were rapidly used for the different enzyme assays as described in Sulpice et al. (2007) for Rubisco and in Gibon et al. (2004) for the other enzymes. The assays were carried out in 96-well microplates using ELx800 microplate readers (Bio-Tek, USA) at the Max Planck Institute of Molecular Plant Physiology (Germany). Rubisco activation state was calculated as the ratio between initial and total Rubisco activity.

C and N Isotope Signature and Nutrient Composition in Green Organs and Grains

The flag leaf blades and sheaths, peduncles, and whole-ears samples used to calculate DW per organ at Zadoks 65 and 75 were finely grounded and used to assess the stable C ($\delta^{13}C$) and N ($\delta^{15}N$) isotope composition and the total C and N contents in the dry matter with an elemental analyzer Flash 1112 EA (Thermo Finnigan, Germany), coupled with an isotope ratio mass spectrometer Delta C IRMS (Thermo Finnigan) at the Scientific-Technical Services of the University of Barcelona (CCiTUB, Spain) as described in Medina et al. (2016). Moreover, grains at Zadoks 75, 85, and 92 (grain hard, not dented by thumbnail) were also collected and dried for 48 h at 70°C for the same analyses. The contents of other macro- and micro-nutrients were also analyzed in green organs collected at Zadoks 65 and 75 (K, Ca, P, Mg, Fe, Mn, Cu) and in grains at Zadoks 92 (K, P, S, Mg, Ca, Mn, Fe, Na, Zn, Cu, Mo). For each sample analyzed, around 500 mg of dried material was mixed with 8 ml of HNO_3 60% and 2 ml H_2O_2 30% in a Teflon container. Then, the samples were subsequently digested at 200°C in a microwave digestion system (ETHOS UP, Milestone, Italy). Afterwards, the solutions were cooled to room temperature and diluted to 25 ml by adding deionized water. Nutrient concentration was determined at the Analysis and Instrumentation Service of IRNASA-CSIC (Spain) with an inductively coupled plasma-optical emission spectrometer (ICP-OES Varian 720-ES, Agilent Technologies, USA). The yield of each nutrient and protein in grains at harvest was calculated by multiplying their concentration by GY.

Statistical Analysis

All the variables were subjected to two-way ANOVA using the general linear model to calculate the effects of N, genotypic variability, and their interaction by using IBM SPSS v23.0 (SPSS

A

Trait	Control				Low nitrogen				*P*-value		
	KNI	DRI	EUR	HAR	KNI	DRI	EUR	HAR	N	G	G×N
GY	ad	abc	ab	a	d	cd	bd	abc	***	**	
biomass	a	ab	ab	a	c	ab	bc	ac	***		*
HI	b	ab	a	ab	ab	b	a	a		**	**
plants.m2	a	ab	ac	a	ac	c	bc	ac	***	*	
ears.plant	b	b	b	b	b	a	ab	b	**	**	*
grains.ear	ab	ab	ab	a	b	ab	ab	a		**	
TGW	ab	ab	ab	b	ab	ab	ab	a	**		
ped.length	ab	a	ab	ab	ab	ab	ab	b	***		
ear.length	b	b	b	a	b	b	b	a		***	
height	a	a	ab	ab	b	b	ab	b	***		
prot.grain											
moisture.grain	ab	ab	ab	b	a	ab	ab	a	**		
SW.grain	ab	ab	a	ab	b	ab	ab	ab		**	
vitreo.grain											
sedim.grain	ab	b	a	a	c	c	c	c	***	**	**
b.grain	c	c	c	c	a	b	a	a	***	***	**
WG.grain											
GI.grain	ac	ab	a	c	ac	ac	a	bc		***	

min max

B

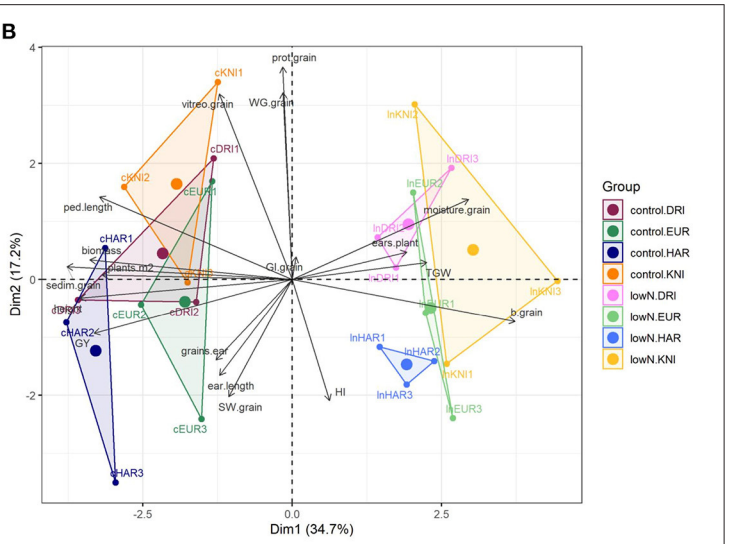

FIGURE 2 | Effects of N supply and genotypic variability on agronomic components and grain quality traits **(A)** and principal component analysis **(B)** in four varieties of field-grown durum wheat (Kiko Nick, Don Ricardo, Euroduro, and Haristide) at two N levels (control vs. low N). In **(A)**, the different letters differ statistically (*, $p < 0.05$; **, $p < 0.01$; ***, $p < 0.001$). The abbreviations are described in **Supplementary Table 1**.

Inc., USA). To analyze the differences between the means of the specific groups, we used the Tukey's honest significant difference (HSD) test. Significance was accepted at $p < 0.05$. The heatmap tables were prepared in Microsoft Excel 2016 using the conditional formatting (Microsoft Corporation, USA), while the rest of the figures were prepared in R environment. The scatter and bar plots were generated using the package *ggplot2*. Stepwise regressions were performed using the *stepAIC()* function, while the proportion of variance explained by each predictor was calculated with the package *relaimpo*. The packages *factoextra* and *FactoMineR* were used to extract and visualize the multivariate data analyses (PCA, principal component analysis). Pearson correlation matrices were built to analyze the relationships between trait pairs using the function *cor()*, and visualized using the package *corrplot*. The abbreviations for each trait used in the figures and tables are summarized in **Supplementary Table 1**.

RESULTS

Effect of N and Genotypic Variability on Durum Wheat Agronomic Components, Grain Quality, and Physiology

Low N reduced GY (22%), biomass (25%), and plants per unit area (29%), as well as peduncle length and plant height, compared to control N, while TGW slightly increased (**Figure 2A**; **Supplementary Table 2**). For GQ, low N significantly reduced sedimentation index and increased moisture content and yellowness index (**Figure 2A**; **Supplementary Table 2**). The different N supplies were undoubtedly separated in the PCA by X-axis, representing a 34.7% of the variability. The four varieties clearly showed differences in agronomic and GQ traits, with a similar trend at each N supply as evidenced by the low number of significant G × N interactions and their distribution in the PCA (**Figure 2**). The variety Haristide had the highest GY regardless of N supply, followed by Euroduro, Don Ricardo, and Kiko Nick (**Figure 2A**). Most changes in agronomic components followed the trend observed in GY, being Kiko Nick the one with lower values and Haristide with higher ones. These differences were slightly more pronounced under low N than control N. In the PCA, Y-axis explained 17.2% of the variance in the data, which was partially related with differences among varieties (**Figure 2B**). The most relevant GQ traits in this axis were grain protein content, WG, GI, and SW.

Ground phenotyping was performed to monitor plant growth, pigment content, and senescence at canopy and leaf levels. Low N supply significantly decreased GA, GGA, and NDVI, and increased CSI from early stages to maturity (**Figure 3**). Minor changes, albeit significant, were observed among varieties, mainly at late-growth stages where Haristide showed a better performance regardless of the N supply (**Figure 3**; **Supplementary Table 2**). Leaf flavonols content was increased under low N compared to control, being significant at anthesis (**Supplementary Figure 1**). The flavonols content was higher in Kiko Nick, followed by Don Ricardo, Euroduro, and Haristide at both growth stages independently of the N supply, while NBI tended to be higher in Haristide and Euroduro.

Low N decreased LRWC significantly at anthesis and MGF, while Haristide and Euroduro had higher LRWC at anthesis than Kiko Nick and Don Ricardo (**Supplementary Table 2**). Regarding the effect of N on organ weights, low N decreased FW at anthesis and MGF and DW at Zadoks 85 in blades, and DW at Zadoks 85 in sheaths and peduncles, but not in ears (**Supplementary Table 2**). Genotypic variability affected organ weights, mainly blades, sheaths, and peduncles at anthesis and

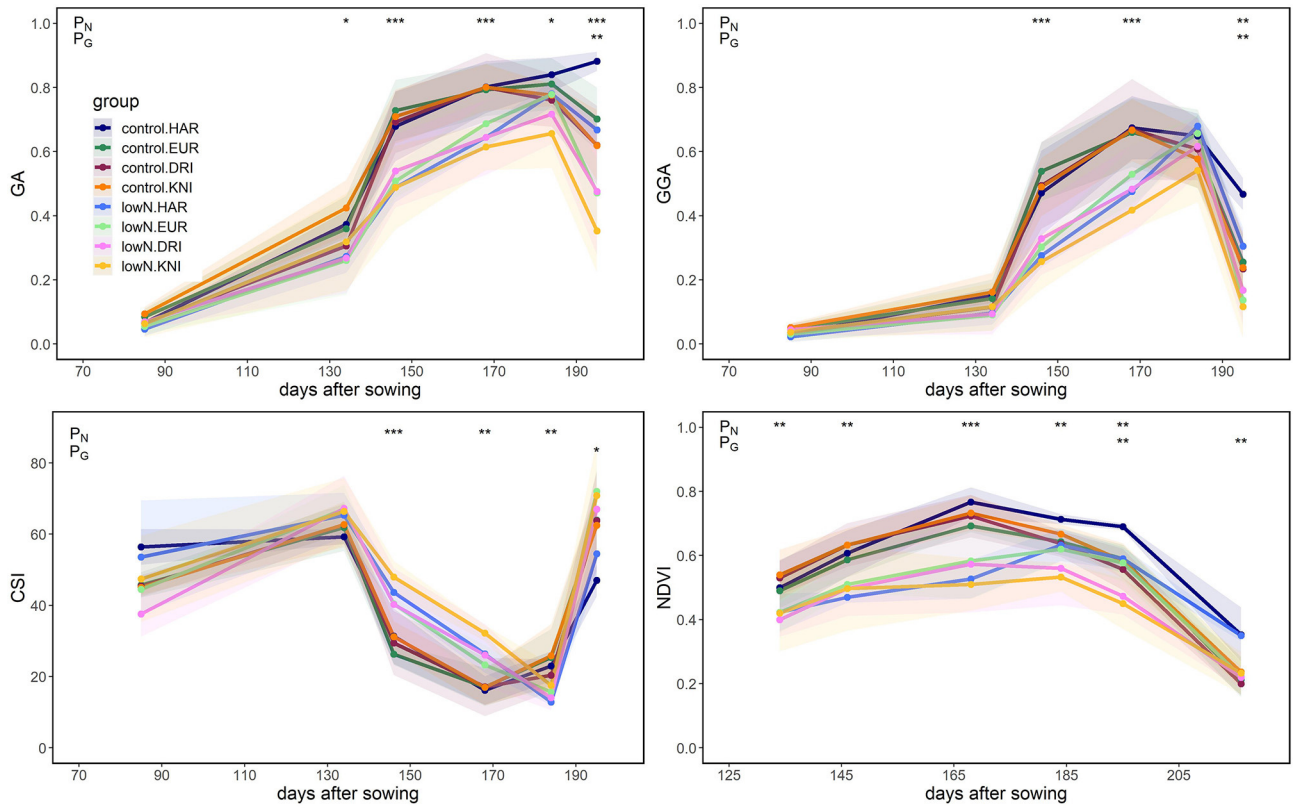

FIGURE 3 | Green area (GA), greener green area (GGA), crop senescence index (CSI), and normalized difference vegetation index (NDVI) in four varieties of field-grown durum wheat (Kiko Nick, Don Ricardo, Euroduro, and Haristide) at two N levels (control vs. low N) measured at the canopy level. Asterisks indicate a significant difference between varieties (G) and N levels (N) according to the two-way ANOVA(*, $p < 0.05$; **, $p < 0.01$; ***, $p < 0.001$). The interaction G × N did not reach significance for these parameters.

MGF, while ear DW was the lowest in Kiko Nick at late-grain filling regardless of N supply.

Correlations Between Agronomic Components and Grain Quality and Physiological Traits

GY was positively correlated with several agronomic components, such as biomass, plants per unit area, grains per ear, peduncle and ear lengths, and plant height (**Figure 4**). GY also correlated with the GQ traits sedimentation index, positively, and, with yellowness index, negatively. In addition, significant positive correlations were also observed between GY and traits, such as LRWC and blade FW at both anthesis and MGF, and blade, sheath, and peduncle DW at late-grain filling. Among the significant correlations between agronomic components and GQ traits, the most interesting were the correlations between GY and grain moisture content, and the sedimentation and yellowness indices. Grain protein correlated positively with vitreousness, WG, leaf chl, and N contents, and negatively with SW, leaf anthocyanins, and some organ weights (**Figure 4**). Biomass was highly correlated with GY and, therefore, the NDVI and RGB canopy indices with higher correlation coefficients as growth progressed (**Figure 4**). The leaf spectral indices were good proxies for GY, yield-related traits, and biomass, particularly flavonols and NBI. These indices were also correlated with several GQ traits, such as grain protein content, vitreousness, sedimentation index, WG, and GI.

Effect of N and Genotypic Variability on Grain Nutrient Compositions in Field-Grown Durum Wheat

We built a PCA with grain and protein yields and 13 grain minerals expressed as concentrations and yields measured at harvest to further characterize GQ under G × N interaction (**Figure 5**). X-axis and Y-axis explained 47.4 and 17.2% of the variance in the data, respectively, and they were associated with changes due to both N treatment and genotypic variability. N effect was clear, while the differences between varieties were similar under control or low N supply. Control N was certainly associated with grain protein and N yields, and nutrients, such as C, S, Fe, P, Cu, and Mn. The high-yielding Haristide had the highest concentrations of nutrients, such as Ca, K, and Na, and the lowest of Zn (**Figure 5**), being statistically significant Ca and Zn by Tukey's HSD test (**Supplementary Table 2**). Considering the nutrient amounts by yields, low N undoubtedly decreased the uptake of most of them, while Haristide was the variety that

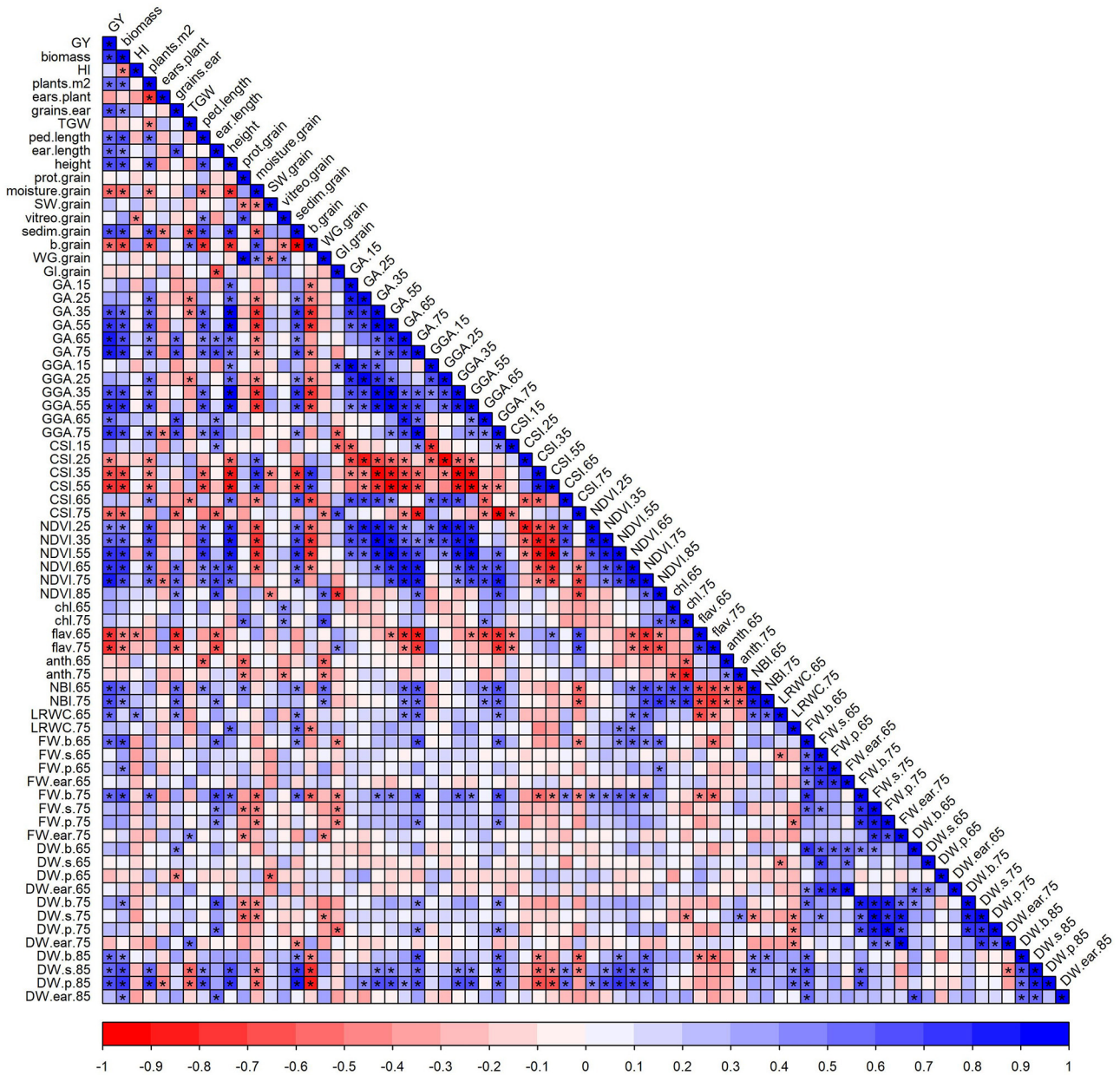

FIGURE 4 | The correlation matrix of agronomic components and grain quality and physiological traits. Each point of the matrix is a Pearson correlation coefficient between two traits (blue, positive correlation; red, negative correlation). Asterisks indicate a significant correlation ($p < 0.05$). The abbreviations are described in **Supplementary Table 1**.

uptakes highest levels of most nutrients and Kiko Nick the least regardless of N supply.

Primary Metabolism and Nutrient Composition in Green Organs of Durum Wheat During Grain Filling Under Contrasting N Supply

We examined the metabolism of photosynthetic green organs by determining carbohydrates and Rubisco protein contents, C-N metabolism enzyme activities, and nutrient and isotope composition. The blade was significantly separated from the other organs in the PCA due to its higher values for most of these traits, e.g., Rubisco protein, Rubisco, PEPCase, GS, and GOGAT activities, and nutrients, such as N, Ca, Mg, Mn, and Cu (**Figure 6**). Initial Rubisco activity was 42–56, 23–39, 14–18, 11–18, and 11–14% in awns, sheaths, peduncles, glumes, and lemmas, respectively, compared to blades depending on N supply and the growth stage (calculated from **Supplementary Table 2**). Similar patterns were observed for total Rubisco activity, which

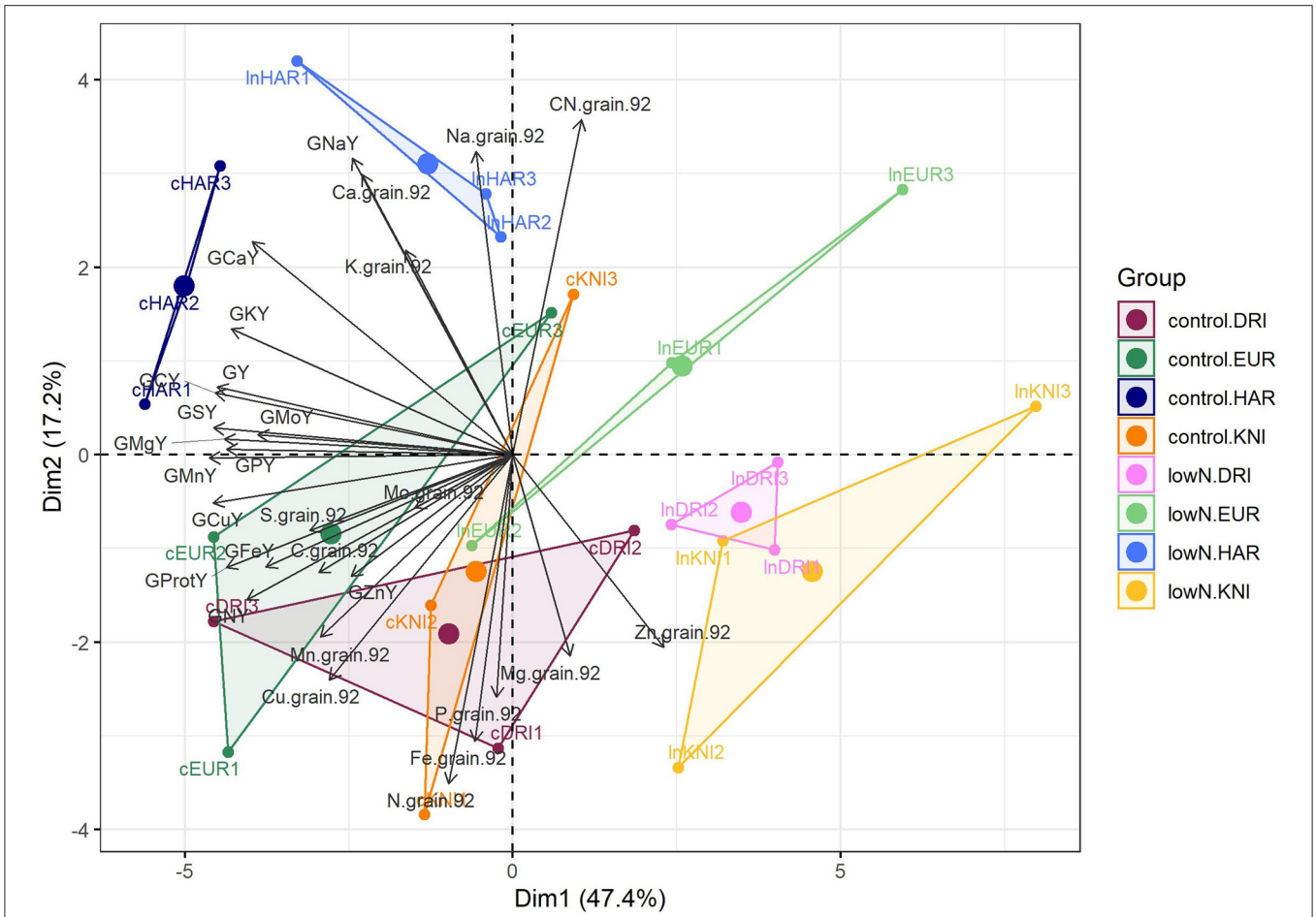

FIGURE 5 | Principal component analysis of grain nutrient compositions and yields at harvest in four varieties of field-grown durum wheat (Kiko Nick, Don Ricardo, Euroduro, and Haristide) at two N levels (control vs. low N). The abbreviations are described in **Supplementary Table 1**.

correlated with protein level ($r = 0.80$), as well as for the other enzymes, except GDH whose values were not so low in the non-foliar organs. Considering X-axis (45.3% of the variability), the closer organ to the blade was the awn. Ear bracts, glumes, and lemmas almost overlapped and were close to awns, being separated from sheaths and peduncles mainly by Y-axis (11.9% of the variability). Ear organs had high levels of GDH activity, Rubisco activation state, and fructose, glucose, and Fe levels at MGF. Sheaths and peduncles were characterized by the highest fructans levels and free carbohydrates (glucose and fructose) at anthesis.

The N effect was relatively similar between organs, but when the position of the centroids was examined per organ and N supply, we observed slightly stronger effects on blades, while, in other organs, such as the ear bracts, it was smaller or almost negligible (**Supplementary Figure 2**). Low N increased the levels of fructose, fructans, and starch in the peduncle and sucrose in blades at anthesis compared to control N (**Supplementary Table 2**). Interestingly, low N decreased sucrose levels in blades, sheaths, and, more significantly, in ear organs at MGF, together with starch. Low N increased Rubisco protein in peduncles and lemmas at anthesis but reduced it in sheaths and peduncles at MGF and in blades at both stages (**Supplementary Table 2**). Low N tended to decrease both initial and total Rubisco activities in most organs, except for a small increase in blades and a stronger increase in peduncles at anthesis. Low N also decreased activities of PEPCase (e.g., in glumes, sheaths, and peduncles), GS, and GOGAT, while GDH was less affected, with an interesting strong increase in blades in low N compared to control N. Although the N effect on grain nutrient composition at harvest was clear (**Figure 5**), its effects were not so evident in the organ-specific nutrient concentrations (**Supplementary Table 2**). Among the most relevant data, lower N supply increased Fe content, especially in glumes, and reduced C content at late stages and, non-significantly, N.

The genotypic variability greatly influenced primary metabolism and nutrient composition in green organs (**Supplementary Figure 3**, **Supplementary Table 2**). Fructose levels were higher in most green organs of high (Haristide and Euroduro) vs. low-yielding (Don Ricardo and Kiko Nick) varieties (**Supplementary Table 2**). Sucrose content was strongly reduced in Haristide in all organs at anthesis, but, at MGF, it was

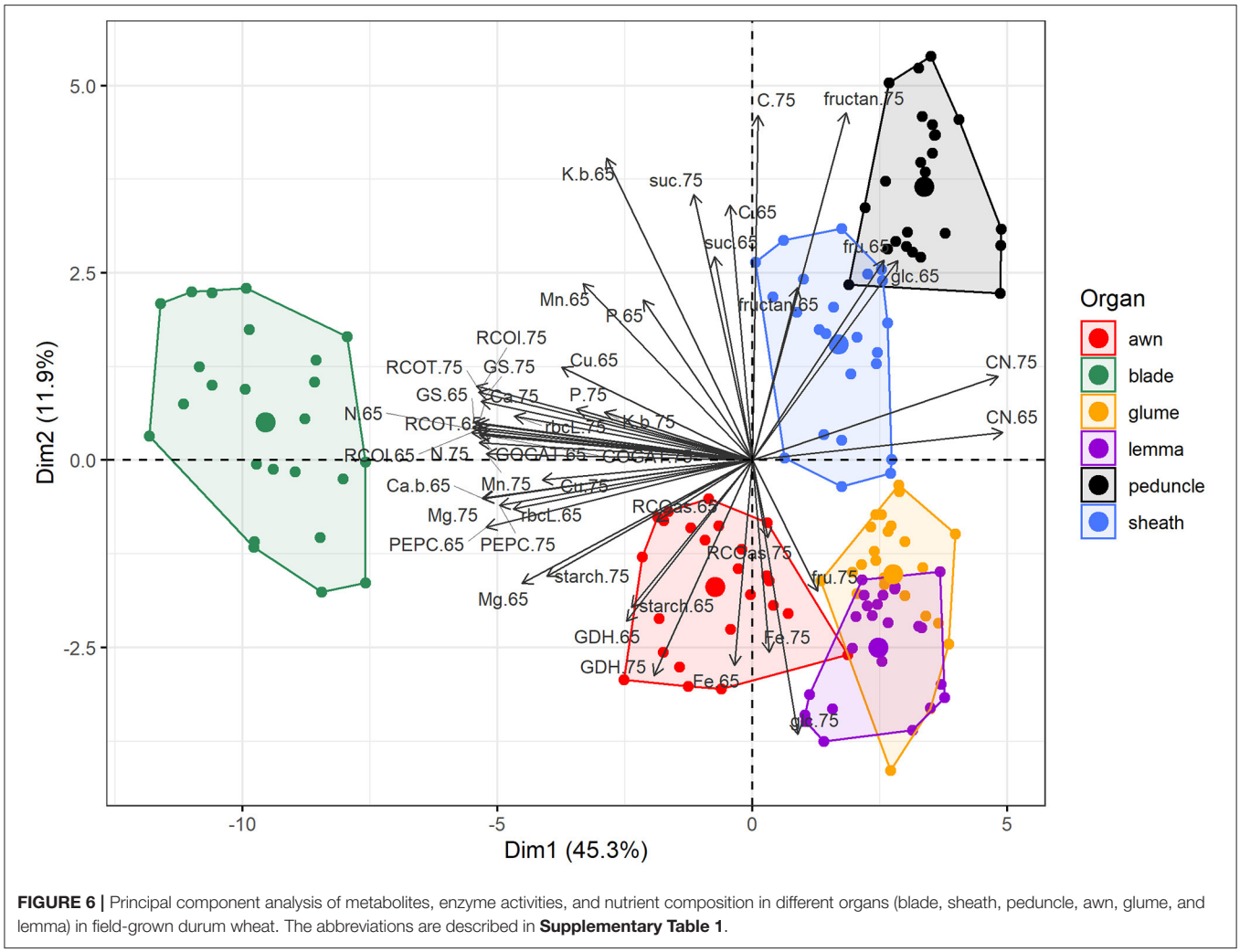

FIGURE 6 | Principal component analysis of metabolites, enzyme activities, and nutrient composition in different organs (blade, sheath, peduncle, awn, glume, and lemma) in field-grown durum wheat. The abbreviations are described in **Supplementary Table 1**.

higher in blades, awns, glumes, and lemmas compared to the other varieties, regardless of N supply. The pattern of changes in starch was very similar to sucrose, while overall fructans decreased in Haristide, except for an increase in peduncles at MGF. Rubisco protein content and activities were organ specific and highly variable between varieties. Due to the amount of traits, treatments, and significant results obtained for the other enzyme activities and nutrients, we focused on their correlations with agronomic components and GQ traits detailed in the following sections. An overview of the most relevant results for each variety and organ is shown in **Supplementary Figure 3**. In summary, the metabolism and nutritional composition of the high-yielding variety Haristide were markedly different from the others at the whole plant.

Changes in Primary Metabolism and Nutrient Composition in Green Organs Between Anthesis and Mid-Grain Filling

Metabolic changes between anthesis and MGF were studied by organ (grouping all varieties as their differences were similar for each N regime) to understand their metabolic evolution during grain filling (**Figure 7**). Glucose content at both N supplies and starch at control N increased in blades and decreased in other organs at MGF compared to anthesis. Fructose content increased in blades, particularly under low N, while decreased in peduncles compared to other organs. Sucrose content was slightly higher in all organs under control N at MGFcompared to anthesis, while it was similar under low N, except for the high increase in peduncles at both N levels. A marked increase in fructans was observed in peduncles, higher under control N. The amount and activity of Rubisco in peduncles increased at MGF under control N but decreased under low N, while they increased in sheaths. In ear organs, i.e., glumes and lemmas, Rubisco protein content tended to decrease, but the initial activity increased, partly due to a better activation state (**Figure 7**). By contrast, Rubisco activity was significantly decreased in blades at MGF under low N. PEPCase activity tended to increase at MGF, being negatively affected by low N, higher in peduncles under control N and lower in glumes. GS activity increased remarkably in glumes under control N and decreased in awns under low N. GOGAT activity was stable in blades, increased in sheaths under low N and

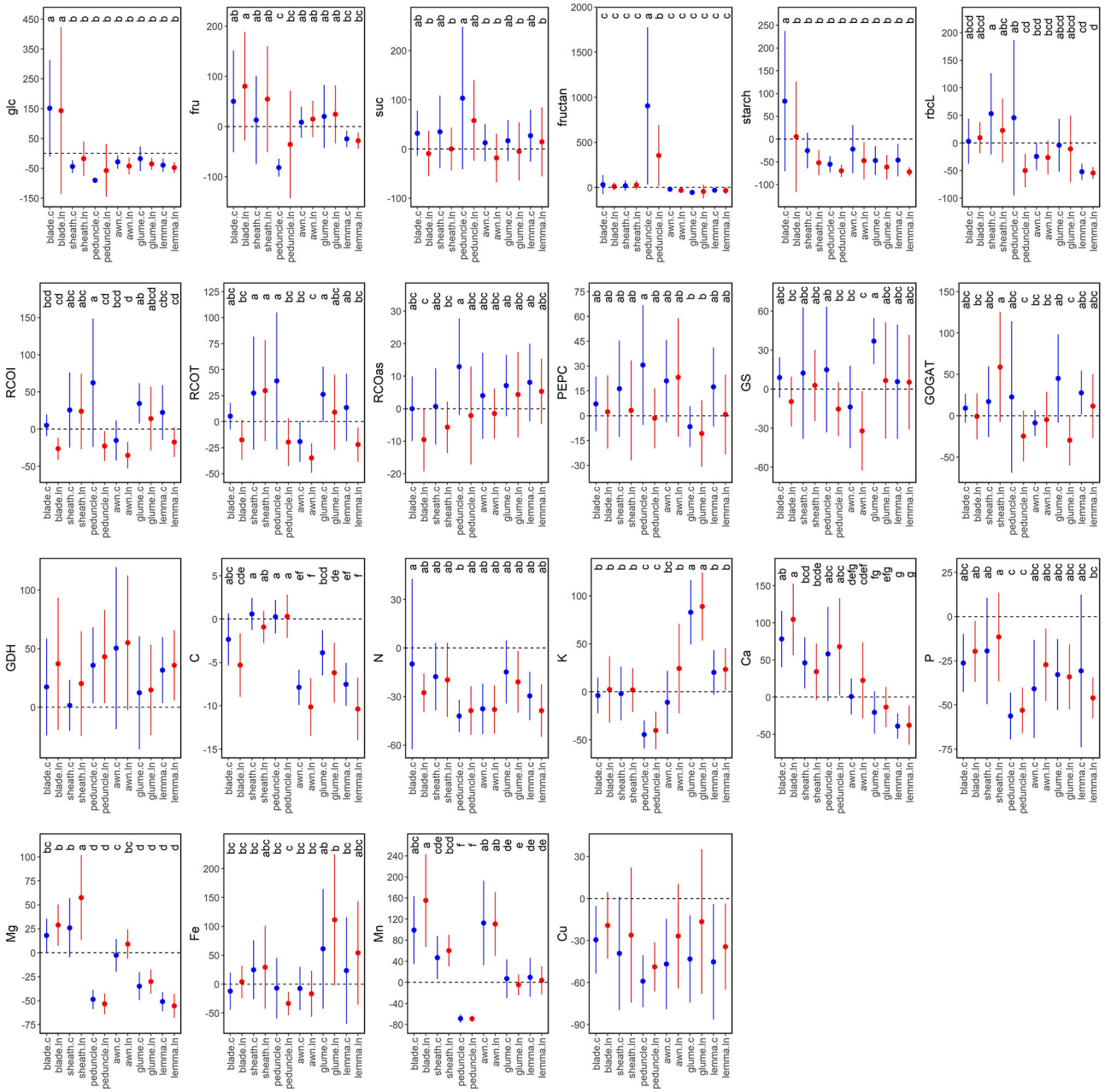

FIGURE 7 | Percentage (%) of variation between anthesis (Zadoks 65, blue) and mid-grain filling (Zadoks 75, red) for the metabolite contents, Rubisco large subunit protein, enzyme activities, and nutrient contents. Each dot is the average of four field-grown durum wheat varieties per organ (blade, sheath, peduncle, awn, glume, and lemma) and N supply (c, control; ln, low N). The different letters differ statistically ($p < 0.05$). The abbreviations are described in **Supplementary Table 1**.

glumes under control N, or decreased in peduncles and glumes under low N. In general, GDH activity was higher at MGF. The nutrients exhibited significant differences between the organs but limited N effects (**Figure 7**). MGF led to a decrease of C in blades and more strongly in ear organs, N, P (more in peduncles), Cu, K, and Mn in peduncles; Ca in ear bracts; and Mg in peduncles and ear bracts, and an increase of K in glumes; Ca in blades, peduncles, and sheaths; Mg in blades and sheaths; Fe in ear bracts; and Mn in blades, sheaths, and awns.

Correlations Between Agronomic Components and Grain Quality Traits With the Metabolic Status of Green Organs

In blades, GY correlated positively with free carbohydrates and negatively with sucrose, fructans, and starch, also observed for biomass (**Figure 8**). Grain protein content was positively associated with total Rubisco and PEPCase activities at MGF, and negatively with Rubisco activation state at anthesis. In sheaths,

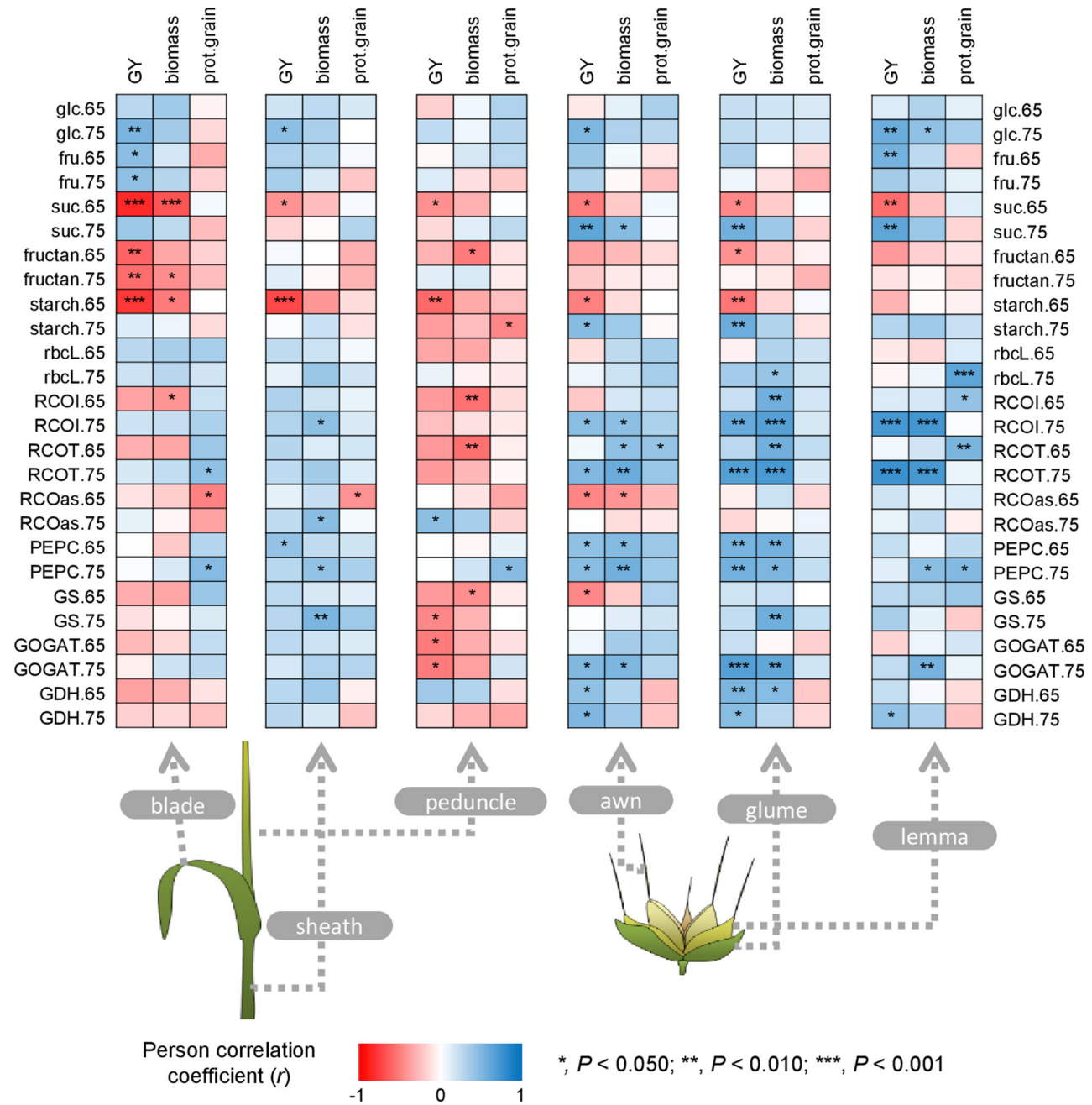

FIGURE 8 | Correlations between metabolic traits in the different green organs at anthesis (Zadoks 65) and mid-grain filling (Zadoks 75) and agronomic components and grain quality traits at harvest. Each point is a Pearson correlation coefficient between two traits (blue, positive correlation; red, negative correlation). Asterisks indicate a significant correlation according to the legend. The abbreviations are described in **Supplementary Table 1**.

GY correlated positively with PEPCase activity at anthesis and glucose content at MGF, and negatively with sucrose and starch contents at anthesis. Biomass correlated with Rubisco, PEPCase, and GS activities at MGF, while grain protein content correlated negatively with Rubisco activation state at anthesis. In peduncles, sucrose, and starch contents at anthesis, GS activity at MGF, and GOGAT activity at both stages correlated negatively with GY. Negative correlations were also observed for biomass and the peduncle biochemical related traits, i.e., fructans, initial and total Rubisco and GS activities at anthesis. Grain protein content only correlated with starch and PEPCase activity at MGF. In awns, glumes, and lemmas, GY generally correlated negatively with sucrose and starch at anthesis and positively with sucrose and starch, initial and total Rubisco and GOGAT activities at MGF,

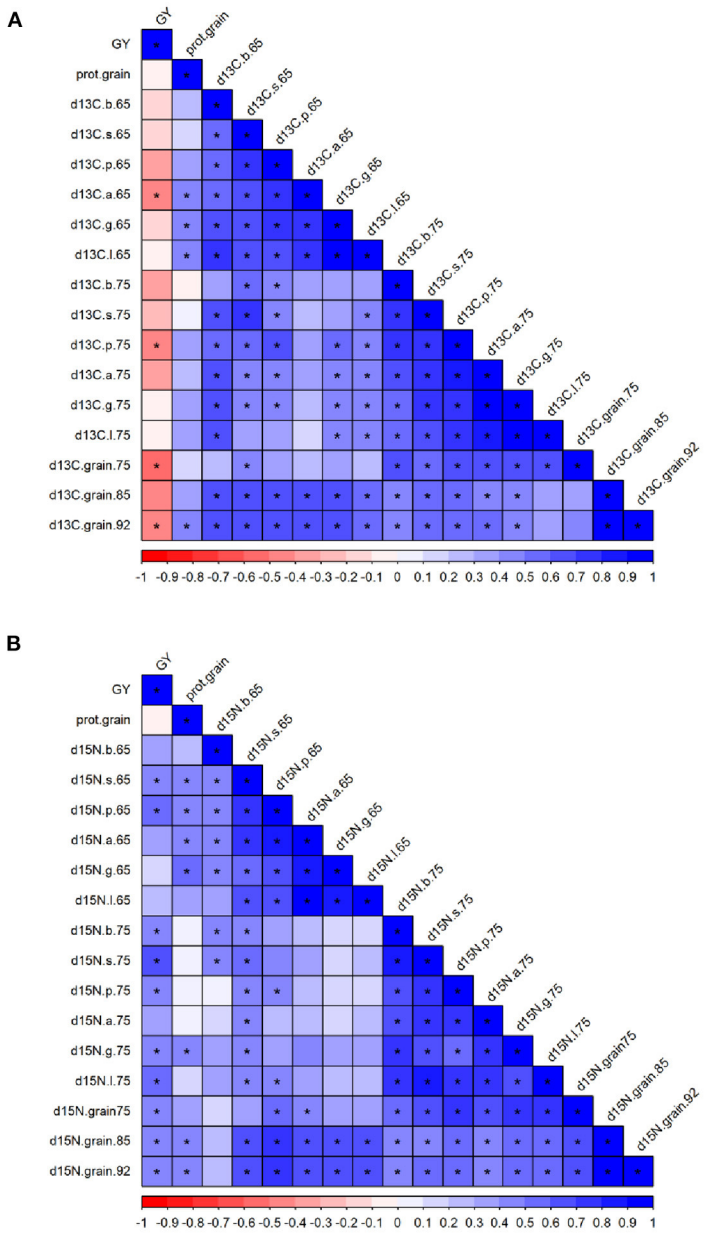

C

Predicted trait (database)	Multivariate model	Estimate	*P*-value	r^2
GY			**0.007**	**0.869**
(d13C)	(Intercept)	-13752		
	d13C.grain.75	-2031	0.002	0.210
	d13C.a.65	-1654	0.003	0.158
	d13C.g.75	2157	0.005	0.088
	d13C.a.75	-2019	0.037	0.062
	d13C.grain.92	8590	0.049	0.061
	d13C.grain.85	-8537	0.041	0.055
	d13C.s.65	1189	0.042	0.047
	d13C.p.65	-932	0.042	0.045
	d13C.b.75	2527	0.023	0.037
	d13C.g.65	1705	0.048	0.035
	d13C.s.75	-2043	0.056	0.028
	d13C.l.65	-1071	0.209	0.024
	d13C.b.65	1081	0.094	0.018
d13C.grain.92			**0.001**	**0.75**
(d13C.organ)	(Intercept)	-7.28		
	d13C.a.65	0.36	0.052	0.182
	d13C.g.65	0.57	0.040	0.169
	d13C.s.75	0.79	0.018	0.129
	d13C.l.65	-0.55	0.086	0.091
	d13C.a.75	0.43	0.141	0.080
	d13C.g.75	-0.47	0.110	0.051
	d13C.b.75	-0.44	0.212	0.049
GY			**0.009**	**0.641**
(d15N)	(Intercept)	5346		
	d15N.s.75	1044	0.119	0.163
	d15N.p.65	1064	0.025	0.157
	d15N.grain.92	3905	0.072	0.089
	d15N.grain.85	-4176	0.073	0.078
	d15N.b.75	-768	0.248	0.069
	d15N.g.75	639	0.229	0.048
	d15N.g.65	-643	0.133	0.038
d15N.grain.92			**0.000**	**0.71**
(d15N.organ)	(Intercept)	0.47		
	d15N.p.65	0.66	0.013	0.308
	d15N.g.65	0.56	0.037	0.212
	d15N.b.75	0.64	0.010	0.143
	d15N.b.65	-0.52	0.034	0.047
prot.grain			**0.001**	**0.736**
(d15N)	(Intercept)	13.48		
	d15N.g.65	2.12	0.006	0.222
	d15N.g.75	1.52	0.024	0.116
	d15N.s.65	1.54	0.009	0.108
	d15N.l.65	-2.25	0.004	0.103
	d15N.grain75	0.69	0.103	0.082
	d15N.b.75	-1.74	0.012	0.069
	d15N.p.75	-1.18	0.102	0.036

FIGURE 9 | The correlation matrix of C **(A)** and N **(B)** isotope composition per organ with grain yield and grain protein content. Asterisks indicate a significant correlation ($p < 0.05$). Multivariate regression models **(C)** explaining grain yield and C and N isotope composition in grain at harvest across varieties under different N supplies. The abbreviations are described in **Supplementary Table 1**.

and PEPCase activity at both growth stages. GY also correlated positively with free carbohydrates in awns and lemmas, and negatively with Rubisco activation state and GS activity in awns at anthesis. Correlations between metabolic traits and biomass in ears were similar to those found for GY, with a remarkable correlation between biomass and Rubisco, PEPCase and GOGAT activities. Grain protein content predominantly correlated with lemma metabolic traits, such as Rubisco protein and Rubisco and PEPCase activities.

We used the isotope signatures of green organs to predict their contribution to grain filling and GY. A high number of significant correlations were observed between the $\delta^{13}C$ of organs and grains (**Figure 9A**). GY correlated negatively with $\delta^{13}C$ of awns at anthesis, peduncles at MGFand grains at MGF and harvest, while grain protein content correlated with $\delta^{13}C$ of awns, glumes, and lemmas at anthesis and grains at harvest. Similar to $\delta^{13}C$, there were a high number of correlations between $\delta^{15}N$ of the organs with the one in grains, GY and grain protein

content (**Figure 9B**). Moreover, we used regression models with the organ-specific isotope compositions to predict GY and grain $\delta^{13}C$, $\delta^{15}N$, and protein content (**Figure 9C**). According to the proportion of variance explained by each predictor (r^2), GY was mainly predicted by $\delta^{13}C$ of grains, awns and glumes, and grain $\delta^{13}C$ at harvest by $\delta^{13}C$ of ear organs and sheaths. Using the $\delta^{15}N$ values, GY was predicted by $\delta^{15}N$ of sheaths, peduncles, grains, blades, and glumes, $\delta^{15}N$ of grains at harvest by $\delta^{15}N$ of peduncles, glumes, and blades, and grain protein content by $\delta^{15}N$ of many organs, predominantly the glumes.

DISCUSSION

We performed a holistic study integrating phenotyping measurements of canopy and flag leaves and biochemical analyses of six foliar and non-foliar photosynthetic organs to identify the traits at the whole plant level, which are related to plant growth, GY, and GQ in field-grown durum wheat. A total of 426 traits were studied in four varieties grown under contrasting N fertilization conditions. The pattern of changes among varieties was similar under both N conditions, as shown by the low G × N interaction. Therefore, we focused our attention mainly on the effects of N and genotypic variability separately.

N Fertilization Has a Significant Effect on Grain Yield and Quality, While Agronomic Differences Between Varieties Were Not Affected by N Availability

An efficient use of N fertilization that meets sustainability is necessary since it is the nutrient that most affects crop production and quality, but it is costly, and its excessive use can cause soil and water pollution (Vicente et al., 2019b; Wang et al., 2021). Then, it is important to identify those physiological and metabolic parameters affected by N, with an impact on GY and GQ. In our study, lower N supply decreased plant biomass by reducing plant height, peduncle length, and tillering, with a direct impact on GY (**Figure 2**). However, under N-limiting conditions, there were less plants per unit area, but they used efficiently their nutrients on producing more ears per plant with larger grains (i.e., higher TGW), as it has been previously shown in barley (Vicente et al., 2019b) and wheat (Liu et al., 2021). Grain protein content is frequently affected by N fertilization (Wang et al., 2021), but our contrasting N levels were not enough to alter it (**Figure 2**). Nevertheless, low N modified moisture content, and sedimentation and yellowness indices, which indicated an impoverishment of grain processing and end-product qualities (Zörb et al., 2018).

The variety with highest GY, Haristide, was characterized by shorter peduncles and longer and heavier ears capable of lodging more grains, parameters associated with higher sink strength (**Figure 2**; **Supplementary Table 2**). Genotypic variability did not alter grain protein content but affected other traits related to grain processing and end-product qualities. The most productive varieties Haristide and Euroduro had higher milling potential (SW), baking quality of wheat flour (sedimentation and yellowness indices) and, only for Haristide, lower gluten strength (GI). In Djouadi et al. (2021), durum wheat yield also correlated with several grain quality traits, but, frequently, a negative correlation is found with grain protein content.

Phenotyping Approaches to Assess the Effect of N and Genotypic Variability on Grain Yield and Quality

Phenotyping approaches are suitable for characterizing plant performance and identifying key attributes for plant growth and production (Kefauver et al., 2017; Vicente et al., 2019b; Prey and Schmidhalter, 2020). We performed ground-based phenotyping to quantify canopy greenness and thus relate it to plant biomass and health (Casadesús et al., 2007; Vergara-Diaz et al., 2016). RGB and spectral indices were good predictors of the N fertilization on green biomass in durum wheat from early stages to maturity (**Figure 3**). These indices tend to saturate at intermediate growth periods, so their use is more valuable at early or late stages, as it happened in our study. Haristide showed a stay-green phenotype compared to the other varieties regardless of the N supply, which implies longer standing photosynthetically active biomass (**Figure 3**). Spectral indices measured at the flag leaf level suggested that Haristide had improved performance due to better N status (NBI index) and lower flavonoid content (**Supplementary Figure 1**), while higher LRWC at anthesis and grain $\delta^{13}C$ indicated a better water status and water use efficiency, respectively (Rebetzke et al., 2002; Araus et al., 2021a).

High-throughput phenotyping has been used to predict yield-related traits in wheat, e.g., using unmanned aerial systems, multispectral cameras, and spectroradiometers (Prey and Schmidhalter, 2020; Garriga et al., 2021; Vatter et al., 2021), but their high cost and user training are drawbacks for their expansion. The vegetative indices used here quantified the greenness by counting pixels in the green-color range or by the spectrum reflected by the vegetation, so their high correlation with biomass and hence GY was not surprising (**Figure 4**). The correlations were higher as growth progressed, indicating that late stages are better for prediction, although this is not an advantage for the use of high-throughput phenotyping in early detection or breeding programs. The best leaf spectral indices for prediction were those estimating flavonoids and N content, which highlighted the relevance of antioxidant capacity and N status for productivity. Thus, the lower flavonoid content of Haristide compared with the other varieties may indicate a reduced need to produce antioxidants to counter the detrimental effects of reactive oxygen species that often occur during stress conditions or senescence (Agati et al., 2020). Canopy indices did not stand out for its prediction of GQ parameters, except for those traits that already correlated with GY (**Figure 4**). However, leaf spectral indices had potential to predict some key GQ traits. In short, our study highlighted the use of low-cost and affordable phenotyping devices (RBG imaging and leaf spectral sensors) to rapidly estimate the effects of N fertilization, to select high-yielding varieties, and to predict GY and GQ.

Nitrogen Fertilization Affects the Uptake and/or Allocation of Micro- and Macronutrients to the Grain, While Ca and Zn Could Play an Important Role in Yield

The concentration of mineral elements in the grain is relevant for GQ and human diet, being determined by the genotype-by-environment interaction (Sanchez-Garcia et al., 2015; Guzmán et al., 2016). The nutrient concentrations varied between N supplies and varieties, with few significant G × N interactions (**Figure 5**). Higher N supply quantitatively increased grain N and thus protein yields, and the uptake and/or allocation of nutrients, such as C, S, Fe, P, Cu, and Mn to the grain. This may be associated with a promotion of root growth under higher N supply that favors the nutrients uptake, as suggested by Mariem et al. (2020). Nevertheless, an assessment of its cost benefit and associated environmental pollution is crucial when selecting the best application rate and timing (Kefauver et al., 2017; Vicente et al., 2019b).

The high-yielding Haristide had higher yields of most nutrients than the other varieties, indicating higher uptake of nutrients from the soil, regardless of nutrient concentration (**Figure 5**). Anyway, the concentration of nutrients in the grain is an important factor affecting the quality parameters by which wheat flours are graded. Haristide was mainly distinguished from the other varieties by a significantly higher Ca and lower Zn concentration, being Ca mainly accumulated in blades (**Supplementary Table 2**). Brennan et al. (2007) reported that Ca application had a direct impact on wheat yields, which can suggest that its better uptake in Haristide could be a key factor to increase production. Indeed, Ca may modulate the absorption and translocation of several elements and maintain the integrity of selective ion transport proteins (Cobalchin et al., 2021). Lower Zn content in Haristide, irrespective of N supply, could suggest a poor root uptake or remobilization from shoots to grains (Liu et al., 2019), which is relevant for human diet to avoid symptoms, such as loss of appetite, growth retardation, rough and peeling skin, and immune system dysfunction (Wang et al., 2020). Uauy et al. (2006) showed that delayed senescence may decrease N, Fe, and Zn content in the grain. Haristide showed a stay-green phenotype, which might explain the lower Zn content found in this variety. In conclusion, N fertilization is crucial to stimulate nutrient uptake, while higher GY was associated with better Ca status but lower Zn.

Canopy Photosynthesis, N Assimilation, and C-N Allocation to the Grain Are the Result of a Common Effort of the Green Organs of the Plant

After characterizing wheat agronomy and canopy, we focused on the metabolism of green photosynthetic organs and their impact on GY and GQ. We hypothesized that non-foliar green organs have special physiological and metabolic features that make them suitable as source organs during grain filling, at least to complement the contribution of the flag leaf. This role has been predicted through other approaches under optimal and, more significantly, under stress conditions (Sanchez-Bragado et al., 2014a,b, 2016, 2020b; Vicente et al., 2018b), although the precise metabolic pathways operating in each part are poorly understood. Multivariate analysis of metabolic and mineral traits indicated that the metabolism in the blades was, undoubtedly, the most active (**Figure 6**). It was followed by the awns, albeit by a wide margin. The different ear bracts, which were very similar to each other, had a similar behavior to the awns. The peduncles and the sheaths were separated from the rest of the organs, suggesting they might have similar functions. Based on the PCA-centroids distribution of **Supplementary Figure 2**, it seems that N effect was more relevant on blades and less on bracts. Nevertheless, the differences were not very large, while Sanchez-Bragado et al. (2014a) found that the whole ear performance and contribution to grain filling improved under high N fertilization.

We measured different metabolism traits, such as Rubisco protein and activity, and the amount of photoassimilates, as an alternative to previous approaches to characterize photosynthetic capacity of non-foliar organs to GY, which were frequently intrusive or causing compensatory effects (Sanchez-Bragado et al., 2016; Rivera-Amado et al., 2020). The protein content and activities of Rubisco, directly involved in the fixation of atmospheric CO_2, were significantly higher in blades, but not negligible in other organs, such as the awns, demonstrating active photosynthetic capacities at late stages, including a high degree of activation state in ear organs (**Supplementary Table 2**). Higher PEPCase activity was shown in blades and awns, which was associated with their higher photosynthetic capacity and the need to process the C fixed, but the activities in the other organs were remarkable (**Supplementary Table 2**). This enzyme is involved in the balance of C and N metabolism by regulating the synthesis of C skeletons for the synthesis and nitrogenous compounds and its possible role in the re-assimilation of CO_2, such as grain respiration (Jia et al., 2015; Shi et al., 2015; Sanchez-Bragado et al., 2020b). Sucrose, which is the main compound used to transport C in cereals (Vicente et al., 2016; Al-Sheikh Ahmed et al., 2020), was highly abundant in all the green organs studied, which could be explained more by their photosynthetic capacity than by sucrose transport. The peduncles and the sheaths were, clearly, the organs where fructans accumulated (**Figure 6**), suggesting their predominant storage function. Takahashi et al. (2001) proposed a long-term storage function in peduncles and short-term in sheaths, involved in diel fluctuations. Starch, a minor storage carbohydrate in wheat (Scofield et al., 2009), is accumulated mainly in blades and, later, in ear organs. Glucose and fructose were predominantly abundant in sheaths and peduncles at earlier stages and in ear organs at both growth stages. The free carbohydrates are frequently derivate from the breakdown of other carbohydrates to transport C through the plant (Cimini et al., 2015), which could indicate that sheaths and peduncles provided C at anthesis (e.g. C from blades), and ears at grain filling. The ear is the youngest organ in the plant, so its delayed senescence (Jia et al., 2015; Vicente et al., 2018b; Tambussi et al., 2021) may indicate that ear organs play a more active role at later stages. According to Takahashi et al. (2001), from late grain-filling, any new assimilate is used for grain growth. These results indicated that not only the blades

but any of the green organs are actively contributing to canopy photosynthesis with an impact on yield. Previous studies pointed out that the photosynthesis of non-laminar organs, mainly the ears, significantly contributed to canopy photosynthesis and, then, GY (Maydup et al., 2010; Jia et al., 2015; Gámez et al., 2020; Araus et al., 2021b). Gross ear photosynthesis was ∼56% of leaf photosynthesis on an area basis (Molero and Reynolds, 2020), while net photosynthesis may be much higher if we subtract the high ear respiration (Gámez et al., 2020; Tambussi et al., 2021) or consider the larger ear area (Olszewski et al., 2018; Sanchez-Bragado et al., 2020b), making ear photosynthesis a promising target for crop improvement.

A previous study suggested that 42% of the N in grains was coming from the ears, using N isotope signatures (Sanchez-Bragado et al., 2017). We combined measurements of N content, isotope composition, and enzyme activities to deepen into N metabolism at the whole plant level. The enzyme profiles revealed active N metabolism functioning in every organ, with higher levels of GS and GOGAT in blades and awns, and GDH in blades and lemmas (**Figure 6**). It may indicate that an important part of N metabolism takes place outside the blades, corroborating at the biochemical level's previous results (Lopes et al., 2006; Sanchez-Bragado et al., 2017). The high GDH activities in ears and, particularly, in lemmas may suggest an important role in plant glutamate homeostasis, involved in C-N signaling (Labboun et al., 2009) and, given their proximity to grains, in the N supply for grain filling at late stages. Organ-specific N levels followed a similar trend that Rubisco traits (high in blades and awns), mainly due to the fact that Rubisco and other photosynthetic structures require a high N budget (Evans and Clarke, 2019). The rest of the nutrients also had higher levels in blades, but very high levels of Fe in the glumes were observed. Fe is essential for photosynthetic processes, heme biosynthesis, and Fe-S cluster assembly (Morrissey and Guerinot, 2009), but its specific role in glumes remains unclear and should be further investigated.

Lower N fertilization significantly inhibited photosynthetic capacity and N assimilation at the whole plant level, except for an upregulation in the peduncle during anthesis (**Supplementary Table 2**). It also promoted the storage of C in peduncles, as reported previously in bread wheat (Scofield et al., 2009), while the high decrease of sucrose and starch levels in ear organs at MGF may suggest that either (i) the ears decreased their capacity to supply C to the grain or other organs under low N, or (ii) most of the C produced is sent out due to the high demand of heterotrophic tissues. Our isotopic results and those of Sanchez-Bragado et al. (2017), together with the better activation state of Rubisco at late stages (**Figure 7**), pointed to the latter.

Metabolic and Nutrient Changes Between Anthesis and Mid-Grain Filling Point to the Specialization of Each Green Organ in the Later Growth Stages

The clear increase in free carbohydrates at MGF in blades may suggest that different C-rich cellular components are degraded to provide nutrients to other organs (**Figure 7**). The decrease of fructose and the drastic increase of fructan levels in peduncles at MGF may indicate that this organ is actively accumulating C, which will be probably used when plant photosynthesis ceases at the end of grain filling (Takahashi et al., 2001). These changes were not observed in sheaths, which could support the hypothesis that they participate more in the diurnal accumulation of fructans (Takahashi et al., 2001). Furthermore, CO_2 fixation by Rubisco was improved at MGF in sheaths, glumes, and, only at control N, in peduncles and lemmas, suggesting a relevant photosynthetic contribution at late stages. The increased Rubisco activity in ears was due to an increase in its activation state, even though protein levels decreased. We hypothesize that these organs may have redistributed efficiently the N stored in this enzyme to other limiting processes. Interestingly, Kanno et al. (2017) observed that rice mutants with lower Rubisco content improved N use efficiency and photosynthesis. While N decreased at MGF in every organ, GDH tended to increase, suggesting that it may act predominantly deaminating glutamate at late stages and, then, reallocating N to the developing grains (Labboun et al., 2009). Low N supply had a clear effect on reducing C assimilation through the observed changes in sucrose levels and Rubisco activation state at the whole plant level, reflecting the strong coordination between C and N metabolism (Vicente et al., 2018a). In general, low N also inhibited PEPCase, GS, and GOGAT activities, probably by limiting their substrate concentrations. In parallel to N, P and Cu also decreased at MGF. The changes in K, Ca, Mg, Fe, and Mn were organ specific. Meanwhile, C decreased in blades and, more significantly, in ear organs, which may suggest a high C contribution of ears at late stages to the developing grains. Overall, the pattern of changes between anthesis and MGF suggested that each organ evolves in a different way, indicating diverse but complementary roles for the control of starch and protein deposition to the grain during the grain-filling phase.

Linear and Stepwise Regressions Highlight the Key Role of Ear Metabolic Traits and Blade Carbohydrates for Durum Wheat Growth and Productivity

Although correlations do not imply cause-effect relationships, we used them to determine the possible contribution of the different photosynthetic organs to grain filling and to identify key traits (**Figure 8**). Accumulation of free carbohydrates and lower sucrose, starch, and fructan contents was positively associated with GY, mainly in blades and the different ear organs. It clearly highlighted that higher productivity is linked to rapid translocation of photoassimilates, predominantly for grain filling since plant growth is ceased at late stages (**Figure 3**). Oppositely, sucrose was positively correlated with GY in ear organs at MGF, suggesting again ears as key C sources for grains. Apart from carbohydrate metabolism, it was surprising that other metabolic traits in blades were not associated with GY (**Figure 7**). However, GY and biomass were linked to a more active C and N metabolism in awns, glumes, and lemmas, as observed with the concomitant association of Rubisco, PEPCase, and sucrose at late stages with GY. The high contribution of ears

to grain filling may be related to its proximity to the grain, delayed senescence, higher light harvesting at the top of the canopy, or even its putative capacity to reassimilate respired CO_2 (Sanchez-Bragado et al., 2020b; Tambussi et al., 2021). Whether awn metabolism or, particularly, its photosynthetic capacity is relevant for GY has been controversial (Sanchez-Bragado et al., 2020a). Our results do suggest this at the biochemical level. Based on the correlations, the sheath appeared to be an organ that performed functions more oriented for plant growth, while the metabolic traits of the peduncle did not have a considerable impact on yield or biomass, even negative correlations between these parameters were observed (**Figure 7**). This may be associated with the advantage of shorter varieties (i.e., peduncles or stems), which favors the contribution of ears to grain filling (Tambussi et al., 2021). The only study to our knowledge, comparing leaf and whole-ear photosynthesis with GY, suggested that the latter correlated better than the former (Abbad et al., 2004). We previously found that Rubisco gene expression in durum wheat ears and leaves, as well as several N-metabolism-related genes, was correlated with higher productivity (Vicente et al., 2018b). Moreover, Vergara-Diaz et al. (2020a) proved that leaf, glume, and lemma metabolomes were determinant for GY in durum wheat. Lastly, Shokat et al. (2020) also reported that antioxidant and C metabolism enzymes in leaves and whole ears correlated with yield traits in bread wheat.

The similarity of the isotope compositions between green organs and grains at harvest has been used as a non-intrusive technique to estimate the relative organ contribution to grain filling (Sanchez-Bragado et al., 2014b, 2017; Tambussi et al., 2021). Our models suggested that the supply of C and N to the grains was, to some extent, due to the contribution of the different organs (**Figure 9**). Moreover, the relative contribution of C from non-foliar organs, in particular the ear organs, stood out above the rest, while, for N, the contribution was more varied in terms of plant parts. Protein content, considered as the most important GQ trait, was mainly associated with the metabolism of lemmas and blades (**Figure 8**), while the isotope signatures suggested a key role also for glumes (**Figure 9**).

CONCLUSIONS

We highlight that our novel characterization of key enzymes activities in six different green organs, together with carbohydrate profiles, mineral compositions, natural isotope compositions, and plant canopy monitoring, was an integrative approach to identify metabolic and physiological targets involved in grain filling. The primary metabolism of green organs suggested that all have important functions in contributing to early and late grain filling. Although, in absolute terms, the blades presented the greatest metabolic activity among the green organs, only their carbohydrate metabolism was associated with GY. The pattern of correlations between key enzyme activities and sucrose in ear organs with GY emphasized the key role of ears during grain filling at the metabolic level (Sanchez-Bragado et al., 2014b, 2017; Vicente et al., 2018b; Shokat et al., 2020; Vergara-Diaz et al., 2020b). Our results showed that, regardless of the N supply, high yield was associated with plants with shorter peduncles and longer ears (high sink strength), stay-green phenotype with more photosynthetically active biomass at late-growth stages, better leaf water and N status, and more active ear metabolism, particularly at MGF (i.e., higher Rubisco, PEPCase, GOGAT, and GDH activities). This study opens the doors to investigate on a larger population of varieties of the molecular and morphological mechanisms operating in non-foliar photosynthetic organs that impact GY and GQ. We predict that advances in organ-specific high-throughput phenotyping and metabolic regulation of source-sink dynamics will strongly contribute to crop improvement under optimal and unfavorable environments, highlighting the need of including ear photosynthesis in the breeding programs as a new target for crop improvement.

DATA AVAILABILITY STATEMENT

The raw data supporting the conclusions of this article will be made available by the authors, without undue reservation.

AUTHOR CONTRIBUTIONS

RV, NA, and JA conceived and supervised the project. RM-P and NA performed the field trials. RM-P prepared the samples and carried out most of the measurements, with help from AS, MH, BE, and RV for enzyme assays, MN-T for grain quality traits, and RM for carbohydrates content and grain nutrient composition. RV and RM-P performed the analyses and designed the tables and figures. RV wrote the manuscript with the assistance of RM-P. All the authors provided critical feedback and contributed to the final manuscript.

FUNDING

This study was supported by the projects AGL2016-76527-R and PID2019-106650RB-C22, funded by the Spanish Ministry of Science and Innovation, and the projects CSI260P20 and CLU-2019-05-IRNASA/CSIC Unit of Excellence funded by the Junta de Castilla y León and co-financed by the European Union (ERDF). We also acknowledge the support of FCT—Fundaçãopara a Ciência e a Tecnologia, I.P., through the R&D Unit GREEN-IT -Bioresources for Sustainability (UIDB/04551/2020 and UIDP/04551/2020). RMP was the recipient of an FPI-INIA fellowship from the Spanish Ministry of Science and Innovation (CPD2016-0107).

ACKNOWLEDGMENTS

We thank the staff from the station of Zamadueñas (ITACyL) for their support during the crop season and technical assistance, especially to B. Gil-Pérez, Y. Pallavicini, M. C. Diez-Fraile, and I. Araus-González. We also thank F.Z. Rezzouk from University

of Barcelona for her support with isotope analyses. Finally, we are also grateful to the staff from IRNASA for their technical assistance with carbohydrate and nutrient composition analyses, particularly to E. Marcos-Barbero for his willingness to help with statistical and ICP analyses.

SUPPLEMENTARY MATERIAL

The Supplementary Material for this article can be found online at: https://www.frontiersin.org/articles/10.3389/fpls.2022.869680/full#supplementary-material

REFERENCES

Abbad, H., El Jaafari, S., Bort, J., and Araus, J. L. (2004). Comparison of flag leaf and ear photosynthesis with biomass and grain yield of durum wheat under various water conditions and genotypes. *Agronomie* 24, 19–28. doi: 10.1051/agro:2003056

Agati, G., Brunetti, C., Fini, A., Gori, A., Guidi, L., Landi, M., et al. (2020). Are flavonoids effective antioxidants in plants? twenty years of our investigat*ion. Antioxidants* 9, 1098. doi: 10.3390/antiox9111098

Al-Sheikh Ahmed, S., Zhang, J., Farhan, H., Zhang, Y., Yu, Z., Islam, S., et al. (2020). Diurnal changes in water soluble arbohydrate omponents in leaves and sucrose associated *TaSUT1* gene expression during grain development in wheat. *Int. J. Mol. Sci.* 21, 276. doi: 10.3390/ijms21218276

Araus, J. L., Kefauver, S. C., Díaz, O. V., Gracia-Romero, A., Rezzouk, F. Z., Segarra, J., et al. (2021a). Crop phenotyping in a context of global change: what to measure and how to do it. *J. Integr. Plant Biol. (in press)*. 64, 592–618. doi: 10.1111/jipb.13191

Araus, J. L., Sanchez-Bragado, R., and Vicente, R. (2021b). Improving crop yield and resilience through photosynthesis optimisation: panacea or pipe dream? *J. Experiment. Bot.* 72, 3936–3955. doi: 10.1093/jxb/erab097

Axford, D. W. E., Mcdermott, E. E., and Redman, D. G. (1978). Small scale tests of bread making quality. *Milling Feed Fert.* 161, 18–20.

Beres, B. L., Rahmani, E., Clarke, J. M., Grassini, P., Pozniak, C. J., Geddes, C. M., et al. (2020). A systematic review of durum wheat: enhancing production systems by exploring genotype, environment, and management (G × E × M) synergies. *Front. Plant Sci.* 11, 1665. doi: 10.3389/fpls.2020.568657

Brennan, R. F., Bolland, M. D. A., and Walton, G. H. (2007). Comparing the calcium requirements of wheat and canola. *J. Plant Nutr.* 30, 1167–1184. doi: 10.1080/01904160701394642

Casadesús, J., Kaya, Y., Bort, J., Nachit, M. M., Araus, J. L., Amor, S., et al. (2007). Using vegetation indices derived from conventional digital cameras as selection criteria for wheat breeding in water-limited environments. *Ann. Appl. Biol.* 150, 227–236. doi: 10.1111/j.1744-7348.2007.00116.x

Chairi, F., Vergara-Diaz, O., Vatter, T., Aparicio, N., Nieto-Taladriz, M. T., Kefauver, S. C., et al. (2018). Post-green revolution genetic advance in durum wheat: the case of Spain. *Field Crops Res.* 228, 158–169. doi: 10.1016/j.fcr.2018.09.003

Cimini, S., Locato, V., Vergauwen, R., Paradiso, A., Cecchini, C., Vandenpoel, L., et al. (2015). Fructan biosynthesis and degradation as part of plant metabolism controlling sugar fluxes during durum wheat kernel maturation. *Front. Plant Sci.* 6, 89–89. doi: 10.3389/fpls.2015.00089

Cobalchin, F., Volpato, M., Modena, A., Finotti, L., Manni, F., Panozzo, A., et al. (2021). Biofortification of common wheat grains with combined Ca, Mg, and K through foliar fertilisation. *Agronomy* 11, 1718. doi: 10.3390/agronomy11091718

Del Pozo, A., Matus, I., Ruf, K., Castillo, D., Méndez-Espinoza, A. M., and Serret, M. D. (2019). Genetic advance of durum wheat under high yielding conditions: the case of Chile. *Agronomy* 9, 454. doi: 10.3390/agronomy9080454

Del Pozo, A., Yañez, A., Matus, I. A., Tapia, G., Castillo, D., Sanchez-Jardón, L., et al. (2016). Physiological traits associated with wheat yield potential and performance under water-stress in a Mediterranean environment. *Front. Plant. Sci.* 7, 987. doi: 10.3389/fpls.2016.00987

Djouadi, K., Mekliche, A., Dahmani, S., Ladjiar, N. I., Abid, Y., Silarbi, Z., et al. (2021). Durum wheat yield and grain quality in early transition from conventional to conservation tillage in semi-arid Mediterranean conditions. *Agriculture* 11, 711. doi: 10.3390/agriculture11080711

Estévez-Geffriaud, V., Vicente, R., Vergara-Díaz, O., Narváez Reinaldo, J. J., and Trillas, M. I. (2020). Application of *Trichoderma asperellum* T34 on maize (*Zea mays*) seeds protects against drought stress. *Planta* 252, 8. doi: 10.1007/s00425-020-03404-3

Evans, J. R., and Clarke, V. C. (2019). The nitrogen cost of photosynthesis. *J. Exp. Bot.* 70, 7–15. doi: 10.1093/jxb/ery366

Gámez, A. L., Vicente, R., Sanchez-Bragado, R., Jauregui, I., Morcuende, R., Goicoechea, N., et al. (2020). Differential flag leaf and ear photosynthetic performance under elevated (CO_2) conditions during grain filling period in durum wheat. *Front. Plant. Sci.* 11, 2064. doi: 10.3389/fpls.2020.587958

Garriga, M., Romero-Bravo, S., Estrada, F., Méndez-Espinoza, A. M., González-Martínez, L., Matus, I. A., et al. (2021). Estimating carbon isotope discrimination and grain yield of bread wheat grown under water-limited and full irrigation conditions by hyperspectral canopy reflectance and multilinear regression analysis. *Int. J. Remote Sens.* 42, 2848–2871. doi: 10.1080/01431161.2020.1854888

Gibon, Y., Blaesing, O. E., Hannemann, J., Carillo, P., Höhne, M., Hendriks, J. H. M., et al. (2004). A robot-based platform to measure multiple enzyme activities in Arabidopsis using a set of cycling assays: comparison of changes of enzyme activities and transcript levels during diurnal cycles and in prolonged darkness. *Plant Cell* 16, 3304–3325. doi: 10.1105/tpc.104.025973

Guzmán, C., Autrique, J. E., Mondal, S., Singh, R. P., Govindan, V., Morales-Dorantes, A., et al. (2016). Response to drought and heat stress on wheat quality, with special emphasis on bread-making quality, in durum wheat. *Field Crops Res.* 186, 157–165. doi: 10.1016/j.fcr.2015.12.002

IPCC (2013). "Climate change 2013: the physical science basis," in *Contribution of Working Group I to the Fifth Assessment Report of the Intergovernmental Panel on Climate Change*. New York, NY: Cambridge University Press.

Jia, S., Lv, J., Jiang, S., Liang, T., Liu, C., and Jing, Z. (2015). Response of wheat ear photosynthesis and photosynthate carbon distribution to water deficit. *Photosynthetica* 53, 95–109. doi: 10.1007/s11099-015-0087-4

Kanno, K., Suzuki, Y., and Makino, A. (2017). A small decrease in Rubisco content by individual suppression of *RBCS* genes leads to improvement of photosynthesis and greater biomass production in rice under conditions of elevated CO_2. *Plant Cell Physiol.* 58, 635–642. doi: 10.1093/pcp/pcx018

Kefauver, S. C., Vicente, R., Vergara-Diaz, O., Fernández-Gallego, J. A., Kerfal, S., López, A., et al. (2017). Comparative UAV and field phenotyping to assess yield and nitrogen use efficiency in hybrid and conventional barley. *Front. Plant. Sci.* 8, 1733. doi: 10.3389/fpls.2017.01733

Labboun, S., Tercé-Laforgue, T., Roscher, A., Bedu, M., Restivo, F. M., Velanis, C. N., et al. (2009). Resolving the role of plant glutamate dehydrogenase. *I.* in vivo real time nuclear magnetic resonance spectroscopy experiments. *Plant Cell Physiol.* 50, 1761–1773. doi: 10.1093/pcp/pcp118

Liu, D.-Y., Liu, Y.-M., Zhang, W., Chen, X.-P., and Zou, C.-Q. (2019). Zinc uptake, translocation, and remobilization in winter wheat as affected by soil application of Zn fertilizer. *Front. Plant Sci.* 10, 426. doi: 10.3389/fpls.2019.00426

Liu, Y., Liao, Y., and Liu, W. (2021). High nitrogen application rate and planting density reduce wheat grain yield by reducing filling rate of inferior grain in middle spikelets. *Crop J.* 9, 412–426. doi: 10.1016/j.cj.2020.06.013

Lopes, M. S., Cortadellas, N., Kichey, T., Dubois, F., Habash, D. Z., and Araus, J. L. (2006). Wheat nitrogen metabolism during grain filling: comparative role of glumes and the flag leaf. *Planta* 225, 165–181. doi: 10.1007/s00425-006-0338-5

Mariem, S. B., González-Torralba, J., Collar, C., Aranjuelo, I., and Morales, F. (2020). Durum wheat grain yield and quality under low and High nitrogen conditions: insights into natural variation in low- and high-yielding genotypes. *Plants* 9, 1636. doi: 10.3390/plants9121636

Maydup, M. L., Antonietta, M., Guiamet, J. J., Graciano, C., López, J. R., and Tambussi, E. A. (2010). The contribution of ear photosynthesis to grain filling in bread wheat (*Triticum aestivum* L.). *Field Crops Res.* 119, 48–58. doi: 10.1016/j.fcr.2010.06.014

Medina, S., Vicente, R., Amador, A., and Araus, J. L. (2016). Interactive effects of elevated [CO_2] and water stress on physiological traits and gene expression during vegetative growth in four durum wheat genotypes. *Front. Plant Sci.* 7, 1738. doi: 10.3389/fpls.2016.01738

Molero, G., and Reynolds, M. P. (2020). Spike photosynthesis measured at high throughput indicates genetic variation independent of flag leaf photosynthesis. *Field Crops Res.* 255, 107866. doi: 10.1016/j.fcr.2020.107866

Morcuende, R., Kostadinova, S., Pérez, P., Martín Del Molino, I. M., and Martínez-Carrasco, R. (2004). Nitrate is a negative signal for fructan synthesis, and the fructosyltransferase-inducing trehalose inhibits nitrogen and carbon assimilation in excised barley leaves. *New Phytol.* 161, 749–759. doi: 10.1046/j.1469-8137.2004.00990.x

Morrissey, J., and Guerinot, M. L. (2009). Iron uptake and transport in plants: the good, the bad, and the ionome. *Chem. Rev.* 109, 4553–4567. doi: 10.1021/cr900112r

Olszewski, J., Makowska, M., Pszczółkowska, A., Okorski, A., and Bieniaszewski, T. (2018). The effect of nitrogen fertilization on flag leaf and ear photosynthesis and grain yield of spring wheat. *Plant Soil Environ.* 60, 531–536. doi: 10.17221/880/2013-PSE

Pérez, P., Rabnecz, G., Laufer, Z., Gutiérrez, D., Tuba, Z., and Martínez-Carrasco, R. (2011). Restoration of photosystem II photochemistry and carbon assimilation and related changes in chlorophyll and protein contents during the rehydration of desiccated *Xerophyta scabrida* leaves. *J. Exp. Bot.* 62, 895. doi: 10.1093/jxb/erq317

Prey, L., and Schmidhalter, U. (2020). Deep phenotyping of yield-related traits in wheat. *Agronomy* 10, 603. doi: 10.3390/agronomy10040603

Ray, D. K., Mueller, N. D., West, P. C., and Foley, J. A. (2013). Yield trends are insufficient to double global crop production by 2050. *PLoS One* 8, e66428. doi: 10.1371/journal.pone.0066428

Rebetzke, G. J., Condon, A. G., Richards, R. A., and Farquhar, G. D. (2002). Selection for reduced carbon isotope discrimination increases aerial biomass and grain yield of rainfed bread wheat. *Crop Sci.* 42, 739–745. doi: 10.2135/cropsci2002.7390

Rivera-Amado, C., Molero, G., Trujillo-Negrellos, E., Reynolds, M., and Foulkes, J. (2020). Estimating organ contribution to grain filling and potential for source upregulation in wheat cultivars with a contrasting source–sink balance. *Agronomy* 10, 1527. doi: 10.3390/agronomy10101527

Royo, C., Soriano, J. M., and Álvaro, F. (2017). "Wheat: a crop in the bottom of the Mediterranean diet pyramid," in *Mediterranean Identities - Environment, Society, Culture,* ed B. Fuerst-Bjeliš. (Rijeka: InTech), pp. 381–399.

Sanchez-Bragado, R., Elazab, A., Zhou, B., Serret, M. D., Bort, J., Nieto-Taladriz, M. T., et al. (2014a). Contribution of the ear and the flag leaf to grain filling in durum wheat inferred from the carbon isotope signature: genotypic and growing conditions effects. *J. Integr. Plant Biol.* 56, 444–454. doi: 10.1111/jipb.12106

Sanchez-Bragado, R., Kim, J. W., Rivera-Amado, C., Molero, G., Araus, J. L., Savin, R., et al. (2020a). Are awns truly relevant for wheat yields? a study of performance of awned/awnless isogenic lines and their response to source–sink manipulations. *Field Crops Res.* 254, 107827. doi: 10.1016/j.fcr.2020.107827

Sanchez-Bragado, R., Molero, G., Reynolds, M. P., and Araus, J. L. (2014b). Relative contribution of shoot and ear photosynthesis to grain filling in wheat under good agronomical conditions assessed by differential organ $\delta^{13}C$. *J. Exp. Bot.* 65, 5401–5413. doi: 10.1093/jxb/eru298

Sanchez-Bragado, R., Molero, G., Reynolds, M. P., and Araus, J. L. (2016). Photosynthetic contribution of the ear to grain filling in wheat: a comparison of different methodologies for evaluation. *J. Exp. Bot.* 67, 2787–2798. doi: 10.1093/jxb/erw116

Sanchez-Bragado, R., Serret, M. D., and Araus, J. L. (2017). The nitrogen contribution of different plant parts to wheat grains: exploring genotype, water, and nitrogen effects. *Front. Plant Sci.* 7, 1986. doi: 10.3389/fpls.2016.01986

Sanchez-Bragado, R., Vicente, R., Molero, G., Serret, M. D., Maydup, M. L., and Araus, J. L. (2020b). New avenues for increasing yield and stability in C_3 cereals: exploring ear photosynthesis. *Curr. Opin. Plant Biol.* 56, 223–234. doi: 10.1016/j.pbi.2020.01.001

Sanchez-Garcia, M., Álvaro, F., Peremarti, A., Martín-Sánchez, J. A., and Royo, C. (2015). Changes in bread-making quality attributes of bread wheat varieties cultivated in Spain during the 20th century. *Euro. J. Agron.* 63, 79–88. doi: 10.1016/j.eja.2014.11.006

Scofield, G. N., Ruuska, S. A., Aoki, N., Lewis, D. C., Tabe, L. M., and Jenkins, C. L. D. (2009). Starch storage in the stems of wheat plants: localization and temporal changes. *Ann. Bot.* 103, 859–868. doi: 10.1093/aob/mcp010

Shi, J., Yi, K., Liu, Y., Xie, L., Zhou, Z., Chen, Y., et al. (2015). Phosphoenolpyruvate carboxylase in Arabidopsis leaves plays a crucial role in carbon and nitrogen metabolism. *Plant Physiol.* 167, 671–681. doi: 10.1104/pp.114.254474

Shokat, S., Großkinsky, D. K., Roitsch, T., and Liu, F. (2020). Activities of leaf and spike carbohydrate-metabolic and antioxidant enzymes are linked with yield performance in three spring wheat genotypes grown under well-watered and drought conditions. *BMC Plant Biol.* 20, 400. doi: 10.1186/s12870-020-02581-3

Stitt, M., Lilley, R., Gerhardt, R., and Heldt, H. (1989). Metabolite levels in specific cells and subcellular compartments of plant leaves. *Methods Enzymol.* 174, 518–552. doi: 10.1016/0076-6879(89)74035-0

Sulpice, R., Tschoep, H., Von Korff, M., Büssis, D., Usadel, B., Höhne, M., et al. (2007). Description and applications of a rapid and sensitive non-radioactive microplate-based assay for maximum and initial activity of D-ribulose-1,5-bisphosphate carboxylase/oxygenase. *Plant Cell Environ.* 30, 1163–1175. doi: 10.1111/j.1365-3040.2007.01679.x

Takahashi, T., Chevalier, P., and Rupp, R. (2001). Storage and remobilization of soluble carbohydrates after heading in different plant parts of a winter wheat cultivar. *Plant Prod Sci* 4, 160–165. doi: 10.1626/pps.4.160

Tambussi, E. A., Maydup, M. L., Carrión, C. A., Guiamet, J. J., and Araus, J. L. (2021). Ear photosynthesis in C_3 cereals and its contribution to grain yield: methodologies, controversies, and perspectives. *J. Exp. Bot.* 72, 3956–3970. doi: 10.1093/jxb/erab125

Uauy, C., Distelfeld, A., Fahima, T., Blechl, A., and Dubcovsky, J. (2006). A NAC gene regulating senescence improves grain protein, zinc, and iron content in wheat. *Science* 314, 1298–1301. doi: 10.1126/science.1133649

Vatter, T., Gracia-Romero, A., Kefauver, S. C., Nieto-Taladriz, M. T., Aparicio, N., and Araus, J. L. (2021). Preharvest phenotypic prediction of grain quality and yield of durum wheat using multispectral imaging. *Plant J. (in press).* 109, 1507–1518. doi: 10.1111/tpj.15648

Vergara-Diaz, O., Vatter, T., Kefauver, S. C., Obata, T., Fernie, A. R., and Araus, J. L. (2020a). Assessing durum wheat ear and leaf metabolomes in the field through hyperspectral data. *Plant J.* 102, 615–630. doi: 10.1111/tpj.14636

Vergara-Diaz, O., Vatter, T., Vicente, R., Obata, T., Nieto-Taladriz, T. M., Aparicio, N., et al. (2020b). Metabolome profiling supports the key role of the spike in wheat yield performance. *Cells* 9, 1025. doi: 10.3390/cells9041025

Vergara-Diaz, O., Zaman-Allah, M. A., Masuka, B., Hornero, A., Zarco-Tejada, P., Prasanna, B. M., et al. (2016). A novel remote sensing approach for prediction of maize yield under different conditions of nitrogen fertilization. *Front. Plant Sci.* 7, 666. doi: 10.3389/fpls.2016.00666

Vicente, R., Bolger, A. M., Martínez-Carrasco, R., Pérez, P., Gutiérrez, E., Usadel, B., et al. (2019a). *De novo* transcriptome analysis of durum wheat flag leaves provides new insights into the regulatory response to elevated CO_2 and high temperature. *Front. Plant Sci.* 10, 1605. doi: 10.3389/fpls.2019.01605

Vicente, R., Martínez-Carrasco, R., Pérez, P., and Morcuende, R. (2018a). New insights into the impacts of elevated CO_2, nitrogen, and temperature levels on the regulation of C and N metabolism in durum wheat using network analysis. *New Biotechnol.* 40, 192–199. doi: 10.1016/j.nbt.2017.08.003

Vicente, R., Pérez, P., Martínez-Carrasco, R., Feil, R., Lunn, J. E., Watanabe, M., et al. (2016). Metabolic and transcriptional analysis of durum wheat responses to elevated CO_2 at low and high nitrate supply. *Plant Cell Physiol* 57, 2133–2146. doi: 10.1093/pcp/pcw131

Vicente, R., Pérez, P., Martínez-Carrasco, R., Usadel, B., Kostadinova, S., and Morcuende, R. (2015). Quantitative RT-PCR platform to measure transcript levels of C and N metabolism-related genes in durum wheat: transcript profiles in elevated [CO_2] and high temperature at different nitrogen supplies. *Plant Cell Physiol.* 56, 1556–1573. doi: 10.1093/pcp/pcv079

Vicente, R., Vergara-Díaz, O., Kerfal, S., López, A., Melichar, J., Bort, J., et al. (2019b). Identification of traits associated with barley yield performance using contrasting nitrogen fertilizations and genotypes. *Plant Sci.* 282, 83–94. doi: 10.1016/j.plantsci.2018.10.002

Vicente, R., Vergara-Díaz, O., Medina, S., Chairi, F., Kefauver, S. C., Bort, J., et al. (2018b). Durum wheat ears perform better than the flag leaves under water stress: gene expression and physiological evidence. *Environ. Exp. Bot.* 153, 271–285. doi: 10.1016/j.envexpbot.2018.06.004

Wang, M., Kong, F., Liu, R., Fan, Q., and Zhang, X. (2020). Zinc in wheat grain, processing, and food. *Front. Nutr.* 7, 124. doi: 10.3389/fnut.2020.00124

Wang, Y., Wang, D., Tao, Z., Yang, Y., Gao, Z., Zhao, G., et al. (2021). Impacts of nitrogen deficiency on wheat (*Triticum aestivum* L.) grain during the medium filling stage: transcriptomic and metabolomic comparisons. *Front. Plant Sci.* 12, 1549. doi: 10.3389/fpls.2021.674433

Xynias, I. N., Mylonas, I., Korpetis, E. G., Ninou, E., Tsaballa, A., Avdikos, I. D., et al. (2020). Durum wheat breeding in the Mediterranean region: current status and future prospects. *Agronomy* 10, 432. doi: 10.3390/agronomy10030432

Zadoks, J. C., Chang, T. T., and Konzak, C. F. (1974). A decimal code for growth stages of cereals. *Weed Res.* 14, 415–421. doi: 10.1111/j.1365-3180.1974.tb01084.x

Zaman-Allah, M., Vergara, O., Araus, J. L., Tarekegne, A., Magorokosho, C., Zarco-Tejada, P. J., et al. (2015). Unmanned aerial platform-based multi-spectral imaging for field phenotyping of maize. *Plant Methods* 11, 1–10. doi: 10.1186/s13007-015-0078-2

Zörb, C., Ludewig, U., and Hawkesford, M. J. (2018). Perspective on wheat yield and quality with reduced nitrogen supply. *Trends Plant Sci.* 23, 1029–1037. doi: 10.1016/j.tplants.2018.08.012

Conflict of Interest: RM-P and NA were employed by Junta de Castilla y León.

The remaining authors declare that the research was conducted in the absence of any commercial or financial relationships that could be construed as a potential conflict of interest.

Publisher's Note: All claims expressed in this article are solely those of the authors and do not necessarily represent those of their affiliated organizations, or those of the publisher, the editors and the reviewers. Any product that may be evaluated in this article, or claim that may be made by its manufacturer, is not guaranteed or endorsed by the publisher.

frontiers | Frontiers in Plant Science

ORIGINAL RESEARCH
published: 18 May 2022
doi: 10.3389/fpls.2022.836665

Comparative Metabolic Analysis Reveals a Metabolic Switch in Mature, Hydrated, and Germinated Pollen in *Arabidopsis thaliana*

Jiang Wang[1,2†], *Shrikaar Kambhampati*[3†], *Doug K. Allen*[3,4] *and Li-Qing Chen*[1,2*]

[1] *Department of Plant Biology, University of Illinois at Urbana-Champaign, Urbana, IL, United States,* [2] *Carl R. Woese Institute for Genomic Biology, University of Illinois at Urbana-Champaign, Urbana, IL, United States,* [3] *Donald Danforth Plant Science Center, St. Louis, MO, United States,* [4] *United States Department of Agriculture, Agricultural Research Service, St. Louis, MO, United States*

Pollen germination is an essential process for pollen tube growth, pollination, and therefore seed production in flowering plants, and it requires energy either from remobilization of stored carbon sources, such as lipids and starches, or from secreted exudates from the stigma. Transcriptome analysis from *in vitro* pollen germination previously showed that 14 GO terms, including metabolism and energy, were overrepresented in *Arabidopsis*. However, little is understood about global changes in carbohydrate and energy-related metabolites during the transition from mature pollen grain to hydrated pollen, a prerequisite to pollen germination, in most plants, including *Arabidopsis*. In this study, we investigated differential metabolic pathway enrichment among mature, hydrated, and germinated pollen using an untargeted metabolomic approach. Integration of publicly available transcriptome data with metabolomic data generated as a part of this study revealed starch and sucrose metabolism increased significantly during pollen hydration and germination. We analyzed in detail alterations in central metabolism, focusing on soluble carbohydrates, non-esterified fatty acids, glycerophospholipids, and glycerolipids. We found that several metabolites, including palmitic acid, oleic acid, linolenic acid, quercetin, luteolin/kaempferol, and γ-aminobutyric acid (GABA), were elevated in hydrated pollen, suggesting a potential role in activating pollen tube emergence. The metabolite levels of mature, hydrated, and germinated pollen, presented in this work provide insights on the molecular basis of pollen germination.

Keywords: untargeted metabolomics, *in vitro* pollen germination, hydrated pollen, germinated pollen, metabolites, mature pollen, starch and sucrose metabolism

OPEN ACCESS

Edited by:
Maria Grazia Annunziata, University of Potsdam, Germany

Reviewed by:
Zhou Li, Sichuan Agricultural University, China
Agnieszka Zienkiewicz, Nicolaus Copernicus University in Toruń, Poland

***Correspondence:**
Li-Qing Chen
lqchen77@illinois.edu

† These authors have contributed equally to this work

Specialty section:
This article was submitted to Plant Metabolism and Chemodiversity, a section of the journal Frontiers in Plant Science

Received: *15 December 2021*
Accepted: *29 March 2022*
Published: *18 May 2022*

Citation:
Wang J, Kambhampati S, Allen DK and Chen L-Q (2022) Comparative Metabolic Analysis Reveals a Metabolic Switch in Mature, Hydrated, and Germinated Pollen in Arabidopsis thaliana. Front. Plant Sci. 13:836665. doi: 10.3389/fpls.2022.836665

INTRODUCTION

Successful pollination in flowering plants is essential to fertilization and seed formation and is a key determinant of seed yield (Johnson et al., 2019). Mature pollen in most plant species is metabolically dormant before anthesis with approximately 15–35% water content (Shi and Yang, 2010). Pollen viability correlates with the degree of dehydration and the composition of carbohydrate and lipid

reserves (Shi and Yang, 2010). Upon interacting with stigma, compatible pollen grains will undergo a rapid rehydration process that is a prerequisite to germination (Moon and Jung, 2020). It takes less than 5 min for pollen to germinate in many monocot species (Heslop-Harrison, 1979; Chen et al., 2008). By contrast, dicot pollen can take an hour to hydrate before germination (Rotsch et al., 2017). Defects in pollen hydration may result in precocious germination in anthers (Johnson and McCormick, 2001) and cause sterility (Fiebig et al., 2000). After hydration, metabolism initiates pollen tube growth from the aperture, which is controlled by multiple cellular and molecular processes (Kim et al., 2019). The rapid growth of pollen tubes is an energy-demanding process that requires mobilization of storage reserves in pollen grains (Goetz et al., 2017) and support from stigma exudates (Goldman et al., 1994; Wolters-Arts et al., 1998) coordinated by a complicated change of metabolic dynamics, protein synthesis, cell signaling, cell-wall remodification, and new cell component biosynthesis (Shi and Yang, 2010; Johnson et al., 2019; Kim et al., 2019; Hafidh and Honys, 2021).

Studies performed with rice and *Arabidopsis* [see review in Moon and Jung (2020) and references therein] analyzed the complexity of biochemical mechanisms initiated during pollen germination and pollen tube growth. In contrast to the wealth of available transcriptome and proteome data, global metabolomic dynamics have not been well-characterized during pollen germination. In particular, knowledge of metabolomic changes during pollen hydration is nearly absent from the literature and metabolite reports on pollen are limited to a small number of specific compounds. Secondary metabolites have been examined in tomato plants during pollen development under heat stress (Paupiere et al., 2017) and sucrose and starch catabolism has been measured in different fractions in the lily (Castro and Clément, 2007). Comprehensive metabolomic analysis during pollen germination has been performed in lilies and tobacco, two bicellular pollen species (Obermeyer et al., 2013; Rotsch et al., 2017), and the Chinese fir, a gymnosperm (Fragallah et al., 2018), but no such studies have been reported with the model plant *Arabidopsis*, a tricellular pollen species, despite the extensive transcriptomic resources available for comparative analysis.

In this study, we examined changes in *Arabidopsis* pollen by surveying metabolite profiles among mature, hydrated, and germinated pollen with an untargeted metabolomic approach. Monosaccharide, polysaccharide, sugar phosphate, lipid, and fatty acid levels changed during the process. In addition, integrated analysis of the metabolomic and publicly available transcriptomic data revealed that sucrose and starch metabolism were significantly elevated in pollen hydration and germination. Several genes that encode transporters and enzymes for phosphorylated sugars as well as lipid synthesis enzymes were differentially expressed in accordance with the changes of their metabolic intermediates, suggesting some concordance with transcript data. The potential roles of several metabolites that were over-represented in hydrated pollen required for the metabolic activation of pollen tube emergence were discussed with reference to transcriptomic data.

MATERIALS AND METHODS

Plant Growth and Pollen Collection

The *Arabidopsis* Col-0 plants were grown under controlled temperature (22°C) with a 16-h light (100–150 μmol m^{-2} s^{-1})/8-h dark photoperiod. The pollen harvesting method, *in vitro* germination medium, and sampling stage for hydrated pollen (45 min after germination) and germinated pollen (4 h after germination) for metabolomic analyses were identical to methods published based on transcriptome analysis of *Arabidopsis* pollen germination (Wang et al., 2008), to enable comparisons. For each repeat, mature pollen grains from the fully opened flowers were collected from more than 1,000 plants using a vacuum cleaner method (Johnson-Brousseau and McCormick, 2004) at around 5 h into the light period.

Culture of *Arabidopsis* Pollen *in vitro*

For mature pollen samples, collected pollen grains were resuspended in 2 ml of ice-cold Pollen Isolation Buffer [PIB, composed of 100 mM $NaPO_4$, pH 7.5, 1 mM EDTA, and 0.1% (v/v) Triton X-100] right after collection followed by centrifuging at 15,000 g for 1 min (4°C). For hydrated pollen and germinated pollen samples, in brief, pollen pellets were washed with 1 ml of liquid Pollen Germination Medium [PGM, composed of 15% (w/v) sucrose, 1.5 mM boric acid, 0.8 mM $MgSO_4$, 1 mM KCl, 5 mM MES, 0.05% (w/v) lactalbumin hydrolysate, 10 μM myo-inositol, 5 mM $CaCl_2$] before they were resuspended in 30 μl of liquid PGM and subsequently cultured in Petri dishes (35 mm in diameter). A 70 μm mesh was used to cover the pollen droplet to create a thin layer for optimal germination for each Petri dish. The Petri dishes were covered and placed in the dark for 45 min or 4 h and collected as hydrated pollen or germinated pollen, respectively. All pollen samples were washed by 1 ml ice-cold ddH_2O three times before being stored in a -80°C freezer.

Starch Staining of *in vitro* Germinated Pollen

Mature, hydrated, and germinated pollen were prepared as aforementioned. Pollen samples were stained using 100 μl iodine solution [composed of 4% (w/v) potassium iodide and 1.27% (w/v) iodine] kept in the dark for 10 min and washed twice using 1 ml ddH_2O before imaged with a compound microscope (Nikon, NY, United States).

Total Metabolite Extraction

Total metabolites from pollen were extracted using a phase separation method previously described (Kambhampati et al., 2021) with slight modifications. Briefly, 10–30 mg (fresh weight) pollen tissue, collected in Eppendorf tubes, was extracted using 700 μL of chilled 7:3 (v/v) methanol: chloroform spiked with 50 μM each of 1.4-piperazinediethanesulfonic acid (PIPES), ribitol, and norvaline as internal standards. After two metal beads were also added to the samples, they were homogenized using a Tissue-Lyser for 5 min at 30 Hz. The samples were incubated on a rotary shaker at 4°C for 2 h after which 300 μL ddH_2O was added. The samples were then centrifuged

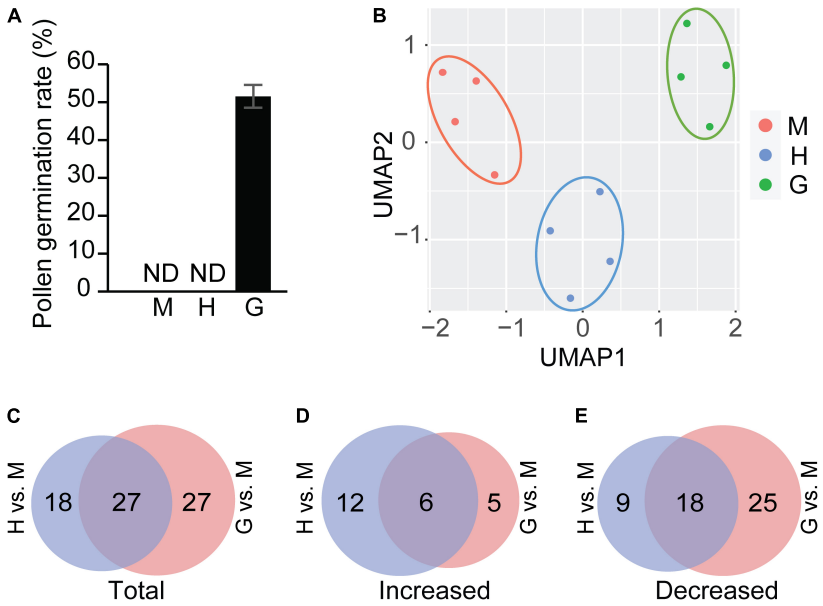

FIGURE 1 | Pollen germination and statistical analysis of metabolites. **(A)** *In vitro* pollen germination assay for mature pollen (M), hydrated pollen (H), and germinated pollen (G). ND: not detected. The means were calculated from multiple repeats (±SE, $n = 6$), with over 420 pollen grains/tubes counted in total. **(B)** UMAP analysis of mature pollen(M), hydrated pollen (H), and germinated pollen (G). **(C)** Venn diagram showing total differential accumulated metabolites in hydrated pollen vs. in mature pollen (H vs. M) and those in hydrated pollen vs. in mature pollen (G vs. M). **(D)** Venn diagram showing increased metabolites in hydrated pollen vs. in mature pollen (H vs. M) and those in hydrated pollen vs. in mature pollen (G vs. M). **(E)** Venn diagram showing decreased metabolites in hydrated pollen vs. in mature pollen (H vs. M) and those in hydrated pollen vs. in mature pollen (G vs. M). Detailed compound information used in the Venn diagrams of panels **(C–E)** was shown in **Supplementary Table 1**.

at 14,000 rpm for 10 min to achieve phase separation and the upper aqueous phase, as well as the lower organic phase, were collected separately. The aqueous phases containing polar and non-polar metabolites were split into two equal parts and dried using a speed vacuum centrifuge (Labconco, Kansas City, MO, United States). The two dried parts were re-suspended in 50 μL 80% (v/v) methanol, and 30% (v/v) methanol for metabolomics analyses using hydrophilic interaction chromatography (HILIC) and reverse phase chromatography, respectively. The organic phase was also dried using a speed vacuum centrifuge and re-suspended in 50 μL of 49:49:2 (v/v/v) mixture of acetonitrile:methanol:chloroform. All samples were filtered using a 0.8 μM PES membrane centrifuge filter (Sartorius, Goettingen, Germany) and transferred to a glass vial for injection into an LC-MS/MS system.

Liquid Chromatography-Tandem Mass Spectrometry

Three different chromatographic methods, including a HILIC, a reverse phased C18 and a reverse phased C8 columns, were used to attain a wide coverage of compound groups. The aqueous fraction of the extraction, which is expected to contain core and specialized metabolic intermediates, was used for HILIC and C18 chromatography, while the organic fraction was used for C8 based chromatography for the separation of lipids. An Eksigent Ekspert microLC 200-chromatography system (Eksigent Technologies, Redwood City, CA, United States) and a CTC Analytics Leap HTS PAL liquid handler hooked to a benchtop Q-Exactive Orbitrap MS (Thermo Scientific, Waltham, MA, United States) were used for all untargeted LC-MS analysis. HILIC separation was achieved using a custom made zic-pHILIC (100 × 0.5 × 3 μm) column obtained from Higgins Analytical Inc. (Mountain View, CA, United States) with the mobile phases, 10 mM ammonium bicarbonate in ddH_2O (solvent A) and 10 mM ammonium bicarbonate in 95:5 (v/v) Acetonitrile: ddH_2O (solvent B) and a flow rate of 15 μL/min. The following gradient was used for HILIC; 0-2 min at 100% B, 3 min at 85% B, 16 min at 50% B, 17 min at 30% B, 18 min at 30% B, 20 min back to 100% B and equilibration up to 30 min. Reverse-phase chromatography was performed using a Targa C18 (100 × 0.3 × 5 μm) column with the mobile phases, 0.1% formic acid in ddH_2O (Solvent A) and 0.1% formic acid in Acetonitrile (Solvent B), and a flow rate of 15 μL/min. The gradient conditions used for the C18 method are as follows; 0-3 min at 2% B, 13 min at 100% B, 16 min at 100% B, 19 min at 2% B, and equilibration up to 30 min. For lipidomics, a custom-made C8 column (100 × 0.5 × 1.7 μm) from Higgins Analytical Inc. (Mountain view, CA, United States) was used with the mobile phases 1% 1 M ammonium acetate, 0.1% acetic acid in ddH_2O (solvent A) and 1% 1 M ammonium acetate, 0.1% acetic acid in 7:3 (v/v) acetonitrile: isopropanol (solvent B), and a flow rate of 40 μL/min. The following gradient, 0–1 min at 55% B, 3 min at 75% B, 8 min at 89% B, 10 min at 99% B, 11 min at 99% B and 12 min at 55% B followed by equilibration up to 18 min, was used, which was modified from Hummel et al. (2011) to adopt to microflow.

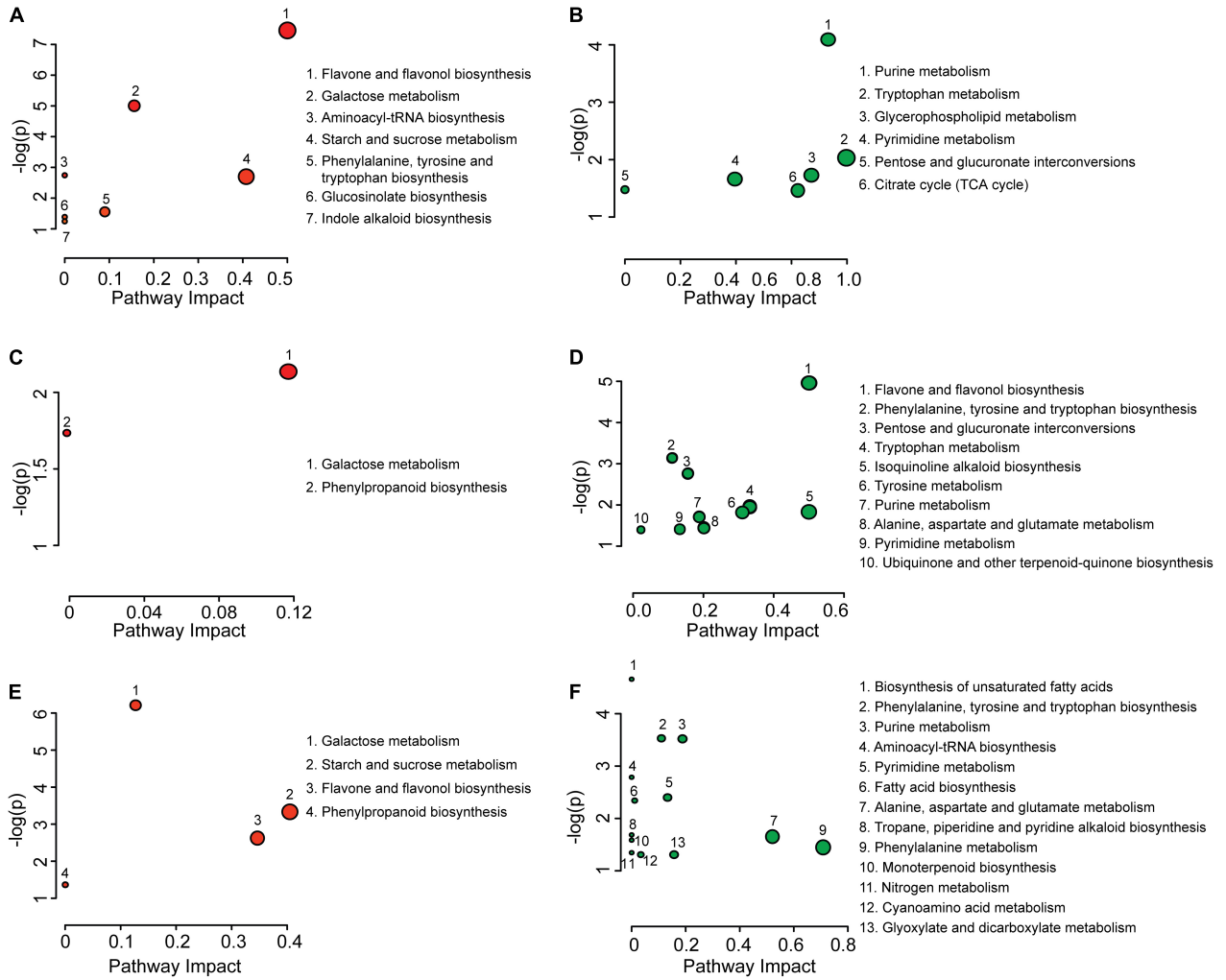

FIGURE 2 | Pathway enrichment analysis of differential metabolites from mature pollen, hydrated pollen, and germinated pollen. Pathway enrichment analysis of increased **(A)** and decreased **(B)** metabolites between mature pollen and hydrated pollen. Pathway enrichment analysis of increased **(C)** and decreased **(D)** metabolites between hydrated pollen and germinated pollen. Pathway enrichment analysis of increased **(E)** and decreased **(F)** metabolites between mature pollen and germinated pollen. For all enrichment analysis $P < 0.05$, the circle size corresponds to the impact of the metabolic pathway, which evaluates the ratio of matched metabolites to overall metabolites in each pathway during the pathway topology analysis.

Data for untargeted metabolomics using all three chromatographic methods were acquired for mass ranges of 70–1,000 m/z by full MS at 70,000 resolution in both positive and negative ionization modes. The automatic gain control (AGC) and maximum injection time (IT) were 5×10^5 and 100 ms, respectively. The heated electrospray ionization (HESI) source was operated with sheath gas, 15 arbitrary units; auxiliary gas, 5 arbitrary units; capillary temperature, 250°C; auxiliary gas heater temperature, 50°C; and S-lens RF level, 50. The spray voltage was 4.2 and 3.9 kV in positive and negative modes, respectively. One sample in each group was also used for the top 12 data-dependent acquisition experiments in both ionization modes to generate MS/MS datasets for compound identification. These experiments involved a full MS scan at 70,000 resolution, AGC target 5×10^5, maximum IT 100 ms and MS/MS scans at 17,500 resolution, AGC target 5×10^4, maximum IT 50, 2.0 m/z isolation window, stepped collision energy of 15, 25, and 35 eV, intensity threshold 1×10^4 and 15-s dynamic exclusion.

Metabolic Data Analysis and Integration of Available Transcriptomic Data

For data analyses, the raw data files in Thermo.RAW format obtained in the profile mode were first centroided by conversion into .mzML format using ProteoWizard (Kessner et al., 2008) with peak picking filter applied. Features were detected and a pre-processed data table was created using the program, MZmine 2.53 (Pluskal et al., 2010), data were normalized using average squared intensities available within the MZmine workflow (Katajamaa and Orešiè, 2005) to enable comparison between different samples and the peak areas were exported to a single combined data table containing 2,235 metabolomic features. Global changes

in metabolome were visualized using UMAP (McInnes et al., 2018). Raw data (.mzML format) are publicly available at National Metabolomics Data Repository [NMDR; Sud et al. (2016)]. A *t*-test was carried out to determine the significantly changed metabolites ($P < 0.05$) in pollen from the hydration or germination stage when compared with the mature pollen stage. The resultant subset of features that showed significant differences were annotated using "Functional Analysis" module of MetaboAnalyst v5.0 (Pang et al., 2021). Notably, for the untargeted metabolome analysis, as the annotated metabolites for the pathway enrichment analysis were predicted using computational algorithms (Li et al., 2013), the content of a specific metabolite needs to be manually verified if it is not provided in our already verified list. Pathway enrichment analysis was performed using the "Pathway Analysis" module of MetaboAnalyst v5.0. A differentially regulated gene list was directly retrieved from supplementary materials of published transcriptomic data by Wang et al. (2008). The differentially regulated genes and the consequential metabolites during the transition from mature to hydrated pollen, and from hydrated to germinated pollen, were integrated using the "Joint Pathway Analysis" module in MetaboAnalyst v5.0 with pathway database selection of "Metabolic pathways (integrated)." "Hypergeometric Test" was used for the enrichment analysis, "Degree Centrality" was selected for the topology analysis, and "Combine *p*-values (pathway-level)" was set as the integration method.

Statistical Analysis

The Shapiro-Wilk test was used to test the normality of data. For the data that passed the normal distribution test, one-way ANOVA followed by multiple comparison tests (Fisher's LSD method) was used for the difference comparisons among multiple subjects. For the data of metabolites (glucose, raffinose, stearic acid, oleic acid, IAA, and quercitin) non-normally distributed, the Kruskal-Wallis ANOVA followed by multiple comparison tests (Dunn's test) was used. All statistical analysis was performed using OriginPro 2021b software (OriginLab Corporation, Northampton, MA, United States).

RESULTS

Pollen Germination Stages and Statistical Analysis

Pollen germination rates were initially evaluated using a light microscope. Consistent with previous observations (Wang et al., 2008), no pollen from mature or hydrated stages was in a germinated form, while ∼52% of observed pollen germinated in the germinated pollen stage (**Figure 1A**). Three different chromatographic methods were used, including hydrophilic interaction chromatography (HILIC), reverse phase chromatography with a C18 column, and lipidomic profiling using a specific reverse phase C8 column. This ensured an extensive coverage of compounds and captured core central and specialized metabolites along with several lipid classes. To obtain a global overview of the metabolomic data, a UMAP (Uniform Manifold Approximation and Projection) analysis (McInnes et al., 2018), was performed to accommodate dimensionality reduction relative to PCA (Principal Component Analysis), and to visualize the data (**Figure 1B**). The four biological replicates for mature, hydrated, and germinated pollen were each clustered together and the clusters were easily distinguished along the UMAP1 dimension. The hydration stage was separated from the mature and germination stages as determined by the second UMAP dimension, suggesting many peak features were uniquely present and/or accumulated at distinct levels in this stage.

After determining the significant changes that occurred in metabolite levels ($P < 0.05$) between mature and hydrated pollen, and between mature and germinated pollen, we noted the significantly increased or decreased metabolites in each pair, with verified identities presented in **Supplementary Table 1**. Compared to mature pollen, a total of 45 and 54 metabolites were significantly altered in hydrated and germinated pollen, respectively. Of these, 27 of the same metabolites were altered in both hydrated and germinated pollen groups (**Figure 1C**). Where metabolite levels increased, the majority (18/23) of metabolites were found in hydrated pollen (**Figure 1D**), suggesting a potential role in metabolic activation before pollen tube emergence (Kim et al., 2019). Where metabolite levels decreased, 25 metabolites were found only in germinated pollen, while nine were found only in the hydrated pollen (**Figure 1E**).

Differential Metabolic Pathway Enrichment Analysis

The metabolite differences were subjected to pathway enrichment analysis (**Figure 2**) where "enrichment" refers to an overrepresentation of the number of metabolites within a pathway that are coordinately elevated or reduced in level. During the transition from mature pollen to hydrated pollen, seven metabolic pathways were overrepresented in metabolites with elevated levels. Six metabolic pathways were overrepresented in metabolites with decreased levels (**Figures 2A,B**). During the transition from hydrated pollen to germinated pollen, two metabolic pathways were overrepresented in metabolites with elevated levels and ten pathways were overrepresented in metabolites with reduced levels (**Figures 2C,D**). When mature and germinated pollen metabolites were compared, four metabolic pathways were overrepresented in metabolites with elevated levels and thirteen metabolic pathways were overrepresented in metabolites with lowered levels (**Figures 2E,F**). Specifically, starch and sucrose metabolism, galactose metabolism, and flavone and flavonol biosynthetic pathways had disproportionate numbers of metabolites with increased levels in both hydrated and germinated pollen. By contrast, purine and pyrimidine metabolic pathways had more metabolites that were lowered in levels in both hydrated and germinated pollen. Interestingly, the quantity of metabolites from two overrepresented pathways increased during the transition from mature pollen to hydrated pollen, and then decreased during the transition from hydrated pollen to germinated pollen. One of the two pathways was the biosynthesis of flavone and flavonol, and the other was

TABLE 1 | Joint pathway analysis of transcriptomics and metabolomics in hydrated pollen and germinated pollen.

	Enriched pathway	Total. compound	Hits. compound	Total. gene	Hits. gene	*P*	Impact
Up in hydrated pollen	Starch and sucrose metabolism	22	3	35	4	<0.001	0.55
	Galactose metabolism	27	5	24	1	<0.001	0.36
Down in hydrated pollen	Linoleic acid metabolism	63	7	78	1	0.042	0.26
	Pentose and glucuronate interconversions	16	2	14	1	0.032	0.21
Up in germinated pollen	Starch and sucrose metabolism	22	1	35	9	0.005	0.48
	Galactose metabolism	27	2	24	3	0.035	0.54
	Glutathione metabolism	26	1	24	8	0.003	0.49
Down in germinated pollen	Pentose and glucuronate interconversions	16	4	14	6	<0.001	0.79
	Glycerophospholipid metabolism	37	3	46	10	0.006	0.61
	Purine metabolism	63	6	78	10	0.03	0.66

Total represents the total number of compounds/genes in each pathway; hits represents the number of compounds/genes that were significantly changed within each pathway.

biosynthesis of phenylalanine, tyrosine and tryptophan. Both pathways had over-represented numbers of elevated metabolites in the hydrated pollen compared to the other two stages, suggesting their potential roles in metabolic activation for pollen tube emergence. Detailed information on pathway enrichment analysis can be found in **Supplementary Table 2**.

Integrative Analysis of Transcriptomics and Metabolomics

To obtain a deeper understanding, we performed a multi-omics analysis that integrated the current metabolomic data with previously published expression levels from transcriptomics (Wang et al., 2008). As shown in **Table 1**, two pathways contained an overrepresented number of metabolites and genes that were either elevated or lowered in level in hydrated pollen compared to mature pollen. Three pathways contained an overrepresented number of genes and metabolites with either heightened or reduced levels in germinated pollen when compared to hydrated pollen. The list of compounds and genes from the joint analysis can be found in **Supplementary Table 3**. To investigate whether metabolic changes were associated with transcriptional changes, we performed a pathway enrichment analysis using the previously published transcriptome data. Unexpectedly, few of the identified pathways (e.g., linoleic acid metabolism, glycerophospholipid metabolism and purine metabolism) from our joint analysis data were significantly enriched in transcriptomics data (**Supplementary Table 4**). This is not surprising as disconcordance between protein and transcript levels is well-documented [Fernie and Stitt, 2012; summarized in Allen (2016)]; however, the results imply that integrative analysis can provide more insight than transcriptomics alone. Consistent with pathway enrichment analysis based only on metabolomics data, we found that starch and sucrose metabolism as well as galactose metabolism were over-represented in both hydrated and germinated pollen in the joint pathway analysis, suggesting that the compounds and enzymes related to soluble carbohydrate metabolism and cell-wall modifications were active during both pollen hydration and germination. In the published transcriptome data (Wang et al., 2008), *AtSUC3 (At2g02860)* and *AtSUC9 (At5g06170)*, which encode plasma-membrane localized sucrose transporters, had increased expression in germinated pollen. *AtSIP2 (At3g57520)*, which encodes a raffinose synthase, had elevated expression in germinated pollen. The gene expression levels were consistent with increased sucrose and raffinose that accumulated in germinated pollen (**Supplementary Table 1**). To investigate whether starch is altered during pollen germination, we performed starch staining using iodine solution on mature, hydrated, and germinated pollen. No clear differences were observed in the starch stains from the pollen in any of the three stages (**Supplementary Figure 2**), consistent with a previous report that no evidence of starch was detected in the mature *Arabidopsis* pollen grains after staining with iodine containing solution (Regan and Moffatt, 1990). As shown in the joint analysis (**Supplementary Table 3**), *AtUGE1 (At1g12780)*, which encodes a UDP-glucose epimerase, was expressed to a higher degree in germinated pollen, and *AtUGE3 (At1g63180)* was also elevated in both hydrated and germinated pollen. Plant UGEs are important to the regulation of cell wall carbohydrate biosynthesis (Rösti et al., 2007), which may contribute to the heightened metabolite levels in galactose metabolism from hydrated and germinated pollen.

Overview of All Differentially Accumulated Metabolites Among Mature, Hydrated, and Germinated Pollen

To give an overall comparison of metabolites among mature, hydrated, and germinated pollen, we summarized intensities in a heatmap of all manually verified metabolites (**Supplementary Table 5**) that passed the statistical threshold during metabolomics analysis (**Figure 3**). Four major clusters of metabolites were identified. The first cluster was enriched with metabolites accumulating in germinated pollen (e.g., raffinose, glucosamine). The second cluster contained metabolites enriched in hydrated pollen, including 2-aminobenzoic acid and oleic acid, and the third cluster represented metabolites elevated in mature pollen (e.g., xylose and fustin). The fourth cluster contained metabolites reduced in germinated pollen such as vitamin K2 and linoleic acid. All lipid species (including both neutral and polar lipids)

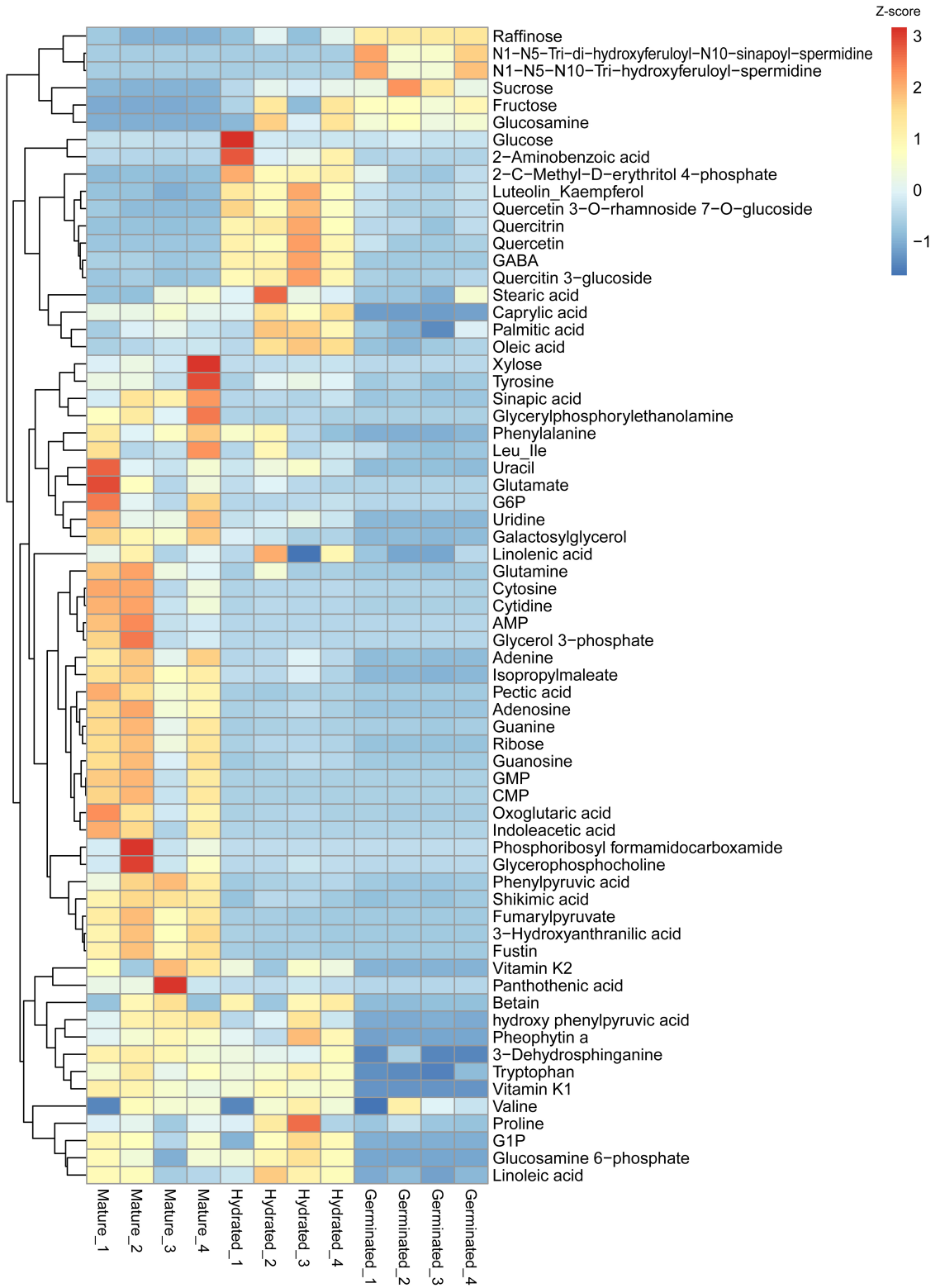

FIGURE 3 | Heatmap showing the identified metabolite differences among mature pollen, hydrated and germinated pollen. Heatmap was created using raw data in intensity converted to z-scores for each metabolite using the "pheatmap" package (Kolde, 2019) in R. The scale bar represents the distance of the raw intensity away from the group mean in units of the standard deviation for a given metabolite. Z-score is negative when the raw intensity is below the mean, positive when above.

were compared in a second heatmap (**Supplementary Figure 1**) and were mostly elevated in mature pollen but reduced in germinated pollen.

Carbon-Related Metabolites Were Differentially Altered in Hydrated and Germinated Pollen

Sugar metabolism and fatty acid metabolism were among the enriched pathways during pollen hydration and germination. The normalized intensities of soluble sugars, fatty acids, lipids, and their adducts were retrieved from the metabolomic data (**Supplementary Table 5**). As shown in **Figures 4A,B**, glucose and fructose content were significantly elevated in hydrated pollen but unchanged in germinated pollen. By contrast, sucrose and raffinose content continued to increase during the transition from mature to hydrated to germinated pollen (**Figures 4C,D**). In contrast, glucose 6-phosphate, a precursor and product of sucrose metabolism, sharply decreased from mature to hydrated pollen (**Figure 4E**). Glucose 1-phosphate, which is also closely related to sucrose, dramatically decreased from hydrated to germinated pollen (**Figure 4F**). There was significantly reduced stored lipid in the form of triacylglycerol (TAG) in germinated pollen after hydration (**Figure 4G**). *AtDGAT (At2g19450)*, which encodes the key diacylglycerol acyltransferase for TAG biosynthesis (Routaboul et al., 1999), was reduced in expression during pollen germination (**Supplementary Table 3**). Other lipid species (e.g., diacylglycerol) were also reduced during pollen germination (**Supplementary Figure 1**). Non-esterified fatty acids including linoleic acid and linolenic acid, the two most abundant unsaturated fatty acids found in *Arabidopsis* flowers (Li-Beisson et al., 2009), decreased in germinated pollen after pollen hydration (**Figure 4H**). Furthermore, palmitic acid, oleic acid, and linolenic acid content peaked in hydrated pollen before decreasing during pollen germination (**Figure 4H**), suggesting they may be involved in metabolic activation during pollen hydration. The lack of the three major fatty acids (palmitic acid, oleic acid and linolenic acid) in the pollen coat is known to result in rapid dehydration of rice pollen grains (Xue et al., 2018). Taken together, the data suggests that lipids stored in mature pollen catabolized to support the energy-demanding pollen germination process. Saccharides, including sucrose and raffinose, accumulated as pollen germination progressed, likely due to the carbon supply from the external sucrose-rich medium provided during *in vitro* germination.

Amino Acids, Hormone, and Flavonoids Changes in Hydrated and Germinated Pollen

In contrast to central carbon intermediates, the levels of detected amino acids (Val, Tyr, Trp, Pro, Phe, Leu/Ile, Gln, Glu; **Supplementary Table 5**) did not change significantly within the three pollen stages (**Figure 5A**). γ-aminobutyric acid (GABA) showed a special pattern (**Figure 5B**), increasing in hydrated pollen followed by a sharp decrease to base level in germinated pollen. The levels of all identified compounds involved in nucleotide metabolism, including adenosine monophosphate (AMP), guanosine monophosphate (GMP), cytidine monophosphate (CMP), guanosine, adenosine, uridine, cytosine, cytidine, guanine, adenine, uracil (**Figure 3**), significantly decreased from mature pollen to hydrated pollen and remained low in germinated pollen (**Figure 5C**). Decreases in uracil and uridine in transition from mature pollen to germinated pollen suggest that the mature pollen grain is primed for rapid translation and protein synthesis upon germination. Indoleacetic acid (IAA) content also declined significantly from mature to hydrated pollen and remained at a low level in germinated pollen (**Figure 5D**). GABA, quercetin and the flavonoids luteolin/kaempferol sharply increased in hydrated pollen before returning to a low level in germinated pollen (**Figures 5E,F**) and may be related to metabolic activation for pollen tube emergence.

DISCUSSION

Before anthesis, pollen undergoes a maturation process which includes dehydration and accumulation of storage reserves. The degree of dehydration is highly correlated with carbohydrates and lipid levels in mature pollen (Shi and Yang, 2010). However, the form of carbohydrates and dehydration status in mature pollen grains varies among plant species (Pacini, 1996; Pacini et al., 2006). Grass pollen grains generally contain a low level of water, a high level of starch, and are short-lived (Shi and Yang, 2010; Kim et al., 2019) compared to dicot pollen grains (*Arabidopsis*), which accumulate a high level of lipids instead of starch (Kuang and Musgrave, 1996; Ischebeck, 2016). It has been well-documented that *Arabidopsis* mature pollen is virtually starch-free (Regan and Moffatt, 1990; Kuang and Musgrave, 1996; Tang et al., 2009; Streb and Zeeman, 2012), which is consistent with the lack of clear starch stains in mature, hydrated, and germinated pollen (**Supplementary Figure 2**). In addition to changes in composition, pollen metabolism responds rapidly upon interacting with stigma cells including translation of mRNA and activation of stored enzymes to engage pollen hydration (Shi and Yang, 2010). Compared to those in mature pollen grain, metabolites from a number of central carbon biosynthetic pathways, e.g., purine and pyrimidine metabolism and fatty acids biosynthesis, were significantly reduced in hydrated pollen or germinated pollen, possibly due to increased turnover (**Figures 2B,D,F**), and consistent with the use of fatty acids (**Figure 4H**) and nucleotides (**Figure 5C**)/purines (**Figure 3**) that are building blocks for growth and were detected at higher levels in mature pollen relative to hydrated or germinated pollen.

Although *Arabidopsis* mature pollen is stored with lipid and carbohydrate reserves, the amount is insufficient to sustain rapid pollen tube growth given its small pollen grain size/volume (De Storme et al., 2013) and additional supplies of sugars are needed during pollen tube growth (Reinders, 2016). This concept was supported with our observations from metabolomic data and the integration of metabolome and transcriptome. We found elevated levels of starch and sucrose metabolism during the transition from mature to hydrated pollen (**Figure 2A** and **Table 1**) and from hydrated to germinated pollen (**Figure 2C**

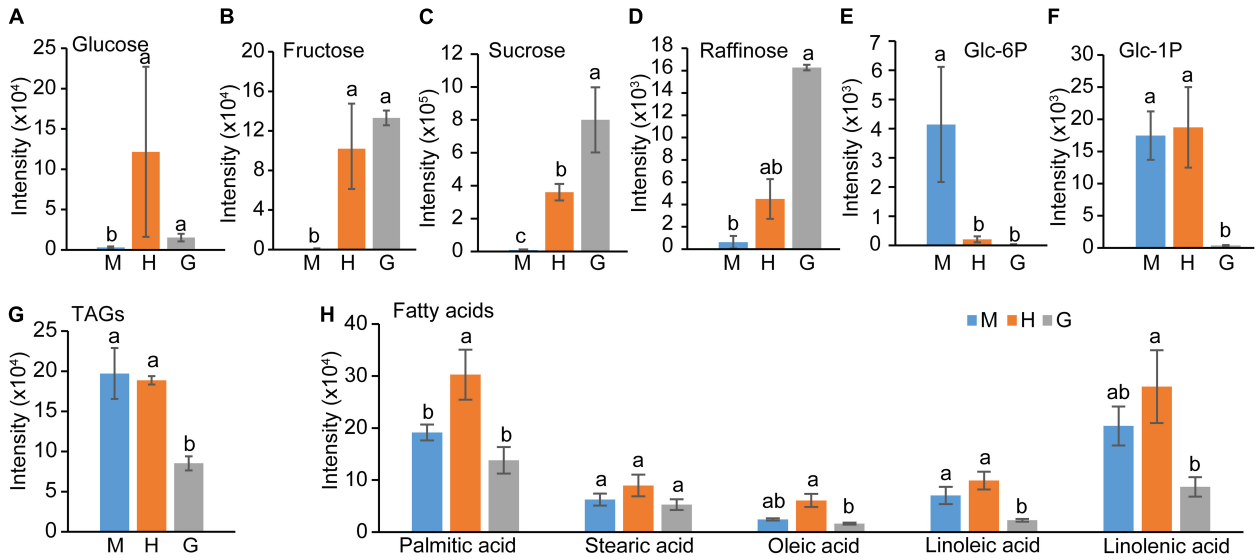

FIGURE 4 | Central carbon intermediates changes among mature pollen (M), hydrated (H) and germinated (G) pollen. **(A)** Glucose, **(B)** Fructose, **(C)** Sucrose, **(D)** Raffinose, **(E)** Glucose-6-phosphate, **(F)** Glucose-1-phosphate, **(G)** total triacylglycerides, **(H)** Fatty acids content in mature, hydrated, and germinated pollen. The means (± SE, $n = 4$) were plotted. The statistically significant differences among mature, hydrated, and germinated pollen for a particular compound were represented by different letters ($P < 0.05$).

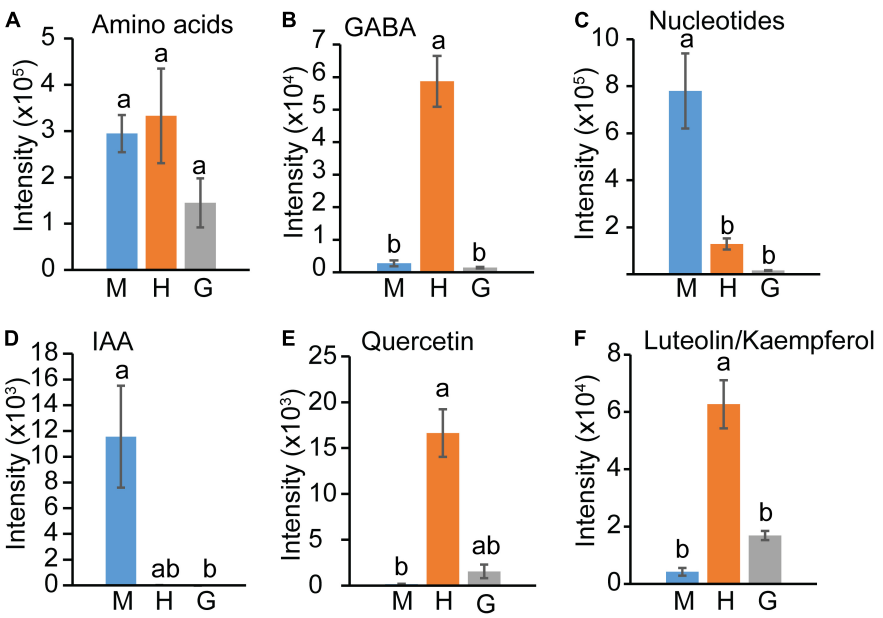

FIGURE 5 | Amino acids, hormone, and flavonoids changes among mature pollen (M), hydrated (H) and germinated (G) pollen. **(A)** Amino acids, **(B)** GABA, **(C)** Nucleotides, **(D)** IAA, **(E)** Quercetin, **(F)** Luteolin/Kaempferol content in mature, hydrated, and germinated pollen. The means (±SE, $n = 4$) were plotted. The statistically significant differences among mature, hydrated, and germinated pollen for a particular compound were represented by different letters ($P < 0.05$).

and **Table 1**), suggesting soluble carbohydrate metabolism is most active in germinated followed by hydrated and mature pollen, respectively. The elevated soluble carbohydrate metabolism can contribute to elevated sucrose and raffinose in germinated pollen (**Figures 4C,D**). The elevated demand for sucrose during pollen germination can be accommodated by expression of sucrose transporters like *AtSUC1* (*At1g71880*), which when absent result in a compromised pollen germination phenotype in mutants without affecting fatty acid content (Sivitz et al., 2008). By contrast, both monosaccharides (glucose and fructose; **Figures 4A,B**) and di- and trisaccharides (sucrose and raffinose; **Figures 4C,D**) contributed to elevated carbohydrate levels in

hydrated pollen. Interestingly, there were significantly higher levels of glucose and fructose in hydrated pollen and maintained at a similar level in germinated pollen after hydration. Based on targeted metabolite quantifications, elevated glucose and fructose were also found in hydrated *Arabidopsis* pollen compared to mature pollen (Wang et al., 2022).

Monosaccharides, including glucose and fructose, do not support *in vitro* pollen germination of *Arabidopsis*, while di- and trisaccharides, including sucrose and raffinose, can support *in vitro* pollen germination of *Arabidopsis* (Hirsche et al., 2017). Because only sucrose was supplied in the *in vitro* germination medium, the elevated glucose and fructose level in hydrated pollen were likely due to sucrose hydrolysis. Plasma-membrane localized sucrose transporters, such as AtSUC1 (Stadler et al., 1999; Sivitz et al., 2008), and alkaline/neutral invertases, such as A/N-InvH (*At3g05820*) that hydrolyze sucrose into fructose and glucose, are highly expressed in pollen (Wang et al., 2008) and *atsuc1* and *invh* mutants exhibit reduced pollen germination and fewer seeds per silique, respectively (Sivitz et al., 2008; Battaglia et al., 2017). When cell-wall invertase activity has been reduced via RNA-interference or an invertase inhibitor, pollen germination rates and seed sets are reduced in both *A. thaliana* and *N. tabacum* (Hirsche et al., 2009). Soluble carbohydrates, especially glucose, are potent signaling molecules involved in many aspects of plant growth (Rolland et al., 2006); thus, the accumulated glucose and fructose in hydrated pollen may initiate signaling events that result in metabolic activation before pollen tube emergence. Increased glucose levels were not observed in germinated pollen, suggesting pollen metabolism limits glucose levels to avoid pollen tube growth inhibition known to occur at high glucose concentrations (Rottmann et al., 2018).

In our results, almost all lipid species accumulated to high levels in mature pollen and were subsequently reduced in germinated pollen (**Supplementary Figure 1**), consistent with the lipid accumulation pattern that was observed in tobacco pollen (Dorne et al., 1988). Neutral lipids including TAG in tobacco pollen were reduced during 6 h of pollen germination, similar to lipid bodies in olive pollen after 7 h of pollen germination (Rodriguez-Garcia et al., 2003). Another study detailed changes in neutral and polar lipid fractions over olive pollen germination (Hernández et al., 2020). Interestingly, they found the fatty acid composition from total lipids was significantly altered, although the TAG content remained unchanged during the first 6 h of germination (Hernández et al., 2020). These results indicate lipid dynamic changes are stage- and species-dependent. As widely reported, an external supply of sucrose is required for *in vitro Arabidopsis* pollen germination, though the presence or absence of sugars had little impact on *in vitro* olive pollen germination or pollen tube growth rates (Zienkiewicz et al., 2013), possibly suggesting lipid reserves are the primary carbon source for olive pollen germination without significant requirement for sugars. On the other hand, a different pattern in sugar accumulation (relative to our study) was reported during tobacco pollen germination (Rotsch et al., 2017). To be specific, sucrose decreased sharply after pollen rehydration although remaining low during pollen germination, while fructose progressively increased as pollen germination proceeded. Tobacco pollen can also germinate without any sugars (Rotsch et al., 2017), suggesting that lipid and sucrose reserves in tobacco pollen are sufficient for subsequent germination. Thus, changes in metabolite levels, such as sugars and lipids, over the pollen germination stages are highly species-dependent and will require further investigations to understand the differences in mechanisms underlying *in vitro* pollen germination.

The GABA content peaked in hydrated pollen (**Figure 5B**). In plants, GABA levels are regulated by stress, signaling, energy production and play a major role in balancing carbon/nitrogen metabolism by linking amino acid metabolism and the TCA cycle through the GABA shunt (Fait et al., 2008). Exogenous GABA stimulates *Arabidopsis* pollen tube growth at low concentrations but inhibits pollen tube growth at high concentrations during *in vitro* pollen germination (Palanivelu et al., 2003), likely through GABA-gated aluminum-activated malate transporter (ALMT) (Ramesh et al., 2015). The mutant of the POP2 gene, which encodes a transaminase that degrades GABA, accumulates a high level of GABA and the pollen tube growth of *pop2* is arrested (Palanivelu et al., 2003), suggesting the GABA level plays a critical role in pollen tube growth/signaling and similar GABA patterns in lily and tobacco pollen germination (Obermeyer et al., 2013; Rotsch et al., 2017) may suggest conserved roles in development across some species.

Auxin is one of the most important hormones to promote cell division and elongation in plants (Zhao, 2010). Auxin plays a critical role in *Arabidopsis* pollen maturation (Cecchetti et al., 2008; Salinas-Grenet et al., 2018), but external auxin treatment reduced *in vitro* pollen germination rate of *Arabidopsis* (Ding et al., 2012). Our observations that IAA is accumulated at high levels in mature pollen, while barely detectable in hydrated pollen and germinated pollen (**Figure 5D**) is consistent with the prior descriptions. However, external IAA can stimulate *in vitro* pollen tube growth of *Nicotiana tabacum* (Chen and Zhao, 2008) and *Torenia fournieri* (Wu et al., 2008), suggesting the role of auxin during pollen tube growth is species-dependent.

The role of flavonoids during pollen germination also varies among different plant species. A male sterile phenotype of flavonoid-deficient mutant was observed in maize (Coe et al., 1981) and petunia (Ylstra et al., 1994), but *Arabidopsis* plants that are deficient in flavonoid biosynthesis appear to be fully fertile (Burbulis et al., 1996). As common flavonoids in plants, quercetin and luteolin/kaempferol accumulate to high levels in hydrated pollen (**Figures 5E,F**), flavone and flavonol biosynthesis was engaged and resulted in elevated metabolite levels during pollen hydration (**Figure 2A**). Our results support flavonoid involvement in the onset of pollen germination, but its role on pollen fertility may be limited in *Arabidopsis*.

As already mentioned, the germinated pollen samples object of this study consisted of both non-germinated and germinated pollen, with an overall germination rate of ∼52%, comparable to previously published rates for *Arabidopsis* [39% in Sivitz et al. (2008); 58% in Qin et al. (2009); 48.9% in Hirsche et al. (2017)]. Pollen germination is a consequence of both the rate of hydration and the speed at which the pollen tube tip is able to accomplish tube emergence (Firon et al., 2012). The fact that a substantial number of pollen grains failed to germinate

in vitro indicates issues connected to the hydration process in non-germinable pollen grains. Although it would be possible to largely separate pollen tubes from non-germinated pollen grains using a 50-μm nylon mesh (Wang et al., 2008), we faced the impossibility of sufficiently remove these non-germinable pollen grains from the hydrated pollen samples on large scale. Thus, what we called germinated pollen samples were mixed samples (germinated and non-germinated) in order to compare them to the mixed samples of hydrated pollen (germinable and non-germinable) and to already published results with similar germination rates. Previously reported metabolomic (Obermeyer et al., 2013; Fragallah et al., 2018) and transcriptomic (Qin et al., 2009) studies on germinated pollen followed a really similar approach, thus, increasing our confidence on the results obtained.

To conclude, a comprehensive metabolome analysis during *Arabidopsis* pollen germination in combination with published transcriptome revealed a complicated metabolic pathway network in support of pollen hydration and germination. The detailed analyses of carbohydrates and fatty acids indicated their roles in carbon metabolism that varied in mature, hydrated, and germinated pollen stages and a unique set of metabolites were identified to accumulate in the hydrated pollen stage, but were barely accumulated in other two stages.

DATA AVAILABILITY STATEMENT

Raw and pre-processed metabolomic data is available at the NIH Common Fund's National Metabolomics Data Repository (NMDR) website, the Metabolomics Workbench, https://www.metabolomicsworkbench.org where it has been assigned Study ID ST002060. The data can be accessed directly via its Project doi: 10.21228/M8570V.

AUTHOR CONTRIBUTIONS

JW and L-QC conceived and designed the experiments. JW and SK conducted the experiments and performed the metabolomics analysis. DA supervised the metabolomics analysis and edited the manuscript. JW, SK, and L-QC wrote the manuscript. All authors contributed to the article and approved the submitted version.

FUNDING

This research was supported by startup funds from the University of Illinois at Urbana–Champaign (to JW, and L-QC). DA was supported by the USDA-ARS and SK by the National Institute of Health (U01 CA235508). Establishment of preliminary conditions for subsequent method development using QTRAP6500 was supported by NSF-MRI funds (DBI-1427621).

ACKNOWLEDGMENTS

We would like to acknowledge the Proteomics and Mass Spectrometry Core Facility at the Danforth Center where data for metabolomics were collected and Brad Evans, Russell Williams, and Michael Wei for instrument support and maintenance.

SUPPLEMENTARY MATERIAL

The Supplementary Material for this article can be found online at: https://www.frontiersin.org/articles/10.3389/fpls.2022.836665/full#supplementary-material

Supplementary Figure 1 | Heatmap showing the identified lipid species differences among mature pollen, hydrated and germinated pollen. Heatmap was carried out on raw intensity data converted to z-scores for each metabolite using the "pheatmap" package in R. The scale bar represents the distance between raw intensity and the population mean in units of the standard deviation for a given metabolite. Z-score is negative when the raw intensity is below the mean, positive when above. DG, diacylglycerol; TG, triacylglycerol; PA, phosphatidic acid; PC, phosphatidylcholine; PI, phosphatidylinositol; PG, phosphatidylglycerol; PE, phosphatidylethanolamine; LPC, lysophosphatidylcholine; LPE, lysophosphatidylethanolamine.

Supplementary Figure 2 | Starch staining of mature, hydrated, and germinated pollen. Mature, hydrated, and germinated pollen collected from 50 flowers were stained using iodine solution. No clear starch stains (dark purple) were observed from mature, hydrated, and germinated pollen.

REFERENCES

Allen, D. K. (2016). Quantifying plant phenotypes with isotopic labeling & metabolic flux analysis. *Curr. Opin. Biotechnol.* 37, 45–52. doi: 10.1016/j.copbio.2015.10.002

Battaglia, M. E., Martin, M. V., Lechner, L., Martínez-Noël, G. M. A., and Salerno, G. L. (2017). The riddle of mitochondrial alkaline/neutral invertases: a novel *Arabidopsis* isoform mainly present in reproductive tissues and involved in root ROS production. *PLoS One* 12:e0185286. doi: 10.1371/journal.pone.0185286

Burbulis, I. E., Iacobucci, M., and Shirley, B. W. (1996). A null mutation in the first enzyme of flavonoid biosynthesis does not affect male fertility in *Arabidopsis*. *Plant Cell* 8, 1013–1025. doi: 10.1105/tpc.8.6.1013

Castro, A. J., and Clément, C. (2007). Sucrose and starch catabolism in the anther of *Lilium* during its development: a comparative study among the anther wall, locular fluid and microspore/pollen fractions. *Planta* 225, 1573–1582. doi: 10.1007/s00425-006-0443-5

Cecchetti, V., Altamura, M. M., Falasca, G., Costantino, P., and Cardarelli, M. (2008). Auxin regulates *Arabidopsis* anther dehiscence, pollen maturation, and filament elongation. *Plant Cell* 20, 1760–1774. doi: 10.1105/tpc.107.057570

Chen, D., and Zhao, J. (2008). Free IAA in stigmas and styles during pollen germination and pollen tube growth of *Nicotiana tabacum*. *Physiol. Plant.* 134, 202–215. doi: 10.1111/j.1399-3054.2008.01125.x

Chen, S., Zhong, W., Liu, M., Xie, Z., and Wang, H. (2008). Pollen grain germination and pollen tube growth in pistil of rice. *Rice Sci.* 15, 125–130. doi: 10.1016/S1672-6308(08)60030-X

Coe, E. H., Mccormick, S. M., and Modena, S. A. (1981). White pollen in maize. *J. Hered.* 72, 318–320. doi: 10.1093/oxfordjournals.jhered.a109514

De Storme, N., Zamariola, L., Mau, M., Sharbel, T. F., and Geelen, D. (2013). Volume-based pollen size analysis: an advanced method to assess somatic and gametophytic ploidy in flowering plants. *Plant Reprod.* 26, 65–81. doi: 10.1007/s00497-012-0209-0

Ding, Z. J., Wang, B. J., Moreno, I., Duplakova, N., Simon, S., Carraro, N., et al. (2012). ER-localized auxin transporter PIN8 regulates auxin homeostasis and

male gametophyte development in *Arabidopsis*. *Nat. Commun.* 3:941. doi: 10.1038/ncomms1941

Dorne, A.-J., Kappler, R., Kristen, U., and Heinz, E. (1988). Lipid metabolism during germination of tobacco pollen. *Phytochemistry* 27, 2027–2031. doi: 10.1016/0031-9422(88)80090-6

Fait, A., Fromm, H., Walter, D., Galili, G., and Fernie, A. R. (2008). Highway or byway: the metabolic role of the GABA shunt in plants. *Trends Plant Sci.* 13, 14–19. doi: 10.1016/j.tplants.2007.10.005

Fernie, A. R., and Stitt, M. (2012). On the discordance of metabolomics with proteomics and transcriptomics: coping with increasing complexity in logic, chemistry, and network interactions scientific correspondence. *Plant Physiol.* 158, 1139–1145. doi: 10.1104/pp.112.193235

Fiebig, A., Mayfield, J. A., Miley, N., Chau, S., Fischer, R., and Preuss, D. (2000). Alterations in CER6, a gene identical to CUT1, differentially affect long-chain lipid content on the surface of pollen and stems. *Plant Cell* 12, 2001–2008. doi: 10.1105/tpc.12.10.2001

Firon, N., Nepi, M., and Pacini, E. (2012). Water status and associated processes mark critical stages in pollen development and functioning. *Ann. Bot.* 109, 1201–1214. doi: 10.1093/aob/mcs070

Fragallah, S., Wang, P., Li, N., Chen, Y., and Lin, S. Z. (2018). Metabolomic analysis of pollen grains with different germination abilities from two clones of Chinese fir (*Cunninghamia lanceolata* (lamb) hook). *Molecules* 23:3162. doi: 10.3390/molecules23123162

Goetz, M., Guivarch, A., Hirsche, J., Bauerfeind, M. A., Gonzalez, M. C., Hyun, T., et al. (2017). Metabolic control of tobacco pollination by sugars and invertases. *Plant Physiol.* 173, 984–997. doi: 10.1104/pp.16.01601

Goldman, M. H. S., Goldberg, R. B., and Mariani, C. (1994). Female sterile tobacco plants are produced by stigma-specific cell ablation. *EMBO J.* 13, 2976–2984. doi: 10.1002/j.1460-2075.1994.tb06596.x

Hafidh, S., and Honys, D. (2021). Reproduction multitasking: the male gametophyte. *Annu. Rev. Plant Biol.* 72, 581–614. doi: 10.1146/annurev-arplant-080620-021907

Hernández, M. L., Lima-Cabello, E., Alché, J., de, D., Martínez-Rivas, J. M., and Castro, A. J. (2020). Lipid composition and associated gene expression patterns during pollen germination and pollen tube growth in olive (*Olea europaea L.*). *Plant Cell Physiol.* 61, 1348–1364. doi: 10.1093/pcp/pcaa063

Heslop-Harrison, J. (1979). Aspects of the structure, cytochemistry and germination of the pollen of rye (*Secale cereale L.*). *Ann. Bot.* 44, 1–47.

Hirsche, J., Engelke, T., Voller, D., Gotz, M., and Roitsch, T. (2009). Interspecies compatibility of the anther specific cell wall invertase promoters from *Arabidopsis* and tobacco for generating male sterile plants. *Theor. Appl. Genet.* 118, 235–245. doi: 10.1007/s00122-008-0892-2

Hirsche, J., Fernandez, J. M. G., Stabentheiner, E., Grosskinsky, D. K., and Roitsch, T. (2017). Differential effects of carbohydrates on *Arabidopsis* pollen germination. *Plant Cell Physiol.* 58, 691–701. doi: 10.1093/pcp/pcx020

Hummel, J., Segu, S., Li, Y., Irgang, S., Jueppner, J., and Giavalisco, P. (2011). Ultra performance liquid chromatography and high resolution mass spectrometry for the analysis of plant lipids. *Front. Plant Sci.* 2:54. doi: 10.3389/fpls.2011.00054

Ischebeck, T. (2016). Lipids in pollen – they are different. *Biochim. Biophys. Acta Mol. Cell Biol. Lipids* 1861, 1315–1328. doi: 10.1016/j.bbalip.2016.03.023

Johnson, M. A., Harper, J. F., Palanivelu, R., and Merchant, S. S. (2019). A fruitful journey: pollen tube navigation from germination to fertilization. *Annu. Rev. Plant Biol.* 70, 809–837. doi: 10.1146/annurev-arplant-050718-100133

Johnson, S. A., and McCormick, S. (2001). Pollen germinates precociously in the anthers of raring-to-go, an *Arabidopsis* gametophytic mutant. *Plant Physiol.* 126, 685–695. doi: 10.1104/pp.126.2.685

Johnson-Brousseau, S. A., and McCormick, S. (2004). A compendium of methods useful for characterizing *Arabidopsis* pollen mutants and gametophytically-expressed genes. *Plant J.* 39, 761–775. doi: 10.1111/j.1365-313X.2004.02147.x

Kambhampati, S., Aznar-Moreno, J. A., Bailey, S. R., Arp, J. J., Chu, K. L., Bilyeu, K. D., et al. (2021). Temporal changes in metabolism late in seed development affect biomass composition. *Plant Physiol.* 186, 874–890. doi: 10.1093/plphys/kiab116

Katajamaa, M., and Orešič, M. (2005). Processing methods for differential analysis of LC/MS profile data. *BMC Bioinformatics* 6:179. doi: 10.1186/1471-2105-6-179

Kessner, D., Chambers, M., Burke, R., Agusand, D., and Mallick, P. (2008). ProteoWizard: open source software for rapid proteomics tools development. *Bioinformatics* 24, 2534–2536. doi: 10.1093/bioinformatics/btn323

Kim, Y. J., Zhang, D. B., and Jung, K. H. (2019). Molecular basis of pollen germination in cereals. *Trends Plant Sci.* 24, 1126–1136. doi: 10.1016/j.tplants.2019.08.005

Kolde, R. (2019). *pheatmap: Pretty Heatmaps Version 1.0.12*. Available online at: https://rdrr.io/cran/pheatmap/ (accessed January 17, 2022).

Kuang, A., and Musgrave, M. E. (1996). Dynamics of vegetative cytoplasm during generative cell formation and pollen maturation in *Arabidopsis thaliana*. *Protoplasma* 194, 81–90. doi: 10.1007/BF01273170

Li, S. Z., Park, Y., Duraisingham, S., Strobel, F. H., Khan, N., Soltow, Q. A., et al. (2013). Predicting network activity from high throughput metabolomics. *PLoS Comput. Biol.* 9:e1003123. doi: 10.1371/journal.pcbi.1003123

Li-Beisson, Y., Pollard, M., Sauveplane, V., Pinot, F., Ohlrogge, J., and Beisson, F. (2009). Nanoridges that characterize the surface morphology of flowers require the synthesis of cutin polyester. *Proc. Natl. Acad. Sci. U.S.A.* 106, 22008–22013. doi: 10.1073/pnas.0909090106

McInnes, L., Healy, J., and Melville, J. (2018). UMAP: uniform manifold approximation and projection for dimension reduction. *arXiv* [preprint]. arXiv:1802.03426, doi: 10.1093/bib/bbab008

Moon, S., and Jung, K. H. (2020). First steps in the successful fertilization of rice and *Arabidopsis*: pollen longevity, adhesion and hydration. *Plants Basel* 9:956. doi: 10.3390/plants9080956

Obermeyer, G., Fragner, L., Lang, V., and Weckwerth, W. (2013). Dynamic adaption of metabolic pathways during germination and growth of lily pollen tubes after inhibition of the electron transport chain. *Plant Physiol.* 162, 1822–1833. doi: 10.1104/pp.113.219857

Pacini, E. (1996). Types and meaning of pollen carbohydrate reserves. *Sex. Plant Reprod.* 9, 362–366. doi: 10.1007/BF02441957

Pacini, E., Guarnieri, M., and Nepi, M. (2006). Pollen carbohydrates and water content during development, presentation, and dispersal: a short review. *Protoplasma* 228, 73–77. doi: 10.1007/s00709-006-0169-z

Palanivelu, R., Brass, L., Edlund, A. F., and Preuss, D. (2003). Pollen tube growth and guidance is regulated by POP2, an *Arabidopsis* gene that controls GABA levels. *Cell* 114, 47–59. doi: 10.1016/S0092-8674(03)00479-3

Pang, Z. Q., Chong, J., Zhou, G. Y., Morais, D. A. D., Chang, L., Barrette, M., et al. (2021). MetaboAnalyst 5.0: narrowing the gap between raw spectra and functional insights. *Nucleic Acids Res.* 49, W388–W396. doi: 10.1093/nar/gkab382

Paupiere, M. J., Muller, F., Li, H. J., Rieu, I., Tikunov, Y. M., Visser, R. G. F., et al. (2017). Untargeted metabolomic analysis of tomato pollen development and heat stress response. *Plant Reprod.* 30, 81–94. doi: 10.1007/s00497-017-0301-6

Pluskal, T., Castillo, S., Villar-Briones, A., and Oresic, M. (2010). MZmine 2: modular framework for processing, visualizing, and analyzing mass spectrometry-based molecular profile data. *BMC Bioinformatics* 11:395. doi: 10.1186/1471-2105-11-395

Qin, Y., Leydon, A. R., Manziello, A., Pandey, R., Mount, D., Denic, S., et al. (2009). Penetration of the stigma and style elicits a novel transcriptome in pollen tubes, pointing to genes critical for growth in a pistil. *PLoS Genet.* 5:e1000621. doi: 10.1371/journal.pgen.1000621

Ramesh, S. A., Tyerman, S. D., Xu, B., Bose, J., Kaur, S., Conn, V., et al. (2015). GABA signalling modulates plant growth by directly regulating the activity of plant-specific anion transporters. *Nat. Commun.* 6:7879. doi: 10.1038/ncomms8879

Regan, S. M., and Moffatt, B. A. (1990). Cytochemical analysis of pollen development in wild-type *Arabidopsis* and a male-sterile mutant. *Plant Cell* 2, 877–889. doi: 10.1105/tpc.2.9.877

Reinders, A. (2016). Fuel for the road – sugar transport and pollen tube growth. *J. Exp. Bot.* 67, 2121–2123. doi: 10.1093/jxb/erw113

Rodriguez-Garcia, M. I., M'rani-Alaoui, M., and Fernandez, M. C. (2003). Behavior of storage lipids during development and germination of olive (*Olea europaea L.*) pollen. *Protoplasma* 221, 237–244. doi: 10.1007/s00709-002-0076-x

Rolland, F., Baena-Gonzalez, E., and Sheen, J. (2006). Sugar sensing and signaling in plants: conserved and novel mechanisms. *Annu. Rev. Plant Biol.* 57, 675–709. doi: 10.1146/annurev.arplant.57.032905.105441

Rösti, J., Barton, C. J., Albrecht, S., Dupree, P., Pauly, M., Findlay, K., et al. (2007). UDP-Glucose 4-Epimerase isoforms UGE2 and UGE4 cooperate in providing

UDP-Galactose for cell wall biosynthesis and growth of *Arabidopsis thaliana*. *Plant Cell* 19, 1565–1579. doi: 10.1105/tpc.106.049619

Rotsch, A. H., Kopka, J., Feussner, I., and Ischebeck, T. (2017). Central metabolite and sterol profiling divides tobacco male gametophyte development and pollen tube growth into eight metabolic phases. *Plant J.* 92, 129–146. doi: 10.1111/tpj.13633

Rottmann, T., Fritz, C., Sauer, N., and Stadler, R. (2018). Glucose uptake via STP transporters inhibits in vitro pollen tube growth in a HEXOKINASE1-dependent manner in *Arabidopsis thaliana*. *Plant Cell* 30, 2057–2081. doi: 10.1105/tpc.18.00356

Routaboul, J. M., Benning, C., Bechtold, N., Caboche, M., and Lepiniec, L. (1999). The TAG1 locus of *Arabidopsis* encodes for a diacylglycerol acyltransferase. *Plant Physiol. Biochem.* 37, 831–840. doi: 10.1016/S0981-9428(99)00115-1

Salinas-Grenet, H., Herrera-Vasquez, A., Parra, S., Cortez, A., Gutierrez, L., Pollmann, S., et al. (2018). Modulation of auxin levels in pollen grains affects stamen development and anther dehiscence in *Arabidopsis*. *Int. J. Mol. Sci.* 19:2480. doi: 10.3390/ijms19092480

Shi, D. Q., and Yang, W. C. (2010). "Pollen germination and tube growth," in *Plant Developmental Biology-Biotechnological Perspectives*, eds E. Pua and M. Davey (Berlin: Springer), 245–282.

Sivitz, A. B., Reinders, A., and Ward, J. M. (2008). *Arabidopsis* sucrose transporter AtSUC1 is important for pollen germination and sucrose-induced anthocyanin accumulation. *Plant Physiol.* 147, 92–100. doi: 10.1104/pp.108.118992

Stadler, R., Truernit, E., Gahrtz, M., and Sauer, N. (1999). The AtSUC1 sucrose carrier may represent the osmotic driving force for anther dehiscence and pollen tube growth in *Arabidopsis*. *Plant J.* 19, 269–278. doi: 10.1046/j.1365-313X.1999.00527.x

Streb, S., and Zeeman, S. C. (2012). Starch metabolism in *Arabidopsis*. *Arabidopsis Book* 10:e0160. doi: 10.1199/tab.0160

Sud, M., Fahy, E., Cotter, D., Azam, K., Vadivelu, I., Burant, C., et al. (2016). Metabolomics Workbench: an international repository for metabolomics data and metadata, metabolite standards, protocols, tutorials and training, and analysis tools. *Nucleic Acids Res.* 44, D463–D470. doi: 10.1093/nar/gkv1042

Tang, L. Y., Nagata, N., Matsushima, R., Chen, Y., Yoshioka, Y., and Sakamoto, W. (2009). Visualization of plastids in pollen grains: involvement of FtsZ1?in pollen plastid division. *Plant Cell Physiol.* 50, 904–908. doi: 10.1093/pcp/pcp042

Wang, J., Yu, Y.-C., Li, Y., and Chen, L.-Q. (2022). Hexose transporter SWEET5 confers galactose sensitivity to *Arabidopsis* pollen germination via a galactokinase. *Plant Physiol.* kiac068. doi: 10.1093/plphys/kiac068

Wang, Y., Zhang, W. Z., Song, L. F., Zou, J. J., Su, Z., and Wu, W. H. (2008). Transcriptome analyses show changes in gene expression to accompany pollen germination and tube growth in *Arabidopsis*. *Plant Physiol.* 148, 1201–1211. doi: 10.1104/pp.108.126375

Wolters-Arts, M., Lush, W. M., and Mariani, C. (1998). Lipids are required for directional pollen-tube growth. *Nature* 392, 818–821. doi: 10.1038/33929

Wu, J. Z., Lin, Y., Zhang, X. L., Pang, D. W., and Zhao, J. (2008). IAA stimulates pollen tube growth and mediates the modification of its wall composition and structure in *Torenia fournieri*. *J. Exp. Bot.* 59, 2529–2543. doi: 10.1093/jxb/ern119

Xue, Z. Y., Xu, X. N., Zhou, Y., Wang, X. N., Zhang, Y. C., Liu, D., et al. (2018). Deficiency of a triterpene pathway results in humidity-sensitive genic male sterility in rice. *Nat. Commun.* 9:604. doi: 10.1038/s41467-018-03048-8

Ylstra, B., Busscher, J., Franken, J., Hollman, P. C. H., Mol, J. N. M., and Vantunen, A. J. (1994). Flavonols and fertilization in *petunia hybrida*: localization and mode of action during pollen tube growth. *Plant J.* 6, 201–212. doi: 10.1046/j.1365-313X.1994.6020201.x

Zhao, Y. D. (2010). Auxin biosynthesis and its role in plant development. *Annu. Rev. Plant Biol.* 61, 49–64. doi: 10.1146/annurev-arplant-042809-112308

Zienkiewicz, A., Zienkiewicz, K., Rejón, J. D., Rodríguez-García, M. I., and Castro, A. J. (2013). New insights into the early steps of oil body mobilization during pollen germination. *J. Exp. Bot.* 64, 293–302. doi: 10.1093/jxb/ers332

Conflict of Interest: The authors declare that the research was conducted in the absence of any commercial or financial relationships that could be construed as a potential conflict of interest.

Publisher's Note: All claims expressed in this article are solely those of the authors and do not necessarily represent those of their affiliated organizations, or those of the publisher, the editors and the reviewers. Any product that may be evaluated in this article, or claim that may be made by its manufacturer, is not guaranteed or endorsed by the publisher.

Advantages of publishing in Frontiers

OPEN ACCESS
Articles are free to read for greatest visibility and readership

FAST PUBLICATION
Around 90 days from submission to decision

HIGH QUALITY PEER-REVIEW
Rigorous, collaborative, and constructive peer-review

TRANSPARENT PEER-REVIEW
Editors and reviewers acknowledged by name on published articles

Frontiers
Avenue du Tribunal-Fédéral 34
1005 Lausanne | Switzerland

Visit us: www.frontiersin.org
Contact us: frontiersin.org/about/contact

REPRODUCIBILITY OF RESEARCH
Support open data and methods to enhance research reproducibility

DIGITAL PUBLISHING
Articles designed for optimal readership across devices

FOLLOW US
@frontiersin

IMPACT METRICS
Advanced article metrics track visibility across digital media

EXTENSIVE PROMOTION
Marketing and promotion of impactful research

LOOP RESEARCH NETWORK
Our network increases your article's readership